Targeting the Mevalonate Pathway Enhances the Efficacy of Epidermal Growth Factor Receptor – Tyrosine Kinase Inhibitors in Head and Neck Squamous Cell Carcinoma

Lenah Mukhtar

Thesis submitted to the University of Ottawa

in partial fulfillment of the requirements for the

Doctor of Philosophy degree in Biochemistry

Specializing in Human and Molecular Genetics

Department of Biochemistry, Microbiology, and Immunology

Faculty of Medicine

University of Ottawa

ABSTRACT

Epidermal growth factor receptor (EGFR) is highly expressed in head and neck squamous cell carcinoma (HNSCC) and non-small cell lung cancer (NSCLC) and is a key regulator of tumor cell growth and survival. Erlotinib, also known as tarceva, (a first-generation) and afatinib, also known as giotrif, (a second-generation) are tyrosine kinase inhibitors (TKIs) of EGFR. These TKIs are recognized therapeutic agents in these tumor types, as they inhibit EGFR signaling but show limited activity as single agents. Novel strategies will likely require EGFR-TKIs combination with an agent(s) that will enhance their therapeutic efficacy. Recently, we have demonstrated that combining statins, inhibitors of the mevalonate pathway, with erlotinib enhanced EGFR inhibition and induced synergistic cytotoxicity through the activation of cellular integrated stress response pathway (ISR) regulated by the induction of activating transcription factor 3 (ATF3). In our Phase I clinical trial, combining rosuvastatin with erlotinib, while demonstrating clinical activity, this treatment also showed statin-induced myopathies likely the result of diminished ubiquinone levels, which limited their utilization. Therefore, alternative strategies are warranted. Targeting geranylgeranyl diphosphate (GGPP) synthesis or its incorporation, a downstream mevalonate metabolite, represents such an approach with the potential to circumvent statin-associated toxicities but retain the efficacy in combination with EGFR inhibitors. In this project, we evaluated the effect of the combination of geranylgeranyl transferase-I inhibitor (GGTI-298) with the EGFR inhibitor, tarceva, (aim 1) and a GGPP synthase inhibitor, digeranyl bisphosphonate (DGBP), with the EGFR inhibitor, afatinib, (aim 2). For aim 1, we demonstrated that GGTI-298 treatment induced ATF3 expression in SCC9 and SCC25 cells and in a cohort of *ex-vivo* tumor tissues. Furthermore, GGTI-298 and tarceva induced synergistic cytotoxicity in SCC cells that was dependent on ATF3 expression, as ATF3 deficient murine embryonic fibroblasts (ATF3-/- MEFs)

displayed attenuated cytotoxicity in response to GGTI-298 alone and in combination with tarceva. Similarly, SCC9 sub-lines that were selected as resistant to GGTI-298 through prolonged exposure to this agent also failed to demonstrate synergy with treatment of GGTI-298 in combination with tarceva. For aim 2, we demonstrated that the specific GGPP synthase inhibitor, DGBP, induced cytotoxicity in SCC cells. We further demonstrated this specificity as specific shRNA targeting of GGPP synthase as well as the inhibitor DGBP significantly enhanced the cytotoxic activity of the EGFR-TKI afatinib in SCC cells. DGBP as well as afatinib treatments induced ATF3 expression in SCC cells *in vitro* and in a cohort of *ex-vivo* tumor tissues. Co-administration of the downstream metabolite GGPP inhibits the induction of ATF3 and the cytotoxic and apoptotic effects associated with DGBP treatment. Furthermore, the synergistic cytotoxicity induced by the combination of DGBP and afatinib in SCC cells was also dependent on the expression of ATF3 through the induction of cellular stress response pathways. Taken together, these results suggest the potential clinical utility of combining downstream mevalonate inhibitors (GGTI-298 or DGBP) with EGFR inhibitors in HNSCC patients as a novel and more refined combination therapeutic approach.

DEDICATIONS

To my parents, husband, and daughter for their prayers, love and support.

ACKOWLEDGMENTS

At first, I would like to thank Allah, the all-knowing, for giving me the strength to carry on. I would also like to dedicate my hard work on this project to the handful of people that helped to make it possible.

Dr. Jim Dimitroulakos, my research supervisor, has played an important role in the success of my PhD project by giving me valuable and constructive feedback, which have collectively helped me attain my goals.

Dr. Ian Lorimer, Dr. Christina Addison, and Dr. Luc Sabourin, thank you for being members of the thesis advisory committee and for all the support and your valuable scientific inputs. Special thanks to Dr. Christina Addison who had an essential role during the last year of my PhD; I cannot thank you enough Dr. Addison for standing by myside when needed.

Many thanks to my lab colleagues, Mohamed Shaad Hasim and Tabassom Baghai, for their great support and help. I'm also extending my gratitude to all members of the Cancer Therapeutics Program at the Ottawa Hospital Research Institute of the Ottawa Hospital, who I have had the pleasure to work with during my project. A special thanks to Dr. Josee Coulombe for her care and encouragement.

Special thanks to my sponsor, The Ministry of Higher Education in Saudi Arabia, represented by The Royal Embassy and the Saudi Arabian Cultural Bureau in Canada, for the full scholarship and for providing all services needed to ease pursuing my studies abroad. Special thanks to my academic advisor at the Saudi Bureau, Dr. Faika El-Nakib for her support during both my masters and my PhD. Special thanks to Dr. Hassan AL- Mohammad, the senior academic regulations officer, at the Saudi Bureau for his assistance during the last year of my PhD.

Finally, I owe my warm thanks to my parents, Fatimah and Emam, my sister, Dina, my brothers, Abdullah, Hussam, Khaled, and Mohammed, my nieces Judie and Jana, my grandmother, aunts, and friends for their encouragement and support, which made it possible for me to finish this work. Special thanks to my mentor, my aunt Abeer Al-Fouti, for her continuous mentoring during my student life. Lastly, special thanks to my loving and caring husband, Zeyad, and my daughter, Sara, for their unconditional love, constant support, and prayers; your encouragement and advice kept me going each and every day. I am truly thankful for having you in my life.

TABLE OF CONTENTS

ABSTRACT ..... **II**

DEDICATIONS ..... **IV**

ACKOWLEDGMENTS ..... **V**

TABLE OF CONTENTS ..... **VII**

LIST OF ABBREVIATIONS ..... **IX**

LIST OF FIGURES ..... **XII**

LIST OF TABLES ..... **XIV**

CHAPTER 1: INTRODUCTION **1**

1.1 Head and Neck Squamous Cell Carcinoma 1

1.1.1 Epidemiology, Histology and Etiology *1*

1.1.2 Current HNSCC Treatment and Challenges *4*

1.2 Epidermal Growth Factor Receptor 6

1.2.1 Structure and Function of EGFR *6*

1.2.2 Dimerization and Activation of EGFR *10*

1.2.3 Signal Transduction via EGFR *14*

1.2.4 Role of EGFR in HNSCC *18*

1.3 EGFR Targeted Therapies 19

1.3.1 Monoclonal Antibodies *19*

1.3.2 Receptor Tyrosine Kinase Inhibitors *20*

1.4 Mevalonate Pathway 24

1.4.1 Biochemistry of the Mevalonate pathway *25*

1.4.2 The Statin family *29*

1.4.3 Statins and EGFR-TKIs Combination *30*

1.5 Downstream Target of Mevalonate Pathway 37

1.5.1 Protein Prenylation *37*

1.5.2 Prenylated Small-GTPases *38*

1.5.3 Inhibitors of Prenylated Proteins *38*

1.6 Metabolic Stress Pathways 41

1.6.1 The LKB1/AMPK Pathway *41*

1.6.2 The Integrated Stress Response Pathway *45*

1.6.3 Activating Transcription Factor 3 ..... *49*

1.6.4 Statins and the Metabolic Stress Pathways *50*

1.7 Rationale 53

1.8 Hypothesis 54

1.9 Overall objective of this study 54

1.10 Specific Aims 54

CHAPTER 2: MATERIALS AND METHODS **55**

2.1 Tissue Culture 55

2.2 Drug Compounds 57

2.3 (4,5-Dimethylthiazol-2-yl)-2,5-Diphenyltetrazolium Bromide (MTT) Assay 57

2.4 Trypan Blue Exclusion Cell Viability Assay 59

2.5 Western Blotting Analysis 60
2.6 Scratch Wound Assay 61
2.7 Propidium Iodide Flow Cytometry 62
2.8 Fluorescence Microscopy 62
2.9 Transcriptome Analysis (RNAseq) 63
2.10 Design and Expression of short-hairpin RNA for GGDPS 64
2.11 Quantitative RT-PCR 64
2.12 *Ex-Vivo* Tumor Analysis 65
2.13 Graphical and Statistical Analyses 66

CHAPTER 3: RESULTS 67

3. INHIBITION OF GGTASE1 ENHANCES TARCEVA EFFICACY IN SQUAMOUS CELL CARCINOMA CELLS: POTENTIAL NOVEL COMBINATION THERAPEUTIC APPROACH 67

3.1 GGPP Reverses Lovastatin Induced Synergy with Tarceva 69
3.2 Synergistic Cytotoxicity of GGTI-298 and Tarceva in SCC Cells 76
3.3 GGTI-298 Induces Multiple Stress Pathways 85
3.4 ATF3 is a GGTI-298 Regulated Gene 89
3.5 Key Role of ATF3 in GGTI-298 Cytotoxicity and Synergy with Tarceva 93

CHAPTER 4: RESULTS 101

4. GERANYLGERANYL DIPHOSPHATE SYNTHASE AS A THERAPEUTIC TARGET: ENHANCING AFATINIB ACTIVITY IN SQUAMOUS CELL CARCINOMA 101

4.1 GGPP Reverses Lovastatin Induced Cytotoxicity 103
4.2 Inhibition of GGDPS Induces Cellular Cytotoxicity 106
4.3 ATF3 is the Key Role for DGBP Cytotoxicity 120
4.4 DGBP Induces ATF3 Through the Activation of the ISR Signaling Pathway 132
4.5 DGBP Synergistically Enhances Afatinib Cytotoxicity 136

CHAPTER 5: DISCUSSION 149

5.1. GGTI - Effects on EGFR Activity and Synergy with EGFR-TKIs 154
5.2 Targeting GGPP Synthase - Potential as Novel Enhancer of EGFR Inhibitors 163
5.3 Conclusion and Future direction 174

APPENDIX I 178

APPENDIX II 195

APPENDIX III 198

REFERENCES 199

LIST OF ABBREVIATIONS

Acronym	Meaning
4EBP1	eukaryotic translation initiation factor 4E binding protein 1
5-FU	5-flourouracil
5UTR	5`-untranslated region
AKT	protein kinase B
AML	acute myeloid leukemia
AMPK	AMP-activated protein kinase
ANOVA	analysis of variance
AR	amphiregulin
Arf	ADP ribosylation factors
ATF	activating transcription factor
ATM	ataxia-telangiectasia mutated
ATP	adenosine triphosphate
BAD	Bcl-2-associated death promoter
BCA	bicinchoninic acid assay
Bcl2	B-cell lymphoma 2
BGP	beta-glycerophosphate
BTC	betacellulin
bZIP	basic leucine zipper
Caspase	cysteine aspartic acid specific protease
Cdc42	Cell division control protein 42 homolog
CDK	cycline depedent kinase
CDKN2A	cyclin-dependent kinase Inhibitor 2A
cDNA	complementary deoxyribonucleic acid
CHOP	CCAAT-enhancer-binding protein homologous protein
CI	combination index
CoQ10	Coenzyme Q10 (aka ubiquinone)
CR1-2	cystein rich domain
CREB	cAMP Responsive Element Binding protein
CRT	chemo-radio therapy
CT	chemotherapy
Ct	threshold cycle
Cys	cystein
DDIT4	DNA-damage-inducible transcript 4
DDR	DNA damage response
DGBP	digeranyl bisphosphonate
DHDDS	dehydrodolichyl diphosphate synthase
DI-IV	domains I-IV
DLT	dose limited toxicity
DMEM	dulbecco's modified eagle medium
DMSO	dimethyl sulfoxide
DR5	death receptor 5
dsRNA	double-stranded RNA
ECL	Electrochemiluminescence
EDTA	ethylenediaminetetraacetic acid
EGF	epidermal growth factor
EGFR	epidermal growth factor receptor
EGFRvIII	EGFR variant III
eIF2	eukaryotic initiation factor 2
eIF4E	eukaryotic translation initiation factor 4E
EMA	european medicines agency
EPG	epigen
EPR	epiregulin
ER	endoplasmic reticulum
ErbB	avian erythroblastosis oncogene B
ERK	extracellular signal regulated kinases
Ets	E26 transformation-specific or E-twenty-six family
FBS	fetal bovine serum
FDA	food and drug administration
FPP	farnesyl diphosphate / farnesyl pyrophosphate
FPPDS	farnesyl diphosphate synthase
Ftase	farnesyltransferase
FTI	farnesyltransferase inhibitor
GADD153	DNA damage- inducible gene 153
GAP	GTPase-activating protein
GAPDH	glyceraldehyde 3-phosphate dehydrogenase
GCN2	general control nonderepressible 2
GDI	guanine nucleotide dissociation inhibitor
GDP	guanosine diphosphate
GEF	guanyl nucleotide exchange factor
GGDPS	geranylgeranyl diphosphate synthase

GGPP	geranylgeranyl diphosphate / geranylgeranyl pyrophosphate
GGTase	geranylgeranyl transferase
GGTI	geranylgeranyl transferase inhibitor
GPCR	G-protein coupled receptors
Grb2	growth factor receptor-bound protein 2
GTP	guanosine triphosphate
Gy	the gray unit
H-Ras	Harvey rat sarcoma viral oncogene homolog
HB-EGF	heparin-binding epidermal growth factor-like growth factor
HCl	hydrochloric acid
HER	human epidermal growth factor receptor
HisRS	histidyl-tRNA synthetase
HMG-CoA	3-hydroxy-3-methyl glutaryl coenzyme A
HMGR	3-hydroxy-3-methyl glutaryl coenzyme A reductase
HN	head and neck tumor tissue
HNSCC	head and neck squamous cell carcinomas
HPV	human papilloma virus
hr	hours
HRI	heme-regulated eIF2a kinase
HRP	horseradish peroxidase
IBP	Isoprenoid biosynthetic pathway
IC50	half maximal inhibitory concentration
ICMT	isoprenylcysteine carboxyl methyltransferase
IgG	immunoglobulin G
IPP	isopentyl diphosphate
ISR	integrated stress response
IV	intravenous
JAK	janus kinase
JNK	c-Jun N-terminal kinases
JUN	a protein that in humans is encoded by the JUN gene
K-Ras	Kirsten rat sarcoma viral oncogene homolog
kDa	kilo dalton
L1-2	ligand binding domain
LA-HNSCC	locally regionally advanced HNSCC
LDL	low-density lipoprotein
LKB1	liver kinase B
LU	lung tumor tissue
mAbs	monoclonal antibodies
MAPK	mitogen-activated protein kinase
MEF	mouse embryonic fibroblast
MEK	mitogen-activated protein kinase kinase
MEL	melanoma tumor tissue
Met	methionine
μM	micro molar
mM	milli molar
mRNA	messenger ribonucleic acid
MTD	maximum tolerated dose
MTT Assay	3-(4,5-Dimethylthiazol-2-yl)-2,5-diphenyltetrazolium bromide assay
MVK	mevalonate kinase
MVP	mevalonate pathway
MYC	avian myelocytomatosis virus oncogene cellular homolog
N-Ras	Neuroblastoma RAS viral oncogene homolog
NBP	nirogenous bisphosphonate
NEAA	non-essential amino acids
Nrg	neuregulin
NSCLC	non-small cell lung
OHRI	ottawa hospital research institute
OS	overall survival
OVCA	ovarian tumor tissue
p21	CIP1/WAF1 CDK inhibitor
p27	Cip/Kip inhibitor
p53	tumor protein 53
PAGE	polyacrylamide gel electrophoresis
PARP	poly (ADP-ribose) polymerase
PBS	phosphate buffered saline
PERK	PKR-like ER kinase
PI3K	phosphoinositide 3-kinase
PIC	pre-initiation complex
PJS	Peutz-Jeghers syndrome
PKC	protein kinase C
PKR	double-stranded RNA-dependent protein kinase
PLCγ	phospholypase Cγ
PMVK	phosphomevalonate kinase
pRb	ritnoblastoma protein
PTB	phosphotyrosine binding
PTEN	phosphatase and tensin homolog
PTI	prenyltransferase inhibitor
PTM	post-translational modification

PUMA (BBC3)	p53 upregulated modulator of apoptosis
R/M HNSCC	recurrent/metastatic HNSCC
Rab	rat sarcoma-related proteins in brain
Rac1	ras-related C3 botulinum toxin
Raf	rapidly accelerated fibrosarcoma
Ran	Ras-related nuclear protein
Rap1	ras-related proteins1 or Ras-proximate-1
Ras	rat sarcoma viral oncogene
RCE1	Ras-converting enzyme 1
RhoA	ras homolog gene family
RIPA	radio immuno precipitation assay
RPM	round per minute
RPMI	roswell park memorial institute medium
RT	radiotherapy
RTK	receptor tyrosine kinase
Sar1	Secretion Associated Ras Related GTPase 1A
SCC	squamous cell carcinoma
SD	standard deviation
Ser	Serine
SH2	Src homology-2
shRNA	short hairpin ribonucleic acid
SOS	son of sevenless
SQS	squalene synthase
STAT	signal transducer and activator of transcription
STRAD	STE20-like kinase domain
TBS	tris buffer saline
TBST	tris-buffered saline with 0.1% tween-20
TGF-a	transforming growth factor-a
Thr	Threonine
THY	thymus tumor tissue
TKI	tyrosine kinase inhibitor
TNM	tumor lymph node metastasis
tRNA	transfer ribonucleic acid
TSC	tuberous sclerosis complex
Tyr	tyrosine
uORF	short upstream open reading frame
UPR	unfolded protein response
V/V	volume/volume
W/V	weight/volume
WT	wild-type
ZOL	Zoledronate

LIST OF FIGURES

Chapter 1: Introduction

Figure 1. 1 The Anatomy of Head and Neck Cancer. 2
Figure 1. 2 The domains of EGFR. 8
Figure 1. 3 EGFR dimerization. 12
Figure 1. 4 EGFR signaling pathway. 16
Figure 1. 5 Common drugs in HNSCC. 23
Figure 1. 6 Mevalonate pathway. 27
Figure 1. 7 The mevalonate pathway and EGFR link. 31
Figure 1. 8 LKB1/AMPK signaling pathway. 43
Figure 1. 9 Integrated stress response pathway. 47
Figure 1. 10 Statins and metabolic stress pathways. 51

Chapter 3: Results

Figure 3. 1 The effect of add back downstream mevalonate metabolites on lovastatin. 70
Figure 3. 2 The effects of GGTI-298 on RhoA prenylation, actin organization, and cellular migration, and viability. 74
Figure 3. 3 The synergistic relationship between lovastatin and erlotinib in SCC cells. 77
Figure 3. 4 The effects of GGTI-298 on tarceva-induction of cytotoxicity and apoptosis in SCC cells. .. 81
Figure 3. 5 The synergistic relationship between GGTI-298 and tarceva in SCC cells. 83
Figure 3. 6 The effects of GGTI-298 on EGFR, AKT, LKB1 and AMPK phosphorylation. 87
Figure 3. 7 The role of ATF3 in GGTI-298 activity. 91
Figure 3. 8 Characterization of SCC9 resistant sub-lines and the effects of GGTI-298 and ATF3 on parental SCC9 and GGTI-resistant clones. 95
Figure 3. 9 The effects of GGTI-298 on ATF3 null MEFs vs. wild-type. 98

Chapter 4: Results

Figure 4. 1 GGPP rescues lovastatin cytotoxicity in SCC and NSCLC cells. 104
Figure 4. 2 Knockdown GGPDS in HeLa. 108
Figure 4. 3 MTT assay evaluating DGBP cytotoxicity in SCC and NSCLC cells. 111
Figure 4. 4 The effect of biochemical add back GGPP on DGBP in SCC cells. 116
Figure 4. 5 Comparison between lovastatin and DGBP effects on the human normal fibroblast 118
Figure 4. 6 The effects of DGBP and afatinib on ATF3 expression in SCC cells. 121
Figure 4. 7 The effects of DGBP and afatinib on ATF3 expression in NSCLC cells. 124
Figure 4. 8 ATF3 is a key regulator of DGBP activity. 128
Figure 4. 9 Add back GGPP prevented DGBP apoptotic effects in SCC cells. 130
Figure 4. 10 DGBP and afatinib induce ATF3 through the ISR Pathway. 134
Figure 4. 11 MTT assay evaluating afatinib cytotoxicity in SCC and NSCLC cells. 139
Figure 4. 12 The synergistic relationship between DGBP and afatinib in SCC cells. 141
Figure 4. 13 The synergistic relationship between DGBP and afatinib in NSCLC cells. 143
Figure 4. 14 The addition of DGBP enhances afatinib-induction of ATF3 in SCC cells. 146

Chapter 5: Discussion

Figure 5. 1 Overall proposed model of the study. 176

Appendix I

Figure S1. Densitometry analysis of Figure 3-1C……....178
Figure S2. Densitometry analysis of Figure 3-6……..….179
Figure S3. Densitometry analysis of Figure 3-7B……...180
Figure S4. Densitometry analysis of Figure 3-8.....……..…...181
Figure S5. Densitometry analysis of Figure 4-4C……....182
Figure S6. Densitometry analysis of Figure 4-6A…….....183
Figure S7. Densitometry analysis of Figure 4-6B……....184
Figure S8. Densitometry analysis of Figure 4-7A…….....185
Figure S9. Densitometry analysis of Figure 4-8A…….....186

Figure S10. Densitometry analysis of Figure 4-8B……..…….....187
Figure S11. Densitometry analysis of Figure 4-9……..…….....188
Figure S12. Densitometry analysis of Figure 4-10A (DGBP & ATF3)……..……..189
Figure S13. Densitometry analysis of Figure 4-10A (DGBP & PARP)……..……..190
Figure S14. Densitometry analysis of Figure 4-10A (afatinib & ATF3)……..…….....191
Figure S15. Densitometry analysis of Figure 4-10A (afatinib & PARP)……..…….....192
Figure S16. Densitometry analysis of Figure 4-14A (ATF3)……..……..193
Figure S17. Densitometry analysis of Figure 4-14A (PARP)……..…….....194

Appendix II

Figure S18. Venn diagram demonstrating the number of the genes that were differentially expressed following the treatment of SCC25 with 10μM lovastatin or 10μM GGTI-298……..195
Figure S19. GO analysis of the differentially expressed genes following 10μM lovastatin and 10μM GGTI-298 in SCC25 …….196
Figure S20. Venn diagram and GO analysis demonstrating the subset of the genes that were differentially induced following the 24hrs treatment of SCC25 with 10μM lovastatin and 10μM GGTI-298……...197

LIST OF TABLES

Chapter 1: Introduction

Table 1.1 High throughput Prestwick Library Screen Hits……..……..35

Appendix III

Table S1. A table highlights the gene names of the 26 upregulated genes following the 24hrs treatment of SCC25 with 10mM lovastatin and 10mM GGTI-298……...198

CHAPTER 1: INTRODUCTION

1.1 Head and Neck Squamous Cell Carcinoma

1.1.1 Epidemiology, Histology and Etiology

Head and Neck Squamous Cell Carcinoma (HNSCC) is the sixth most common form of cancer (1), with an annual incidence of approximately 932,000 new cases and 379,000 deaths diagnosed worldwide in 2015 (2,3). Cancer of the head and neck consists of a heterogeneous group of aggressive epithelial malignancies of different anatomical sites of the upper aerodigestive tract (Figure 1.1) including lip, oral cavity, nasopharynx, oropharynx, hypopharynx, and larynx (4). HNSCC represents about 90 - 95% of all head and neck tumors (5), where the tongue is the most common part of the oral cavity associated with SCC (6). The overall long-term survival remains poor with an approximately 50% survival rate of HNSCC patients with advanced disease of less than five years (7). In fact, tongue cancer has an even lower survival rate compared to other parts of the oral cavity (6,8).

Figure 1. 1 The Anatomy of Head and Neck Cancer.

This figure shows the common anatomical sites of the head and neck cancer. For the National Cancer Institute © 2017 Terese Winslow LLC, U.S. Govt. has certain rights.

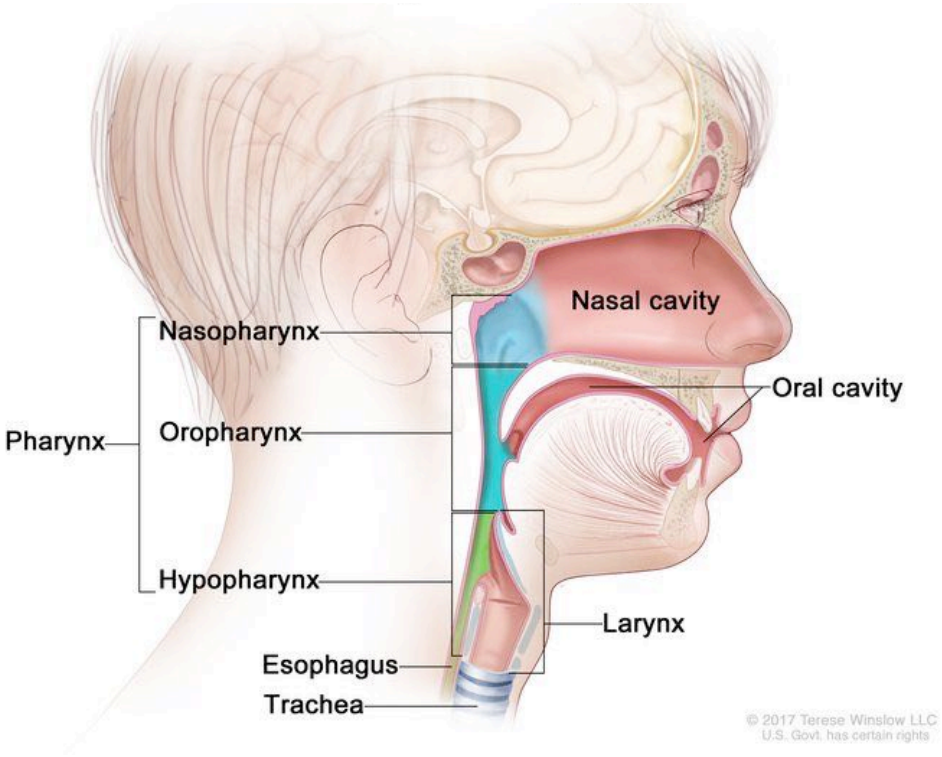
Nasal cavity
Nasopharynx
Oral cavity
Pharynx
Oropharynx
Hypopharynx
Larynx
Esophagus
Trachea
© 2017 Terese Winslow LLC
U.S. Govt. has certain rights

The most common identified predisposing factors of HNSCC are tobacco use and alcohol consumption (9). Recently, infection with human papillomavirus (HPV) has been associated with a significant subset of HNSCC patients in Canada and other Western countries, especially in the oropharynx cancers (9,10). HPV is a double-stranded DNA virus that infects the squamous epithelium. HPV-16 and HPV-18 are primarily associated with the development of HNSCC and cervical cancer (11). Viral oncoproteins E5, E6, and E7 are accessory proteins that coordinate viral genome amplification, and they usually contribute to HPV-mediated HNSCC oncogenesis (6,12). E5 oncoprotein modulates the receptor tyrosine kinase EGFR expression by preventing its internalization and degradation leading to increased EGFR-induced cellular proliferation (6,13). E6 oncoprotein is a ubiquitin ligase that targets and degrades the p53 tumor suppressor, thereby compromising p53-dependent cell-cycle arrest and apoptosis (6,14). E7 oncoprotein binds and inhibits the tumor suppressor pRb (6,15). The binding of E7 to pRb releases the E2F transcription factor and inhibits the transcription of the cyclin-dependent kinase (CDK) inhibitors p21 and p27 leading to cell-cycle progression through the G1 phase, thereby enhancing cellular proliferation (6). The outcome of HPV association has led to the division of HNSCC into two subsets with distinctive molecular and clinical profiles: HPV-positive cancers (generally are non-smokers with a better prognosis), and HPV-negative cancers (smokers and a worse prognosis) (16).

1.1.2 Current HNSCC Treatment and Challenges

Due to HNSCC heterogeneity, treatment planning and prognostication are often challenging to obtain (17). The standard treatment of HNSCC is based on the anatomical locality of the primary tumor, and TNM staging of the disease (1,18). The prognosis of HNSCC patients usually depends on the stage of cancer at presentation. Based on the TNM system, HNSCC is classified into three broad stages: early stage (I/II), locally-regionally advanced stage (LA stage,

III/IVA), and recurrent/metastatic disease stage (R/M stage, IVB) that are determined by the extent of the tumor, the presence of lymph-node, and tumor metastatic disease (7). HNSCC treatment involves several modalities including surgery, radiotherapy (RT), and chemotherapy (CT) depending on the overall health status of the patients. Surgery frequently involves either classic open surgery or minimally invasive procedures, depending on the anatomy and tumor features, to resect the tumor in which clear margins can be achieved and function is preserved or improved (4). Radiation therapy ranges from 60Gy – 70Gy and utilizes ionizing radiation that induces DNA-damage which activates the DNA damage response, and induces cell death (4,19). The US Food and Drug Administration (FDA) approved five conventional CT drugs for HNSCC including cisplatin, 5-fluorouracil (5-FU), methotrexate, docetaxel, and bleomycin (1). Cisplatin is a member of the platinum family that covalently binds and damages DNA through their alkylating group (1). 5-FU, bleomycin, and methotrexate are antimetabolites, which prevent DNA/RNA synthesis (1), and docetaxel is a member of taxane family that inhibits microtubules disassembly and arrests cells in the G2/M phase which leads to apoptosis (1).

Generally, patients harboring early stage disease, representing approximately 30% of all HNSCC patients, are potentially curable with a single treatment (either surgery or RT); while advance stages require a combined modality of surgery, RT and CT depending on the expected outcomes and the treatment toxicities (7). Cisplatin-based chemo-radiotherapy (CRT) is the standard treatment option for the LA-HNSCC which represents the majority of HNSCC cases (7,16). However, these therapies are aggressive, and about 10 - 30% of these LA-HNSCC cases develop metastasis, mostly in the lung (7,20). Treatment options for the R/M HNSCC patients are limited, and involve palliative platinum-based CT with best supportive care with median overall survival (OS) of approximately 7 months (7,21,22). However, these treatment options lack

specificity for tumor cells and are often associated with toxicities during or shortly after treatment (e.g., fatigue, nausea, alopecia, neutropenia, anemia, mucositis, dermatitis, hoarseness of voice, and myelosuppression) without improving the OS (7,23). Due to the significant challenges associated with these conventional therapies, new selective and effective treatments with limited side effects are urgently required. Therefore, the treatment of advanced HNSCC has expanded to include biological molecular targeted therapies. These agents act specifically against key components of cellular pathways involved in tumor growth, progression, and survival (24). One such approach revolves around targeting the activity of epidermal growth factor receptor (EGFR) whose overexpression (90 – 100% of tumor) in HNSCC can drive tumor cell proliferation and survival (1,16,25). EGFR is a well-recognized therapeutic target in HNSCC, and its targeting has therapeutic potential.

1.2 Epidermal Growth Factor Receptor

1.2.1 Structure and Function of EGFR

EGFR, also referred to as erbB1(avian erythroblastosis oncogene B) and HER1 (human epidermal growth factor receptor), is a cell surface receptor that belongs to ErbB receptor tyrosine kinase (RTK) family (26,27). This RTK family includes four members: ErbB1 (EGFR/HER1), ErbB2 (HER2/Neu), ErbB3 (HER3), and ErbB4 (HER4) (28,29) that share 37% sequence identity (28–30). Where EGFR, ErbB2, and ErbB4 contain catalytic kinase domains and can form heterodimeric pairs with each other (29–31), ErbB2 has no known binding ligand, and the structure of its extracellular region differs significantly from EGFR, while ErbB3 contains an impaired kinase catalytic domain (28,31). Both ErbB2 and Erb3 can pair and form heterodimers with the other ErbB family members (28–30). RTKs are the key regulators for cellular communication and

coordination of complex cellular processes such as proliferation, survival, differentiation, migration, and apoptosis (27).

EGFR is one of the most studied RTK in biology (30), and it plays essential roles in the control of cellular functions during embryogenesis and in the regulation of metabolic and physiological processes (27). EGFR is expressed in a range of tissues mostly epithelial, mesenchymal, and neuronal origin, and in different organs such as the skin and the gastrointestinal tract (28,31–33). EGFR was discovered in the 1960s by Stanley Cohen, and it was the first receptor to be characterized as a protein-tyrosine kinase (31,34,35).

EGFR (Figure 1.2) is a 170 kDa plasma membrane glycoprotein (35) (containing 1186 amino acids) encoded by the *EGFR* gene at the 7p12 locus (28,31). It consists of a heavily glycosylated extracellular ligand-binding domain (~620 residues) at the N-terminus, a single short hydrophobic lipophilic transmembrane domain (~24 residues) that allows for anchorage to the cell, and an intracellular domain (~270 residues) that is flanked by juxtamembrane (~40 residues) and a continuous kinase active site (~232 residues) with multiple phosphorylation sites at the C-terminus. Autophosphorylation sites include seven tyrosine residues (Tyr-845, 992, 1045, 1068, 1086, 1148, 1173) (28,31). Phosphorylation of EGFR on serine (Ser-1142) and threonine (Thr-654) residues are involved in a mechanism for regulation of receptor kinase activity and internalization (28,31). Glycosylation is crucial for protein-protein interactions that occur between protein ligand and its cognate receptor (36). The extracellular domain is composed of four subdomains (Figure 1.2): DI (L1), DII (CR1), DIII (L2), and DIV (CR2) (28,31). These domains are alternately arranged from the N- to the C-terminus as follows: L1-CR1-L2-CR2, where domains I and III are involved in the ligand binding, and domains II and IV are cysteine-rich domains involved in receptors dimerization (28,31).

Figure 1. 2 The domains of EGFR.

This figure shows the structure of EGFR, where EGFR receptor is comprise of: [1] the extracellular region that consists of 4 domains at the N-terminal: D1 (L1), D2 (CR1), D3 (L2), and DIV (CR2), [2] Transmembrane domain, and [3] intracellular domain, which contains juxtramembrane, tyrosine kinase, and regulatory region at the C-terminal. Figure adapted and modified from Kathryn M. Ferguson, 2008 (282).

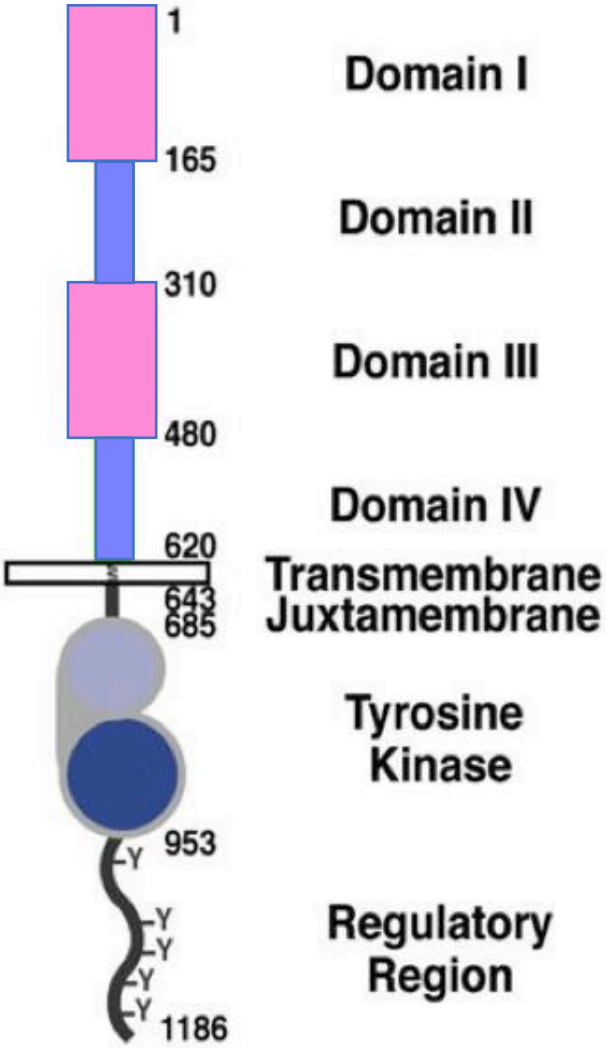
1
Domain I
165
Domain II
310
Domain III
480
Domain IV
620
Transmembrane
643
685
Juxtamembrane
Tyrosine
Kinase
953
Y
Y
Y
Y
Y
Regulatory
Region
1186

1.2.2 Dimerization and Activation of EGFR

EGFR is activated either by ligand-dependent or –independent manner depending on the context. In the absence of ligand, where the activation signal is missing, the extracellular domain of EGFR exists in equilibrium state between the auto-inhibited closed (tethered where domain II that is required for dimerization is buried into domain IV by the intramolecular interactions) and open confirmation (untethered where domain II is exposed and available for dimerization) (37,38). ErbB2, which has no ligand-binding domain, has a conformation that resembles the ligand-activated state, making this receptor constitutively active (39).

Ligand-induced dimerization is a typical process for ErbB RTK activation and induction of downstream signal transduction cascades (38,40). There are several polypeptide growth factor ligands with similar structures, that bind and activate ErbB receptors, which are divided into four groups (31). The first group binds to EGFR and consists of the epidermal growth factor (EGF), epigen (EPG), transforming growth factor-α (TGF-α), and amphiregulin (AR); the second group binds to EGFR and ErbB4 and consists of betacellulin (BTC), heparin-binding epidermal growth factor-like growth factor (HB-EGF), and epiregulin (EPR); the third group binds to ErbB3 and ErbB4 and consists of neuregulin-1 (Nrg-1) and neuregulin-2 (Nrg-2); and the fourth group binds to ErbB4 and consists of neuregulin-3 (Nrg-3) and neuregulin- 4 (Nrg-4) (31). Moreover, EGFR has been shown to be activated by cellular stresses (41,42), and G-protein coupled receptors (GPCR) (43). EGF is the ligand with the highest affinity for the EGFR receptor (28).

Under normal conditions (Figure 1.3), EGF binds to its receptor and shifts the equilibrium towards dimer formation, in which two EGF ligands bind simultaneously to both DI and DIII of the extracellular domain, and stabilize the receptors in their untethered form (38,39). This binding draws the receptors closer to one another and induces conformational changes in the receptors,

where DII (CR1) becomes exposed allowing for receptor homo-dimerization between two EGFR proteins or hetero-dimerization between EGFR and another ErbB family member (38,39). Following receptor dimerization (Figure 1.4), the Tyr kinase domain becomes activated leading to auto- or trans-phosphorylation of Tyr residues on the intracellular catalytic domain (39). This phosphorylation involves the transfer of the γ-phosphate of adenosine triphosphate (ATP) to Tyr hydroxyl groups on downstream target proteins, initiating signaling cascades (39). EGF-EGFR complex then migrates from the caveolae/raft component of the cell membrane to the bulk membrane component and clusters into clathrin-coated pits and subsequently internalizes in endosomes, in which EGFR will either be targeted for lysosomal degradation or recycled back to the cell surface starting a new signaling cascade (29,39).

Figure 1. 3 EGFR dimerization.

This figure explains how EGF ligand induces EGFR dimerization. (i) Unligated EGFR form a tethered conformation, in which DII is buried into DIV. (ii) EGF binds to DI and DIII of EGFR simultaneously and induces spatial rearrangement of DII and DIV forming extended conformation. (iii) Consequently, the dimerization arm of DII becomes expose to interact with another receptor. Figure adapted and modified from Chetan Yewale *et al*. 2013 (36) © with permission from Elsevier.

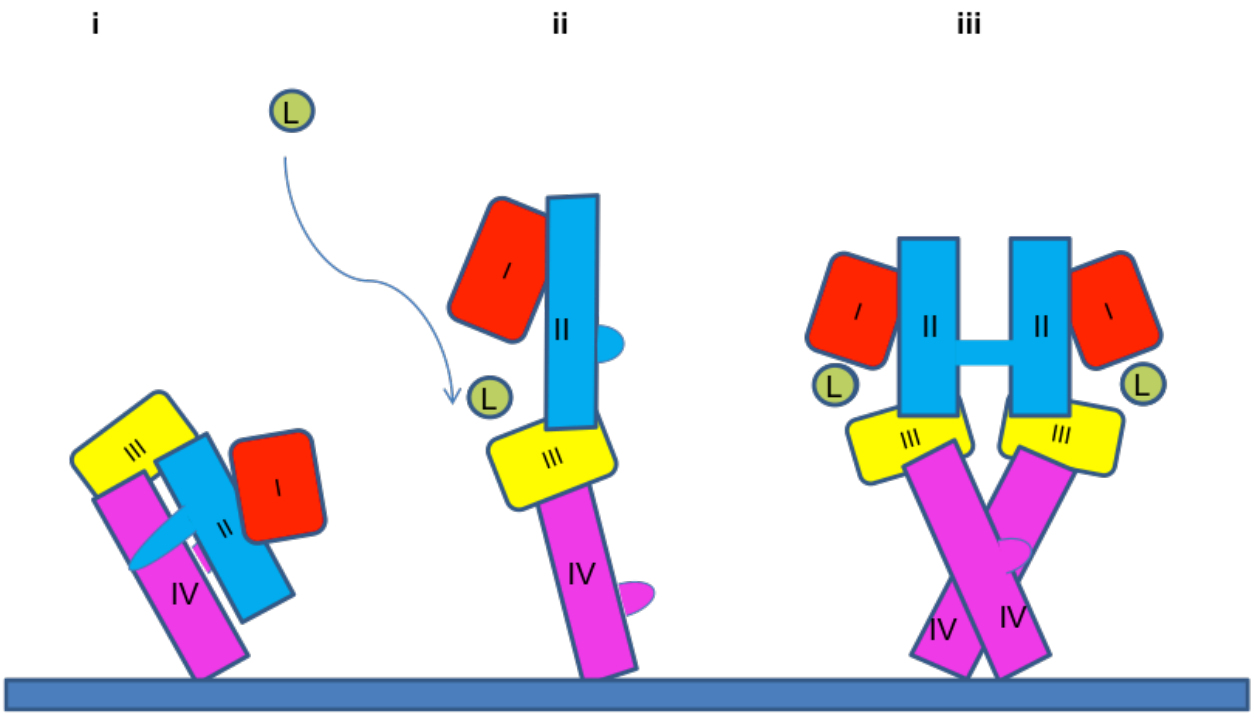
i
ii
iii
L
I
II
III
IV

1.2.3 Signal Transduction via EGFR

Upon EGFR dimerization and phosphorylation of Tyr residues, the kinase domains at the carboxy tail provide specific docking sites for recruiting downstream cytoplasmic signaling proteins containing Src homology-2 (SH2) domain, leading to the activation of intracellular signaling pathways (36). These include the Rat Sarcoma/ Rapidly Accelerated Fibrosarcoma/Mitogen-activated protein kinase kinase/Extracellular signal regulated kinase (Ras/Raf/MEK/ERK), Phosphoinositide 3-kinases/Protein kinase B (PI3K/AKT), Janus kinase/Signal transducer and activator of transcription (JAK/STAT), and Phospholipase Cγ/Protein kinase C (PLCγ/PKC) (28,44). Importantly, the Ras/Raf/MEK/ERK and PI3K/AKT mediate signals implicated in cellular proliferation, survival, apoptosis, angiogenesis, migration, as well as cell motility (Figure 1.4) (44).

The Ras/Raf/MEK/ERK pathway, also referred to as MAPKinase pathway, plays an essential role in regulating cell proliferation and survival (45–47). It can be activated by a variety of growth or stress factors (46). An important adaptor protein that mediates the induction of this signalling pathway is the adaptor protein growth factor receptor-bound protein 2 (Grb2), which is constitutively bound to guanyl nucleotide exchange factor-Son of sevenless (GEF-Sos) (45–47). Upon EGFR activation, Grb2 docks to the phosphorylated Tyr-1068 and Tyr-1086 EGFR amino acid residues (45–47) and together with Sos are recruited to the plasma membrane and brought into close proximity with the guanine nucleotide-binding protein Ras (45–47). Sos accelerates the exchange of the inactive guanosine diphosphate (GDP) for the active guanosine triphosphate (GTP) and transforms Ras-GDP into its active conformation Ras-GTP (45–47). The activated Ras recruits the serine/threonine kinase Raf to the plasma membrane where it can be phosphorylated and activated (45–47). As a result, MEK and ERK (also referred to as MAPK) are subsequently

phosphorylated and activated (45–47). Active ERK translocates to the nucleus and regulates the expression of many downstream genes involved in cell proliferation (Myc, Ets, and CREB) and apoptotic regulatory molecules (Bad, Bcl-2, and caspase 9) (45–47).

The PI3K/AKT pathway is involved in cellular proliferation, survival, and migration (45,48). PI3K is a dimeric enzyme that contains both kinase (p110) and adaptor (p85) subunits (45,48). Following EGFR activation, p85 binds to the phosphorylated Tyr residues via its SH2 domain (45,48), then, recruits p110 to the plasma membrane leading to the activation and phosphorylation of the serine/threonine kinase AKT (45,48). Activation of AKT prevents apoptosis by phosphorylating and inactivating the pro-apoptotic protein BAD and caspase-9 (45,48). Up regulation of the PI3K or deletion of phosphatase and tensin homolog (PTEN), a negative regulator of the PI3K/AKT signaling pathway, can lead to cellular transformation in many cancers including HNSCC (49).

Figure 1. 4 EGFR signaling pathway.

This figure demonstrates the two major pathways activated by EGFR activation. Two EGF ligands bind to 2 EGFR in 2:2 stoichiometry, which leads to receptor dimerization and phosphorylation of Tyr residues at the C-terminus of the EGFR. Phosphorylation of Tyr resides leads to the activation of MAPK (ERK) and AKT pathways. These pathways drive crucial cellular functions, such as proliferation and survival. Consequently, EGF-EGFR complex internalizes and either undergoes lysosomal degradation or EGFR recycles back to the cell membrane to start a new cycle. Red stars indicate phosphorylation. Figure adapted and modified from Javier Martinez-Useros and Jesus Garcia-Foncillas, 2015 (7).

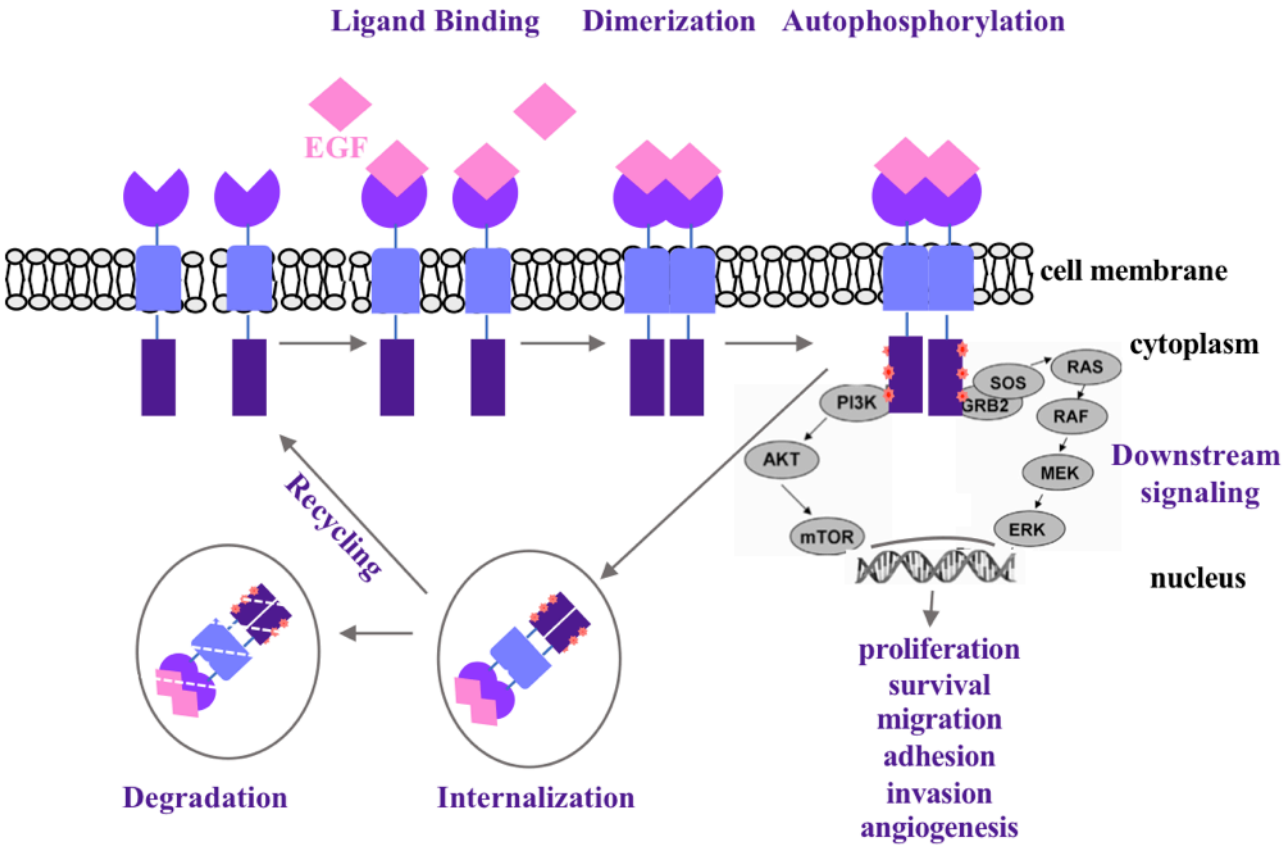
Ligand Binding
Dimerization
Autophosphorylation
EGF
cell membrane
cytoplasm
SOS
RAS
PI3K
GRB2
RAF
AKT
MEK
Downstream signaling
mTOR
ERK
nucleus
Recycling
proliferation
survival
migration
adhesion
invasion
angiogenesis
Degradation
Internalization

1.2.4 Role of EGFR in HNSCC

The complexity and the importance of EGFR signaling pathway in cell growth and survival highlights its potential role in cancer development as it can provide constant signals for cell proliferation, survival, angiogenesis, and metastasis, which are the essential hallmarks of cancers (50). While EGFR signaling is tightly controlled in healthy cells, EGFR dysregulation has been observed in HNSCC, non-small-cell lung cancer (NSCLC), glioblastoma, pancreatic, renal, colorectal, breast, ovarian, prostate, and bladder carcinomas (33). About $1x10^4$ – $1x10^5$ EGFR is expressed per normal cell, but tumor cells can express more than $2x10^6$ receptors per cell (36). This dysregulation can result from different mechanisms such as receptor overexpression, overproduction of growth factor ligands, ligand-independent receptor activation, cross-talk with other receptors, activating mutations, alterations in the dimerization process, limited endocytosis of activated receptor, and deficiency of specific phosphatases deactivating the phosphorylated EGFR tyrosine residues (7,9,28).

High EGFR expression has been associated in HNSCC with advanced tumor stage, resistance to standard therapies (chemo- and radiotherapy), and with poor patient prognosis (18,25,51). A correlation between high EGFR expression and a reduction in overall survival rates has been demonstrated in HNSCC patients (25,26). Increased EGFR expression has been linked to poor OS, short disease-free survival, and higher locoregional relapse rates (25,52). In addition to EGFR overexpression, higher ErbB2 and ErbB3 expression was also reported in HNSCC and had been linked to reduced treatment response and poor outcomes in laryngopharyngeal cancer (25,53). Therefore, EGFR is a suitable target for the development of more efficacious therapies in HNSCC.

1.3 EGFR Targeted Therapies

Currently, EGFR is the only molecular target in HNSCC for which there are pharmacologic therapeutic interventions approved by the FDA (54). There are 2 classes of EGFR-targeted therapies (Figure 1.5): monoclonal antibodies (mAbs) and receptor tyrosine kinase inhibitors (TKIs) (1). These 2 therapeutic approaches have shown limited but promising clinical results.

1.3.1 Monoclonal Antibodies

mAbs are intravenously (IV) administrated (28) and function by competing with EGFR-native ligand through binding of the extracellular ligand-binding domain of the EGFR, preventing both receptor dimerization and EGFR downstream signaling (25,51). EGFR mAb binding leads to increased EGFR internalization and lysosomal degradation (24), and can also enhance the function of the immune system via opsonization of cancer cells (51). The most common mAb studied in HNSCC is cetuximab (IMC-225, Erbitux; IM-Clone Systems, Bridgewater, NJ, USA) (16,55). Cetuximab is a chimeric mouse-human monoclonal IgG antibody that binds to the EGFR at its extracellular ligand-binding domain, with an affinity of approximately 5 to 10-fold higher than that of its endogenous ligands (56). It then blocks EGFR Tyr kinase phosphorylation and downregulates EGFR-mediated transduction pathways (28). Cetuximab demonstrated beneficial preclinical activities both *in vitro* and *in vivo* as a single agent and in combination with chemo- or radiotherapy in a variety of human cancer cells including HNSCC, colorectal, pancreatic, prostate, and ovarian cancer cells (16,28,57). To date, cetuximab is approved by the FDA and European Medicines Agency (EMA) for HNSCC in three specific applications: [1] in combination with radiation for LA- advanced disease, [2] as a monotherapy for R/M disease after failure of platinum chemotherapy, and [3] in combination with cisplatin plus 5-FU for the first-line therapy in R/M HNSCC (2,9,25).

1.3.2 Receptor Tyrosine Kinase Inhibitors

Tyrosine kinase represents an excellent target for the development of cancer drugs (7) where tyrosine kinase inhibitors (TKIs) are generally ATP mimetics that are low molecular weight compounds that are orally administrated (31). They inhibit the intracellular kinase domain of the EGFR by either reversibly or irreversibly binding to the ATP binding site at K745 (58) and prevent the autophosphorylation of the receptor's kinase activity and its downstream signaling (31). The most clinically advanced TKIs in HNSCC are gefitinib (ZD1839, Iressa, AstraZeneca; Wilmington, DE), erlotinib (OSI 774, Tarceva, Genetech; South San Francisco, CA), and afatinib (BIBW2992, Giotrif/Gilotrif, Boehringer Ingelheim; Germany) (9).

Both erlotinib (tarceva) and gefitinib (iressa) are first-generation low-molecular-weight quinazoline-based TKIs that act as reversible competitive inhibitors of ATP. The FDA has approved these TKIs for the treatment of NSCLC in 2003 and 2004, respectively (59,60). The antitumor activity of erlotinib as a single agent or in a combinational therapy has also been observed in patients with advanced HNSCC and NSCLC and has shown promising clinical activity (25,60,61). The MTD of erlotinib on an extended daily schedule is 150 mg/daily (60), and in 2005, a double-blinded phase III trial, BR.21, erlotinib demonstrated improved OS compared to placebo in NSCLC patients as a single agent (62). However, in HNSCC, erlotinib as a monotherapy showed limited activity in two phase II trials in patients with R/M disease (16,63,64). The most common side effects observed with erlotinib and gefitinib are an acneiform skin rash, diarrhea, mucositis, and anemia (60). Investigations of these first-generation inhibitors have yielded somewhat disappointing results in R/M HNSCC, with overall response rates of 1.4 – 10.6% (7,63,65,66). Of interest, these reversible EGFR TKIs are especially effective in NSCLC patients with activating EGFR mutations in exons 18 to 21 encoding the tyrosine kinase domain of the EGFR. According

to a recent systematic review in a total of 53 studies, the prevalence of these activating mutations in HNSCC is about 2.8%, which is not so common (67,68). However, one conflicting report in 2017 by Al-Ali group showed that 57% out of its 47 Saudi HNSCC cases harbor EGFR mutations in exons 19 to 21, and these activating EGFR mutations were correlated with advanced stage tumors, indicating the involvement of the geographical areas in the commonality of these mutations (69). The presence of these activating mutations show enhanced ATP binding that also improves the binding and sensitivity to erlotinib and gefitinib and increases the progression-free survival in this subset of 10% of NSCLC patients (60,70,71). However, some of these NSCLC patients develop resistance against these TKIs, due to the emergence of T790M mutation in EGFR that hinders TKI binding (72–74). This resistance could be avoided to some extent via treatment with the second-generation drugs like afatinib (75).

Afatinib (giotrif) is a second-generation irreversible small oral molecule ATP-competitive 4-anilinoquinazoline derivative TKI (76) that covalently binds to the kinase domains of EGFR, HER2, and HER4 (76). Importantly, afatinib is a potent inhibitor of both the wild-type and the activating mutant EGFR. The FDA approved afatinib for the first-line therapy of metastatic NSCLC patients who have EGFR exon 19 deletions or exon 21 substitution ($EGFR^{L858R}$) (76,77). It is also approved by EMA as a monotherapy for LA-HNSCC or metastatic NSCLC patients with $EGFR^{T790M}$ (73,72). In a recent study, afatinib was able to overcome cetuximab-resistance in HNSCC cells (79), and in a Phase II randomized study, afatinib demonstrated antitumor activity comparable to cetuximab in R/M HNSCC (80). Afatinib has been tested clinically in a variety of solid tumors, where the MTD is 40 mg/daily (76). Afatinib has shown encouraging Phase II and III clinical outcomes in the treatment of HNSCC (77,81). Interestingly, several studies have demonstrated that afatinib treatment significantly improved the OS compared to erlotinib (60,75–

77,82,83). Generally, HNSCC patients show limited response to EGFR-TKIs treatment, especially in the context of $EGFR^{WT}$ disease (60,76,77,84). Therefore, enhancing the efficacy of these EGFR-TKIs likely requires their incorporation in novel rational combination-based therapeutic approaches.

Figure 1. 5 Common drugs in HNSCC.

This figure shows the current FDA approved targeted therapies against HNSCC include mAb cetuximab, the first-generation EGFR-TKIs (erlotinib and gefitinib) and the second-generation afatinib. Figure adapted and modified from Javier Martinez-Useros and Jesus Garcia-Foncillas, 2015 (7).

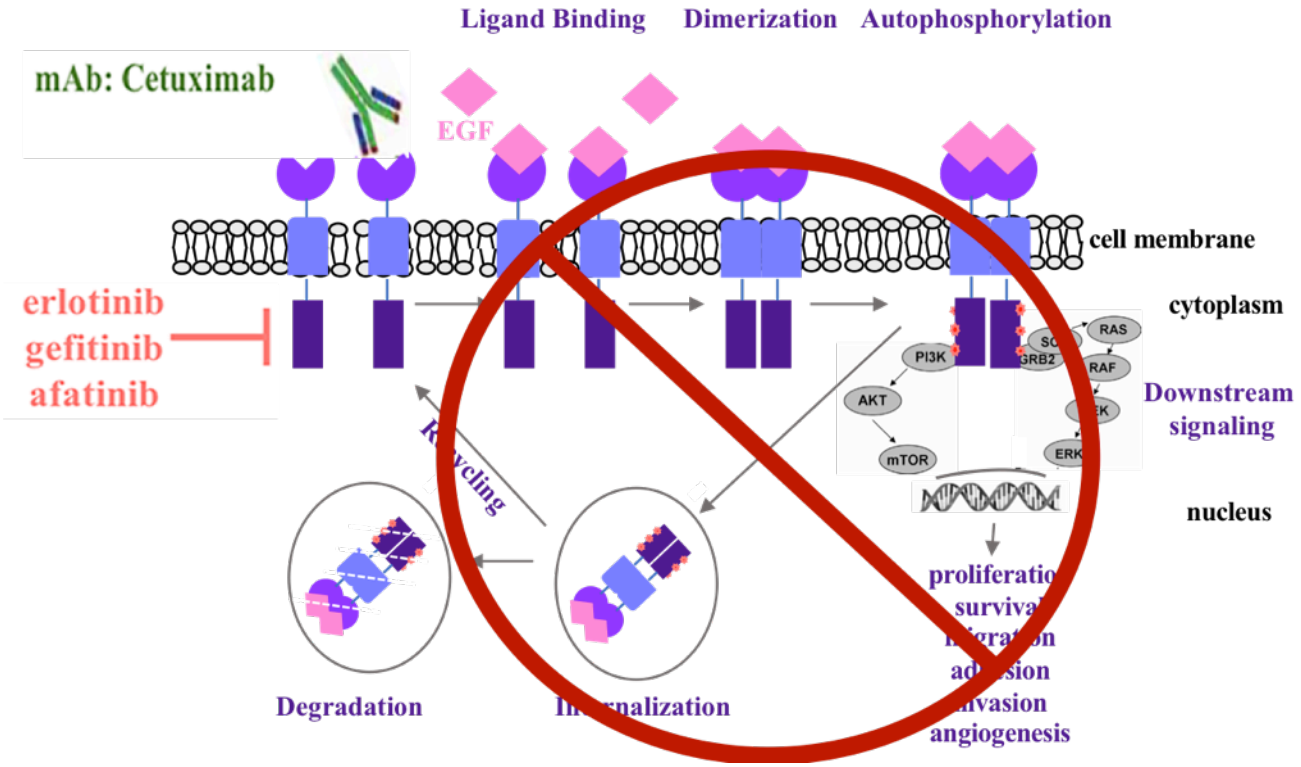
Ligand Binding
Dimerization
Autophosphorylation
mAb: Cetuximab
EGF
cell membrane
cytoplasm
erlotinib
gefitinib
afatinib
RAS
PI3K
RAF
AKT
mTOR
ERK
Downstream signaling
nucleus
Degradation
proliferation
survival
adhesion
invasion
angiogenesis

1.4 Mevalonate Pathway

1.4.1 Biochemistry of the Mevalonate pathway

Mevalonate pathway (MVP) (Figure 1.6) also known as the isoprenoid biosynthetic pathway (IBP) is ubiquitously expressed in all living organisms (85). This metabolic pathway is crucial for many cellular functions including regulation of gene expression, electron transport, reproduction, and signal transduction (85,86). This pathway converts mevalonate into sterol isoprenoids, such as cholesterol, and non-sterol isoprenoids (85).

The first step in this pathway is the synthesis of the 3-hydroxy-3-methylglutaryl-CoA (HMG)-CoA from acetyl-CoA through acetoacetyl-CoA (85,86). 3-hydroxy-3-methylglutaryl-CoA reductase (HMGR) enzyme catalyzes the conversion of HMG-CoA to mevalonate (85,86). HMGR is the rate-limiting enzyme of this pathway and one of the most highly regulated enzymes in nature (85,86). Mevalonate is converted to mevalonate diphosphate by mevalonate kinase (MVK) and phosphomevalonate kinase (PMVK) enzymes (85,86). Isopentyl diphosphate (IPP) is formed by the decarboxylation of mevalonate diphosphate by diphosphomevalonate decarboxylase enzyme (85,86). IPP is then converted to dimethylallyl diphosphate (DMAPP) by IPP isomerase enzyme in a reversible reaction (85). IPP and DMAPP are referred to as the simple isoprenoids, because they contain a single 5-carbon unit (85,87). IPP and DMAPP are condensed to form the 10-carbon geranyl diphosphate (GPP) (85,86). The addition of IPP to GPP leads to the production of the 15-carbon farnesyl diphosphate (FPP) by farnesyl diphosphate synthase (FDPS) enzyme (85,86). FPP is used in the production of ubiquinone (also called: co-enzyme Q10) (85). The addition of IPP to FPP by geranylgeranyl diphosphate synthase (GGDPS) enzyme leads to the production of the 20-carbon geranylgeranyl diphosphate (GGPP) (85,86). Alternatively, the addition of IPP to FPP by dehydrodolichyl diphosphate synthase (DHDDS) results in the GGPP

isomer (2*Z*,6*E*,10*E*- GGPP) that is utilized for dolichol synthesis (85). Squalene synthase (SQS) condenses two FPP molecules to make squalene (85,86). Squalene is used by human and animal cells in the *de novo* production of cholesterol biosynthesis through 19 additional reactions (85,86).

The end products of MVP are essential for cellular homeostasis (86,87). Cholesterol serves as a precursor for the synthesis of steroid hormones, lipoproteins, vitamin D, and bile acid and it is an essential component of the cell membrane in maintaining cell membrane structure, integrity, and fluidity (86,87). Dolichol is a carrier molecule of oligosaccharides in N-linked protein glycosylation used for the production of glycoproteins (86,87). Ubiquinone is an inner component of the mitochondria that involved in mitochondrial respiration and electron transport chain to form ATP (86,87). IPP is an essential substrate for the modification of certain tRNAs that promotes translation fidelity in ribosomes (86,87). The intermediate isoprenoid FPP and GGPP are used in the post-translational modifications of prenylated small-GTPases proteins for their activation and their cellular localization to the plasma membrane in order to activate downstream signaling pathways (86–88).

Figure 1. 6 Mevalonate pathway.

This figure shows a schematic diagram of the mevalonate pathway. HMGR is the rate-limiting enzyme in this pathway, and statins are the inhibitor for HMGR. Statins deplete cholesterol synthesis and downregulate all downstream isoprenoids such as FPP and GGPP. Bisphosphonate is another drug that targets and inhibits the activity of FPP synthase, therefore inhibits both FPP and GGPP. Figure adapted and modified from T.Zhao, 2011 (283).

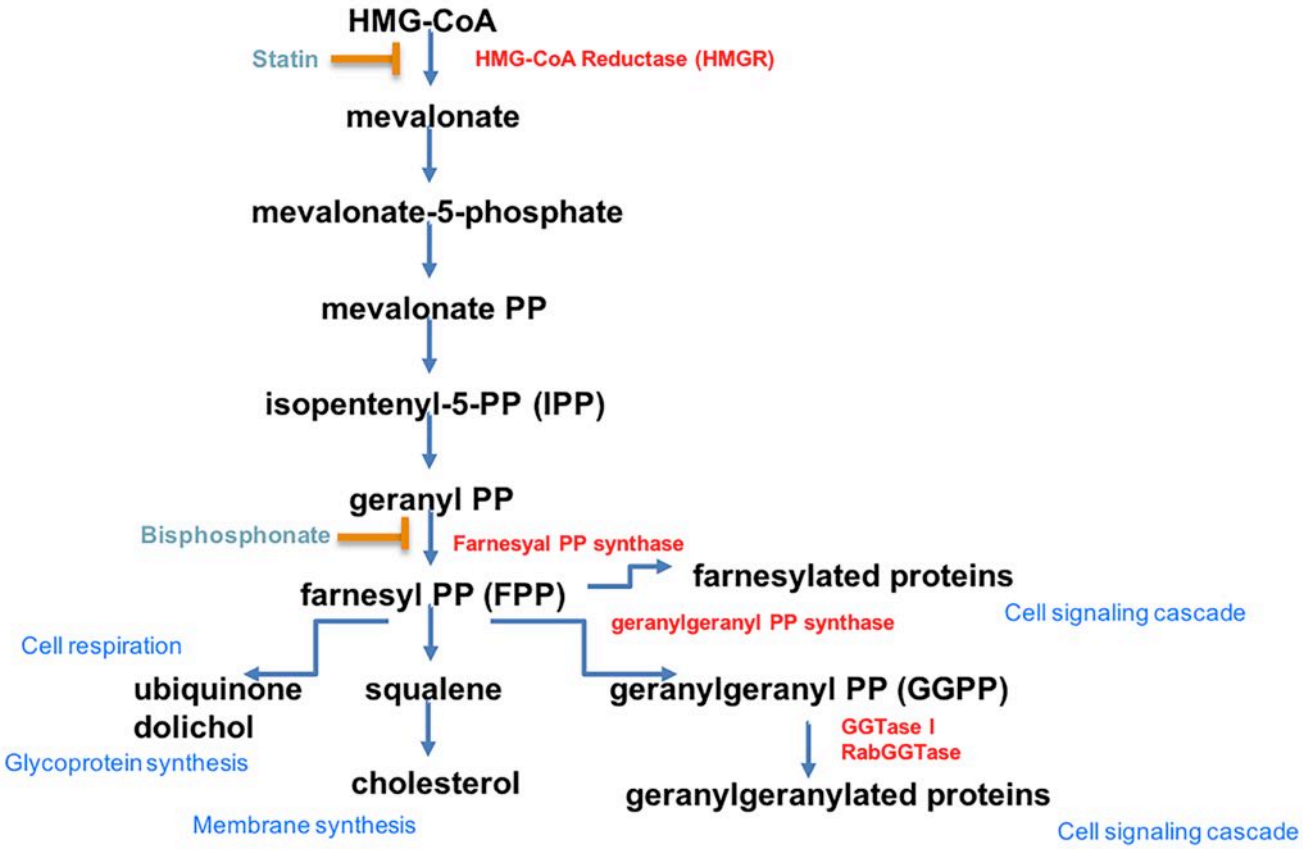
HMG-CoA
Statin
HMG-CoA Reductase (HMGR)
mevalonate
mevalonate-5-phosphate
mevalonate PP
isopentenyl-5-PP (IPP)
geranyl PP
Bisphosphonate
Farnesyal PP synthase
farnesylated proteins
Cell signaling cascade
farnesyl PP (FPP)
geranylgeranyl PP synthase
Cell respiration
ubiquinone
dolichol
Glycoprotein synthesis
squalene
geranylgeranyl PP (GGPP)
GGTase I
RabGGTase
cholesterol
geranylgeranylated proteins
Membrane synthesis
Cell signaling cascade

1.4.2 The Statin family

Several studies have demonstrated that generally cancer cells have elevated activity of MVP suggesting that malignant cells are highly dependent on MVP metabolites compared to their normal cell counterparts (86,89,90). Statins are competitive inhibitors targeting HMGR (91), where they bind to the active site of HMGR with up to a 1000x times higher affinity than its natural substrate (91). They are lipid-lowering drugs that are widely prescribed to reduce cholesterol levels and reduce the morbidity and mortality of cardiovascular diseases (86,92). The statin family drugs are divided mainly into two groups depending on their origin and biochemical characteristics: type-1 involves statins derived from fungal fermentation such as mevastatin (Compactin), lovastatin (Mevacor), pravastatin (Lipostat), and simvastatin (Zocor). Type-2 includes chemically synthetic statins such as fluvastatin (Lescol), rosuvastatin (Crestor), atrovastatin (Lipitor), cervistatin (Baycol), and pitavastatin (Livalo) (86). In 1971, Akira Endo identified Mevastatin as the first cholesterol-lowering drug (91). Both types of statins share a common side chain that exists either in a closed ring (inactive, lactone prodrug) form or an open ring (active, acid) form, where the open active form blocks the catalytic domain on HMGR by mimicking the intermediate reaction formed within the active site of the reductase enzyme (93). All statins are administrated orally as active hydroxyl acids, except lovastatin and simvastatin, which are administrated as lactone prodrugs and then hydrolyzed to hydroxy acid form (92,94).

Multiple studies have shown the anticancer effects of statins as a monotherapy or in combination with several anticancer agents (86,92,95) in a variety of cancers both *in vitro* and *in vivo* including cancer models of HNSCC (96,97) and NSCLC (98). The antitumor effect of statins result from the decreased levels of mevalonate and its downstream products, which affects critical cell functions such as membrane integrity, cell signaling, protein synthesis and cell cycle

progression (86,95). Our laboratory has previously identified high dose statins as potent inducers of tumor specific-apoptosis particularly in various pediatric malignancies, acute myeloid leukemia and SCC cells (99–102). These observations led directly to 2 Phase I clinical trials in AML and SCC patients (99,103); these trials suggested the therapeutic potential of statins would also require their utilization in combination based therapeutic strategies.

1.4.3 Statins and EGFR-TKIs Combination

HMG-CoA reductase and EGFR-targeted therapies may be linked due to the potential of mevalonate metabolites to affect the function or expression or localization of EGFR or proteins downstream of the EGFR signaling pathway (Figure 1.7) (104,105). Cholesterol is required for the proper functioning and localization of the EGFR (106). Dolichol is involved in the glycosylation of the EGFR, which allows the receptor to change conformation and bind its ligand properly (85). FPP and GGPP are involved in farnesylation and geranylgeranylation post-translational modifications of the small-GTPases which are required for their activation (86,107). Once activated, these prenylated proteins can then regulate RTK mediated cell proliferation, cell survival, intracellular trafficking and cell motility (86). Therefore, depletion of mevalonate metabolites through inhibition of HMG-CoA reductase has the potential to inhibit both the EGFR and its downstream signaling cascades.

Figure 1. 7 The mevalonate pathway and EGFR link.

This figure demonstrates how EGFR pathway is connected to mevalonate pathway. The end products of mevalonate pathway are vital for EGFR signaling such as dolichol for EGFR glycosylation, cholesterol for membrane fluidity, FPP and GGPP are involved in the post-translational modification (PTM) and activation of Ras and Rho/Rab GTPase proteins, respectively. PTM of these GTPase proteins include (i) prenylation of the cys residue at -CAAX in the C-terminal by either Ftase or GGTase, (ii) cleavage of –AAX by RCE1 and (iii) methylation of the cys by ICMT. Activated Ras involved in ERK and AKT pathways, which are important for cells proliferation and survival. Activated Rho is crucial for actin organization and cells motility, while activated Rab involved in EGFR internalization and degradation. Yellow star indicates prenylated protein. Figure adapted and modified from Javier Martinez-Useros and Jesus Garcia-Foncillas, 2015 (7) and Mingyun Shen, 2015 (123) © with permission from Elsevier.

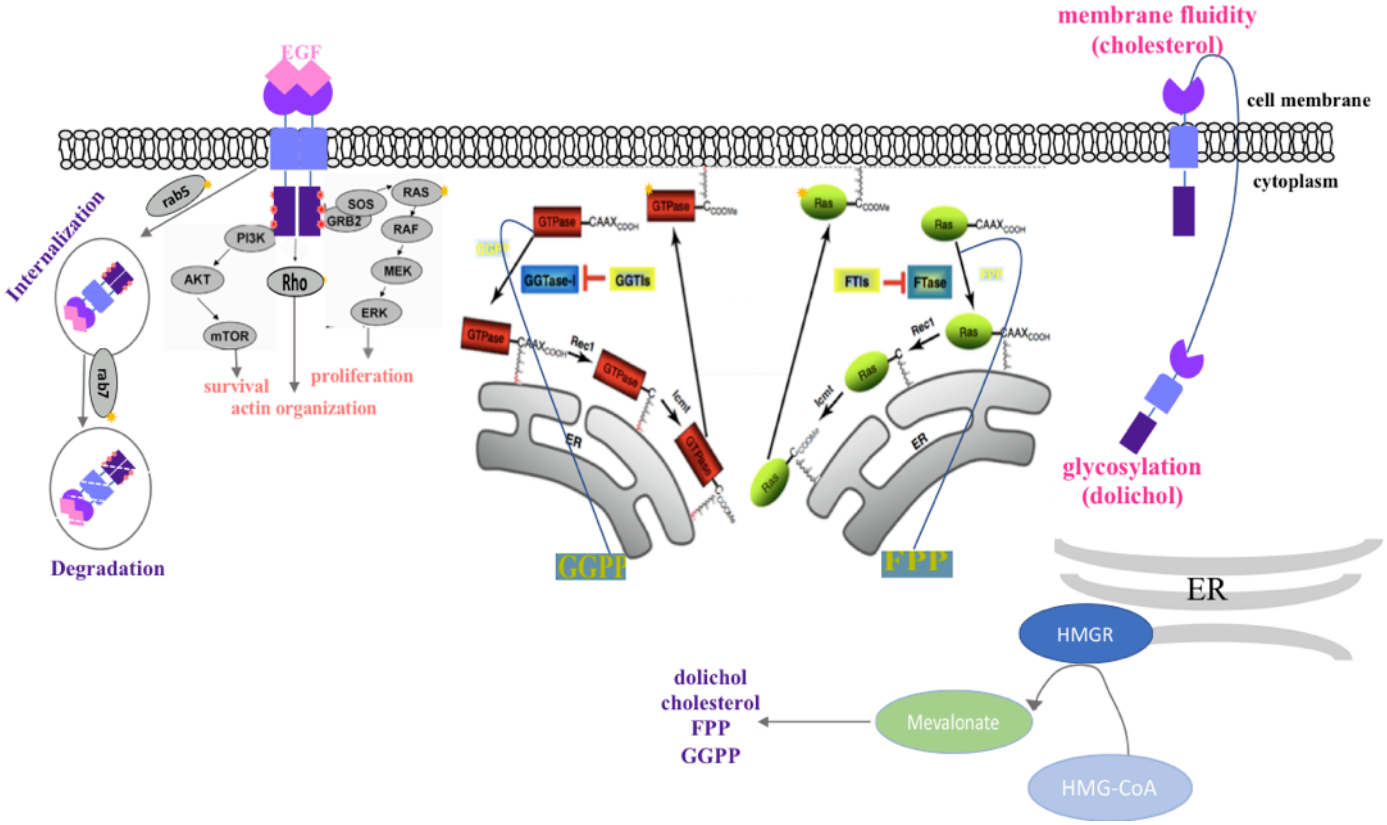
membrane fluidity
(cholesterol)
cell membrane
cytoplasm
EGF
rab5
Internalization
PI3K
AKT
mTOR
SOS
GRB2
RAS
RAF
MEK
ERK
Rho
survival
actin organization
proliferation
rab7
Degradation
GTPase
CAAX
GGTase-I
GGTIs
Rec1
Icmt
ER
GGPP
Ras
FTIs
FTase
FPP
glycosylation
(dolichol)
ER
HMGR
Mevalonate
HMG-CoA
dolichol
cholesterol
FPP
GGPP

To this end, we have demonstrated that the addition of lovastatin to gefitinib (iressa) induced synergistic cytotoxicity in a panel of HNSCC, NSCLC, cervical and colon carcinoma cell lines through the induction of a potent apoptotic response (104,105,108). Interestingly, this combination is robust and specific as demonstrated by our Prestwick Library screen of 1200 approved FDA compounds. The purpose of the original screen was to identify an agent that would increase the cytotoxicity of lovastatin in HNSCC cell lines SCC9 and SCC25 and the NSCLC A549 cell line (Table 1.1) (109). From this screen, we identified gefitinib and erlotinib as 2 of only 12 enhancers of lovastatin-induced cytotoxicity (109). The reverse screen identified 2 mevalonate pathway inhibitors as enhancers of erlotinib in these same cell lines (109). We subsequently assessed the effect of statin usage in patients enrolled in BR.21 Phase III trial, the first Phase III study to demonstrate a survival advantage in NSCLC patients with erlotinib, and showed a survival advantage in patients with statin usage in the erlotinib treated patients (105). These pre-clinical data taken together were the basis of our recently completed Phase I study at the Ottawa Hospital Research Institute evaluating rosuvastatin and erlotinib in combination (ClinicalTrials.gov Identifier: NCT00966472) (110). These agents were chosen based on their superior clinical performances (110). Patients with a wide variety of solid tumors were assessed including breast, prostate, and pancreatic cancers that are not generally considered to be sensitive to EGFR-TKI treatments (100,111). Of particular interest, there were six evaluable patients in this trial with NSCLC and SCC. Three were on study the for greater than 150 days with 2 of these patients on study for greater than 275 days (110). For these patients with advanced disease that have failed all standard therapies, this represents a significant improvement over expected outcomes for single-agent erlotinib treatment (62). However, statin-induced myopathy in approximately 30% patients

limited the utilization of this approach suggesting that a more refined therapy that mimics the efficacy but circumvents the toxicity of statins is warranted.

The incidence of statin-related myopathologies ranges between 5 – 29% of all treated patients (110) and is a dose-dependent side effect of all statins (112). Statin-treated patients frequently display decreased muscle coenzyme Q10, a mevalonate metabolite, suggesting that statin treatments may lead to mitochondrial dysfunction (113,114). Patients are also susceptible to statin-induced myopathy due to variations in genes encoding proteins involved in statin uptake and biotransformation such as cytochrome P450 (113). Evaluating downstream mevalonate pathway inhibitors and/or delineating the downstream regulators of statin-induced apoptosis may uncover such therapeutic targets.

Table 1.1 High throughput Prestwick Library Screen Hits.

This table explains the library screen of 1200 FDA approved compounds in a combination of either lovastatin or erlotinib in SCC9 and SCC25 HNSCC cell lines. The screen was done using MTT cell viability assay. Hits were determined as an agent that enhanced the cytotoxic effect of either drugs to a greater extent than the drug alone. Agents that enhances lovastatin cytotoxicity are shown in the upper panel, whereas erlotinib enhances are shown in the lower panel. Table adapted and modified from Khalil Dayekh, 2014 (109) © with permission from American Association for Cancer Research.

Enhancers of Lovastatin-Induced Cytotoxicity

EGFR Inhibitors	Cardiac Glycoside	Chemotherapy	Microtubule Polymerization	Block Protein Transport
gefitinib	lanatoside	daunorubicin	colchicine	monensin
tarceva		doxorubicin		

Enhancers of Erlotinib-Induced Cytotoxicity

Mevalonate Pathway	Anti-Metabolites	Chemotherapy	Microtubule Polymerization	Block Protein Transport
fluvastatin	methotrexate	gemcitabine	colchicine	monensin
alendronate	floxuridine	doxorubicin		

1.5 Downstream Target of Mevalonate Pathway

1.5.1 Protein Prenylation

The core products of MVP are FPP and GGPP, which are post-translational moieties incorporated into small-GTPase proteins through protein prenylation (115) (Figure 1.7). Prenylation is divided into two types: farnesylation (resulting from the addition of FPP) and geranylgeranylation (resulting from the addition of GGPP) and it plays essential roles in membrane localization and activation of these small-GTPase proteins (115). The last four amino acids (-CAAX) at the C-terminal of small-GTPase proteins determines the type of prenylation (116). FPP and GGPP are covalently attached to cysteines at the C-termini of small-GTPase proteins (115). Farnesylation is catalyzed by farnesyl transferase (FTase) enzyme, where FTase uses FPP as a prenyl group to transfer a FPP moiety to the -CAAX motif (C is cysteine, A is an aliphatic residue, and X is either serine, alanine, methionine, glutamine, or cysteine) of their target proteins (Ras and RhoB) (88,115,117). Geranylgeranylation is catalyzed by geranylgeranyl transferases I (GGTase-I) and -II (GGTase-II, also known as Rab GGTase) where GGTases-I uses GGPP as a prenyl group to transfer GGPP moiety to the -CAAX motif (X is either leucine or isoleucine) of their target proteins (RhoA, Rac1, and Rap1), while proteins with -CC or -CXC C-termini are doubly geranaylgeranaylated by GGTase-II and use GGPP as a prenyl group to transfer GGPP moiety to Rab proteins (88,115,117). Following prenylation, the three C-terminal amino acids (-AAX) are cleaved from the small-GTPase proteins by Ras-converting enzyme 1 (Rce1) enzyme (88,115,117). Then, the new C-terminus is methylated by isoprenylcysteine carboxyl methyltransferase (ICMT) enzyme (88,115,117). In the case of proteins that are geranylgeranylated by GGTase-II, GGTase-II substrates have two cysteines at their C-termini that

are both geranylgeranylated which requires Rab escort protein (REP) in order to present the unprenylated substrate to GGTase-II (88,115,117).

1.5.2 Prenylated Small-GTPases

According to a recent estimate, more than 200 proteins, 2.0% by mass, are prenylated in mammalian cells (115). The largest group of prenylated proteins is the monomeric small-GTPase proteins superfamily (117) including Ras, Rho, Rab, Arf, and Ran (118). The change between GDP-bound inactive and GTP-bound active forms, the binary switches of all small-GTPase protein function, contributes to intracellular signaling cascades that drive cellular proliferation, differentiation, survival, motility, transformation, and apoptosis (86,119). Ras GTPase proteins, which includes H-, K-, and N-Ras, are critical mediators of cell proliferation and differentiation; Ras homologous (Rho) proteins, which includes RhoA, Rac1, and Cdc42, play roles in gene expression, actin cytoskeleton reorganization, cell shape, and cell movement; Ras-like protein in brain (Rab) and Secretion Associated Ras Related GTPase1A/ADP-ribosylation factor (Sar1/Arf) proteins are mediators of vesicle transport; while Ras-related nuclear proteins (Ran) are involved in the transport of macromolecules between the nucleus and cytoplasm and in the microtubule organization during cell division (119). Dysregulation of these proteins has been associated with tumor carcinogenesis and progression in many cancers (119).

1.5.3 Inhibitors of Prenylated Proteins

Interest in blocking Ras farnesylation as anticancer drugs was driven by the realization that a significant percentage of human cancers (8 - 93% depending on the tumor type) harbor activating oncogenic mutations in the *RAS* genes (120), and that Ras GTPase proteins require farnesylation modification for their transformation (121). This led to the discoveries of prenytransferase inhibitors (PTIs) as potential anticancer drugs including farnesyltransferase inhibitors (FTIs) that

inhibit the transfer of FPP, and geranylgeranyltransferase-I inhibitors (GGTIs) which directly inhibit the transfer of GGPP (117,121,122). Several selective PTI inhibitors have been developed and tested for their antitumor effects both *in vitro* and *in vivo* (86,115,123). Several FTIs have been developed and effectively prevented proper functioning of Ras proteins (123). Clinically, tipifarnib (R115777), the first FTIs tested in clinical trials for various cancers showed significant antitumor activity with acceptable toxicity in hematological malignancies; yet the results of Phase III trials were disappointing without improvement in the OS in patients with solid tumors (123–125).

Most GGTIs are CAAX-competitive inhibitors (123). A number of GGTIs have been tested both *in vitro* and *in vivo*, including GGTI-298 and GGTI-2418 (123). GGTIs have been shown to impair tumor cell proliferation and induce cell cytotoxicity in cell cultures and animal models (123,126,127). GGTI-2418 is the only GGTI inhibitor that has entered Phase I clinical trials, and in contrast to statins, GGTI-2148 did not show any muscle pathology in treated patients (123,128,129). Given these results, further investigation of GGTIs as antitumor agents in HNSCC is warranted and may provide an approach to enhance efficacy of EGFR-TKIs without the muscle toxicities with high-dose statins observed during our Phase I combination trials.

An alternative way to impair protein prenylation is through depletion of FPP and GGPP cellular pools. FPP synthase is readily targeted by nitrogen-containing bisphosphonates (NBPs) (130). Generally, NBPs are used in the treatment of bone-related diseases including osteoporosis, Paget's syndrome, and bone metastases due to their high affinity for binding to calcium (130). NBPs function by inhibiting the formation of FDPS, thus depleting FPP pools and other downstream isoprenoids including GGPP (130). Zoledronate (ZOL), a heteroaromatic compound, is one of the most commonly studied FDPS inhibitor, and it was approved for multiple myeloma and metastatic bone cancers (130).

To understand the mechanism of statins and NBPs by which they interfere with cancer cell progression, add-back experiments, which consists of adding exogenous downstream mevalonate metabolites, have been performed in various cell lines *in vitro* (131). It was found the addition of exogenous GGPP, not FPP, prevented cellular apoptosis induced by statins and NBPs; therefore, the anticancer effects of both drugs were correlated with the depletion of GGPP and inhibition of protein geranylgeranylation (131). Likewise, when statins and ZOL potentiate the anticancer effects of some CT agents, the addition of GGPP prevented the synergy that was observed with the drug combination (132,133). These observations highlight the importance of GGPP in cancer cell function and survival (86,131).

Our collaborator Dr. David F. Wiemer at the University of Iowa has developed a compound library of GGDPS inhibitors (131). One such compound is digeranyl bisphosphonate (DGBP) (134) that specifically depletes GGPP cellular pool and subsequent protein geranylgeranylation (135). DGBP is a first-generation agent, where it was the most potent inhibitor described when these studies were initiated (136). DGBP is a synthetic experimental structural diphosphate analog chemical inhibitor (135). DGBP has a different molecular target, selectivity, and cellular effects compared with other bisphosphonates, where it specifically inhibits the activity of GGPP synthase (135). Previous work on DGBP showed that DGBP significantly reduces MDA-MB-231 breast cancer cell migration and motility (137). Also, DGBP was found to induce apoptosis in a variety of cancer types (131,135,138–140). The exogenous addition of GGPP prevented most of the effects observed with DGBP, suggesting specific inhibition of GGDPS by DGBP. Most importantly, a recent published work showed that inhibiting GGDPS by VSW1198, another GGDPS inhibitor, was associated with a transient liver but not muscle toxicity as seen in statin treatment (141). This temporary liver toxicity was likely a consequence of higher drug levels in

the liver, and was observed for one week post injection, and it was associated with slight elevation of transaminase levels only, which linked to the standard pattern seen in hepatic injury (141,142). These data indicated that GGDPS can be targeted and represents a further downstream MVP target with the potential to enhance EGFR-TKIs efficacy.

1.6 Metabolic Stress Pathways

Healthy cells can adapt to environmental changes such as the availability of nutrients and growth signals (143,144). Under metabolic stress, cellular stress pathways can be activated and attempt to alleviate the stress or if the stress cannot be overcome to induce apoptosis (144–148). The common stressors that trigger metabolic stress are glucose deprivation, amino acid starvation, growth factor withdrawal, hypoxia, and conditions that affect ATP synthesis (147–149). A number of signaling pathways regulate the cellular response to these stressors including growth factor signaling (EGFR/AKT signaling pathway) (148,149), the Liver Kinase B1 (LKB1)/AMP-Activated Protein Kinase (AMPK) pathway that is a sensor of cellular energy (ATP) levels (144,148), and the Integrated Stress Response (ISR) (147,148,150). These stress pathways share common downstream targets including the inhibition of global protein translation and the induction of cell-cycle arrest and apoptosis (144,147,148,151).

1.6.1 The LKB1/AMPK Pathway

The LKB1/AMPK pathway (Figure 1.8) serves as a metabolic checkpoint in the cell, that is activated under conditions of low ATP resulting from low nutrients and leading to arresting cell growth (144). LKB1 is serine/threonine kinase 11 (STK11) that was originally identified as a tumor suppressor gene on human chromosome 19p13, which is inactivated and responsible for Peutz-Jeghers syndrome (PJS) (144,152). It is also mutated in a variety of cancers, particularly in

30% NSCLC (144,153,154) and 20% of cervical carcinomas (144,155). LKB1 acts as a master upstream kinase, directly phosphorylating and activating AMPK (144,146). During nutrient starvation and under low energy levels, when intracellular AMP increases and intracellular ATP decreases, LKB1 complexes with its two regulatory subunits, STRAD and MO25, and directly phosphorylates and activates AMPK (144,146). LKB1 is involved in HNSCC carcinogenesis (156), and tumors with low basal levels of AMPK activity respond well to cetuximab treatments (157).

Figure 1. 8 LKB1/AMPK signaling pathway.

This figure demonstrates the activation of LKB1/AMPK pathway. Under low ATP, STRAD and MO25 bind to the LKB1 and export the complex into the cytoplasm. Then, AMP binds to LKB1 complex and activates AMPK. AMPK then phosphorylates the TSC2 (tumor suppressor tuberin) and inhibits the activation of mTOR (mammalian target of rapamycin), leading to the inhibition of translation initiation factor 4E binding protein 1 (4EBP1). Consequently, this leads to the inhibition of global protein translation. Figure adapted and modified from S.E. Korsse, M.P. Peppelenbosch, W. van Veelen, 2013 (284) © with permission from Elsevier.

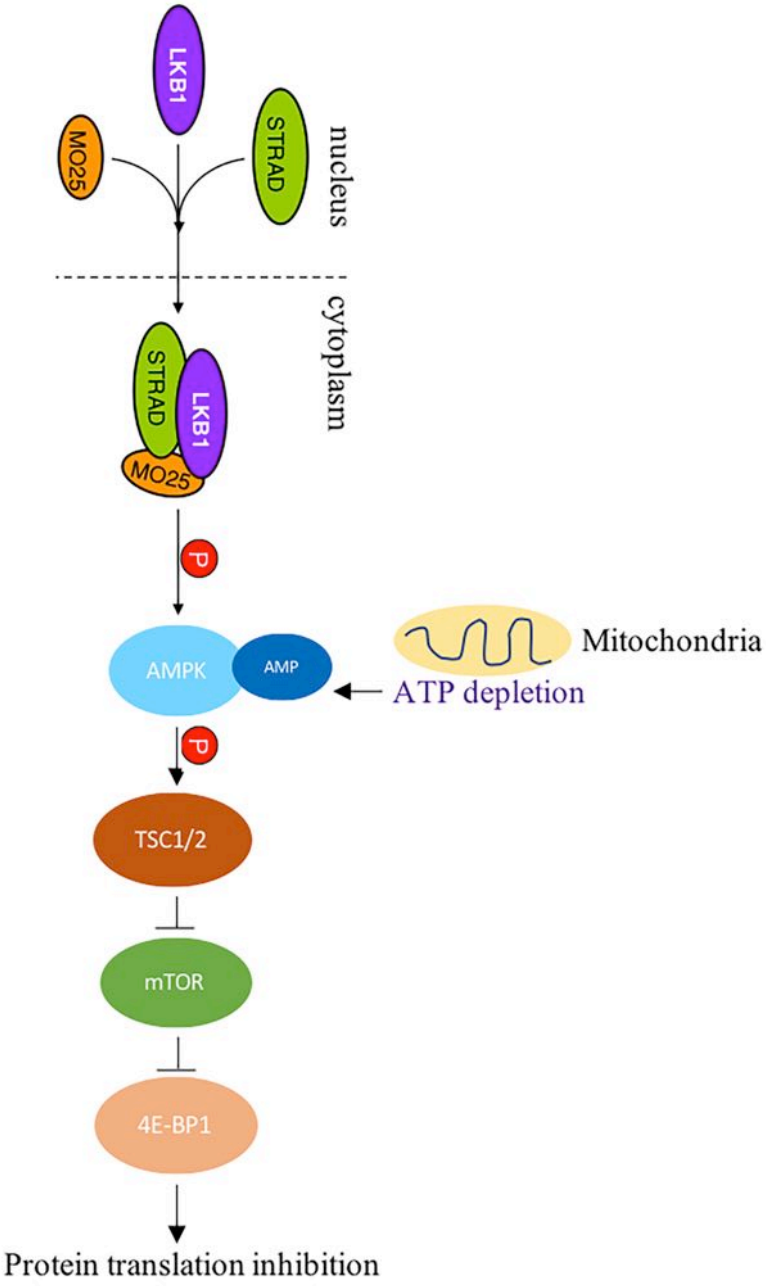
LKB1
MO25
STRAD
nucleus
cytoplasm
STRAD
LKB1
MO25
P
AMPK
AMP
Mitochondria
ATP depletion
P
TSC1/2
mTOR
4E-BP1
Protein translation inhibition

1.6.2 The Integrated Stress Response Pathway

The integrated stress response (ISR) pathway (Figure 1.9) is a conserved signaling pathway in all eukaryotic cells, which is activated by a wide range of physiological and pathological changes (147). Hypoxia, glucose starvation, amino acid deprivation, endoplasmic reticulum (ER) stress, viral infection and oncogene activation are the most common stressors activating this pathway (147,150,158–161). The core event in this pathway is the phosphorylation of the catalytic subunit of the eukaryotic translation initiation factor 2 (eIF2α) (147) that inhibits global protein translation. In mammalian cells, eIF2α phosphorylation is catalyzed by a family of four serine/threonine (S/T) kinases (162) including general control non-derepressible 2 (GCN2), PKR-like ER kinase (PERK), double-stranded RNA-dependent protein kinase (PKR), and heme-regulated eIF2α kinase (HRI) (150,162). These kinases act as early responders to different stress stimuli (147). All four eIF2a kinases share homology in their kinase catalytic domains but retain different regulatory domains depending on their response to distinct stresses (147,162). GCN2 is highly conserved from yeast to humans, and it is activated by the binding to the uncharged de-acetylated transfer RNAs (tRNAs) via histidyl-tRNA synthase related domain in response to amino acid starvation (147,158,160). PERK is activated by sensing ER stress such as the accumulation of the unfolded proteins (147). PKR is activated by double-stranded RNA (dsRNA) during viral infection (163). ER stress, growth factor depletion, cytokines, and bacterial infection have also been shown to activate PKR, but in a dsRNA-independent manner (147,164). HRI is mainly expressed in erythrocytes, and it detects heme reduction during erythrocyte differentiation (165).

Each of these kinases phosphorylates eIF2α (150). eIF2α phosphorylation prevents the assembly of the preinitiation complex (PIC) and leads to a reduction in global protein synthesis, whereas the phosphorylation of eIF2α enhances the translation of specifically selected genes

including activating transcription factor 4 (ATF4), allowing cell survival and recovery (147,150,166). However, if the intensity of the stressor or its duration were severe, ATF4 would adapt and bind additional components aiding apoptosis (147,150,166). Conversely, dephosphorylation of eIF2α leads to signal termination of the ISR, and it returns protein synthesis back to normal (147,167).

ATF4 is a basic leucine zipper (bZIP) transcription factor that belongs to the activating transcription factor/cyclic AMP response element binding protein (ATF/CREB) family (168). It is an unstable protein with a short half-life (approximately less than 1 hour) under normal conditions (168,169). ATF4 is the key protein in cellular fate in response to ISR activation (169). One of the best-studied mechanisms of ISR-mediated apoptosis is through ATF4-mediated activation of C/EBP homologous protein (CHOP, and also known growth arrest DNA damage-inducible gene 153 (GADD153)) (147). CHOP belongs to CCAAT/enhancer-binding protein transcription factor that is up regulated in response to cellular stress and promotes apoptosis through the up regulation of BH3-only pro-apoptotic BCL-2 family PUMA (direct p53-mediated apoptosis), or up regulation of the death receptor (DR5) (147,150,170,171). CHOP regulates the expression of PUMA in response to ER stress (170). In two different studies, PUMA suppressed tumor growth of HNSCC cells and sensitized these cells to cisplatin as well as erlotinib through the induction of apoptosis (172–174). Biochemically, PUMA induces both p53-dependent and -independent apoptosis in various human cancers through mitochondrial dysregulation and caspase activation (172,173).

Figure 1. 9 Integrated stress response pathway.

This figure explains the activation of ISR and ATF3 pathway. During environmental stresses, PKR, HRI, PERK, and GCN2 kinases are activated, which lead to the phosphorylation of eIF2α. Consequently, eIF2α phosphorylation leads to global translational attenuation and the translation/activation of non-Cap-dependent mRNA (ATF4) to relieve the stress. If the levels of the stress are too high, ATF4 leads to the activation of ATF3 and CHOP leading to apoptosis. ATF3 is also activated by other mechanisms including MAPKinases and DNA damage response.

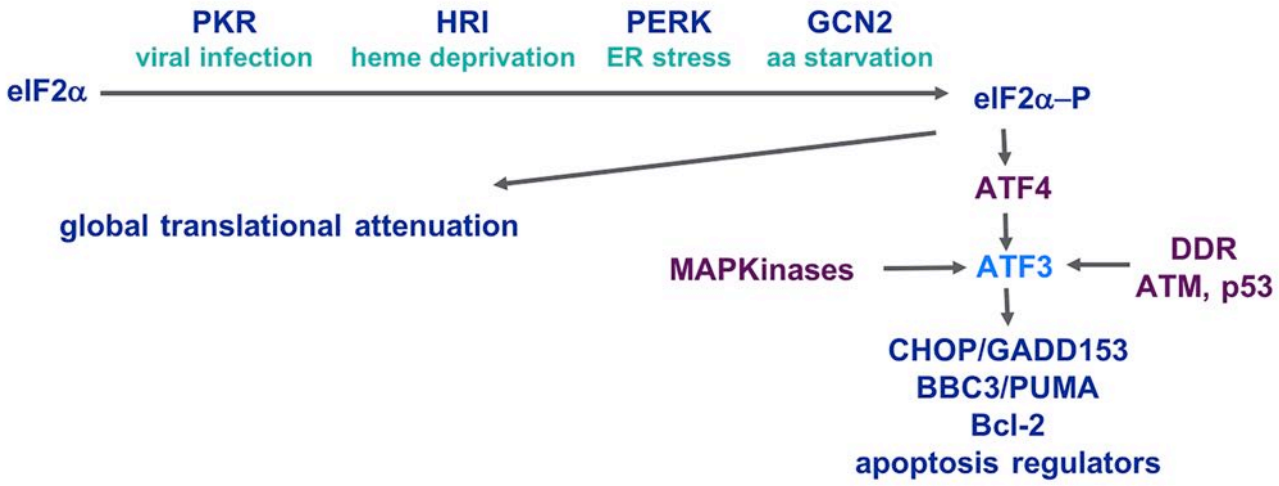
PKR
viral infection
HRI
heme deprivation
PERK
ER stress
GCN2
aa starvation
eIF2α
eIF2α–P
global translational attenuation
ATF4
MAPKinases
ATF3
DDR
ATM, p53
CHOP/GADD153
BBC3/PUMA
Bcl-2
apoptosis regulators

1.6.3 Activating Transcription Factor 3

Activating transcription factor 3 (ATF3) is another member of ATF/CREB family of bZIP transcription factors (175) Its leucine zipper motif is responsible for the homo- or hetero-dimerization with other ATF/CREB family members. The *ATF3* gene is located on chromosome 1q, and its 181 amino acids form a 21 kDa protein (175). Its mRNA level is low or undetectable in most cells, but is significantly increased upon the exposure of cells to stress signals (176). *In vitro* studies have shown that ATF3 has dual functions in cancer by promoting either cell death or survival under defined physiological or pathological conditions (177). In response to DNA damage agents, UV, or anticancer drugs, ATF3 has been shown to induce cell apoptosis and inhibit tumorigenesis in NSCLC, breast, ovarian, and colon carcinomas (177,178).

ATF3 is commonly induced by three cellular pathways (Figure 1.9): the DNA damage response (p53), the MAPKkinase pathway (p38, JNK, and ERK), and the ISR (179,180). Chemo- or radiotherapeutic agents induce DNA damage and trigger the activation of p53 then ATF3, which are involved in cell cycle arrest, DNA repair and apoptosis (179). Cisplatin was shown to activate ATF3 through the MAPKinase pathway, and ATF3 was essential for cisplatin-induced cytotoxicity (179–181). Under ER stress or amino acid starvation, the kinases PERK or GCN2 phosphorylate eIF2a and activate the ISR pathway leading to ATF4 induction, followed by the up regulation of ATF3 and CHOP leading to apoptosis (147,182). ATF4 is a known upstream regulator of ATF3 (147), where ATF4 deletion blocks the expression of both ATF3 and CHOP in response to ER stress and amino acid starvation, while the depletion of ATF3 had no impact of CHOP expression during these stressors (182). Recently, it has been shown that ATF3 activation is required for the activation of PUMA and DR5 (175).

1.6.4 Statins and the Metabolic Stress Pathways

Previous work in our laboratory have shown that lovastatin treatment in HNSCC cells *in vitro* induced apoptosis through the induction of metabolic stress (Figure 1.10). First, we showed the involvement of lovastatin in the growth factor withdrawal which is manifested through the inhibition of ligand-induced EGFR (105); where lovastatin inhibited ligand-induced EGFR dimerization, internalization, trafficking, and autophosphorylation, as well as inhibited EGF-induced AKT phosphorylation in HNSCC cells (104,105). The effect of lovastatin on EGFR dimerization was regulated by lovastatin's ability to target the cytoskeleton through targeting the Rho proteins (105), which confirms the link between the mevalonate pathway and EGFR signaling.

Second, we demonstrated the involvement of lovastatin in the induction of LKB1/AMPK pathway that senses ATP depletion (148); lovastatin treatment in HNSCC cells impaired mitochondrial function, decreased ADP/ATP ratios, and induced the expressions of LKB1 and AMPK. Additionally, the cytotoxic effects of lovastatin were attenuated in LKB1 null MEFs indicating a role for this pathway in regulating lovastatin-induced cytotoxicity. Interestingly, combining metformin, a drug that is used to treat type-2 diabetes and a potent inducer of LKB1, to gefitinib enhanced cytotoxicity of gefitinib only in LKB1 expressing HNSCC cell lines (148).

Third, found that lovastatin treatment induced GCN2 activation of the ISR pathway (166). Lovastatin treatment induced eIF2α phosphorylation and inhibited global protein translation (166). Lovastatin induced the expression of ATF4, ATF3 and CHOP in HNSCC cells (166,183). This was the first study to demonstrate that lovastatin is a potent inducer of the ISR (166). Taken together, lovastatin included cellular apoptosis via metabolic stress induction, representing potential viable therapeutic targets.

Figure 1. 10 Statins and metabolic stress pathways.

This figure demonstrates the effect of lovastatin in the metabolic stress pathways: EGFR withdrawal, LKB1/AMPK activation, and the integrated stress response. Lovastatin can modulate the activity of these three metabolic stress pathways by dysregulating the expression and activity of key regulators of these pathways. The green arrow indicates activation while red arrow indicates inhibition of the proteins. Figure adapted and modified from TT Zhao, 2010 (105) with permission from © Springer Nature; Laurie Ma, 2012 (148); and Nima Niknejad, 2007 (166) with permission from © American Society for Biochemistry and Molecular Biology.

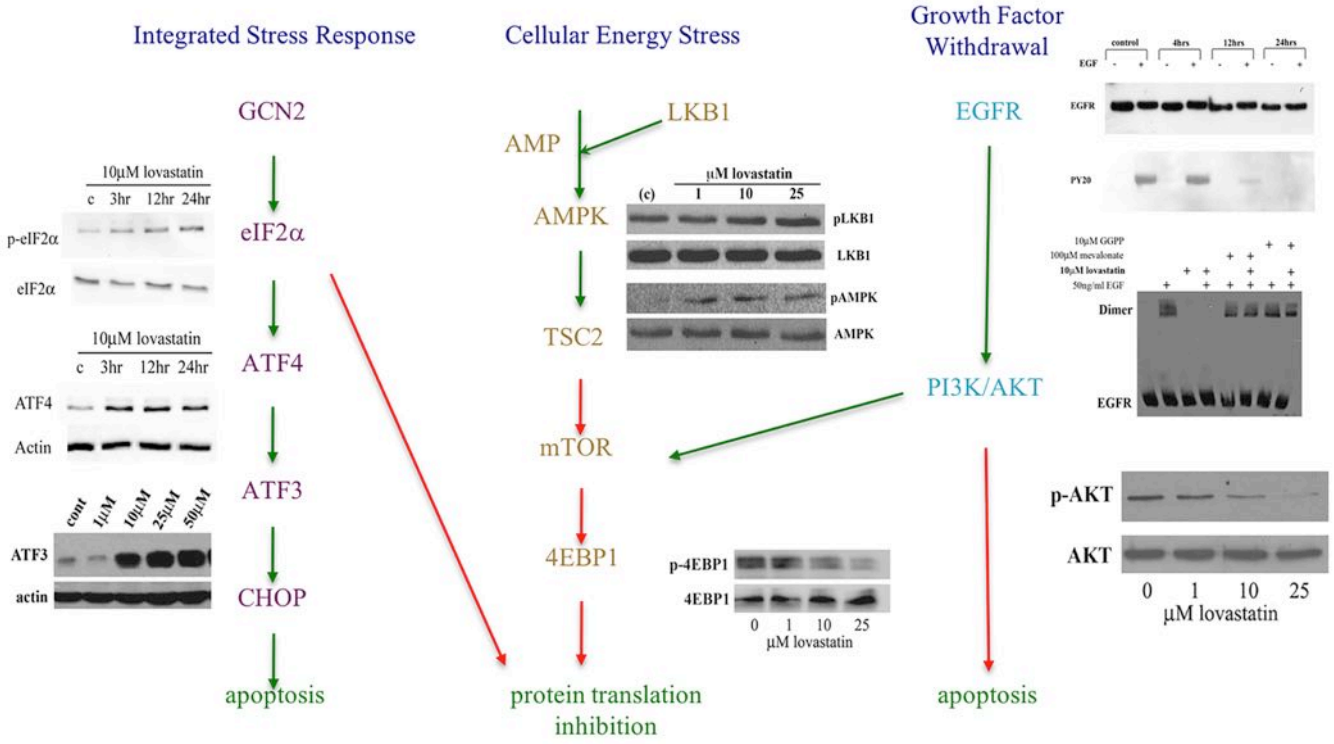
Integrated Stress Response
GCN2
10μM lovastatin
c 3hr 12hr 24hr
p-eIF2α
eIF2α
eIF2α
10μM lovastatin
c 3hr 12hr 24hr
ATF4
Actin
ATF4
cont 1μM 10μM 25μM 50μM
ATF3
actin
ATF3
CHOP
apoptosis
Cellular Energy Stress
LKB1
AMP
AMPK
μM lovastatin
(c) 1 10 25
pLKB1
LKB1
pAMPK
AMPK
TSC2
mTOR
4EBP1
p-4EBP1
4EBP1
0 1 10 25
μM lovastatin
protein translation
inhibition
Growth Factor
Withdrawal
EGFR
control 4hrs 12hrs 24hrs
EGF
EGFR
PY20
10μM GGPP
100μM mevalonate
10μM lovastatin
50ng/ml EGF
Dimer
EGFR
PI3K/AKT
p-AKT
AKT
0 1 10 25
μM lovastatin
apoptosis

1.7 Rationale

Treatment of advanced HNSCC has mainly consisted of a combination of surgery and radiation, or combined radiation with chemotherapy (25). Unfortunately, these standard therapies are associated with significant patient toxicities without improving the OS of these patients (25,184). EGFR-TKIs have been evaluated as potential therapies in a number of cancers, including HNSCC, where EGFR is overexpressed and plays a vital role in HNSCC pathogenesis (25). Unfortunately, as a monotherapy, EGFR-TKIs have yielded limited results (16). Since the end products of mevalonate pathway are crucial for EGFR activation (104), previous studies from our laboratory have demonstrated that the combination of the mevalonate pathway inhibitor, lovastatin, with EGFR-TKIs induced robust synergistic cytotoxicity (104). However, the use of high-dose statins in combination with erlotinib in our recent Phase I clinical trial although demonstrating clinical activity was limited due to significant statin-induced muscle pathologies (110). Downstream mevalonate pathway targets that can recapitulate the efficacy of statins without inducing muscle pathologies may represent a more refined therapeutic approach. Our recent data demonstrated that the downstream mevalonate metabolite GGPP could rescue statin induced cytotoxicity and their synergy in combination with EGFR-TKIs. Importantly, depletion of the mevalonate metabolite ubiquinone likely triggers statin-induced muscle pathologies. Therefore, targeting GGPP synthesis or its incorporation may recapitulate the efficacy of statin without affecting ubiquinone levels whose depletion drives their muscle pathologies.

1.8 Hypothesis

Inhibiting GGPP synthase and/or GGPP protein modifications affects tumor cell proliferation and survival, and in combination will enhance the inhibitory effect of EGFR-TKI.

1.9 Overall objective of this study

To identify agents that recapitulate the efficacy of statin-induced apoptosis and enhance the activity of EGFR-TKIs but circumvent their associated toxicities.

1.10 Specific Aims

1) Evaluate downstream mevalonate pathway enzyme geranylgeranyl transferase-I (GGTase-I) as a therapeutic target in combination with EGFR-TKIs.

2) Evaluate downstream mevalonate pathway enzyme geranylgeranyl diphosphate (GGPP synthase) as a therapeutic target in combination with EGFR-TKIs.

CHAPTER 2: MATERIALS AND METHODS

2.1 Tissue Culture

The SCC (SCC9, SCC25, CAL27 and HeLa), NSCLC (Calu6, H23, A549, HCC4006, HCC827, and HCC1975) and the human normal fibroblast (WI-38) cell lines were purchased from American Type Culture Collection ATCC (Rockville, MD). SCC9 and SCC25 are HPV- HNSCC and obtained from the tongue of 25- and 70- year-old males, respectively. SCC9 and SCC25 are good HNSCC cell models because they overexpress wild-type EGFR. Both SCC9 and SCC25 were the foci of this study and were authenticated employing short tandem repeat genetic profiling (Centre for Applied Genomics, Toronto, ON). According to ATCC, Cal27 were initially identified as SCC, however, Zeng's group have identified Cal27 as an oral adenosquamous carcinoma cell line (185). These lines (SCC9, SCC25, and Cal27) are wild-type EGFR and have *CDKN2A*, *Kras* and *TP53* mutations in their genomes (186). HeLa, a cervical SCC, is HPV+ and it is the most widely used model cell line for studying cancer biology. It is a good model of squamous cell carcinoma, which although derived from different tissue type (i.e. cervical), it is a similar tumor type to those of which I mainly studied; and herein, because it is easily transfectable, it was used as a transfection model for shGGDP synthase using pLKO-Tet-On (Invitrogen). In addition, numerous attempts to transfect HNSCC cell lines failed, and thus we were forced to used alternative relevant model system as a result. The adenocarcinoma NSCLC cells (Calu6, H23, A549) are wild-type *EGFR* and *Kras* mutant. The lung adenocarcinoma cell lines (HCC4006, HCC827, and HCC1975) are wild-type *Kras* and mutant to *EGFR*; where HCC4006 harbour the EGFR ΔL747-E749 mutation, HCC827 are mutated in EGFR at ΔE746-E750, and HCC1975 contain two-point mutations in EGFR L858R and T790M. These mutant EGFR NSCLC cell lines were a generous gift from Dr. Ming Tsao (Princess Margaret Cancer Centre, Toronto, ON) and C.

Addison (Ottawa Hospital Research Institute, Ottawa, ON). SCC9, SCC25, and Cal27 cells are sensitive to lovastatin-induced apoptosis, HeLa is moderately sensitive, while NSCLC cells are relatively resistant to lovastatin. WI-38, a normal human lung fibroblast, is a control cell line was used to compare the basal expression levels of GGPP and HMGCR in the tumor and normal lines.

The murine embryonic fibroblasts (MEFs) ATF3-/- are deficient in ATF3 expression through gene knockout and their wild-type counterparts ATF3+/+ were kindly provided by Dr. T. Hai, (Ohio State University, Columbus, OH), which were previously described in (187). The primary MEFs were isolated from day-13.5 wild type C57BL/6 or ATF3 knockout embryos and immortalized following the 3T9 protocol (187). CHOP-/- MEFs (188), and GCN2-/- MEFs (158,189) were kindly provided by Dr. D. Ron (Skirball Institute, New York), while ATF4-/- MEFs (158,190) were kindly provided by Dr. D. Park (University of Ottawa, Ottawa, Ontario, Canada). All these MEFs shared the same genetic background, where they were all derived from the C57BL/6J mice strain, and the genomic region encoding the ATF3, ATF4, GCN2, and CHOP was replaced in embryonic stem cells using a neomycin resistance replacement cassette, yielding a null allele. In addition, it was not mentioned if the cassette has any effect on the expression of neighbouring gene loci (158,187,188,190). These MEF cells were used to determine the effect of the absence of ATF3 expression on lovastatin, GGTI-298, DGBP, and afatinib cytotoxicity. The SCC9 GGTI-298 resistant clones designated (GGTI-R1 to R4) were derived from continuous treatment of the parental SCC9 cell line with 10μM GGTI-298 for 28 days and surviving single cells were isolated and propagated in control media. All cells except the EGFR-mutant NSCLC cells were grown and maintained in Dulbecco's modified Eagle's medium (DMEM) (Media Services, Ottawa Regional Cancer Centre); ATF4-/- and GCN2-/- needed special media requirements and were maintained in DMEM with 10% non-essential amino acids (NEAA)

solution (Thermo Fisher scientific, Waltham, Massachusetts, USA). EGFR mutant NSCLC (HCC4006, HCC827, and HCC1975) cells were grown and maintained in Roswell Park Memorial Institute medium (RPMI) (Thermo Fisher Scientific, Waltham, Massachusetts, USA). Both medias were supplemented with 1% (v/v) penicillin/streptomycin (Sigma Aldrich, St Louis, MO, USA) and 10% (v/v) fetal calf serum (Hyclone). Incubation settings were maintained at 37ºC and 5% CO_2 in a HERA cell incubator (Kendro Laboratory Products, Newton, CT).

2.2 Drug Compounds

Erlotinib hydrochloride (tarceva) was purchased from BioVision (Mountain View, CA). Afatinib was purchased from Selleck Chem (Houston, TX). Both tarceva and afatinib were suspended and diluted to 10mM stock in dimethyl sulfoxide (DMSO). Lovastatin was obtained from Apotex (Toronto, ON) and suspended in ethanol to 10mM. GGTI-298 was purchased from Sigma-Aldrich (St Louis, MO, USA) and suspended in DMSO to 10mM solution. DGBP was kindly provided by Dr. D. Wiemer and Dr. R. Hohl (University of Iowa, Iowa City, IA) and suspended in distilled water to 10mM. SCC, NSCLC, WI-38, as well as ATF3+/+ and ATF3-/- MEFs, cells were exposed to GGPP and mevalonate, which were purchased from Sigma-Aldrich (St Louis, MO, USA) and were used as previously described in (191). All drug concentrations and treatment times throughout the thesis were determined based on what has been previously reported in the literature to be optimal and from our own laboratory results from the MTT cells viability assay (97,104,121,135,192).

2.3 (4,5-Dimethylthiazol-2-yl)-2,5-Diphenyltetrazolium Bromide (MTT) Assay

All the cell lines were seeded on 96-well flat-bottomed plates (Corning Costar #3595, Corning, NY, USA) in 75µl/well. Cells were seeded at different densities (previously determined

by optimization) due to variation in doubling rates and differences in metabolic activity. The cells were left to incubate overnight at 37 °C and 5% CO2 to allow for attachment and recovery. On the next day, for aim 1, cells were either pretreated with either 10μM solvent control, 1μM or 10μM lovastatin (with or without 10μM GGPP or 100μM mevalonate) or 5μM GGTI-298 for 24hrs followed by tarceva (0.001-10μM) for 48hrs; or a combination treatment of 1μM or 10μM tarceva with GGTI-298 (1-10μM) for a total of 72hrs. For aim 2, cells were treated with either afatinib (0.001-10μM) or DGBP (1-30μM) alone for 48hrs or 72hrs, respectively; or the combination of both drugs for 72hrs consisting of either pre-treatment with 20μM DGBP followed by afatinib (0.001-10μM) or DGBP (1-30μM) pre-treatment for 24hrs followed by 5μM afatinib for further 48hrs; or a combination of DGBP (1-30μM) and 10μM GGPP co-administration for a total of 72hrs. Drugs were prepared at 2X concentration in 75μl and added to the plates already containing 75μl of media for a final volume of 150μl. Each treatment condition was performed in a total of 8 technical replicate wells for every biological replicate. Following treatments, 42μl of 10μg/ml MTT tetrazolium reagent (Sigma-Aldrich) dissolved in phosphate buffered saline (PBS) was added and incubated for 2 hours at 37ºC followed by cell lysis and MTT solubilization with 84μl of lysis solution (0.01N HCl in 10% sodium dodecyl sulphate (SDS) (Sigma-Aldrich, St. Louis, MO)) at 37ºC for 24hrs. MTT activity was measured by reading absorbance at 570 nm using a BioTek Synergy MX plate reader and analyzed using Gen5 software (BioTek, Winooski, VT). Cellular viability was assessed, where the values of the mean were calculated as the percentage of viability relative to a blank column of wells (no cells), which represents no viability, and an untreated column of wells as well as the DMSO treated control column wells which represents the healthy cells. The combination effects of lovastatin with tarceva, GGTI-298 with tarceva, or DGBP with afatinib were determined by the Chou-Talalay method (193) using CalcuSyn (also called

CompuSyn) computer software (Biosoft, Cambridge, GBR). The dose-effect curves of each drug alone and in combination were produced by MTT assay results. These data were entered into the CalcuSyn software and combination index (CI) values were graphed on fraction affected-CI (Fa-CI) plots. A CI < 1 is synergistic interaction, CI = 1 is additive, and CI > 1 is antagonistic.

2.4 Trypan Blue Exclusion Cell Viability Assay

Cells were seeded at $1x10^5$ - $2x10^5$ cells/well depending on the cell type. Next day, the cells were treated at 90% confluency with medium, 10μM solvent control, or with [1] 10μM lovastatin; [2] 10μM tarceva; [3] 5μM GGTI-298; [4] 10μM GGTI-298; [5] 5μM afatinib; [6] 20μM DGBP; [7] 100μM mevalonate; [8] 10μM GGPP, or combination treatment of [1] 100μM mevalonate or 10μM GGPP10μM with 10μM lovastatin; [2] 100μM mevalonate or 10μM GGPP with 10μM GGTI-298; [3] 100μM mevalonate or 10μM GGPP with 10μM GGTI-298 + 10μM tarceva; [4] 20μM DGBP with 5μM afatinib; [5] 20μM DGBP with 10μM GGPP. Then, the treated cells were incubated for 48hrs and 72hrs (depending on the treatment condition) at 37ºC and 5% CO_2. Following treatment, the media were aspirated, and the cells were washed with 3ml of PBS. The PBS was aspirated and 200μl of trypsin (Cellgro, Manassas, VA, USA) was added to each well for 4-10 minutes at 37ºC depending on the level of adherence of each cell type. Cells were then resuspended in 800μl of media and cell suspension was then transferred into a sample cup and cells were counted using the Vi-CELL® XR cell viability analyzer (Beckman Coulter, Mississauga, ON) by performing the trypan blue dye exclusion method to determine cell number and viability per well. In this assay, a cell suspension is mixed with the trypan blue, where viable cells with intact cell membranes will exclude the dye, whereas dead cells will not (194). The average and standard deviation for each cell line and treatment were calculated and plotted on a graph using

GraphPad Prism. For each cell line, biological triplicates of this experiment were performed in 6-well tissue culture plates (Corning Incorporated, Corning NY).

2.5 Western Blotting Analysis

Cells were treated for either 24hrs, 48hrs, or 72hrs (depending on the drug), then on a cold surface, media was aspirated and cells were washed with cold PBS, followed by lysis with RIPA buffer (50mM Tris-Cl, 150mM NaCl, 1mM EDTA, 1% (v/v) Triton X-100, 0.25 % (w/v) sodium deoxycolate and 0.1% (w/v) SDS and pH 7.5) supplemented with 1X protease inhibitor cocktail (Sigma Aldrich), 17.5mM beta-glycerophosphate and 0.2mM Sodium orthovanadate (Sigma-Aldrich, St-Louis, MO, USA). When probing with phospho (EGFR or AKT) antibodies, cells were stimulated for 15 minutes with 50ng/ml Epidermal Growth Factor (EGF) diluted from a 50µg/ml stock in 10 mM acetic acid/0.1% bovine serum albumin (Sigma) before lysis with RIPA buffer (100). Plates were scraped using rubber policemen and the lysis solution was transferred to a 1.5mL tube. The homogenized samples were placed on ice for 30 minutes and then centrifuged for 30 minutes at 14000 RPM at 4ºC. Supernatants were collected into 1.5mL tubes and stored at -80ºC. Total protein concentration was quantified using Pierce BCA protein assay protocol (Thermo Scientific) and protein absorbance read on a BioTek Synergy MX plate reader and analyzed using Gen5 software (BioTek, Winooski, VT) at 562nm. Protein samples were resolved by SDS-PAGE and transferred onto polyvinylidene fluoride (PVDF) membranes (Immobilon-P, Millipore, Billerica, MA, USA). Blocking the membrane was performed with 5% BSA (Bovine Serum Albumin) (Sigma-Aldrich) in Tris-Buffered Saline with 0.1% Tween-20 (TBS-T) and Western blotted with the following primary antibodies overnight at 4ºC: anti-β-actin from Sigma-Aldrich (St. Louis, USA); anti-HMG-CoAR, anti-GGPS1 (E-1), anti-cdc42 (B-9), anti-Rab5 (D-11), anti-Rap1 (E-6), anti-pan-Ras (C-4), anti-PUMA (BBC3) (G-3) and anti-ATF3 (C-19) from

Santa Cruz (Dallas, USA); anti-pY20 and anti-Rac1 from Transduction Laboratories, BD Bioscences (Mississauga, ON); anti-EGFR, anti-Akt, anti-pAkt (Ser 473), anti-LKB1, anti-pLKB1 (Ser 428), anti-AMPK, anti-pAMPK (Thr 172), anti-RhoA (67B9), anti-PARP, and anti-caspase3 from Cell Signaling Technology (Lake Placid, NY, USA). All the antibodies were diluted 1/1000, except for anti-actin (1/10000), anti-ATF3 (1/500), anti-Ras (1/500), and anti-Rap1 (1/500). Dilution of antibodies was made in 5% BSA. Blots were washed 3 times with TBS-T for 5 minutes each wash, then incubated for 1 hour at room temperature with the appropriate HorseRadish Peroxidase (HRP)-tagged secondary antibody (anti-rabbit (1/3000) and anti-mouse (1/3000), Jackson ImmunoResearch, West Grove, PA, USA). Visualization of the protein bands was performed using the Clarity Western ECL substrate (BioRad) and developed using the Syngene Bio-Imaging System (Syngene, Frederick, MD). Densitometric analysis was performed using the ImageJ software from National Institute of Health (NIH, Rockville, Maryland, US). The density of the non-phosphorylated antibody band and the density of the phosphorylated antibody band were each normalized with that of the actin antibody band, then the normalized density of the phosphorylated band was divided by the normalized density of the non-phosphorylated band. The density of the rest of the antibodies used throughout the thesis were normalized with that of the actin antibody. Error bars reflect the standard deviation from the mean (±SD) from 3 independent experiments. All the densitometric data are found in the appendix I.

2.6 Scratch Wound Assay

SCC25 and SCC9 cells were seeded into 6-well tissue culture plates and grown in DMEM supplemented with 10% FBS and 1% Pen/Strep at a density that ensures a confluent state (~90%) the next day. The following day, the cell monolayers were scratched using a P20 pipette tip. Media were removed, and cells were washed twice with warm PBS. Cells were then treated as control or

with 5μM GGTI-298. Five images per well were taken using a digital camera attached to an Eclipse TE2000-U microscope (Nikon, Mississauga, ON) for time 0 hours. Additional images were taken at 24 hours post-wounding and during treatment. Wound diameters for the 5 images taken for each condition, were measured and averaged and percentage wound closure was calculated using the following formula: [(average wound diameter at 24 hours – average wound diameter at 0 hours) / wound diameter at 0 hours] x 100.

2.7 Propidium Iodide Flow Cytometry

One million of SCC9 and SCC25 cells were seeded in 10cm plates and incubated overnight to allow for attachment and recovery. The following day, cells were treated either with 10μM GGTI-298 alone or in combination with 10μM tarceva for 48 hours. Adherent and cells in suspension were collected by centrifugation and fixed in 3ml of cold 80% ethanol overnight at -20^0C. Prior to analysis, cell pellets were washed with PBS resuspended in staining buffer containing 25μg/ml propidium iodide (Sigma-Aldrich) and 40μg/ml RNase A (BioShop, Burlington, Ontario, Canada) and incubated for a minimum of 1 hour in the dark at room temperature. Data (10000 events) was acquired on an EPICS XL flow cytometer (Beckman Coulter, Brea, California, USA) with FL2 laser channel and analyzed with Modfit software (Verity Software House, Topsham, ME, USA).

2.8 Fluorescence Microscopy

In a six-well tissue culture dish, SCC25 were seeded at $2x10^5$ cells in each well containing a 1cm x 1cm microscope coverslip. The following day, cells were treated with solvent control media, 1μM, or 5μM GTTI-298 and were incubated for 24h at 37ºC. Following treatments, cells were fixed with 4% PBS buffered paraformaldehyde for 15 minutes at 37ºC followed by three

washes with PBS. The cells were then permeabilized using 0.1% Triton X-100 (Sigma) in PBS for 15 minutes and followed by 3 washes with PBS. In order to label the actin cytoskeleton, cells were incubated with 100µL/well of reconstituted rhodamine-conjugated phalloidin (Cytoskeleton) in PBS for 15 minutes at room temperature. After 2 washes with PBS, the coverslips were mounted on microscope slides with DAPI (diluted in 50% glycerol) containing immunofluorescent mounting medium. Cells were then visualized with fluorescent microscopy (AxioCam HR, Carl Zeiss).

2.9 Transcriptome Analysis (RNAseq)

SCC25 cells were treated with either 10µM lovastatin or 10µM GGTI-298 for 24hrs. Total RNA was isolated employing the RNeasy Isolation Kit (Qiagen). mRNA expression profiling was determined using NuGen reagents (www.nugeninc.com). After amplification, libraries compatible with Illumina NGS methods were prepared using the Ovation Ultra Low Library Prep Kit (NuGen). The quality of each library was assessed using a Bioanalyzer 2100 (Agilent Technologies). Kappa Library Quant Kits (KappaBiosystems; www.kapabiosystems.com) were used for library quantitation. Cluster generation and 2 x 36 bp paired-end sequencing were performed over a single lane using the Illumina GAIIx or HiSeq Genome Analyzer workstation. We obtained approximately 42 million reads per sample with 89-90% of reads mapped back to the genome. The Illumina CASAVA pipeline was used to generate fastq sequence files. TopHat/Cufflink pipeline was used for mapping reads to the genome and quantification of gene expression (195). Computational assessments were conducted by the Ottawa Bioinformatics Core Facility. Following analysis Gene Ontology enrichment analysis was performed using PANTHER (www.pantherdb.org) (196).

2.10 Design and Expression of short-hairpin RNA for GGDPS

Two 20 and 21-mer sequences targeting GGDPS mRNA are; #1- 5'-ATCCTTCCCACTATTTCACC-3' and #2- 5'-TTCCCACTATTTCACCACAGA-3' (GenBank accession number is AB016043.1) were cloned into Lentiviral vector "all-in-one" pLKO-doxycycline-inducible shRNA system (Invitrogen) to generate stable cell lines with controlled shRNA expression. As a control, we employed the GFP-targeted oligonucleotide 5′CATGCGTCCACTCTTCCTC-3′ (accession number NC_011521). These sequences were BLAST confirmed for specificity. The forward and reverse synthetic 60 nt oligonucleotides (Integrated DNA Technologies, Coralville, IA) were designed, annealed, and inserted into the AgeI/EcoRI sites of pLKO vector, following the manufacturer's instructions (Oligoengine, Seattle, WA). These constructs express a 20 and 21 mer targeting 2 independent locations within GGPDS mRNA or GFP (control shRNA) mRNAs. The Lentiviral packaging cell line, 293T (Clonetech Laboratories, Mountain View, CA) was used for stable virus production according to the manufacturer's instructions. Briefly, packaging cells were transfected with GGPDS-shRNA plasmids#1 and #2, or GFP-shRNA plasmid using FuGENE® HD Transfection Reagent (Promega, Madison, Wisconsin, USA). After generation of stable clones, HeLa cells were infected with viral supernatant using 4μg/ml polybrene. Stably transfected clones expressing shRNAs were selected using 1μg/ml puromycin.

2.11 Quantitative RT-PCR

SCC25 and SCC9 cell lines were treated with either GGTI-298 or lovastatin for 24hrs and mRNA extracted using the RNeasy® kit (Qiagen, Germantown, MD, USA) following the manufacturer's protocol. The concentration of RNA was quantified using Take3 Micro-Volume plate and BioTek Synergy MX plate reader and analyzed using Gen5 software (BioTek, Winooski,

VT). One µg of total RNA was used for reverse transcription to cDNA using a High Capacity cDNA reverse transcription kit (Applied Biosystems) in an ABI Thermal Cycler (Applied Biosystems, Foster City, USA). The total PCR reaction volume of 20µl contained 2µl of cDNA, 1µl TaqMan Gene Expression Assay Primer/Probe (20x), 10µl of TaqMan Universal PCR Master Mix (2x) (Applied Biosystems, 4304437) and 7µl of RNase-free water. The endogenous control for the assay was the housekeeping gene, human GAPDH (20x) (Applied Biosystems, HS4333764-F). The reaction was performed in a 7500 Real-Time PCR system (Applied Biosystems). TaqMan Primers/Probes; HMG-CoAR, HS00168352; GGPPS1, HS01536492; ATF3, HS00231069; PUMA/BBC3, HS00248075; RhoB, HS03676562.

2.12 *Ex-Vivo* Tumor Analysis

Tumor tissue from HNSCC (HN), NSCLC (LU), melanoma (MEL), ovarian (OVCA) and thymus (THY) cancer patients undergoing routine surgical procedures were obtained and analyzed in this study that was approved by the Ottawa Hospital Research Ethics Board (Protocol# 20120559-01H). Areas containing tumor were identified by routine pathological gross examinations. Approximately 2mm cores were obtained using a sterile biopsy punch that was further sliced with a scalpel to obtain approximately 2x1x1mm tumor slices. The slices were randomized, and 3 slices were placed into each well of 24-well plate and cultured in DMEM (HyClone) supplemented with 10% heat-inactivated FBS (Medicorp) and 100-units/ml-antibiotic/antimycotic solution (Sigma). After 48h drug treatments with either 10µl GGTI-298, 25µl GGTI-298, 50µl DGBP or 25µl afatinib, the tumor slices were processed for RNA extraction and RT-PCR analysis of ATF3 mRNA levels as described above in triplicate. Initial tumor cell viability was assessed by addition of a 10% Alamar Blue (Invitrogen) solution and measured in Synergy Mx Monochromator-Based Multi-Mode Microplate Reader using Gen5 software, both

from Biotek Instruments (Winooski, VT) at 560 nm excitation wavelength and 590 nm emission wavelength.

2.13 Graphical and Statistical Analyses

The presented graphical data and statistical analyses were plotted and analyzed using GraphPad Prism software versions 6.0 and then 8.0 (GraphPad, La Jolla, CA) of 2-3 independent performed biological experimental replicates. Statistical differences for single comparison were determined using two-tailed unpaired t-test with a 95% confidence interval. Statistical differences for multiple comparisons were determined using a non-parametric one-way or two-way ANOVA test, depending on the experiment, with a 95% confidence interval using the Bonferroni multiple comparison test correction. Significance between columns for trypan blue exclusion viability assay and for RT-qPCR data were determined by one-way ANOVA using Bonferroni multiple comparison test. For MTT viability curves, significance was determined by two-way ANOVA employing a Bonferroni multiple comparison test. Results with $p<0.05$ were deemed significant. Statistically significant differences were determined as $P < 0.05$ from 2-3 independently performed biological experiments. In each replicate, cells consistently showed significance and no variability in significance was seen from experiment to experiment.

CHAPTER 3: RESULTS

3. Inhibition of GGTase1 Enhances Tarceva Efficacy in Squamous Cell Carcinoma Cells: Potential Novel Combination Therapeutic Approach

Stephanie Zahr[1,2#], Lenah Mukhtar[1,2#], Khalil Dayekh[1,2], Jennifer E.L. Hanson[1], Stephanie Johnson-Obaseki[3], Michael J. Odell[3], Carolyn Nessim[4], Patrick J. Villeneuve[4], Glenwood D. Goss[5] and Jim Dimitroulakos[1,2*].

[1]Centre for Cancer Therapeutics at the Ottawa Hospital Research Institute; and [2]Faculty of Medicine and the Department of Biochemistry at the University of Ottawa, Ottawa, Ontario, Canada. Departments of [3]Otolaryngology, [4]Surgery and [5]Medical Oncology the Ottawa Hospital, Ottawa, Ontario, Canada

# Contributed equally to this work

*Correspondence should be addressed to J.Dimitroulakos, E-mail: Jim.Dimitroulakos@rmp.uhn.ca

Key words: geranylgeranyl transferase, GGTI, EGFR, erlotinib, Head and Neck Cancer, mevalonate pathway

Contribution of Authors: The content of this manuscript was written by Dr. J. Dimitroulakos with the help of L. Mukhtar and K. Dayekh. L. Mukhtar performed the experiments of Figures 1A, 1B, 1C, 6A, 6B, 7B, 8A, 8B, and 8C. S. Zahr performed the experiments of Figures 2A, 2B, 2C, 3A, 3B, 4A, 4B, 4C, 4D, 5A, and 5B. K. Dayekh performed the experiments of Figures 7A, and 7C. J. Hanson performed the experiments of Figures 7D, 9A, 9B, and 9C. S. J-Obaseki, M. Odell, C. Nessim, P. Villeneuve, and D. Goss provided the *ex. vivo* tissues samples. J. Dimitroulakos helped in the synergy analyses of Figures 3 and 5. Number of these figures are supplemental figures in the manuscript.

Summary

Targeting the epidermal growth factor receptor (EGFR), with inhibitors such as tarceva (also known as erlotinib), represents a promising therapeutic option in advanced squamous cell carcinomas (SCC). However, they lack significant efficacy as single agents. Recently, we identified the ability of statins, which target mevalonate synthesis, to induce synergistic cytotoxicity with tarceva in SCC cells through activation of a cellular stress pathway regulated by the activating transcription factor 3 (ATF3). The resulting Phase I trial of rosuvastatin and tarceva, while showing clinical activity, also showed statin-induced muscle pathology which limited this approach and was likely the result of diminished ubiquinone levels. Downstream mevalonate pathway enzymes may represent novel therapeutic targets in SCC cells. Geranylgeranyl pyrophosphate (GGPP), a common protein-lipid membrane anchor was a key regulator of lovastatin-induced synergy in combination with tarceva. Employing an inhibitor of the GGTase-I enzyme, GGTI-298 treatment induced ATF3 expression in SCC9 and SCC25 cells and in a cohort of *ex-vivo* tumor tissues. Furthermore, GGTI-298 and tarceva induced synergistic cytotoxicity in SCC cells that was dependant on ATF3 expression as ATF3 deficient murine embryonic fibroblasts displayed attenuated cytotoxicity in response to GGTI-298 alone and in combination with tarceva. Similarly, SCC9 sub-lines that were selected as resistant to GGTI-298 through prolonged exposure to this agent also failed to demonstrate synergy with GGTI-298 in combination with tarceva. These results suggest the potential clinical utility of combining GGTI-298 inhibitor with tarceva in SCC patients as a novel and more refined combination therapeutic approach.

3.1 GGPP Reverses Lovastatin Induced Synergy with Tarceva

Two HNSCC cell line models, SCC9 and SCC25, were employed in this study to evaluate the potential of mevalonate pathway metabolites to reverse the cytotoxicity of lovastatin both alone (Figure 3.1A) and in combination with tarceva (Figure 3.1B). Employing the MTT cell viability colorimetric assay (197), SCC9 and SCC25 cells were treated with lovastatin alone or in combination with either 100μM mevalonate or 10μM GGPP co-administered for 48hrs to assess effects on cell viability. In both cell lines, mevalonate and GGPP co-administration reversed lovastatin-induced cytotoxicity as cell viability returned to approximately 100% (Figure 3.1A). In the combination treatment, SCC9 and SCC25 cells were first pre-treated for 24hrs with solvent control, 10μM lovastatin (alone), 10μM lovastatin+100μM mevalonate or 10μM lovastatin+10μM GGPP followed in each case by tarceva treatment (0.001-10μM) for further 48hrs. In both cell lines, mevalonate and GGPP addition reversed lovastatin-enhanced cytotoxicity in combination with tarceva in these cell lines as cell viability returned to the levels induced by tarceva alone (Figure 3.1B). These results also demonstrate the specificity of these mevalonate metabolites, as cytotoxicity was not affected in tarceva treatment by their co-administration. Based on these data, the basal expression levels of mevalonate metabolites were tested in SCC, NSCLC, and WI-38 cell lines (Figure 3.1C). Using Western blot, all the cancer cell lines expressed both GGDPS and HMGR at the protein level, while in WI-38, the expression of these two enzymes was less than the cancerous cell lines (Figures 3.1C). H23 and HeLa had the highest expression of these proteins. These results were supported by a graphical representation of densitometric quantification of 3 independently performed biological replicates as shown in the appendix (Figure S1) in which HMGCR and GGDPS levels were normalized to actin levels. These results suggested that GGPP synthase and HMGR might be involved in the tumorigenesis of the cancerous cell lines.

Figure 3. 1 The effect of add back downstream mevalonate metabolites on lovastatin.

(A) MTT cell viability assay of the co-administration of 100μM mevalonate or 10μM GGPP in SCC9 and SCC25 cells following 48hrs of lovastatin treatments. (B) MTT assay results are showing the effect of 10μM lovastatin induced cytotoxicity in combination with tarceva (erlotinib) by the co-administration of either 100μM mevalonate or 10μM GGPP in SCC9 and SCC25 cells. Pre-treatment with lovastatin (10μM) alone or in combination with either 100μM mevalonate or 10μM GGPP for 24hrs was followed by the addition of tarceva for a further 48hrs. (C) Representative Western blot analysis of basal expression of HMG-CoAR and GGPS1 in a variety of SCC (SCC9, SCC25, Cal27, and HeLa), NSCLC (Calu6, H23 and A549) and a normal fibroblast (WI-38) cell lines. For the Western blots, actin expression is used as a loading control. The quantification of the band intensities is found in appendix S1. The error bars represent the standard deviation from the mean (±SD) of 3 biological replicates (n=3). Statistical significance determined by two-way ANOVA with $P<0.05$ and with Bonferroni's post-hoc. Asterisks in the MTT graphs are determined to have a statistically significant difference when comparing the single treatment to the control treated cells or by comparing the combination drugs to a single drug for each cell line.

P- value: *$P<0.05$, **$P<0.01$, ***$P<0.001$.

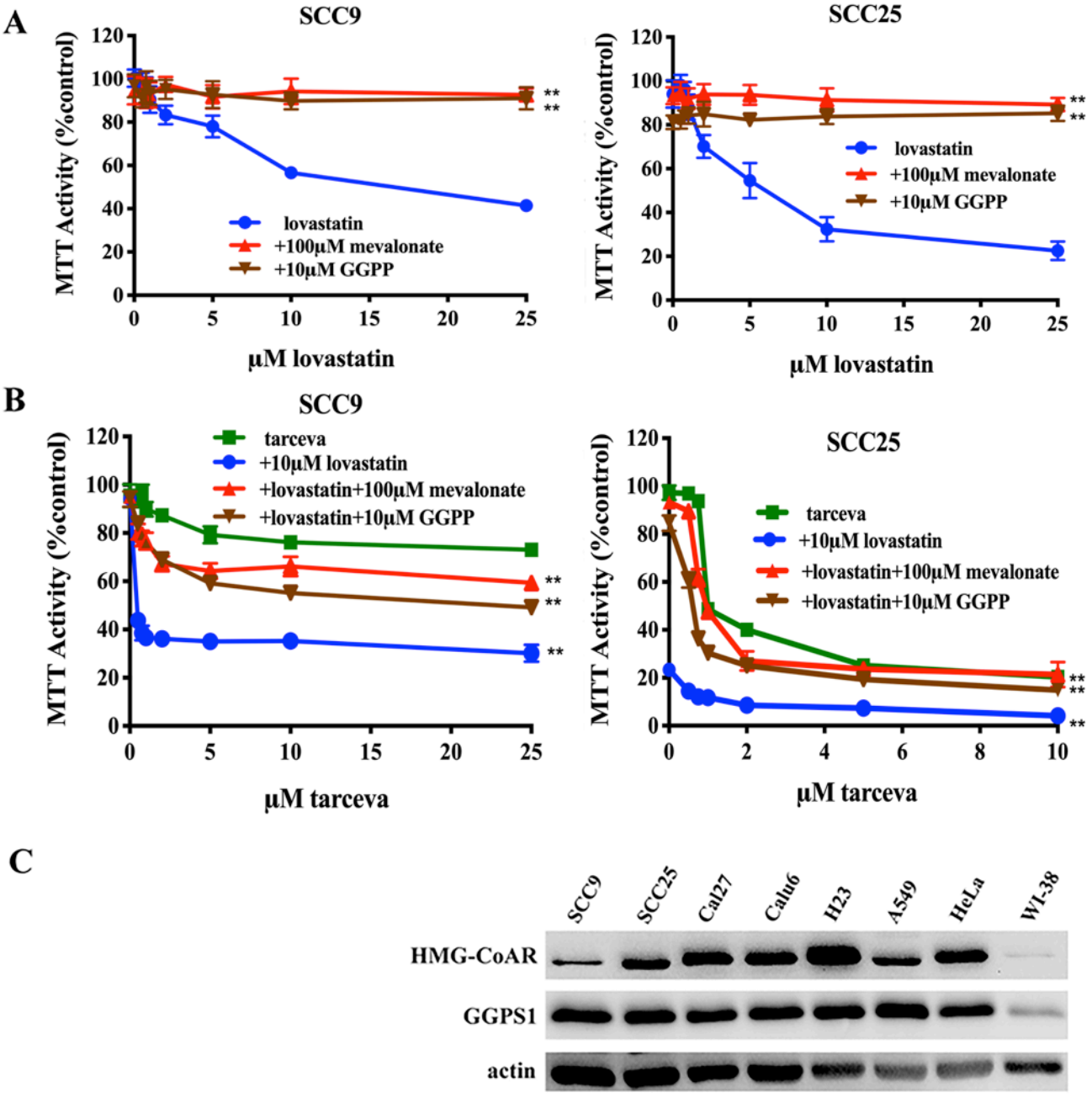
A
SCC9
SCC25
MTT Activity (%control)
μM lovastatin
lovastatin
+100μM mevalonate
+10μM GGPP
**
B
SCC9
SCC25
tarceva
+10μM lovastatin
+lovastatin+100μM mevalonate
+lovastatin+10μM GGPP
μM tarceva
C
SCC9
SCC25
Cal27
Calu6
H23
A549
HeLa
WI-38
HMG-CoAR
GGPS1
actin

Based on these results, we focussed on the potential of targeting the downstream mevalonate pathway enzymes that specifically incorporate GGPP to proteins. GGTase-I has a number of well-established clinically relevant specific inhibitors including GGTI-298 (198,199) that was evaluated in this study. We initially evaluated the specificity of GGTI-298 to target specific GGTase-I modified proteins including RhoA, Cdc42, and Rac1 that play significant roles in actin cytoskeleton reorganization (200). The effects of inhibiting protein geranylgeranylation with GGTI-298 were evaluated in SCC9 and SCC25 cells by Western immunoblotting. Lack of GGPP modification can result in mobility shifts due to the lack of protease cleavage of three terminal amino acids following GGPP addition (121). RhoA, Cdc42, and Rac1 showed a slight shift in the mobility on the gel following either 10μM lovastatin or 5μM GGTI-298 treatments in both SCC9 and SCC25 cells. This effect was reversed with the co-administration of 10μM GGPP with lovastatin but not with GGTI-298 (Figure 3.2A). Rab5 is doubly geranylgeranylated with RabGGTase (GGTase-II) and was used as a control. The shift in mobility on the gel for rab5 is observed in the lovastatin treated cells but not the GGTI-298 treated cells (Figure 3.2A). Hence, GGTI-298 specifically targets the prenylation of geranylgeranylated proteins mediated by GGTase-I, such as the RhoA.

These Rho (RhoA, Cdc42) and Rac GTPase proteins regulate a wide variety of cellular processes including cytoskeletal organization and play a role in cell motility and invasion (201). We next evaluated the effects of GGTI-298 on cell migration of SCC9 and SCC25 cells in a scratch wound assay. Confluent cell monolayers were scratched to create a wound opening, and five different areas were evaluated along the wound opening from which the average diameter was calculated. Percentage wound closure at 24 hours was calculated in comparison to the wound diameter at time 0hr (Figure 3.2B). GGTI-298 significantly reduced the migration of SCC9 and

SCC25 cells as compared to untreated cells. Cell counts of SCC9 and SCC25 treated with 5μM GGTI-298 showed no significant change in cell number compared to the control treated cells after 24hrs of treatment (Figure 3.2B); hence, the treatment of GGTI-298 inhibited HNSCC cells migration and motility. In an attempt to determine the effects of protein geranylgeranylation on cytoskeletal organization, actin architecture was visualized with rhodamine-conjugated phalloidin, which has a high affinity for F-actin following 1μM and 5μM GGTI-298 treatment for 24 hours in SCC25 cells. Increasing concentration of GGTI-298 caused stress fiber dissolution as visualized by fluorescence microscopy (Figure 3.2C).

Figure 3. 2 The effects of GGTI-298 on RhoA prenylation, actin organization, and cellular migration, and viability.

(A) Lovastatin and GGTI-298 treatments induce enhanced expression and mobility shifts of Rho family of proteins (RhoA and Cdc42 and Rac1), visualized by Western blot analysis of SCC9 and SCC25 cell lines. Treatments were with 10μM lovastatin or 5μM GGTI-298 for 24hrs. Rab5 mobility shift was evident only with lovastatin treatment. Treatment with 10μM GGPP alone or in combination with 10μM lovastatin or 5μM GGTI-298 were also evaluated with co-administration of 10μM GGPP. Expression levels of actin were assayed as the loading control. (B) SCC9 and SCC25 migration was measured as percentage wound closure as described in Methods section. Average wound closure measurement at five different points along wound edge was quantified at time points 0hr and 24hrs. Bars represent pooled mean with standard error. GGTI-298 significantly reduced cell migration in SCC9 ($p<0.001$) and SCC25 ($p<0.001$) cells. Treatment of 5μM GGTI-298 in SCC9 and SCC25 had no significant effect of cell viability evaluated by trypan blue exclusion cell viability assay following 24hrs of treatment. Representative phase contrast images are also shown following 24hrs of treatment at x10 magnification. (C) Fluorescence microscopy examining the effects of increasing concentrations of GGTI-298 on actin cytoskeletal organization in SCC25 cells. Rhodamine phalloidin staining of solvent control, 1μM, and 5μM GGTI-298 for 24 hours. Nuclei were counterstained with DAPI. Original magnification x60. Scale bar = 20 μm. Statistical significance was determined by one-way ANOVA with $P<0.05$ and with Bonferroni's post-hoc analysis. Data in this figure were obtained by Stephanie Zahr.

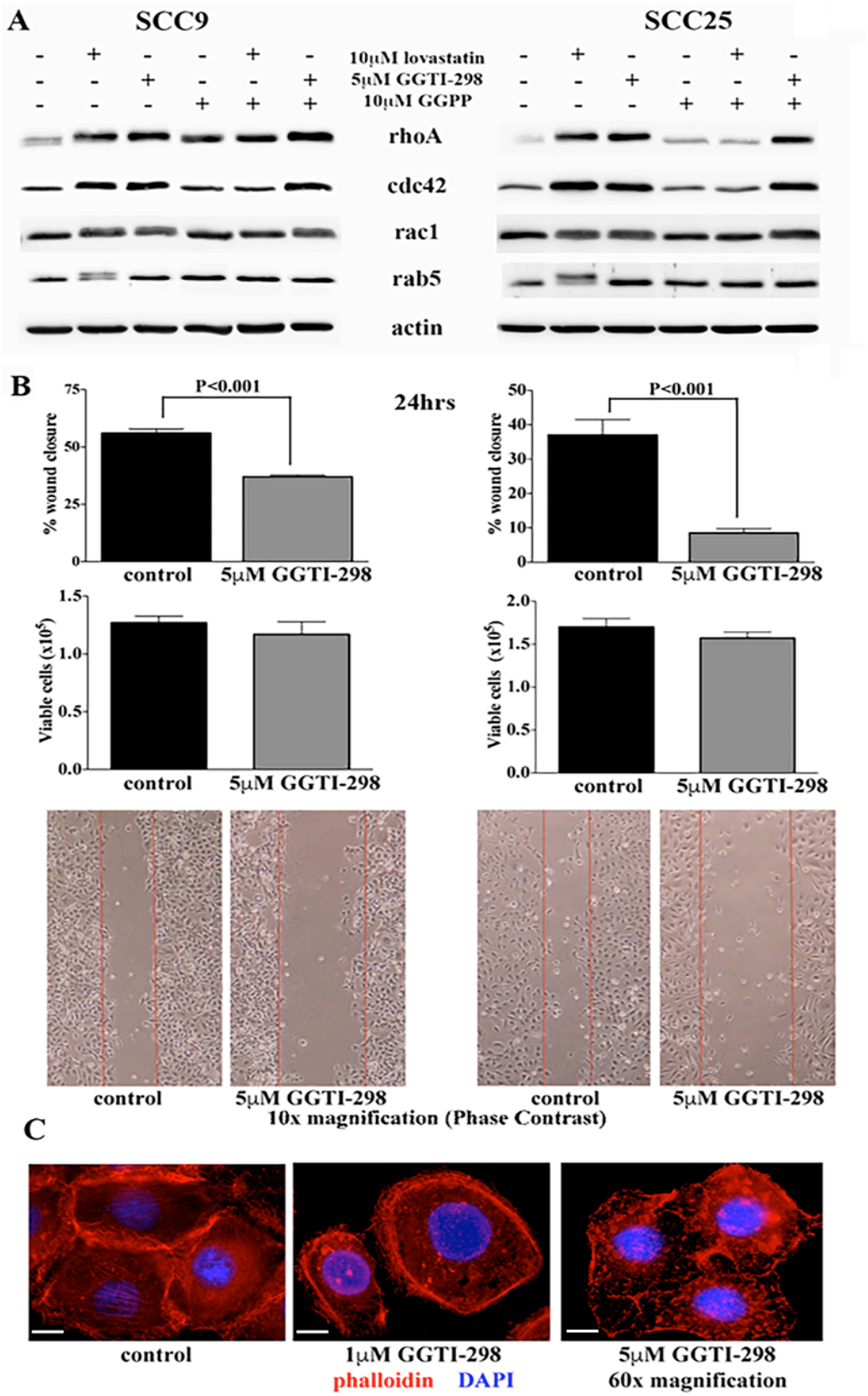
A
SCC9
SCC25
10μM lovastatin
5μM GGTI-298
10μM GGPP
rhoA
cdc42
rac1
rab5
actin
B
24hrs
P<0.001
% wound closure
control
5μM GGTI-298
Viable cells (x10^5)
10x magnification (Phase Contrast)
C
control
1μM GGTI-298
5μM GGTI-298
phalloidin DAPI
60x magnification

3.2 Synergistic Cytotoxicity of GGTI-298 and Tarceva in SCC Cells

The sensitivity of SCC9 and SCC25 HNSCC cell lines to the combination of GGTI-298 with tarceva was initially determined by MTT assay. Previous studies have demonstrated that lovastatin in combination with iressa (gefitinib) enhances cytotoxicity in HNSCC cells (105). We reassessed the combination of lovastatin with the receptor tyrosine kinase inhibitor, tarceva by MTT assay. Cells were treated with tarceva (0.5-10μM) for 48hrs either alone or with 1μM or 10μM lovastatin pre-treatment (24hrs) in combination for a total of 72hrs (Figure 3.3A and B). We showed dose dependant inhibition of SCC growth with increasing the concentration of tarceva in both cell lines; however, the addition of lovastatin enhances the cytotoxicity effects of tarceva in these tested cell lines (Figure 3.3A and B). To understand the nature of this combination effect, the Chou-Talalay analysis method was used to distinguish between additive and synergistic interactions (193). Fraction effect (on cell viability) plots were generated to show the combination effect (CI). CI values of 1 are additive, less than 1 are synergistic, and more than 1 are antagonistic. In HNSCC cell lines, SCC9 and SCC25, tarceva in combination with 1μM lovastatin demonstrated that the decrease in cell viability with these agents in combination determined by MTT assay was consistently synergistic in nature (Figure 3.3A and B).

Figure 3. 3 The synergistic relationship between lovastatin and tarceva in SCC cells.

MTT assay and Combination Index analyses demonstrating synergistic cytotoxicity with tarceva and (0.5 and 10μM) lovastatin in combination treatment of SCC9 (A) and SCC25 cell lines (B). The cell lines were pre-treated with 1 or 10μM lovastatin for 24hrs followed by tarceva combination treatments for a further 48hrs. The Fraction Affected/ Combination Index Plots were determined by MTT analysis where Combination Indices (CI) <1 are considered synergistic, CI >1 are considered antagonistic, and CI=1 are considered additive. Statistical significance was determined by two-way ANOVA with $P<0.05$ and with Bonferroni's post-hoc. Asterisks in the MTT graphs are determined to have a statistically significant difference when comparing the single treatment to the control treated cells or by comparing the combination drugs to a single drug for each cell line.

P- value: *$P<0.05$, **$P<0.01$, ***$P<0.001$.

Data in this figure were performed and analyzed by Stephanie Zahr.

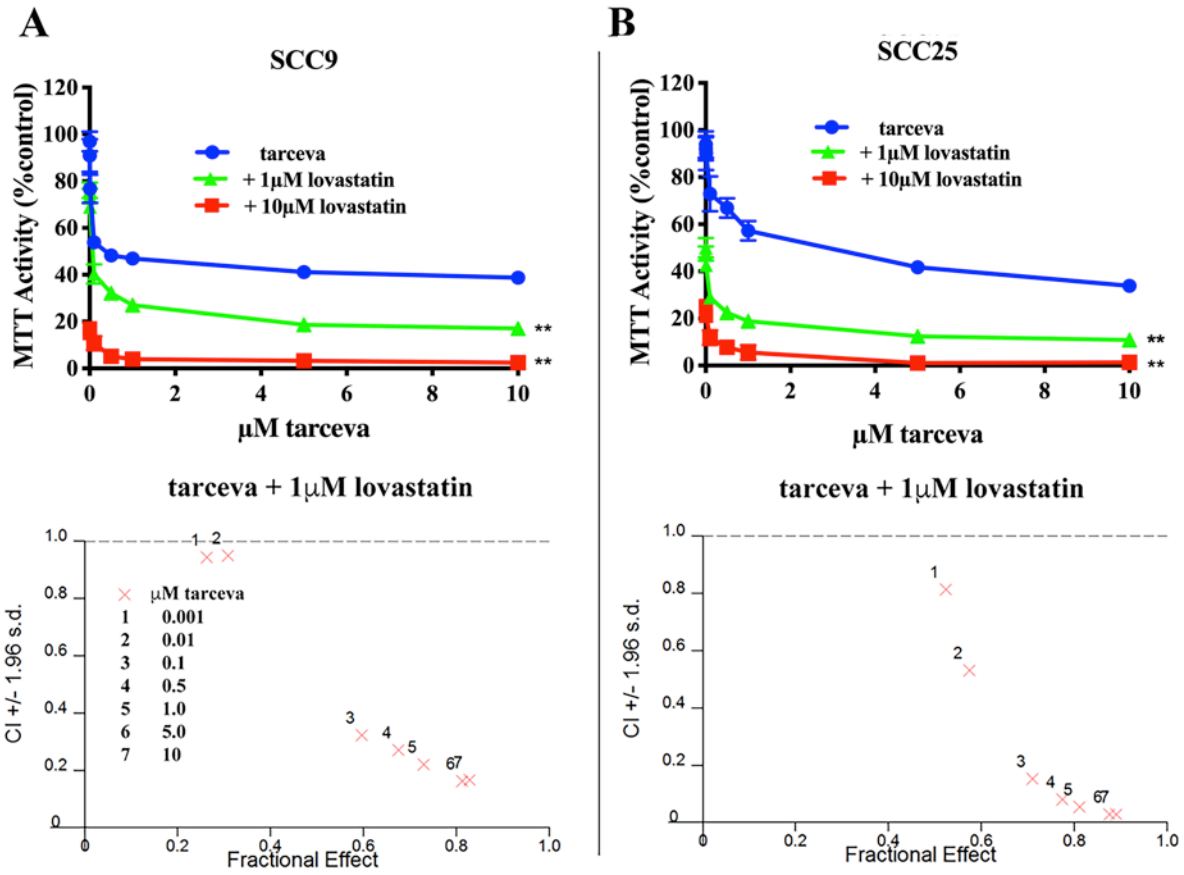
A
SCC9
MTT Activity (%control)
tarceva
+ 1μM lovastatin
+ 10μM lovastatin
**
**
μM tarceva
tarceva + 1μM lovastatin
CI +/- 1.96 s.d.
μM tarceva
1 0.001
2 0.01
3 0.1
4 0.5
5 1.0
6 5.0
7 10
Fractional Effect
B
SCC25
MTT Activity (%control)
tarceva
+ 1μM lovastatin
+ 10μM lovastatin
**
**
μM tarceva
tarceva + 1μM lovastatin
CI +/- 1.96 s.d.
Fractional Effect

The results of (Figure 3.3) were compared to the effects of combining varying concentrations of GGTI-298 (0.1-10μM) pre-treatment for 24hrs either alone or with 1μM or 10μM tarceva in combination for a further 48 hours (Figure 3.4A) in SCC9 and SCC25 cell lines. We demonstrated that GGTI-298 single treatment, similar to our results with lovastatin, showed a more potent cytotoxic response in SCC25 cells compared to SCC9 cells. The combination of GGTI-298 with tarceva showed significant cytotoxicity in both cell lines (Figure 3.4A) that mimicked the effects of lovastatin in combination with tarceva in these cells (Figure 3.3). We confirmed the sensitivity of the HNSCC cell lines to the combination of GGTI-298 with tarceva by trypan blue exclusion cell viability assay (194). Cells were treated with a control, 10μM tarceva, 10μM GGTI-298 single treatments or the combination of 10μM tarceva with 10μM GGTI-298 for 48hrs (Figure 3.4B). The combination of tarceva with GGTI-298 showed enhanced cytotoxicity in both SCC9 and SCC25 cells compared to either agent alone.

Using flow cytometric analysis of propidium iodide-stained DNA in SCC9 and SCC25 cell lines, we evaluated the role of the induction of apoptosis as the mechanism by which the combination of GGTI-298 and tarceva induces enhanced cytotoxicity. Apoptotic bodies that contain nuclear fragments are visualized as a pre-G1 peak in the DNA histogram that is characteristic of this programmed cell death modality (202). Similarly, SCC9 and SCC25 cell lines with the combination of 10μM GGTI-298 and 10μM tarceva showed a significant increase in the induction of pre-G1 apoptotic bodies with this combination compared to either agent alone (Figure 3.4C). To further confirm that the combined enhanced cytotoxicity with tarceva and GGTI-298 were due to induction of apoptosis, we evaluated the cleavage of apoptotic marker poly ADP ribose polymerase (PARP) by Western blot analysis. SCC9 and SCC25 cells were treated with 1μM, 5μM, and 10μM GGTI-298 alone or in combination with 10μM tarceva for 48 hours (Figure 3.4D).

In this assay, increased levels of cleaved PARP (cPARP) represent an increase in apoptosis. Thus, the combination of 1, 5 or 10μM GGTI-298 with 10μM of tarceva showed a significant increase in the levels of cPARP compared to either agent alone.

To understand the nature of this combination effect, the Chou-Talalay analysis method was used to distinguish between additive and synergistic interactions (Figure 3.5). In HNSCC cell lines, SCC9 and SCC25, GGTI-298 in combination with either 1 or 10μM tarceva demonstrated that the decrease in cell viability with these agents in combination determined by MTT assay was consistently synergistic in nature (Figure 3.5A and B). Therefore, the combination of GGTI-298 and tarceva displayed enhanced synergistic cytotoxicity in HNSCC cells likely through targeting of protein geranylgeranylation.

Figure 3. 4 The effects of GGTI-298 on tarceva-induction of cytotoxicity and apoptosis in SCC cells.

(A) MTT assay evaluating cytotoxicity of GGTI-298 and (1 and 10μM) tarceva in combination in SCC9 and SCC25 cell lines. The cell lines were pre-treated with 0.1-10μM GGTI-298 for 24hrs followed by either 1μM or 10μM tarceva combination treatment for a further 48hrs. (B) Cell viability was further assessed employing trypan blue exclusion assay showing enhanced cytotoxicity with GGTI-298 and tarceva combination treatment compared to each agent alone with the same treatment strategy as above. (C) Flow cytometric analysis of sub-G1 apoptotic fraction as determined by propidium iodide staining of cellular DNA content comparing the response of SCC9 and SCC25 cell lines treated as in (B). Bar graph representation and standard error from 3 independent studies. (D) Western blot analysis of PARP cleavage (cPARP) upon 48hr treatment with increasing concentrations of 1μM, 5μM, and 10μM GGTI-298 alone or in combination with 10μM tarceva for 24hrs in SCC9 and SCC25 cells. Actin is used as a loading control. Statistical significance was determined by two-way ANOVA with $P<0.05$ and with Bonferroni's post-hoc. Asterisks in the MTT graphs are determined to have a statistically significant difference when comparing the single treatment to the control treated cells or by comparing the combination drugs to a single drug for each cell line, while significant differences between column groups are displayed as P-values above the comparison.

P- value: *$P<0.05$, **$P<0.01$, ***$P<0.001$.

Data in this figure were obtained by Stephanie Zahr.

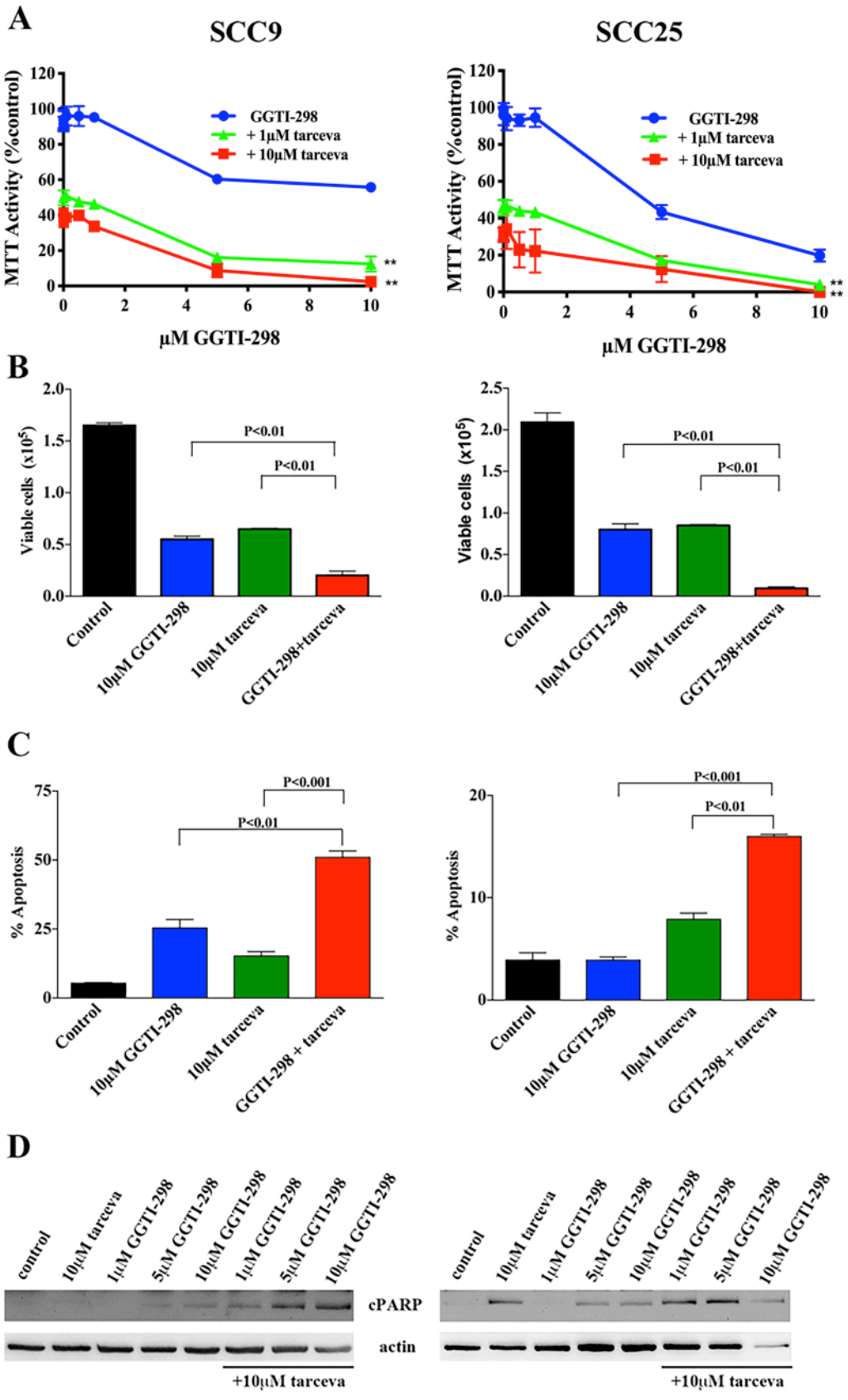
A
SCC9
SCC25
MTT Activity (%control)
GGTI-298
+ 1μM tarceva
+ 10μM tarceva
μM GGTI-298
B
Viable cells (x10^5)
P<0.01
P<0.01
Control
10μM GGTI-298
10μM tarceva
GGTI-298+tarceva
C
% Apoptosis
P<0.001
P<0.01
Control
10μM GGTI-298
10μM tarceva
GGTI-298 + tarceva
D
control
10μM tarceva
1μM GGTI-298
5μM GGTI-298
10μM GGTI-298
cPARP
actin
+10μM tarceva

Figure 3. 5 The synergistic relationship between GGTI-298 and tarceva in SCC cells.

Fraction Affected/ Combination Index Plots determined by MTT analysis of cell viability show the synergistic effect of GGTI-298 (0.1-25μM, 24hr pre-treatment) in combination with 1μM or 10μM tarceva (further 48hr treatment) in SCC9 and SCC25 cells. Combination Indices (CI)<1 are considered synergistic, CI>1 are considered antagonistic, and CI=1 are considered additive. Data in this figure were obtained by Stephanie Zahr.

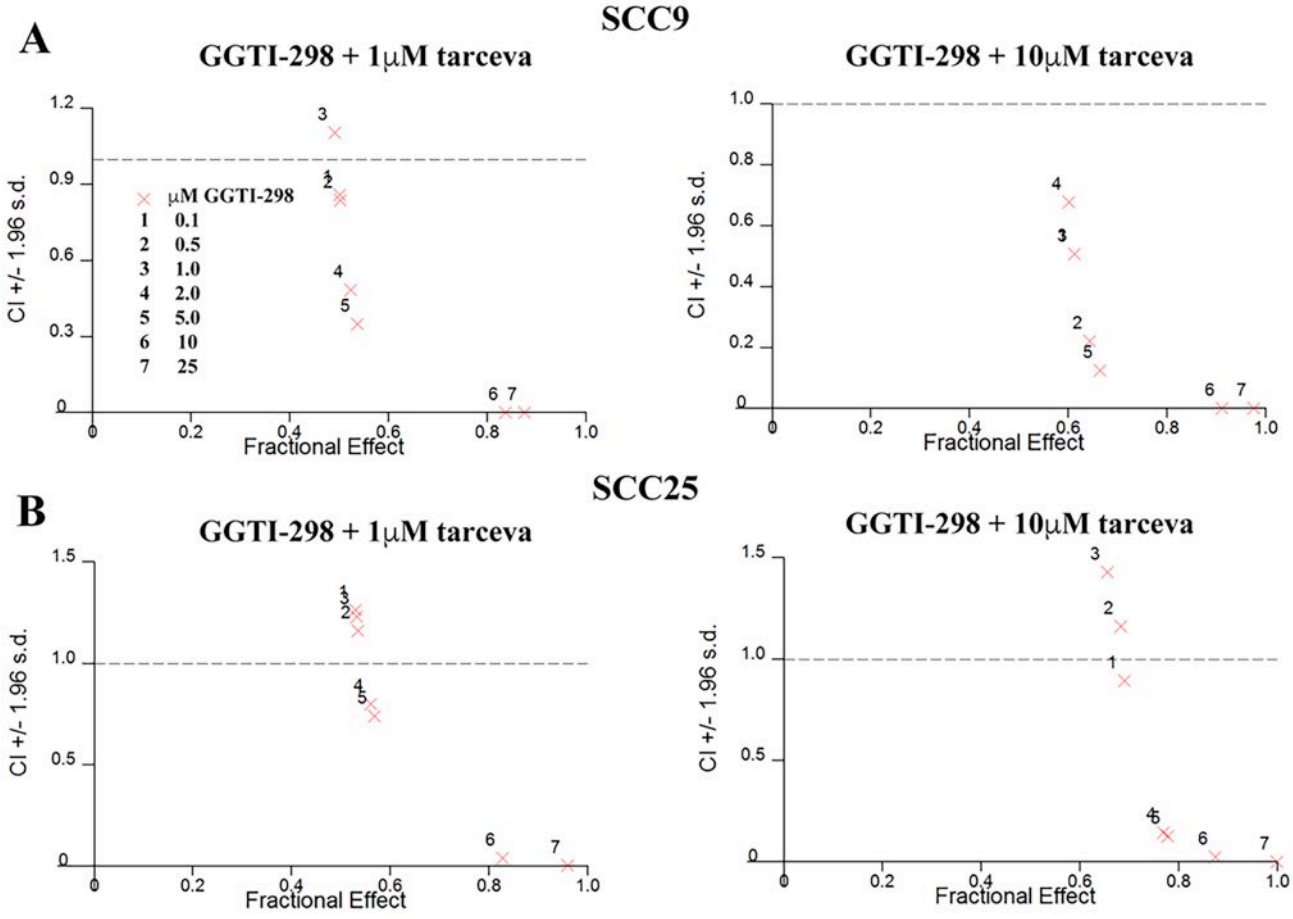
SCC9
A
GGTI-298 + 1μM tarceva
GGTI-298 + 10μM tarceva
CI +/- 1.96 s.d.
Fractional Effect
μM GGTI-298
1 0.1
2 0.5
3 1.0
4 2.0
5 5.0
6 10
7 25
SCC25
B
GGTI-298 + 1μM tarceva
GGTI-298 + 10μM tarceva
CI +/- 1.96 s.d.
Fractional Effect

3.3 GGTI-298 Induces Multiple Stress Pathways

In our recent work, we have demonstrated the ability of lovastatin to induce metabolic stress through [1] the activation of the ISR regulated by the induction of ATF3 (166), [2] the inhibition of ligand-induced EGFR/AKT activation (105), and [3] the activation of energy stress through the induction of LKB1/ AMPK (148). Here, we evaluated the effect of GGTI-298 on the key regulators of the growth factor withdrawal and the energy stress pathways (Figure 3.6).

We first evaluated the effect of GGTI-298 treatment on the phosphorylation status of EGFR and the downstream signaling cascade target AKT, which has a role in cell survival (45,48). Serum-starved SCC25 cells were treated with 1μM tarceva as a control or GGTI-298 (0.5μM, 1μM, 5μM, and 10μM) for 24hrs followed by 50ng/ml EGF stimulation for 15mins and compared with untreated control cells with and without EGF stimulation. The phosphorylation of EGFR and functional activation of the AKT pathways were evaluated by Western blot analysis, employing phospho-specific antibodies recognizing the active form and control antibodies for total EGFR and AKT. The addition of GGTI-298 inhibited ligand-induced activation of EGFR and AKT proteins as the phosphorylated pEGFR and pAKT levels were decreased as shown by Western blot analysis (Figure 3.6A). These results were supported by a graphical representation of densitometric quantification of 3 independently performed biological replicates as shown in the appendix (Figure S2) in which pEGFR and pAKT levels were normalized to total EGFR and AKT levels, confirming the downregulation of these phosphorylated proteins following GGTI-298 treatment.

Next, we evaluated the potential of GGTI-298 to activate LKB1/AMPK in SCC25 cells by evaluating their phosphorylation levels (Figure 3.6B). LKB1/AMPK pathway is the sensor for cellular energy status pathway, which is activated under low intracellular ATP associated with nutrient deprivation or hypoxia. Treatment of SCC25 cells with 10μM lovastatin as a control or

(0.5μM, 1μM, 5μM, and 10μM) GGTI-298 induced the expression levels of phosphorylated LKB1 and AMKPα in a dose-dependent manner. These results were supported by a graphical representation of densitometric quantification of 3 independently performed biological replicates as shown in the appendix (Figure S2) in which pLKB1 and pAMPK levels were normalized to total LKB1 and AMPK levels, confirming the upregulation of these phosphorylated proteins following GGTI-298 treatment. The same results were seen in SCC9 cells (data not shown).

Figure 3. 6 The effects of GGTI-298 on EGFR, AKT, LKB1 and AMPK phosphorylation.

(A) Representative Western blot analysis of EGFR and AKT phosphorylation following treatment with increasing concentrations of GGTI-298 and with 1μM tarceva as a control for a total of 24 hours in serum-free media in SCC25 cells. Total EGFR and AKT were used as a loading control. (B) Representative Western blot analysis of LKB1 and AMPK phosphorylation following treatment with increasing concentrations of GGTI-298 and with 10μM lovastatin as a control for a total of 24 hours in SCC25 cells. Total LKB and AMPK were used as a loading control, along with actin used as a loading control to total protein levels. The quantification of the band intensities is found in appendix S2. The error bars represent the standard deviation from the mean (±SD) of 3 biological replicates (n=3).

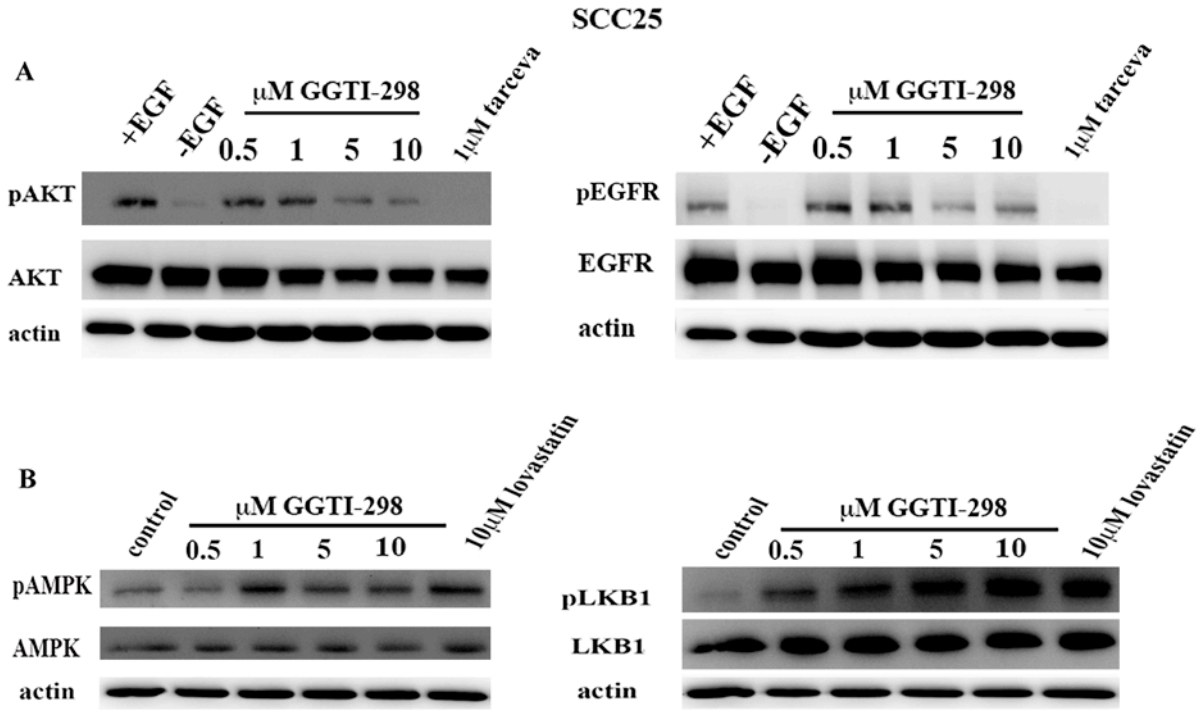
SCC25
A
+EGF
-EGF
μM GGTI-298
0.5
1
5
10
1μM tarceva
pAKT
AKT
actin
pEGFR
EGFR
actin
B
control
μM GGTI-298
0.5
1
5
10
10μM lovastatin
pAMPK
AMPK
actin
pLKB1
LKB1
actin

3.4 ATF3 is a GGTI-298 Regulated Gene

In order to gain further insight on the common potential mechanism of action of lovastatin and GGTI-298 in SCC25 cells, we performed RNA-seq full transcriptome analysis (203) of untreated control compared to either 24hr 10μM lovastatin or 10μM GGTI-298 treatment. From the analysis, we identified 213 genes which that were differentially expressed following 10mM lovastatin as a single drug treatment ($Log_2N\pm2$). Among these 213 genes, 93 genes were upregulated, and 120 genes were downregulated. Additionally, 372 genes were differentially expressed following 10mM GGTI-298 as a single drug treatment ($Log_2N\pm2$). Among these 372 genes, 268 genes were upregulated, and 104 genes were downregulated. The gene ontology summary is found in the appendix II (Fig S18 and S19).

Significant differences in expression of greater than two-fold that were common to both treatments were identified and included 65 genes that were differentially expressed. Among these 65 genes, 26 induced genes were found in relevant pathways, such as growth factor signaling, apoptosis regulators, death ligand pathway, and calcium homeostasis. The gene ontology summary is found in the appendix II (Fig S20 A and B), and Table S1. ATF3 was one of the top 20 genes that were significantly induced in both lovastatin and GGTI-298 treatments (FDR = 6.18E-10). Of significance, ATF3, known ATF3 target genes (PUMA/BBC3, RhoB, Fas, DDIT4) and regulators of ATF3 expression (JNK, JUND, c-JUN) (176,204) were significantly induced in both lovastatin and GGTI-298 treatments (Figure 3.7A). Western blot analyses confirmed GGTI-298 induction of ATF3 that was dose-dependent in both SCC9 and SCC25 cells following 24hrs of treatments (0.5-10μM) (Figure 3.7B). These results were supported by a graphical representation of densitometric quantification of 3 independently performed biological replicates as shown in the appendix (Figure S3) in which ATF3 levels were normalized to actin levels, confirmed the upregulation of the ATF3

levels following GGTI-298 treatment. Next, we employed quantitative RT-PCR to validate the differential expression of two ATF3 target genes identified by our RNA-seq screen above. Both lovastatin and GGTI-298 treatments (1 and 10μM for 24hrs) induced significant PUMA/BBC3 and RhoB expression in both SCC9 and SCC25 cells (Figure 3.7C).

To evaluate the potential of GGTI-298 to induce ATF3 mRNA expression in a more clinically relevant model, we assessed *ex-vivo* HNSCC tumor tissue in culture from 3 different HNSCC patients undergoing surgery at our Institute (HN01-03). We also similarly evaluated a melanoma sample (MEL-01), 2 ovarian carcinomas (OVCA01-02) and a thymus tumor (THY-01). Tissue samples were processed (183) following surgical excision into 2x1mm slices, randomized with 3 tissue slices evaluated per treatment (Figure 3.7D) and analyzed by quantitative RT-PCR performed in triplicate. In the *ex-vivo* tissue samples evaluated, 5 of 7 showed induction of greater than 1.5-fold of ATF3 mRNA levels following 10 and 25μM GGTI-298 treatments for 48hrs. Taken together, these data demonstrate that GGTI-298 treatment induce both ATF3 expression and its target genes in SCC9 and SCC25 cells as well as induce ATF3 expression from a variety of tumor tissues *ex-vivo*.

Figure 3. 7 The role of ATF3 in GGTI-298 activity.

(A) Table of a subset of genes that were up regulated by both 10μM lovastatin and 10μM GGTI-298 treatments for 24hrs in SCC25 cells identified by RNA-seq analysis. The list includes the transcription factor ATF3 and its target genes BBC3/PUMA, RhoB, Fas, and DDIT4 as well as genes that regulate ATF3 expression including JNK, JUND and c-JUN (highlighted in red font). **(**B) Representative Western blot analysis of ATF3 expression following 24hr treatment of 0.5-10μM GGTI-298 with 10μM lovastatin treatment as a comparator. Actin expression is employed as a loading control. The quantification of the band intensities is found in appendix S3. The error bars represent the standard deviation from the mean (±SD) of 3 biological replicates (n=3). (C) Quantitative RT-PCR analysis of 1 and 10μM treatment for 24hrs of both lovastatin and GGTI-298 in SCC9 and SCC25 cells. mRNA levels were determined and normalized to GAPDH levels. BBC3/PUMA and RhoB gene expressions were evaluated. **(**D) ATF3 mRNA was also analyzed by Q-RT-PCR following solvent control, 10 and 25μM GGTI-298 in surgically excised *ex-vivo* tissues from 3 HNSCC (HN), 1 melanoma (MEL), 2 ovarian carcinomas (OVCA) and 1 thyroid cancer (THY) patients. Fold changes were calculated following normalization to *gapdH* levels (ΔΔCt) and expressed as means (±SD) (*n* = 3). The error bars represent SD from the mean of three replicates. Data in figures 7A and 7C were obtained by Khalil Dayekh; data in figure in 7D were done by Jennifer Hanson.

A

RNA-seq Analysis- Common Lovastatin and GGTI-298 Regulated Genes

Apoptosis Regulators	Death Ligand Pathways	Growth Factor Signaling	Calcium Homeostasis
AMIGO2	Fas	EGF	S100A8
ACTN2	TRAIL-R	FGF	S100A9
ATF3	TRADD	NGF	SLC8A1
BBC3/PUMA	FLIP	FGFR	MAL
BMF		PDGFR	
LGALS7		Ras	
rhoA		JNK	
rhoB		JUND	
		c-JUN	
		DDIT4	

SCC25 10μM lovastatin or 10μM GGTI-298 (24hr treatments)

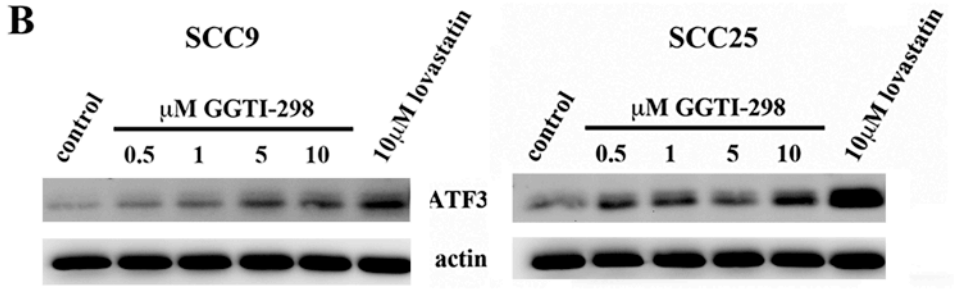

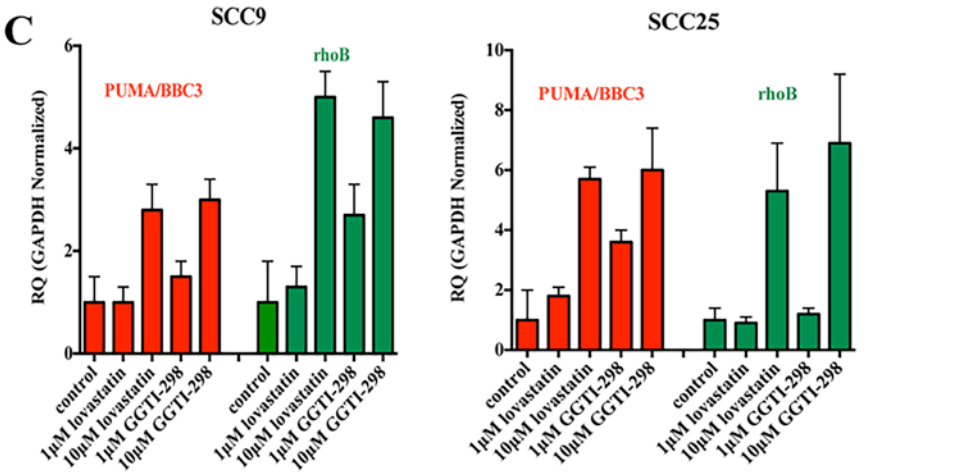

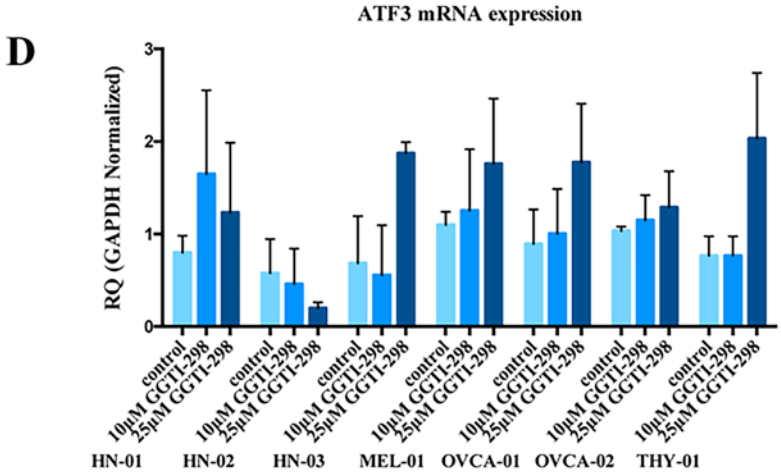

3.5 Key Role of ATF3 in GGTI-298 Cytotoxicity and Synergy with Tarceva

In this study, we developed a series of GGTI-298 resistant clones from the SCC9 cell line (designated GGTI-R1-4). The lethal concentration (LC) 50 (MTT activity reduced by 50%) in GGTI-298 treated cells for 48hrs was approximately 12μM for the SCC9 parental line and greater than 50μM for each of the 4 resistant sub-lines (GGTI-R1-4) (Figure 3.8A). Next, using Western blot, we assessed the effects of GGTI-298 in the 3 metabolic stress pathways mentioned above (Section 3.3) by evaluating whether the expression levels of the key proteins in these pathways were altered in the parental SCC9 compared to their resistant clones. Following 24hr of 10μM GGTI-298 treatment, as expected, the parental SCC9 cell line showed downregulation of pEGFR and pAKT (Figure 3.8B). In addition, the expression of pLKB1, ATF3, and RhoA were induced following GGTI-298 (Figure 3.8B). However, the expression of these key proteins was altered in the resistant clones (Figure 3.8B). These results were supported by a graphical representation of densitometric quantification of 3 independently performed biological replicates as shown in the appendix (Figure S4) in which pEGFR, pAKT, pLKB1 levels were normalized to total EGFR, AKT, and LKB1 levels; whereas ATF3 and RhoA levels were normalized to actin levels. Of a particular interest, the induction of ATF3 in response to GGTI-298 treatment in the parental SCC9 was also evident in GGTI-R1 and R3 but absent in GGTI-R2 and R4 (Figure 3.8B), suggesting a potential role for ATF3 as well as other targets in regulating GGTI-298 cytotoxicity in SCC9 cells. Employing the MTT viability assay, we confirmed that in the parental SCC9 cells, 5μM GGTI-298 24hr pre-treatment followed by 48hr treatment with 0.5-10μM tarceva enhanced the cytotoxicity of tarceva in these cells (Figure 3.8C). In the SCC9-GGTI-R1 and R2 sub-lines, GGTI-298 treatments failed to enhance tarceva induced cytotoxicity (Figure 3.8C). This suggests

a potential role for ATF3 in regulating GGTI-298 cytotoxicity and synergy with tarceva in HNSCC cells.

Figure 3. 8 Characterization of SCC9 resistant sub-lines and the effects of GGTI-298 and ATF3 on parental SCC9 and GGTI-resistant clones.

(A) MTT viability assay comparing the response of parental SCC9 cells to its resistant variants GGTI-R1-4 cell lines after GGTI-298 treatment. Cells were treated with 0.5–10μM GGTI-298 for 48hrs, and cell viability was assessed with the activity of the control untreated cells taken to be 100%. (B) Representative Western blot analysis of SCC9 cells and GGTI-R1-4 treated for 24hrs showing different expression levels of pEGFR, pAKT, pLKB1, RhoA, and ATF3. The quantification of the band intensities is found in appendix S4. The error bars represent the standard deviation from the mean (±SD) of 3 biological replicates (n=3). Lack of ATF3 induction was seen in 2 out of the 4 resistant sub-lines. Actin expression is employed as a loading control. (C) MTT analysis of parental SCC9 cells (left panel) and its sub-lines GGTI-R1 and R2 (right panel) following 48hrs treatments with tarceva with or without a 24hr pre-treatment with 5μM GGTI-298. The error bars represent the standard deviation from the mean (±SD) of 3 biological replicates (n=3). Statistical significance was determined by one-way ANOVA (A) or two-way ANOVA (C) with $P<0.05$ and with Bonferroni's post-hoc. Asterisks in the MTT graphs are determined to have a statistically significant difference when comparing the single treatment to the control treated cells or by comparing the combination drugs to a single drug for each cell line.

P- value: *$P<0.05$, **$P<0.01$, ***$P<0.001$.

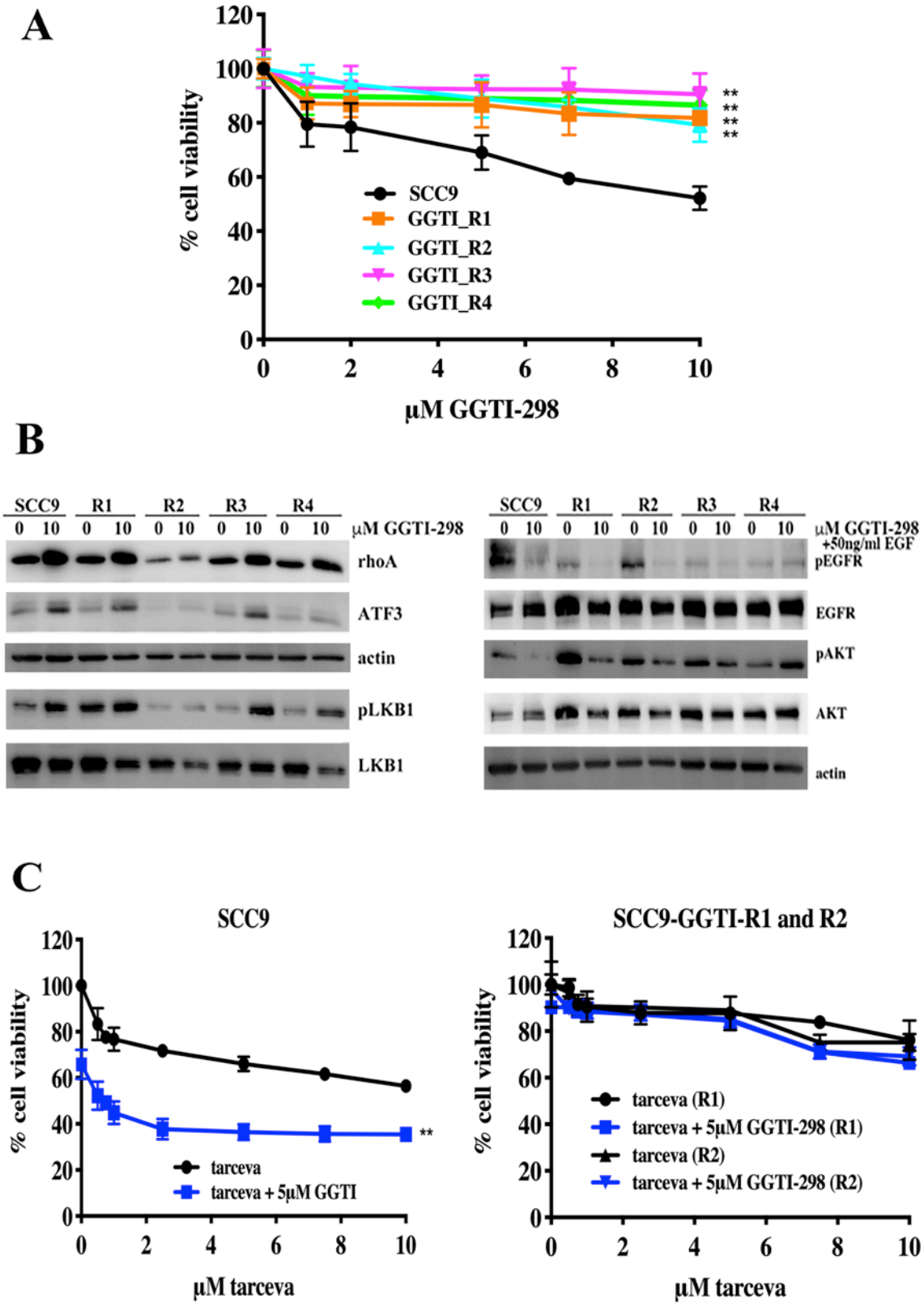
A
% cell viability
µM GGTI-298
SCC9
GGTI_R1
GGTI_R2
GGTI_R3
GGTI_R4
**
B
SCC9
R1
R2
R3
R4
µM GGTI-298
rhoA
ATF3
actin
pLKB1
LKB1
µM GGTI-298 +50ng/ml EGF
pEGFR
EGFR
pAKT
AKT
C
SCC9
% cell viability
µM tarceva
tarceva
tarceva + 5µM GGTI
SCC9-GGTI-R1 and R2
tarceva (R1)
tarceva + 5µM GGTI-298 (R1)
tarceva (R2)
tarceva + 5µM GGTI-298 (R2)

To establish the role of ATF3 in regulating the cytotoxicity of both lovastatin and GGTI-298, we evaluated the cytotoxic effects of these agents in ATF3 null (-/-) cells and their respective wild-type (+/+) murine embryonic fibroblast (MEF) counterparts. MTT cell viability assays demonstrated ATF3-/- MEFs to be resistant to both lovastatin and GGTI-298 treatments (0.1-25μM, 48hrs) (Figure 3.9A). Then, we evaluated ATF3 expression levels following 5 and 10μM 24hr treatments for both lovastatin and GGTI-298 in wild-type and ATF3-/- MEFs. These agents readily induced ATF3 only in the wild-type cells that was also associated with cleaved PARP (a marker of apoptosis) and PUMA/BBC induction that were significantly attenuated in the ATF3 null cells as determined by Western blot analysis (Figure 3.9B). Employing these MEFs cell lines, we also evaluated the potential of either lovastatin (1μM, 24hr pre-treatment) or GGTI-298 (5μM, 24hr pre-treatment) to enhance the cytotoxicity of tarceva (0.001-10μM, further 48hr treatment) using the MTT assay. With both agents' significant cytotoxicity was observed only in the wild-type MEFs but not in the ATF3-/- deficient MEFs (Figure 3.9C). These results demonstrate a role for ATF3 in regulating both the cytotoxicity induced by GGTI-298 as well as its ability to enhance the cytotoxicity of tarceva.

Figure 3. 9 The effects of GGTI-298 on ATF3 null MEFs vs. wild-type.

(A) MTT analysis of wild-type and ATF3-/- MEFs following 48hr treatment with 0.1-25μM lovastatin or GGTI-298. (B) Western blot analysis of ATF3 expression, PARP cleavage (cPARP) and PUMA/BBC3 in wild-type and ATF3-/- MEFs following 1 and 10μM treatment of both lovastatin and GGTI-298 for 24hr. Actin expression is employed as a loading control. (C) MTT analysis of wild-type and ATF3-/- MEFs following 48hrs treatment with tarceva with or without a 24hr pre-treatment with 1μM lovastatin (left panel) or 5μM GGTI-298 (right panel). Data in this figure were obtained by Jennifer Hanson.

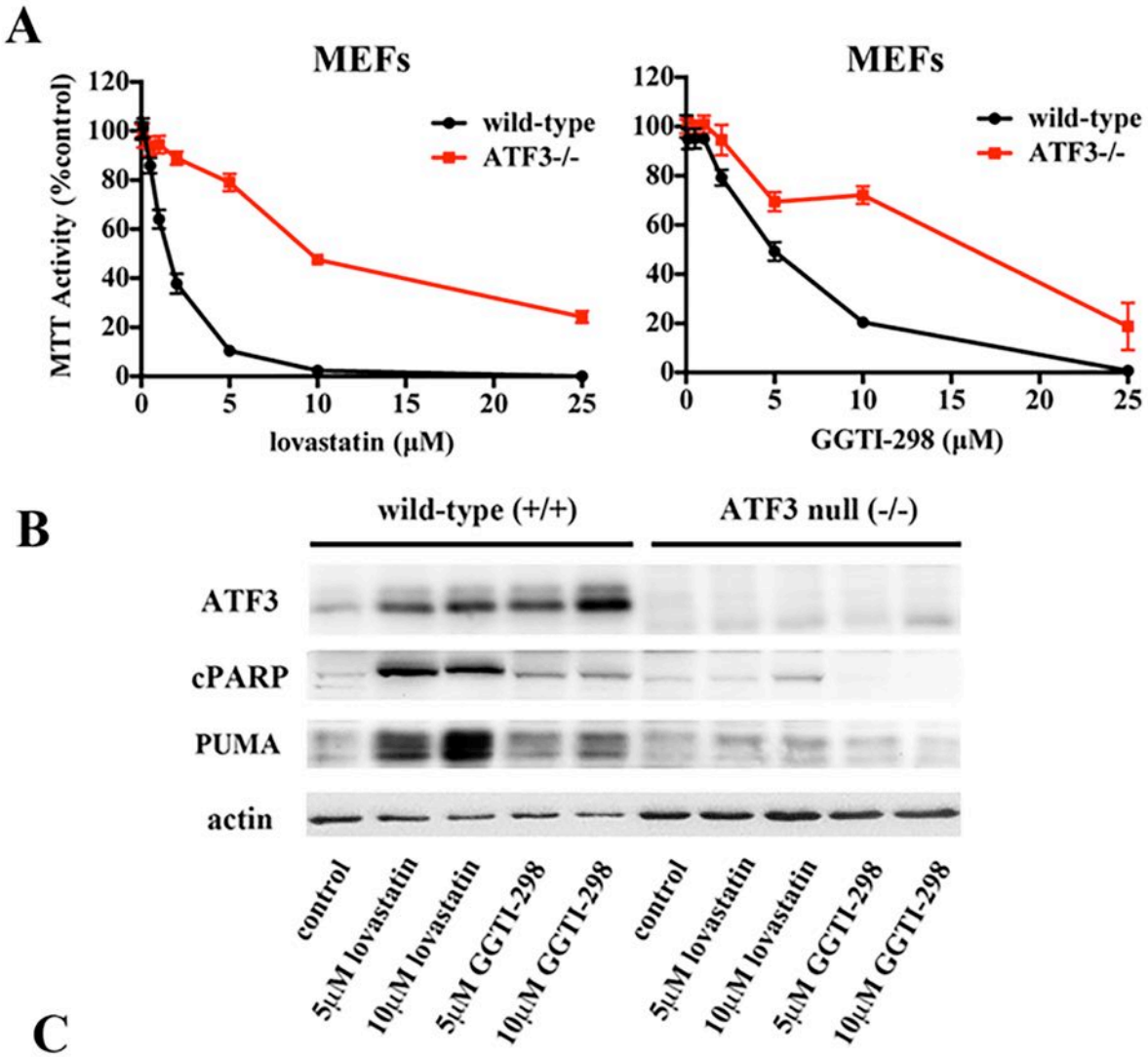
A
MEFs
wild-type
ATF3-/-
MTT Activity (%control)
lovastatin (μM)
GGTI-298 (μM)
B
wild-type (+/+)
ATF3 null (-/-)
ATF3
cPARP
PUMA
actin
control
5μM lovastatin
10μM lovastatin
5μM GGTI-298
10μM GGTI-298
C
wild-type+1μM lovastatin
ATF3-/- +1μM lovastatin
wild-type+5μM GGTI
ATF3-/- +5μM GGTI
tarceva (μM)

Conclusions

In this study, we first evaluated the effects of GGTI-298 on the metabolic stress pathways that regulate statin-induced cytotoxicity. GGTI-298 induced ATF3 expression in SCC9 and SCC25 and in a cohort of *ex vivo* tumor tissues from different solid malignancies. Importantly, ATF3 expression regulated both GGTI-298 cytotoxicity and its synergy with tarceva in HNSCC cells. Additionally, SCC9 sub-lines that were selected as resistant to GGTI-298 also failed to demonstrate synergy with GGTI-298 in combination with tarceva. In conclusion, these results suggest the potential clinical utility of combining GGTI inhibitor with tarceva in SCC patients as a novel and more refined combination therapeutic approach.

Alternatively, targeting GGPP synthase will deplete cellular pools of GGPP similar to statin treatment and could also represents a viable therapeutic target as well with the potential to more closely mimic the anticancer effects of statins and may show improved specificity and minimize off-target effects of GGTI treatment in HNSCC patients. In Chapter 4 we investigated the combinational effects of GGPP synthase inhibitor and EGFR-TKI in HNSCC.

CHAPTER 4: RESULTS

4. Geranylgeranyl diphosphate synthase as a Therapeutic Target: Enhancing Afatinib Activity in Squamous Cell Carcinoma

Lenah Mukhtar[1,2], Jennifer E. L. Hanson[1], David F. Wiemer[6], Raymond J. Hohl[7], Stephanie Johnson-Obaseki[3], Carolyn Nessim[4], Patrick J. Villeneuve[4], Glenwood D. Goss[1] and Jim Dimitroulakos[1,2*].

[1]Centre for Cancer Therapeutics at the Ottawa Hospital Research Institute; and [2]Faculty of Medicine and the Department of Biochemistry at the University of Ottawa, Ottawa, Ontario, Canada. [3]Departments of [3] Otolaryngology and [4]Surgery at the Ottawa Hospital, Ottawa, Ontario, Canada

[6]Department of Chemistry, University of Iowa, Iowa City, IA

[7]Penn State Cancer Institute, Hershey, PA

*Correspondence should be addressed to J.Dimitroulakos, E-mail: Jim.Dimitroulakos@rmp.uhn.ca

Key words: Geranylgeranyl diphosphate synthase, DGBP, EGFR, afatinib, Head and Neck Cancer, Non-Small Cell Cancer, mevalonate pathway

Contribution of Authors: L. Mukhtar performed all the reported experiments in this chapter, except Figure 4-6C, which was done by J. Hanson. L. Mukhtar wrote the manuscript with the help of J.Dimitroulakos. S. J-Obaseki, M. Odell, C. Nessim, P. Villeneuve, and D. Goss provided the *ex. vivo* tissues samples. D. Weiemer and R. Hohl provided the drug DGBP. Number of these figures are supplemental figures in the manuscript.

Final manuscript draft awaiting submission

Summary

Epidermal growth factor receptor (EGFR) drives growth and cell survival and is highly expressed in head and neck squamous cell carcinomas (HNSCC), representing a viable therapeutic target. Erlotinib (also known as tarceva), a first-generation, and afatinib (also known as gilotrif), a second-generation, EGFR inhibitors demonstrate limited activity as single agents in HNSCC. Combination therapies will be required to enhance their efficacy. Recently, we demonstrated that combining statins, inhibitors of the mevalonate pathway, with tarceva induced synergistic cytotoxicity through the induction of cellular stress responses regulated by the activating transcription factor 3 (ATF3). In our Phase I clinical trial combining rosuvastatin with tarceva, clinical activity was shown, but statin-induced myopathies limited the efficacy of this approach. In this study, we have demonstrated that depletion of geranylgeranyl diphosphate (GGPP), a downstream mevalonate metabolite, is responsible for both lovastatin and the specific GGPP synthase inhibitor, digeranyl bisphosphonate (DGBP)-induced cytotoxicity in squamous cell carcinoma (SCC) cells. We further demonstrated that both specific shRNA targeting of GGPP synthase, as well as the inhibitor DGBP, significantly enhances the cytotoxic activity of afatinib in SCC cells. DGBP as well as afatinib treatment induced ATF3 expression in SCC cells *in vitro* and in a cohort of *ex-vivo* tumor tissues. In addition, DGBP treatment induced apoptosis that is mediated through cleavage of apoptotic proteins caspase 3 and PARP. Co-administration of GGPP inhibits the induction of ATF3 and cytotoxicity associated with DGBP treatment. Furthermore, the synergistic cytotoxicity induced by the combinations of DGBP and afatinib in SCC cells was dependent on their enhanced expression of ATF3 in combination through the induction of cellular stress response pathways. This strategy suggests the potential clinical utility of combining GGPP synthase inhibitors with afatinib in SCC.

4.1 GGPP Reverses Lovastatin Induced Cytotoxicity

The co-administration of mevalonate rescues the cytotoxic effect of lovastatin (105). Herein, we expanded this biochemical add back approach by testing other downstream mevalonate metabolites in SCC and NSCLC cell lines employing the MTT (Figure 4.1A) and trypan blue exclusion cell viability assays (194) (Figure 4.1B). Cells were treated with varying concentrations of lovastatin (1-20μM for MTT or 10μM for trypan blue) alone, or with the combination of commercially available mevalonate metabolites (10μM GGPP or 100μM mevalonate) for 48hrs. In both assays, the exogenous addition of GGPP or mevalonate rescued the cytotoxic effect of lovastatin in the cell lines tested. The co-administration of both metabolites prevented lovastatin-induced cytotoxicity as cell viability remained to 90-100% (Figures 4.1A and B). These results demonstrated that the depletion of GGPP pools significantly contributes to the anti-tumor effects of lovastatin. Based on these results, we focused on the potential of targeting GGPP synthesis as a therapeutic approach to enhance EGFR targeted therapy.

Figure 4. 1 GGPP rescues lovastatin cytotoxicity in SCC and NSCLC cells.

(A) MTT cell viability assay of the co-administration of 100μM mevalonate or 10M GGPP in SCC (SCC9, SCC25, and HeLa) and NSCLC (A549, Calu6, and H23) cell lines following 48hrs of lovastatin treatment. (B) Trypan blue exclusion cell viability assay of SCC9, and SCC25 cell lines confirming the MTT assay after the add-back experiment. Cells were treated with control, 10μM lovastatin, 100μM mevalonate, 10μM GGPP, or the combination of 10μM lovastatin and 100μM mevalonate or 10μM lovastatin and 10μM GGPP for 72hrs. The error bars represent the standard deviation from the mean (±SD) of 3 biological replicates (n=3). Statistical significance was determined by two-way ANOVA with $P<0.05$ and with Bonferroni's post-hoc. Asterisks in the MTT graphs are determined to have a statistically significant difference when comparing the single treatment to the control treated cells or by comparing the combination drugs to a single drug for each cell line, while significant differences between column groups are displayed as P-values above the comparison.

P- value: *$P<0.05$, **$P<0.01$, ***$P<0.001$.

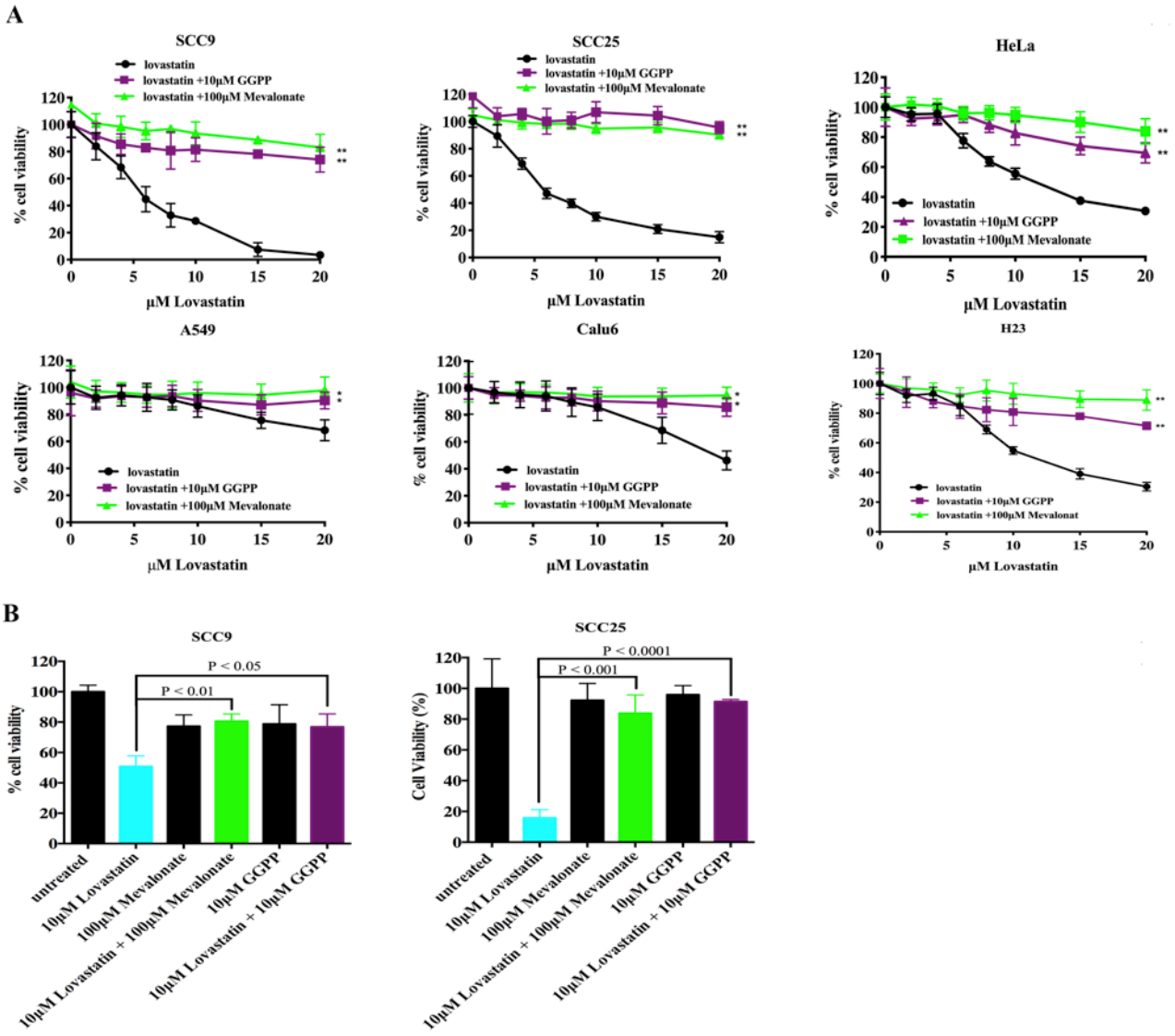
A
SCC9
lovastatin
lovastatin +10μM GGPP
lovastatin +100μM Mevalonate
% cell viability
μM Lovastatin
SCC25
HeLa
A549
Calu6
H23
B
SCC9
P < 0.05
P < 0.01
% cell viability
untreated
10μM Lovastatin
100μM Mevalonate
10μM Lovastatin + 100μM Mevalonate
10μM GGPP
10μM Lovastatin + 10μM GGPP
SCC25
P < 0.0001
P < 0.001
Cell Viability (%)

4.2 Inhibition of GGDPS Induces Cellular Cytotoxicity

We evaluated whether depletion of intracellular GGPP pools, by directly targeting GGPP synthase, mimics statin-mediated anti-tumor activities. We first expressed two distinct shRNA sequences specifically targeting the GGPP synthase gene (*GGDPS1*, GGDPS1-sh1 and GGDPS1-sh2) and GFP as a control using a doxycycline-inducible shRNA system to control shRNA expression in HeLa cells (Figure 4.2). We believe that an inducible expression system is required to ensure their consistent and robust inhibition, and to allow expansion of cells and to obtain stable clones in case knocking out impairs cells growth. Also as GGDPS enzyme plays important roles in maintaining cellular homeostasis (131,205), an inducible system without continuous expression of the shRNAs would be more appropriate in this context for analyzing their effects on EGFR activity. Stable clones were generated and tested for GGDPS1 knockdown following treatment with varying concentrations of doxycycline. Effective depletion of GGDPS1 protein levels were assessed by Western blot (Figure 4.2A) analyses. Unlike the control, GGDPS1 was downregulated at the protein level in a concentration-dependent manner following increasing doxycycline concentration after 48hrs (Figures 4.2A) with both shRNAs tested. Densitometric quantification of blotted GGDPS1 levels normalized to actin highlighted the reduction of GGDPS1 expression following doxycycline treatments (Figure 4.2B), with more than 70% reduction in the GGPP levels after 1000ng/ml doxycycline treatment. Next, the effect of knocking down GGPP synthase on HeLa tumor cell-sensitivity to afatinib was evaluated by MTT cell viability assay (Figure 4.2C). HeLa cells were pretreated with 1000ng/ml doxycycline for 48hrs followed by afatinib treatment for 72hrs. In both doxycycline-treated HeLa-GGDPS1-sh1 and -sh2 cells, the cytotoxic effects of afatinib were significantly enhanced (Figure 4.2C) demonstrating that targeting GGDPS augmented afatinib cytotoxicity. In the control HeLa-GFP cells, doxycycline treatment did not

significantly enhance the cytotoxic effect of afatinib (Figure 4.2D). To exclude the effect of doxycycline on cell viability, HeLa cells were treated with doxycycline series (100-2000ng/ml) for 96hrs; doxycycline treatment alone did not affect cell viability in these transfected cells (Figure 4.2D).

Figure 4. 2 Knockdown GGPDS in HeLa.

(A) HeLa cells stably expressing GFP as a control, GGDPS1-sh1 or GGDPS1-sh2 were treated with doxycycline series for 48hrs confirming the knockdown of GGDPS at protein level by Western blotting (triplicate biological replicates were performed in all cases). In both blots, actin was used as a loading control. (B) Densitometry analysis of GGDPS1 levels normalized to actin. (C) MTT cell viability demonstrating the effect of the addition of afatinib to doxycycline series in HeLa cells expressing GGDPS1-sh1 or GGDPS1-sh2. The addition of doxycycline enhanced the cytotoxic effect of afatinib treatments. (D) MTT cell viability demonstrating the effect of the addition of afatinib to doxycycline series in HeLa cells expressing GFP-sh. The addition of doxycycline did not significantly enhance the cytotoxic effect of afatinib treatments (Left). MTT cell viability demonstrating the effect of doxycycline series in HeLa cells expressing GFP-sh control or GGDPS1-sh1 or GGDPS1-sh2. Doxycycline did not affect the cell viability in these transfected cells (Right). The error bars represent the standard deviation from the mean (±SD) of 3 biological replicates (n=3). Statistical significance was determined by two-way ANOVA with $P<0.05$ and with Bonferroni's post-hoc. Asterisks in the MTT graphs are determined to have a statistically significant difference when comparing the single treatment to the control treated cells or by comparing the combination drugs to a single drug for each cell line, while significant differences between column groups are displayed as P-values above the comparison.

P- value: *$P<0.05$, **$P<0.01$, ***$P<0.001$.

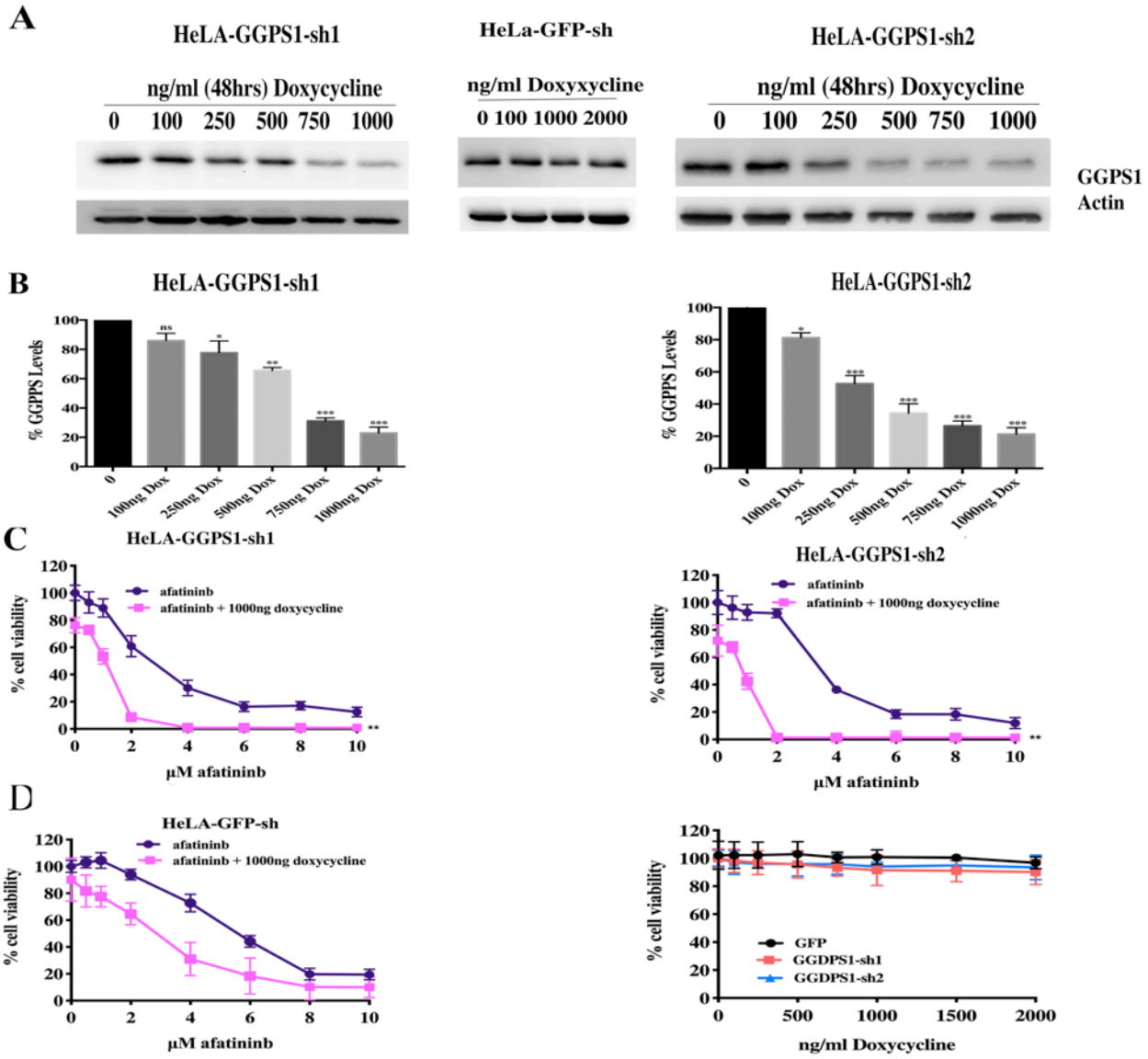
A
HeLA-GGPS1-sh1
ng/ml (48hrs) Doxycycline
0 100 250 500 750 1000
HeLa-GFP-sh
ng/ml Doxyxycline
0 100 1000 2000
HeLA-GGPS1-sh2
ng/ml (48hrs) Doxycycline
0 100 250 500 750 1000
GGPS1
Actin
B
HeLA-GGPS1-sh1
% GGPPS Levels
0
100ng Dox
250ng Dox
500ng Dox
750ng Dox
1000ng Dox
HeLA-GGPS1-sh2
C
HeLA-GGPS1-sh1
% cell viability
afatininb
afatininb + 1000ng doxycycline
µM afatininb
HeLA-GGPS1-sh2
D
HeLA-GFP-sh
GFP
GGDPS1-sh1
GGDPS1-sh2
ng/ml Doxycycline

As a therapeutic approach, digeranyl bisphosphonate (DGBP) specifically inhibits the activity of GGDPS thus resulting in depletion of GGPP cellular pools (134,135). Herein, we evaluated the potential of DGBP as a more clinically relevant therapeutic approach to enhance the activity of afatinib. The anticancer effects of DGBP have been previously reported as a single agent in a limited set of tumor cell lines (131,135,138,140,206). Initially, we specifically tested the sensitivity of SCC and NSCLC cells in contrast to the normal human fibroblast (WI-38) cell line to DGBP using MTT cell viability assay following 72hrs treatment. In this analysis, we demonstrated that DGBP induces cytotoxicity in SCC and NSCLC cells in a concentration-dependent manner (Figure 4.3). Varying sensitivities were observed in SCCs, where SCC25 were most sensitive, SCC9 and HeLa were moderately sensitive; NSCLC cells were relatively resistant, while WI-38 cells were not affected (Figure 4.3).

Figure 4. 3 MTT assay evaluating DGBP cytotoxicity in SCC and NSCLC cells.

(A) MTT assay and IC50 calculations evaluating the cytotoxicity of SCC (SCC9, SCC25, and HeLa) and WI-38 cell lines after treating the cells with DGBP series for 72hrs. (B) MTT assay and IC50 calculations evaluating the cytotoxicity of NSCLC (H23, HCC4006, HCC827, and HCC1975) cell lines after treating the cells with DGBP series for 72hrs. WI-38 are resistant to the cytotoxic effects of DGBP.

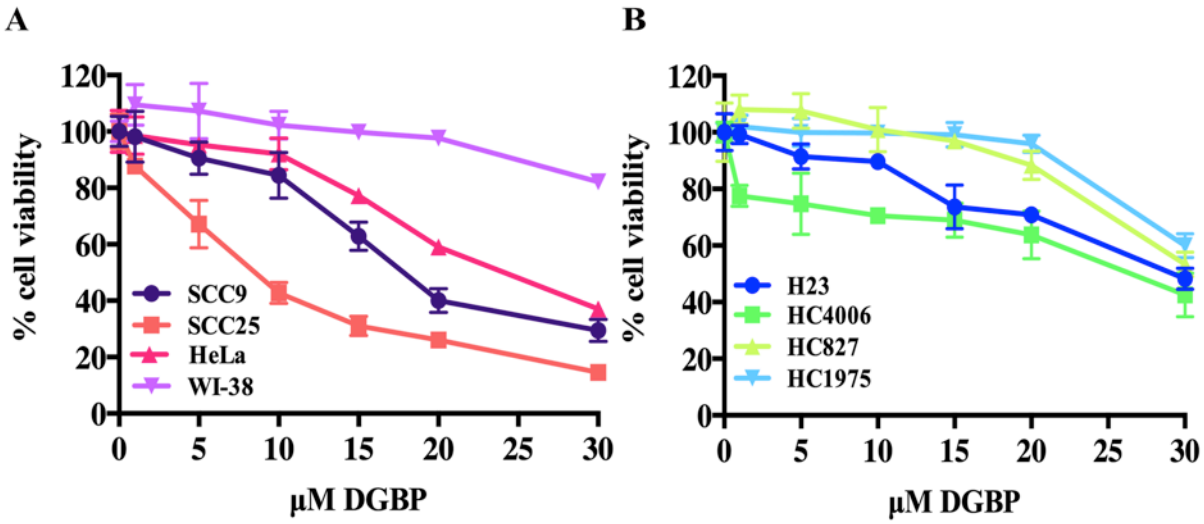

Cell	IC50 (µM DGBP)
SCC9	17.63
SCC25	7.76
HeLa	23.89
WI-38	N/A

Cell	IC50 (µM DGBP)
H23	29.13
HCC4006	27.4
HCC827	30.77
HCC1975	42.56

To confirm target specificity with these DGBP treatment, biochemical add-back experiments with GGPP co-administration were performed to assess its effects on DGBP induced cytotoxicity in these SCC cells using both MTT cell viability and trypan blue exclusion assays (194) (Figure 4.4A and B). SCC cells were treated with varying concentrations of DGBP (1-30μM DGBP) in the presence or absence of exogenous 10μM GGPP for 72hrs. Co-treatment with GGPP prevented the cytotoxic effects of DGBP, with cell viability remaining at approximately 100% as determined by MTT assay (Figure 4.4A). For trypan blue exclusion assay, cells were treated with solvent control, 20μM DGBP, 10μM GGPP, or the combination of 20μM DGBP and 10μM GGPP for 72hrs. In concert with the MTT assay, the addition of GGPP negated the cytotoxic effects of DGBP (Figure 4.4B). These results demonstrated the importance of GGPP cellular pool depletion as a key regulator of DGBP-induced cytotoxicity.

To further assess the specificity of DGBP to targeting GGDPS, we evaluated its ability to target the GGPP modification of Rap1 and RhoA proteins, which play significant roles in gene expression and actin cytoskeleton reorganization, respectively (135,140). Since the inhibition of GGPP can cause the accumulation of FPP, which is the substrate for Ras protein farnesylation, we evaluated DGBP effects on Ras protein as well. The pan-Ras antibody recognizes both farnesylated and non-farnesylated forms of Ras protein, and the inhibition of Ras farnesylation is usually indicated by the appearance of an upper-slower migrating band (135). Using Western blotting, the effect of inhibiting protein geranylgeranylation with DGBP was evaluated in these SCC cell lines. Western blot analysis of Rap1 and RhoA proteins confirmed their induction along with a slight shift in gel mobility for Rap1 following DGBP treatment indicative of the absence of their prenylation (Figure 4.4C).

The upregulation and mobility shift are associated with lack of geranylgeranylation in a number of studies (121), where lack of GGPP modification can result in mobility shifts due to the lack of protease cleavage of three terminal amino acids (-aax) following GGPP addition, where Rap1 show a slight shift in the mobility on the gel following DGBP treatment. This mobility shift was not clearly seen in RhoA. Similarly to a recent study (138), we found treatment with 20μM DGBP for 48hrs increased expression of Rap1 and RhoA in SCC cells (Figure 4.4C). As expected, DGBP did not affect the farnesylation or expression of Ras protein (Figure 4.4C). These changes in protein expression were reversed by the addition of exogenous 10μM GGPP (Figure 4.4C). These results were supported by a graphical representation of densitometric quantification of 3 independently performed biological replicates as shown in the appendix (Figure S5) in which RAP1, RhoA and pan-Ras levels were normalized to actin levels. Although our data showed the induction of Rap1 and RhoA expression, these proteins remain inactive due to their lack of GGPP, as our previous study and a recent report by Agabiti *et al* suggested that the induction of RhoA or Rac1 by lovastatin or DGBP resulted in inactive RhoA or Rac1 protein, respectively (105,138). This confirmed DGBP ability to inhibit the geranylgeranylation of small-GTPase proteins such as Rap1 and RhoA, but not the farnesylation of Ras, through the depletion of cellular GGPP pools.

Next, to determine whether DGBP has preferential effects on the viability of malignant versus normal cells, we tested lovastatin and DGBP activities on normal human fibroblast (WI-38) cells. Using MTT assay, WI-38 were treated either with lovastatin series (1-10μM) for 48hrs or DGBP series (1-30μM) for 72hrs with or without GGPP metabolite (Figures 4. 5A and B). In contrast to the pattern observed after lovastatin treatment (Figure 4.5A), DGBP treatment did not show significant effects on cell viability (Figure 4.5B). Similar data were obtained using trypan

blue exclusion assay (194) (Figure 4.5A and B) where lovastatin decreased cell viability in WI-38, while DGBP not, indicating DGBP affects only cancer cells not the normal cells.

Figure 4. 4 The effect of biochemical add back GGPP on DGBP in SCC cells.

(A) MTT analysis demonstrating the co-administration of exogenous 10μM GGPP to DGBP series showing rescuing in the cytotoxic effect of DGBP in SCC cell lines. (B) The biochemical add-back experiment was further assessed employing trypan blue exclusion assay and showed the addition of exogenous 10μM GGPP prevented the cytotoxicity of 20μM DGBP in SCC cell lines. The error bars represent the standard deviation from the mean (±SD) of 3 biological replicates (n=3). Statistical significance was determined by two-way ANOVA with $P<0.05$ and with Bonferroni's post-hoc. Asterisks in the MTT graphs are determined to have a statistically significant difference when comparing the single treatment to the control treated cells or by comparing the combination of drugs to a single drug for each cell line, while significant differences between column groups are displayed as P- values above the comparison. P- value: *$P<0.05$, **$P<0.01$, ***$P<0.001$. (C) Representative Western blot demonstrating the induction of Rap1 and RhoA expression, but not Ras protein, in SCC cell lines following treatment with 20μM DGBP. The addition of exogenous 10μM GGPP returned the expression levels of Rap1 and RhoA to the basal level. Expression levels of actin were assayed as the loading control for total protein normalization. The quantification of the band intensities is found in appendix S5. The error bars represent the standard deviation from the mean (±SD) of 3 biological replicates (n=3). Statistical analysis was performed by one-way ANOVA using the Bonferroni multiple comparison test. P- value: *$P<0.05$, **$P<0.01$.

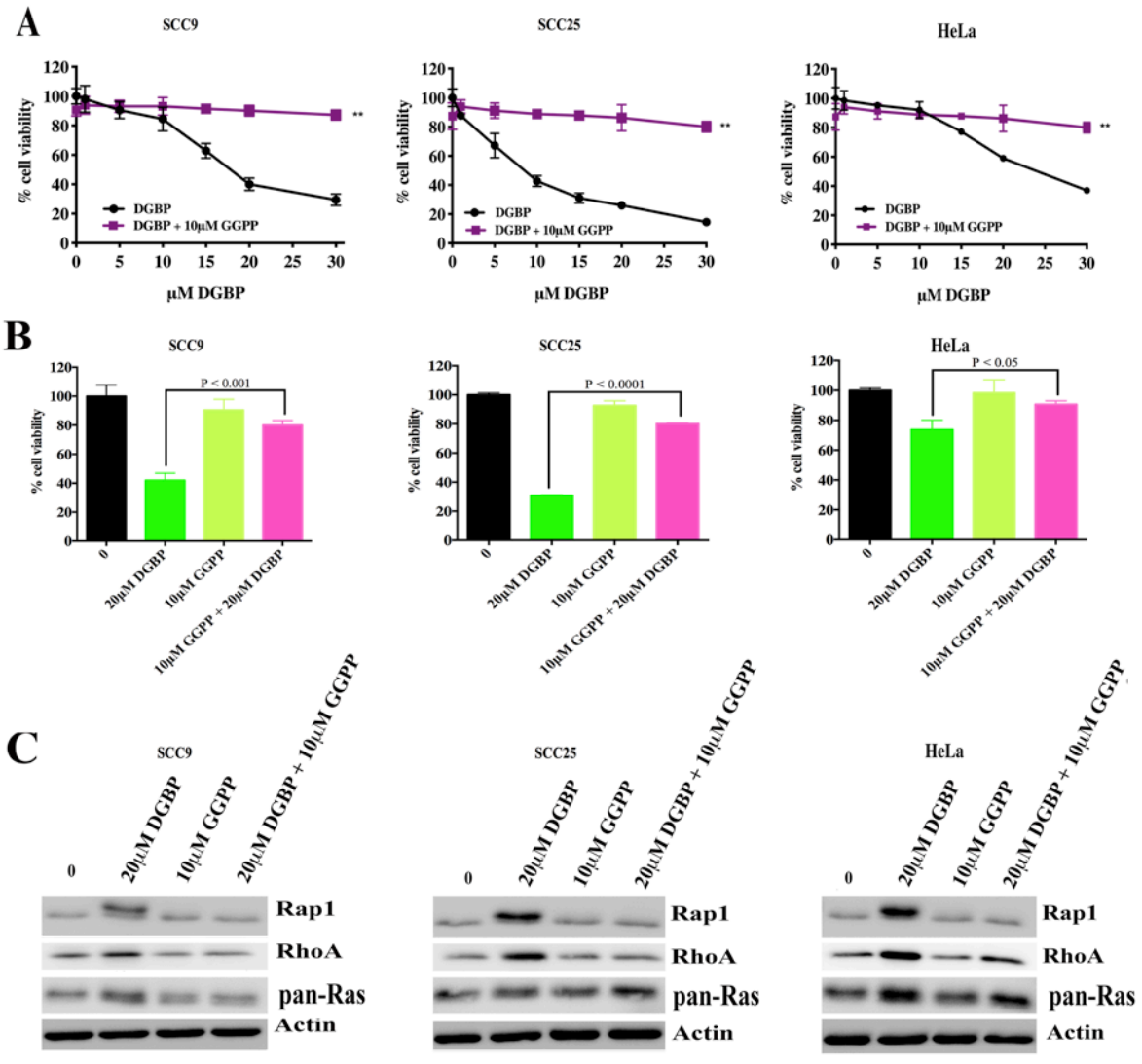
A
SCC9
SCC25
HeLa
% cell viability
DGBP
DGBP + 10μM GGPP
**
μM DGBP
B
SCC9
SCC25
HeLa
P < 0.001
P < 0.0001
P < 0.05
% cell viability
0
20μM DGBP
10μM GGPP
10μM GGPP + 20μM DGBP
C
SCC9
SCC25
HeLa
0
20μM DGBP
10μM GGPP
20μM DGBP + 10μM GGPP
Rap1
RhoA
pan-Ras
Actin

Figure 4. 5 Comparison between lovastatin and DGBP effects on the human normal fibroblast.

(A) MTT and trypan blue exclusion cell viability assays of the co-administration of 100μM mevalonate or 10μM GGPP in WI-38 cell line following 48hrs of lovastatin treatments. (B) MTT and trypan blue exclusion cell viability assays of the co-administration of 10μM GGPP in WI-38 cell line following 72hrs of DGBP treatments. The error bars represent the standard deviation from the mean (±SD) of 2 biological replicates (n=2). Statistical significance was determined by two-way ANOVA with $P<0.05$ and with Bonferroni's post-hoc. Asterisks in the MTT graphs are determined to have a statistically significant difference when comparing the single treatment to the control treated cells or by comparing the combination of drugs to a single drug for each cell line, while significant differences between column groups are displayed as P-values above the comparison.

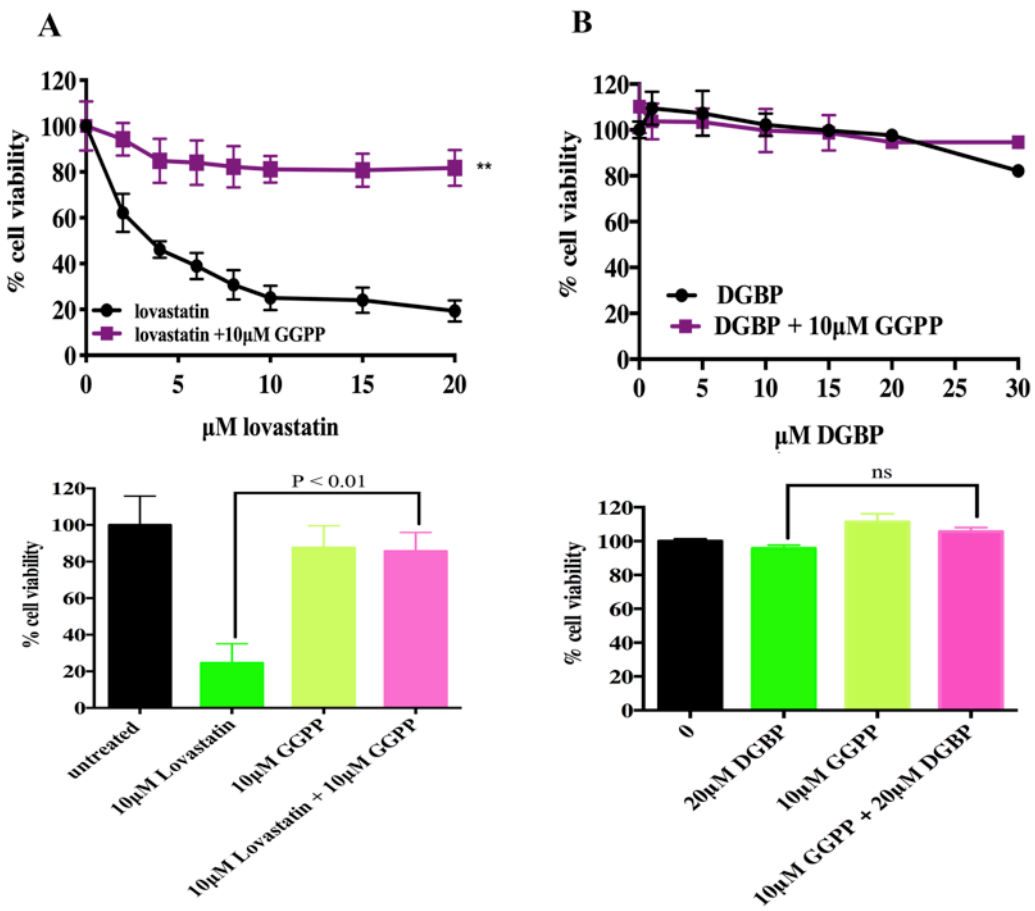
WI-38
A
% cell viability
120
100
80
60
40
20
0
0
5
10
15
20
lovastatin
lovastatin +10µM GGPP
**
µM lovastatin
% cell viability
P < 0.01
untreated
10µM Lovastatin
10µM GGPP
10µM Lovastatin + 10µM GGPP
B
% cell viability
DGBP
DGBP + 10µM GGPP
0
5
10
15
20
25
30
µM DGBP
% cell viability
ns
0
20µM DGBP
10µM GGPP
10µM GGPP + 20µM DGBP

4.3 ATF3 is the Key Role for DGBP Cytotoxicity

In our recent reports, we identified ATF3 as a key regulator of lovastatin-mediated cytotoxicity in SCC cells (109,166,183,191). To assess the role of ATF3 in regulating the cytotoxicity of DGBP, we evaluated the ability of DGBP to induce ATF3 expression by Western blotting in SCC9 and SCC25 following treatment with varying concentrations of DGBP (1- 30μM DGBP) for 48hrs and 72hrs (Figure 4.6A). ATF3 expression was up regulated in both cell lines in both a time- and concentration-dependent manner (Figure 4.6A). The up regulation of ATF3 was accompanied by an increase in the levels of cleaved PARP (cPARP), a marker of cellular apoptosis in both cell lines (Figure 4.6A). These results were supported by a graphical representation of densitometric quantification of 3 independently performed biological replicates as shown in the appendix (Figure S6) in which ATF3 and cPARP levels were normalized to actin and PARP levels, respectively, confirming the upregulation of these proteins following DGBP treatment.

Next, we evaluated the ability of afatinib to induce ATF3 expression by Western blotting in SCC9 and SCC25 following treatment of the cells with varying concentrations of afatinib (1-10μM afatinib) for 48hrs (Figure 4.6B). ATF3 expression was up regulated in both cell lines, and this induction also occurred in a concentration-dependent manner (Figure 4.6B). The up regulation of ATF3 was accompanied by an increase in the levels of cleaved PARP (Figure 4.6B). These results were supported by a graphical representation of densitometric quantification of 3 independently performed biological replicates as shown in the appendix (Figure S7) in which ATF3 and cPARP levels were normalized to actin and PARP levels, respectively, confirming the upregulation of these proteins following afatinib treatment.

Figure 4. 6 The effects of DGBP and afatinib on ATF3 expression in SCC cells.

(A) Representative Western blot analysis demonstrating the up regulation of ATF3, and cPARP expression in SCC9 and SCC25 following 48hrs and 72hrs treatments with DGBP series (1-30μM). The quantification of the band intensities is found in appendix S6. The error bars represent the standard deviation from the mean (±SD) of 3 biological replicates (n=3). Statistical analysis was performed by one-way ANOVA using the Bonferroni multiple comparison test. *P<0.05, **: p≤0.01. (B) Representative Western blot analysis demonstrating the up regulation of ATF3, and cPARP expression in SCC9 and SCC25 following 48hrs with afatinib series (1-10μM). In all blots, actin is used as a loading control. The quantification of the band intensities is found in appendix S7. The error bars represent the standard deviation from the mean (±SD) of 3 biological replicates (n=3). Statistical analysis was performed by one-way ANOVA using the Bonferroni multiple comparison test. *P<0.05, **: p≤0.01.

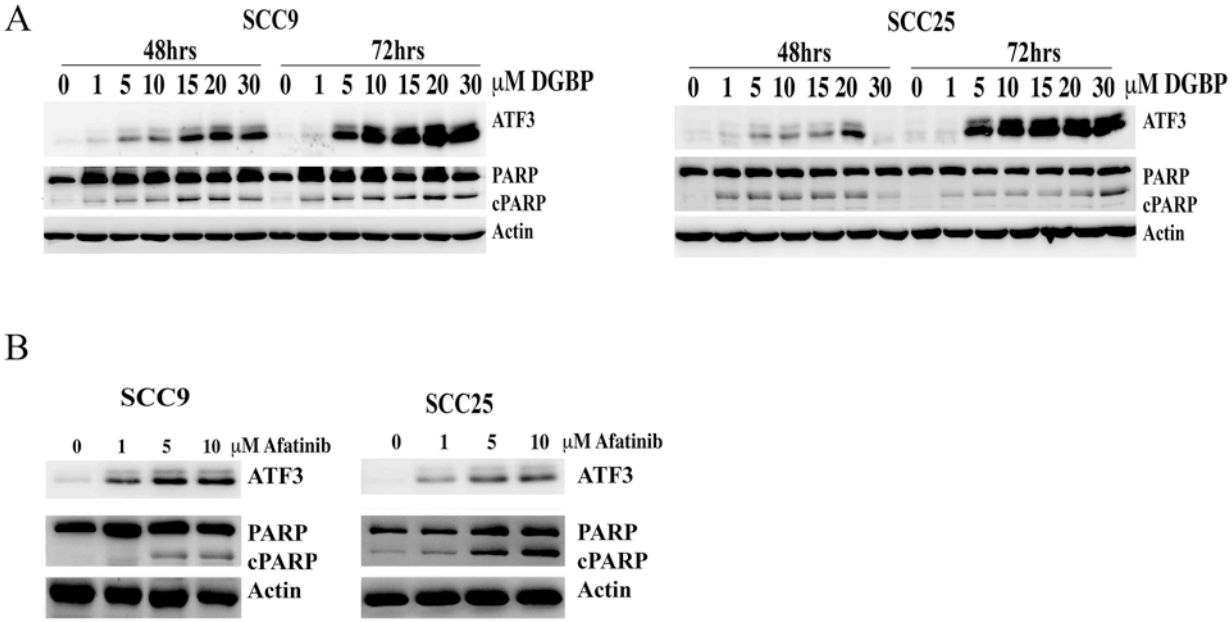
A
SCC9
48hrs
72hrs
0 1 5 10 15 20 30 0 1 5 10 15 20 30 μM DGBP
ATF3
PARP
cPARP
Actin
SCC25
48hrs
72hrs
0 1 5 10 15 20 30 0 1 5 10 15 20 30 μM DGBP
ATF3
PARP
cPARP
Actin
B
SCC9
0 1 5 10 μM Afatinib
ATF3
PARP
cPARP
Actin
SCC25
0 1 5 10 μM Afatinib
ATF3
PARP
cPARP
Actin

In addition to SCC, we have also evaluated ATF3 expression in NSCLC adenocarcinoma cells following treatments with DGBP and afatinib by Western blot. In NSCLC cell lines (H23, HCC4006, and HCC827), ATF3 expression was induced in these NSCLC cells following treatment with either drug (10μM afatinib or 20μM DGBP) similarly to the positive control (2μg cisplatin), which is a known ATF3 inducer. ATF3 induction was accompanied by the cleavage of the apoptotic marker PARP (Figure 4.7A). These results were supported by a graphical representation of densitometric quantification of 3 independently performed biological replicates as shown in the appendix (Figure S8) in which ATF3 and cPARP levels were normalized to actin and PARP levels, respectively, confirming the upregulation of these proteins following DGBP and afatinib treatment.

To evaluate the potential of DGBP and afatinib to induce ATF3 mRNA expression in a more clinically relevant model, we assessed *ex-vivo* tumor tissues from 3 HNSCC (HN01-03) and 2 NSCLC (LU01-02) patients that underwent surgery at our Institute. Tissue samples were processed (183) following surgical excision into 2x1mm slices, randomized with 3 tissue slices evaluated per treatment and analyzed by quantitative RT- PCR performed in triplicate. In the *ex-vivo* tissue samples evaluated, 4 of 5 treated patient samples showed greater than 1.5-fold induction of ATF3 mRNA levels following 48hrs treatment with 50μM DGBP or 25μM afatinib (Figure 4.7B). Taken together, these data demonstrate that both DGBP and afatinib treatments induce ATF3 expression in ex-vivo tumor samples and SCC cell lines.

Figure 4. 7 The effects of DGBP and afatinib on ATF3 expression in NSCLC cells.

(A) Representative Western blot analysis demonstrating the up regulation of ATF3, and cPARP expression in H23, HCC4006, and HCC827 NSCLC cells following 48hrs treatment with DGBP or afatinib, or 24hrs treatment with 2μg cisplatin. In all blots, actin is used as a loading control. The quantification of the band intensities is found in appendix S8. The error bars represent the standard deviation from the mean (±SD) of 3 biological replicates (n=3). Statistical analysis was performed by one-way ANOVA using the Bonferroni multiple comparison test. *P<0.05, **: p≤0.01. (B) Quantitative RT-PCR analysis of ATF3 mRNA expression following solvent control, 50μM DGBP and 25μM afatinib in surgically excised *ex-vivo* tissues from 3 HNSCC (HN) and 2 NSCLC (LU) patients. Fold changes were calculated following normalization to *gapdH* levels (ΔΔCt) and expressed as means (±SD). The error bars represent SD from the mean (±SD) of 3 biological replicates (n=3).

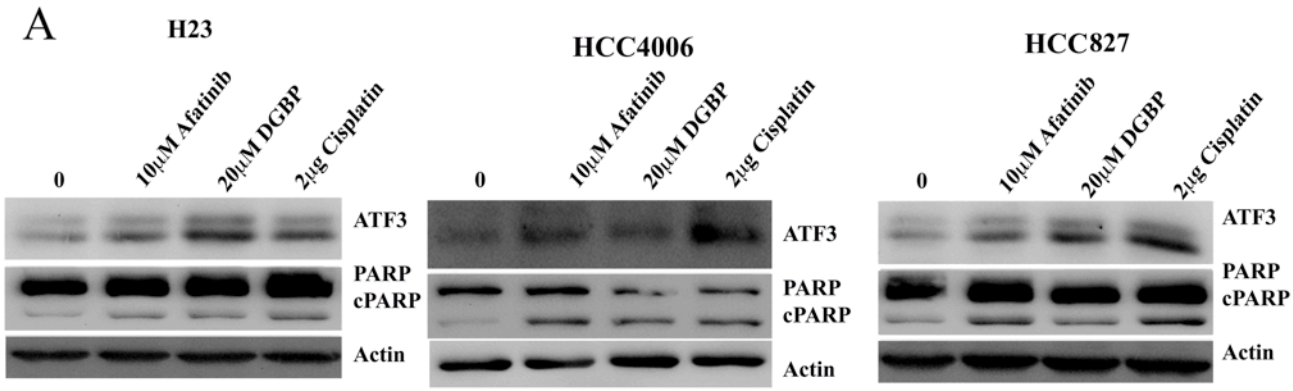
A
H23
HCC4006
HCC827
0
10μM Afatinib
20μM DGBP
2μg Cisplatin
ATF3
PARP
cPARP
Actin

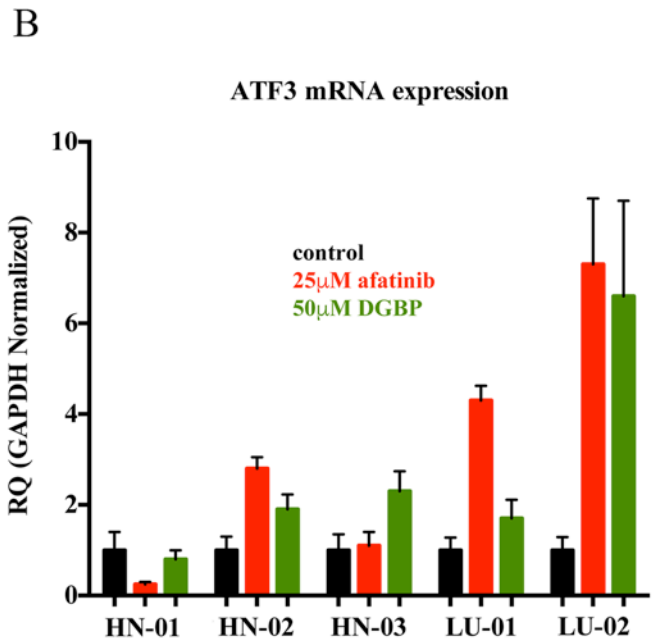
B
ATF3 mRNA expression
RQ (GAPDH Normalized)
10
8
6
4
2
0
control
25μM afatinib
50μM DGBP
HN-01
HN-02
HN-03
LU-01
LU-02

To confirm the importance of ATF3 in mediating the cytotoxicity of DGBP, we employed ATF3 knockout mouse embryonic fibroblasts (ATF3-/- MEFs) and their respective wild-type (WT MEFs) counterparts. We evaluated ATF3 expression levels by Western blotting following DGBP treatment (1- 30μM DGBP) for 48hrs. ATF3 expression was up regulated in the WT MEFs and was also associated with increased cPARP which was attenuated in the ATF3-/- counterparts (Figure 4.8A). These results were supported by a graphical representation of densitometric quantification of 3 independently performed biological replicates as shown in the appendix (Figure S9) in which ATF3 and cPARP levels were normalized to actin and PARP levels, respectively, confirming the upregulation of these proteins in the wild type in contrast to the ATF3 null MEFs.

Caspase activation is a hallmark of the induction of apoptosis (207). Caspases regulate apoptosis through targeted degradation of cellular apoptotic proteins PARP (207). To confirm the cytotoxic effects of DGBP resulted from increased apoptosis, the cleavage of caspase3 was evaluated by Western blotting in WT and ATF3-/- MEFs (Figure 4.8B). DGBP markedly increased ATF3 expression, cleaved PARP and cleaved caspase3 at 20μM following 48hrs. Interestingly, ATF3 expression, cPARP, and c-caspase3 activation were diminished by the co-incubation with 10μM GGPP in WT MEFs, while attenuated in the ATF3-/- MEFs (Figure 4.8B). These results were supported by a graphical representation of densitometric quantification of 3 independently performed biological replicates as shown in the appendix (Figure S10) in which ATF3, cPARP and cCaspase3 levels were normalized to actin, PARP, and Caspase3 levels, respectively confirming the involvement of GGPP inhibition in the apoptotic effects of the DGBP. Taken together, ATF3 is a novel mediator for DGBP cytotoxicity.

Next, to confirm the role of GGPP depletion in the cytotoxic and apoptotic effects of DGBP, the cleavage of both PARP and caspase3 were evaluated by Western blotting in SCC cells

(Figure 4.9). DGBP markedly increased ATF3 expression, cleaved PARP and cleaved caspase3 at 20μM following 72hrs, and the addition of GGPP prevented the expression of these proteins (Figure 4.9). These results were supported by a graphical representation of densitometric quantification of 3 independently performed biological replicates as shown in the appendix (Figure S11) in which ATF3, cPARP and cCaspase3 levels were normalized to actin, PARP, and Caspase3 levels, respectively. These results confirmed the involvement of GGPP in the apoptotic effects of DGBP, where lack of GGPS1 causes depletion of cellular GGPP pool, and that causes the apoptotic effect of DGBP.

Figure 4. 8 ATF3 is a key regulator of DGBP activity.

(A) Representative Western blot analysis demonstrating the up regulation of ATF3, and cPARP expression in WT and ATF3 null MEFs following 48hrs treatment with DGBP series (1-30μM). The quantification of the band intensities is found in appendix S9. The error bars represent the standard deviation from the mean (±SD) of 3 biological replicates (n=3). Statistical analysis was performed by one-way ANOVA using the Bonferroni multiple comparison test. *P<0.05, **: p≤0.01. (B) Representative Western blot demonstrating the induction of ATF3, cPARP, and caspase3 expression in WT and ATF3 null MEFs cell lines following the treatment of 20μM DGBP. The addition of exogenous 10μM GGPP returned the expression levels of ATF3, cPARP, and caspase3 to the basal level. Expression levels of actin were assayed as the loading control. The quantification of the band intensities is found in appendix S10. The error bars represent the standard deviation from the mean (±SD) of 3 biological replicates (n=3). Statistical analysis was performed by one-way ANOVA using the Bonferroni multiple comparison test. *P<0.05, **: p≤0.01.

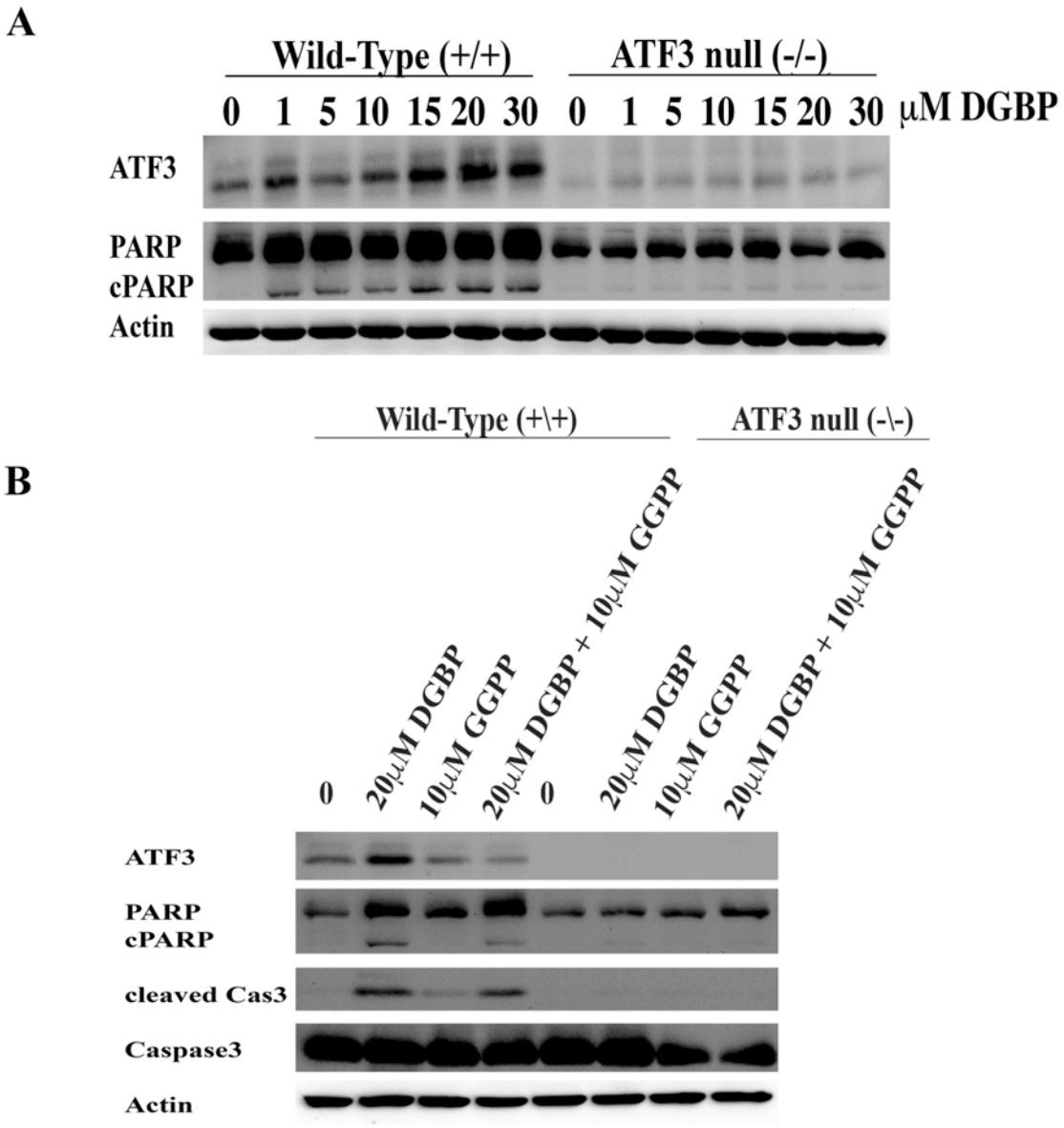
A
Wild-Type (+/+)
ATF3 null (-/-)
0 1 5 10 15 20 30 0 1 5 10 15 20 30 μM DGBP
ATF3
PARP
cPARP
Actin
B
Wild-Type (+\+)
ATF3 null (-\-)
0
20μM DGBP
10μM GGPP
20μM DGBP + 10μM GGPP
0
20μM DGBP
10μM GGPP
20μM DGBP + 10μM GGPP
ATF3
PARP
cPARP
cleaved Cas3
Caspase3
Actin

Figure 4. 9 Add back GGPP prevented DGBP apoptotic effects in SCC cells.

Representative Western blot demonstrating the induction of ATF3, cPARP, and caspase3 expression in SCC cell lines following treatment with 20μM DGBP. The addition of exogenous 10μM GGPP returned the expression levels of ATF3, cPARP, and caspase3 to the basal level. Expression levels of actin were assayed as the loading control. The quantification of the band intensities is found in appendix S11. The error bars represent the standard deviation from the mean (±SD) of 3 biological replicates (n=3). Statistical analysis was performed by one-way ANOVA using the Bonferroni multiple comparison test. *P<0.05, **: p≤0.01.

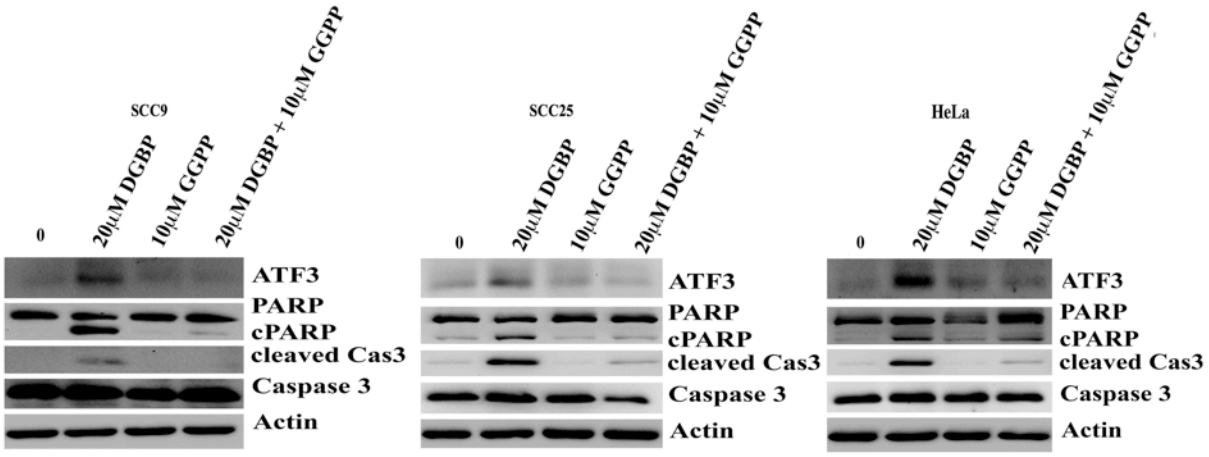
SCC9
SCC25
HeLa
0
20μM DGBP
10μM GGPP
20μM DGBP + 10μM GGPP
ATF3
PARP
cPARP
cleaved Cas3
Caspase 3
Actin

4.4 DGBP Induces ATF3 Through the Activation of the ISR Signaling Pathway

We evaluated the role of ATF3 and the integrated stress response (ISR) pathway, (an important inducer of ATF3 expression), as potential mediators of DGBP induced cytotoxicity. Previously, we demonstrated that lovastatin treatment of SCC cells induces ATF3 expression through the ISR via activation of GCN2 (general control nonderepressible 2), leading to the expression of ATF4, ATF3, and CHOP, which regulate the induction of apoptosis by the ISR (147,150,166). In this study, we employed knockout mouse embryonic fibroblast models (GCN2-/-, ATF4-/-, and CHOP-/-MEFs) and compared them to the wild-type and ATF3-/- MEFs to evaluate the role of the ISR as potential regulators of DGBP- or afatinib- induced ATF3 expression and cytotoxicity. Treatment of wild-type MEFs with DGBP (1-30μM) or afatinib (1-10μM) resulted in the up regulation of ATF3 and cleavage of PARP that was attenuated in MEFs lacking GCN2-/-, ATF4-/- and ATF3-/-. As expected, the levels of ATF3 were not affected in CHOP-/- MEFs as CHOP is downstream of ATF3 in this pathway (166) (Figure 4.10A). These results were supported by a graphical representation of densitometric quantification of 3 independently performed biological replicates as shown in the appendix (Figures S12-S15) in which ATF3 and cPARP levels were normalized to actin and PARP levels, respectively, confirming the upregulation of these proteins in the wild type in contrast to the other null MEFs.

Next, we evaluated the cytotoxic effects of DGBP and afatinib in these MEFs using an MTT cell viability assay (Figure 4.10B). This series of MEFs were treated with DGBP (1-30μM) and afatinib (1-10μM) for 48hrs. Following these treatments, wild-type MEFs demonstrated enhanced sensitivity to both drugs, compared to the null MEFs tested (GCN2, ATF4, ATF3, and CHOP) (Figure 4.10B). These results were confirmed using trypan blue exclusion assays and by comparing responses to either vehicle control or 20μM DGBP (for 72hrs) or 5μM afatinib (for

48hrs) (Figure 4.10C). Taken together, these results demonstrated that activation of the ISR pathway mediates the cytotoxicity of both DGBP and afatinib through the activation of GCN2, ATF4, ATF3, and CHOP; this drives cellular induced apoptosis.

Figure 4. 10 DGBP and afatinib induce ATF3 through the ISR Pathway.

(A) Representative Western blot demonstrating ATF3 induction following DGBP and afatinib treatment in WT and GCN2, ATF4, and CHOP null MEFs (triplicate biological replicates were performed in all cases). In all blots, actin is used as a loading control. Figure 4-8A was reproduced here in Figure 4-10A for comparison to the other cell lines and for convenience to the reader. The quantification of the band intensities is found in appendices S12, S13, S14, and S15. The error bars represent the standard deviation from the mean (±SD) of 3 biological replicates (n=3). Statistical analysis was performed by one-way ANOVA using the Bonferroni multiple comparison test. *P<0.05, **: p≤0.01. (B) MTT assay comparing the responses of WT and all null MEFs following treatments of the cells with either DGBP series or afatinib series. (C) Trypan blue exclusion cell viability assay of WT and all null MEFs cell lines, where cells were treated with control, 20μM DGBP, or 5μM afatinib for 48hrs. The error bars represent the standard deviation from the mean (±SD) of 2 biological replicates (n=2). Statistical significance was determined by two-way ANOVA with P<0.05 and with Bonferroni's post-hoc. Asterisks in the MTT graphs are determined to have a statistically significant difference when comparing the wile type to the null MEFs, while significant differences between column groups are displayed as P-values above the comparison.

P- value: *P<0.05, **P<0.01, ***P<0.001.

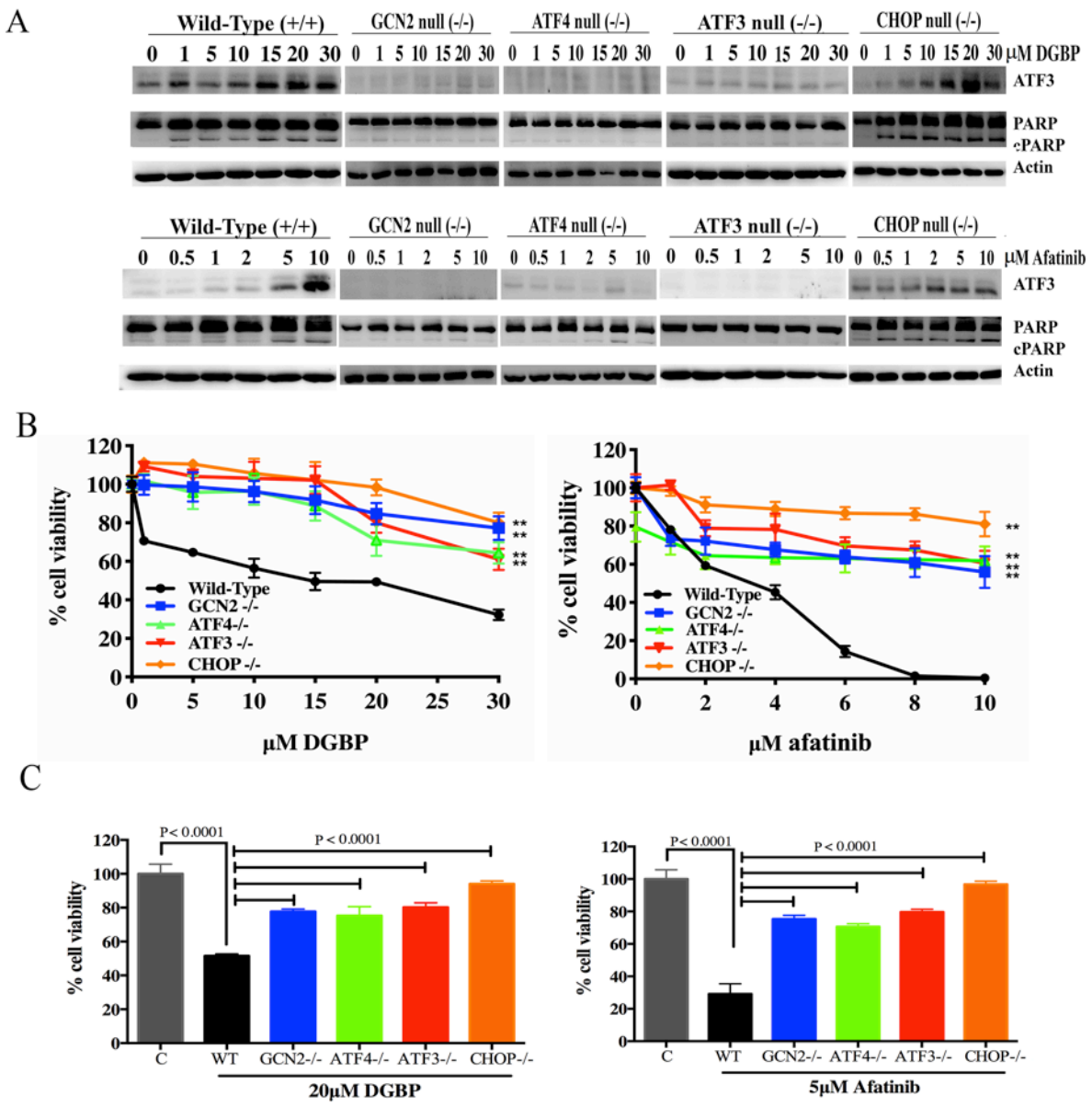
A
Wild-Type (+/+)
GCN2 null (-/-)
ATF4 null (-/-)
ATF3 null (-/-)
CHOP null (-/-)
0 1 5 10 15 20 30 µM DGBP
ATF3
PARP
cPARP
Actin
0 0.5 1 2 5 10 µM Afatinib
B
% cell viability
Wild-Type
GCN2 -/-
ATF4-/-
ATF3 -/-
CHOP -/-
µM DGBP
µM afatinib
C
P< 0.0001
P < 0.0001
C
WT
GCN2-/-
ATF4-/-
ATF3-/-
CHOP-/-
20µM DGBP
5µM Afatinib

4.5 DGBP Synergistically Enhances Afatinib Cytotoxicity

In our recent work, we identified that lovastatin and tarceva induced synergistic cytotoxicity in SCC cells that was dependent on ATF3 expression (109,166). Our goal in this study is to identify more specific agents that enhance EGFR-TKIs activity without the toxicities associated with high-doses statin used in our clinical trial (110). First, the sensitivity of afatinib was tested on SCC, NSCLC, and WI-38 cell lines using MTT cell viability assay following 48hrs treatment (Figure 4.11). From this analysis, we found that afatinib induces cytotoxic effects in SCC cells in a concentration-dependent manner, where SCC9 and SCC25 were sensitive, HeLa were moderately sensitive (because they have less EGFR gene compared to SCC9 and SCC25), while WI-38 were resistant (Figure 4.11A). The NSCLC HCC4006 and HCC827 cell lines were highly sensitive (Figure 4.11B); HCC1975 were moderately sensitive, while H23 were resistant (Figure 4.11C).

Next, we evaluated the sensitivity of SCC cell lines to the combination of DGBP with afatinib by MTT assay. Cells were treated with afatinib (1-10μM) for 48hrs either alone or with 20μM DGBP pre-treatment (24hrs) in combination for a total of 72hrs (Figure 4.12A). We demonstrated that the addition of DGBP enhances the cytotoxic effects of afatinib in the SCC cell lines tested (Figure 4.12A). Next, employing MTT after pre-treating SCC with DGBP series (1-30μM) for 24hrs following by the addition of 5μM afatinib for 48hrs, we observed similar results to those previously observed where the addition of afatinib enhanced the cytotoxicity of DGBP in SCC (Figure 4.12B). The enhanced cytotoxicity of this combination was confirmed by trypan blue exclusion cell viability assay. SCC cells were treated with control, 5μM afatinib or 20μM DGBP alone or in combination for 72hrs and the average number of the viable cells was calculated from 3 independent biological experiments. The results show that in all SCC cell lines tested, the

combination of DGBP with afatinib was significantly better at inhibiting cell viability than either drug alone (Figure 4.12C).

To determine the nature of this combination, the Chou-Talalay analysis was employed to determine if the cytotoxic effect of DGBP and afatinib in combination was either an additive, synergistic, or antagonistic interaction. Fraction affected (from cell viability) plots were generated to show the combination index (CI) (Figure 4.12D). In all 3 SCC cell lines, the combination of DGBP and afatinib demonstrated a reduction in the cell viability as determined by MTT assay which was synergistic (Figure 4.12D). The same experiments of (Figure 4.12) were replicated on the NSCLC cell lines (H23, HCC4006, and HCC827); where the sensitivity of NSCLC cell lines to the combination of DGBP with afatinib was evaluated by both MTT and trypan blue exclusion assays (Figure 4.13). NSCLC cells were treated with afatinib (0.001-10μM) for 48hrs either alone or with 20μM DGBP pre-treatment (24hrs) in combination for a total of 72hrs (Figure 4.13A). The addition of DGBP augments the cytotoxic effects of afatinib in the NSCLC cell lines tested (Figure 4.13A). Next, employing MTT after pre-treating NSCLC with DGBP series (1-30μM) for 24hrs followed by the addition of 5μM afatinib (for H23) or 0.05μM (for HCC4006 and HCC827) for 48hrs resulted in similar effects to those observed in SCC cells, where the addition of afatinib enhanced the cytotoxicity of DGBP in NSCLC (Figure 4.13B). The enhanced cytotoxicity of this combination was confirmed by trypan blue exclusion cell viability assay. NSCLC cells were treated with control, 5μM afatinib (for H23) or 0.05μM (for HCC4006 and HCC827), or 20μM DGBP alone or in combination for 72hrs and the average number of the viable cells was calculated from 3 independent biological experiments. The results show that in all NSCLC cell lines tested, the combination of DGBP with afatinib was significantly better at inhibiting cell viability than either drug alone (Figure 4.13C).

Next, the Chou-Talalay analysis was used to determine if the cytotoxic effect of DGBP and afatinib in combination was either additive, synergistic, or antagonistic interactions. In all 3 NSCLC cell lines, the combination of DGBP and afatinib demonstrated that the reduction in the cell viability as determined by MTT assay was synergistic (Figure 4.13D). Taken together, the combination of afatinib with DGBP showed enhanced cytotoxicity and decreased viability in all mentioned cell lines compared to either agent alone (Figure 4.13).

Figure 4. 11 MTT assay evaluating afatinib cytotoxicity in SCC and NSCLC cells.

(A) MTT assay and IC50 calculations evaluating cytotoxicity of SCC (SCC9, SCC25, and HeLa) and WI-38 cell lines after treating the cells with afatinib series for 48hrs. (B) MTT assay evaluating cytotoxicity of NSCLC (HCC4006 and HCC827) cell lines after treating the cells with afatinib series for 48hrs. (C) MTT assay evaluating cytotoxicity of NSCLC (H23 and HCC1975) cell lines after treating the cells with afatinib series for 48hrs. Note that lower concentrations of afatinib were used in HCC4006 and HCC827 as these cells were highly sensitive to afatinib. The error bars represent the standard deviation from the mean (±SD) of 3 biological replicates (n=3).

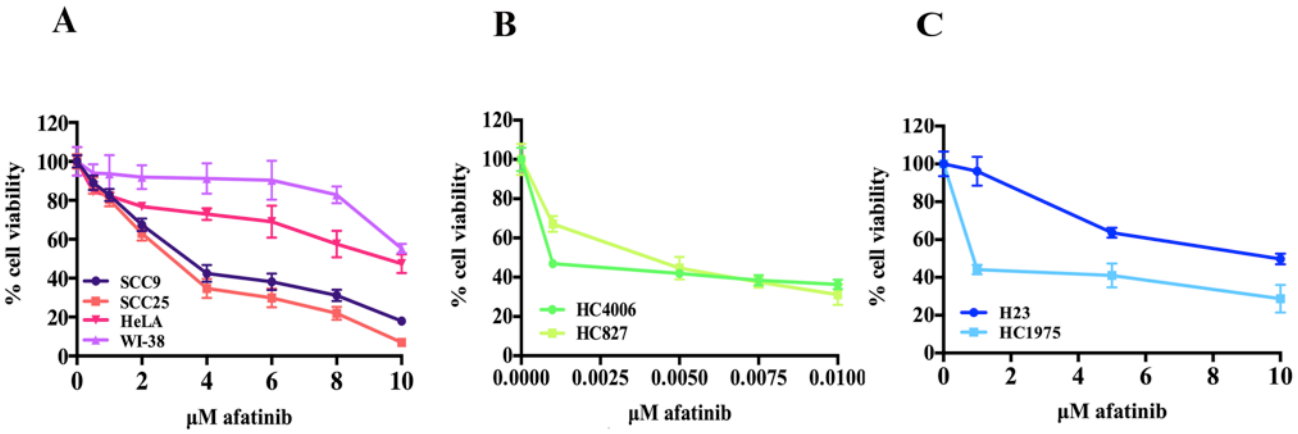

Cell	IC50 (µM Afatinib)
SCC9	3.6
SCC25	2.87
HeLa	9.45
WI-38	10.98

Cell	IC50 (µM Afatinib)
HCC827	0.0033
HCC4006	1.65x10-4

Cell	IC50 (µM Afatinib)
H23	9.08
HCC1975	0.95

Figure 4. 12 The synergistic relationship between DGBP and afatinib in SCC cells.

(A) MTT analysis demonstrating the cytotoxicity of the combination of afatinib and 20μM DGBP in SCC cell lines. Cells were treated with either afatinib series (0.001-10μM) alone for 48hrs or pretreated with 20μM DGBP for 24hrs following by afatinib series for further 48hrs a total of 72hrs. (B) MTT analysis demonstrating the cytotoxicity of the combination of DGBP and 5μM afatinib in SCC cell lines. Cells were treated with either DGBP series (1-30μM) alone for 72hrs or pre-treated with DGBP series for 24hrs following the addition of 5μM afatinib for further 48hrs a total of 72hrs. (C) Trypan blue exclusion cell viability confirming the enhancement of the combination of DGBP and afatinib effects compared to each agent alone. The error bars represent the standard deviation from the mean (±SD) of 3 biological replicates (n=3). Statistical significance was determined by two-way ANOVA with $P<0.05$ and with Bonferroni's post-hoc. Asterisks in the MTT graphs are determined to have a statistically significant difference when comparing the single treatment to the control treated cells or by comparing the combination drugs to a single drug for each cell line, while significant differences between column groups are displayed as P-values above the comparison. P- value: *$P<0.05$, **$P<0.01$, ***$P<0.001$. (D) Fraction Affected/ Combination Index Plots determined by MTT analysis of cell viability show the synergistic effect of DGBP (1-30μM, 24hr pre-treatment) in combination with 5μM afatinib for a total of 72hs in SCC cell lines. Combination Indices (CI) <1 are considered synergistic, CI >1 are considered antagonistic, and CI=1 are considered additive.

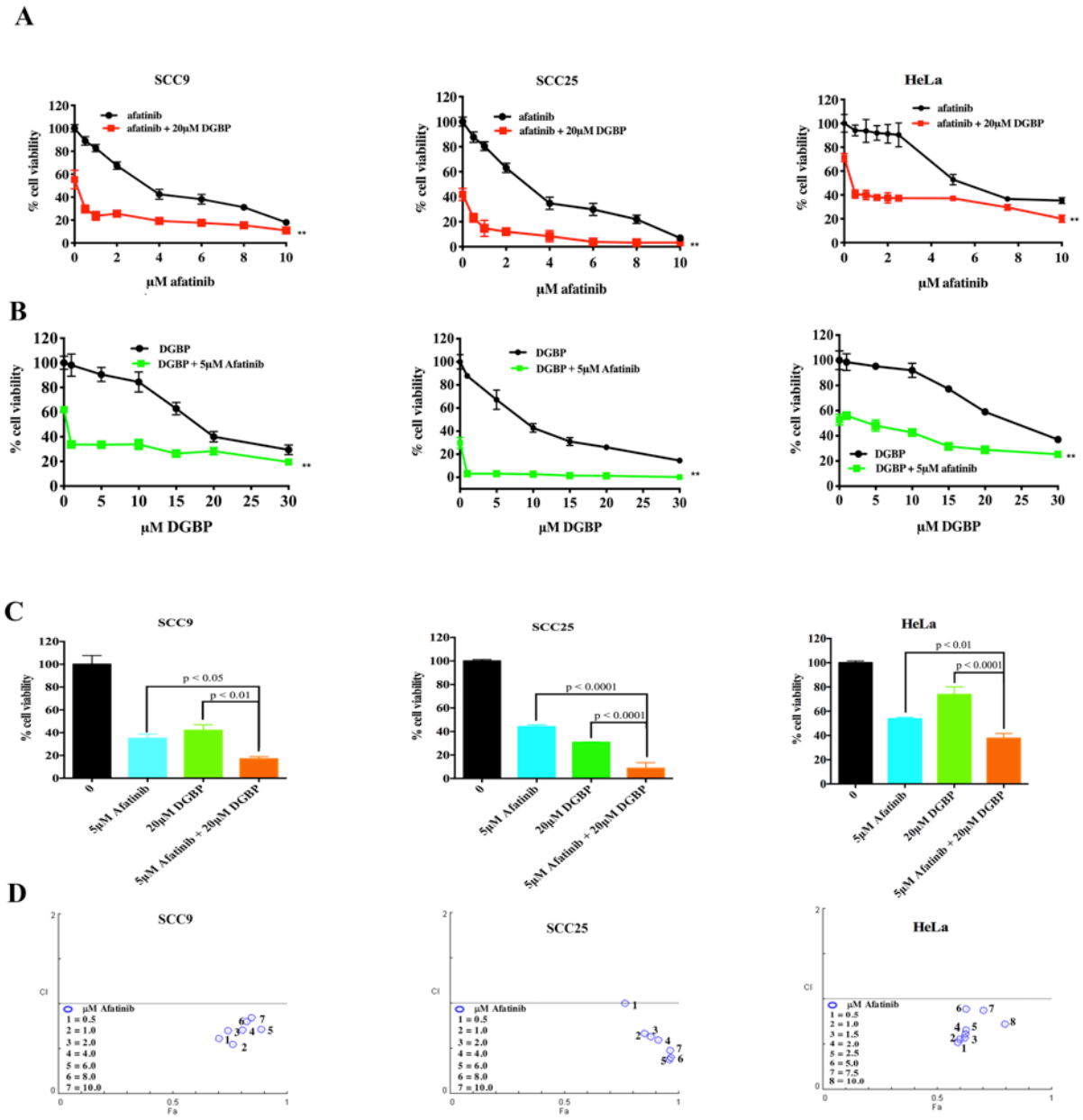
A
SCC9
SCC25
HeLa
% cell viability
afatinib
afatinib + 20μM DGBP
μM afatinib
B
DGBP
DGBP + 5μM Afatinib
DGBP + 5μM afatinib
μM DGBP
C
p < 0.05
p < 0.01
p < 0.0001
0
5μM Afatinib
20μM DGBP
5μM Afatinib + 20μM DGBP
D
CI
Fa
μM Afatinib
1 = 0.5
2 = 1.0
3 = 2.0
4 = 4.0
5 = 6.0
6 = 8.0
7 = 10.0
1 = 0.5
2 = 1.0
3 = 1.5
4 = 2.0
5 = 2.5
6 = 5.0
7 = 7.5
8 = 10.0

Figure 4. 13 The synergistic relationship between DGBP and afatinib in NSCLC cells.

(A) MTT analysis demonstrating the cytotoxicity of the combination of afatinib and 20μM DGBP in NSCLC cell lines. Cells were treated with either afatinib series (0.001-10μM) alone for 48hrs or pretreated with 20μM DGBP for 24hrs followed by afatinib series for a further 48hrs for a total of 72hrs. (B) MTT analysis demonstrating the cytotoxicity of the combination of DGBP and 5μM afatinib (for H23) or 0.05μM (for HCC4006 and HCC827). Cells were treated with either DGBP series (1-30μM) alone for 72hrs or pre-treated with DGBP series for 24hrs following the addition of 5μM (for H23) or 0.05μM (for HCC4006 and HCC827) afatinib for a further 48hrs for a total of 72hrs. (C) Trypan blue exclusion cell viability confirmed the enhancement of the combination of DGBP and afatinib effects compared to each agent alone. The error bars represent the standard deviation from the mean (±SD) of 3 biological replicates (n=3). Statistical significance was determined by two-way ANOVA with $P<0.05$ and with Bonferroni's post-hoc. Asterisks in the MTT graphs are determined to have a statistically significant difference when comparing the single treatment to the control treated cells or by comparing the combination drugs to a single drug for each cell line, while significant differences between column groups are displayed as P-values above the comparison. P- value: *$P<0.05$, **$P<0.01$, ***$P<0.001$. (D) Fraction Affected/ Combination Index Plots determined by MTT analysis of cell viability show the synergistic effect of DGBP (1-30μM, 24hr pre-treatment) in combination with 5μM afatinib for a total of 72hs in NSCLC cell lines. Combination Indices (CI) <1 are considered synergistic, CI >1 are considered antagonistic, and CI=1 are considered additive.

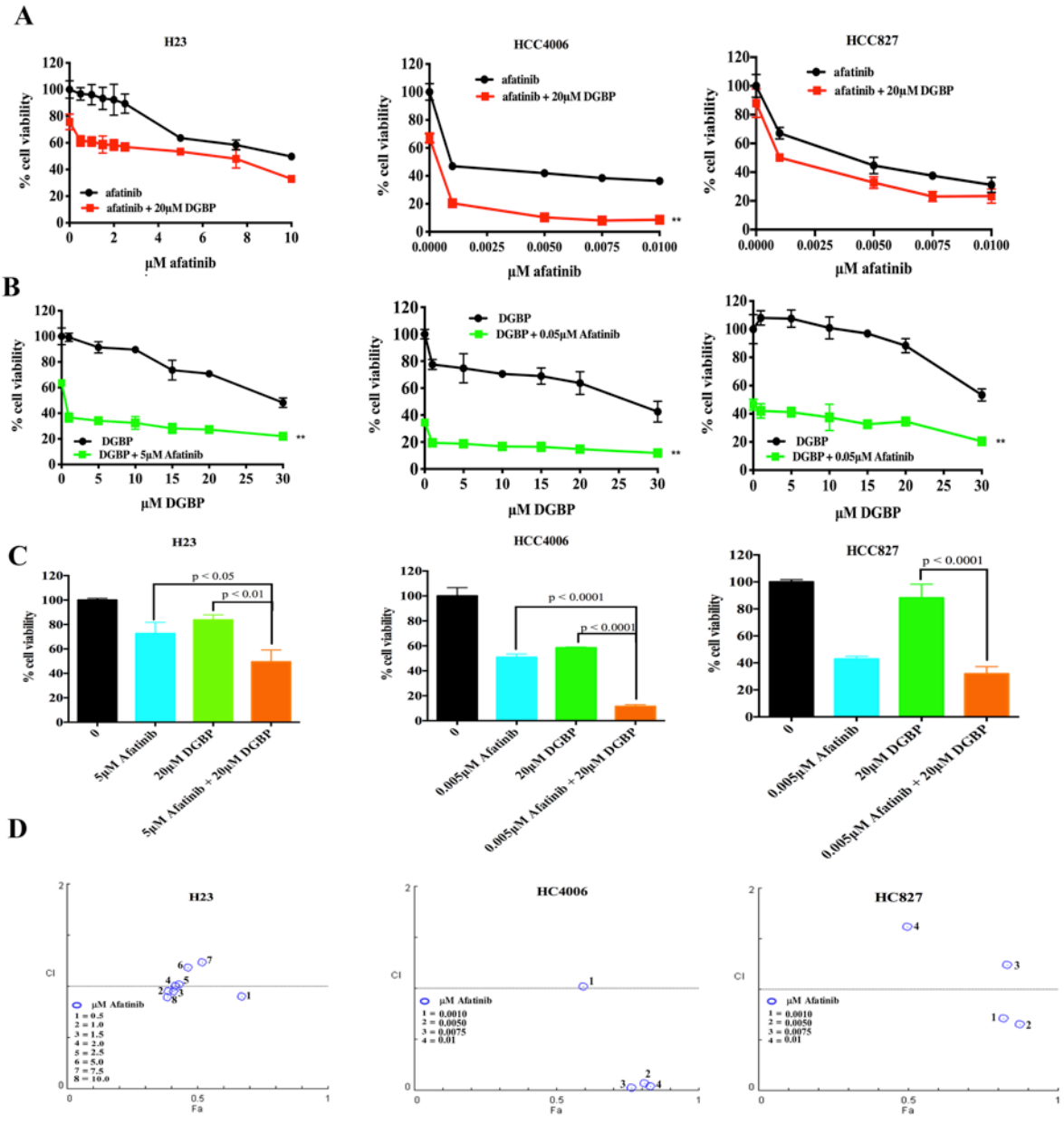
A
H23
HCC4006
HCC827
% cell viability
afatinib
afatinib + 20μM DGBP
μM afatinib
B
DGBP
DGBP + 5μM Afatinib
DGBP + 0.05μM Afatinib
μM DGBP
C
p < 0.05
p < 0.01
p < 0.0001
0
5μM Afatinib
20μM DGBP
5μM Afatinib + 20μM DGBP
0.005μM Afatinib
0.005μM Afatinib + 20μM DGBP
D
CI
Fa
μM Afatinib

We then evaluated the potential role of the ISR, and in particular ATF3, as mediators of the synergy between DGBP and afatinib combination treatments. Elevated and sustained expression of ATF3 can drive cellular apoptosis and combining ATF3 inducing-agents may enhance their cytotoxicity (12, 15). SCC9 and SCC25 cells were treated with afatinib (1, 5, 10μM) for 48hrs either alone or in combination with 20μM DGBP for a total of 72hrs. DGBP treatments enhanced ATF3 induction by afatinib in both cell lines, and this induction was accompanied by the enhancement in the levels of cPARP (Figure 4.14A). These results were supported by densitometric quantification shown in the appendix (Figure S16 and S17) in which ATF3 and cPARP levels normalized to actin and PARP levels, respectively, confirming the upregulation of these proteins following DGBP and afatinib combinational treatment.

Using WT and ATF3 null MEFs, we also evaluated the potential of adding 20μM DGBP (24hrs pre-treatment) to enhance the cytotoxicity of 48hrs afatinib (0.5-10μM) treatment by employing the MTT assay. Significant enhancement in afatinib cytotoxicity was observed only in the WT but not in the ATF3-/- null MEFs after the addition of DGBP (Figure 4.14B). These MTT results were confirmed using Trypan blue exclusion assay where following treatment with solvent control, 5μM afatinib and 20μM DGBP alone or in combination for 72hrs; the average number of viable cells was calculated from 2 independent experiments. As seen in Figure 4.14C, synergistic inhibitory effects were seen on cell viability using the drugs combination, while non-significant effects were observed in ATF3-/- cells regardless of drug treatment. Taken together, these results demonstrate ATF3 as a mediator of DGBP and afatinib-mediated cytotoxicity and importantly as a mediator of DGBP and afatinib synergistic cytotoxicity.

Figure 4. 14 The addition of DGBP enhances afatinib-induction of ATF3 in SCC cells.

(A) Representative Western blot analysis of SCC9 and SCC25 demonstrating ATF3 and cPARP expressions following the combination treatment of DGBP and afatinib for 72hrs, where the addition of 20μM DGBP to afatinib series (1-10μM) enhances ATF3 expression. In all blots, actin is used as a loading control. Afatinib treatment alone as shown in Figure 4-6B is shown again here in Figure 4-14A for comparison purposes and for convenience to the reader to assess the levels of induction of ATF3 expression and PARP cleavage following afatinib alone vs. the combination of afatinib and DGBP. The quantification of the band intensities is found in appendices S16 and S17. The error bars represent the standard deviation from the mean (±SD) of 3 biological replicates (n=3). Statistical analysis was performed by one-way ANOVA using the Bonferroni multiple comparison test. *P<0.05, **: p≤0.01. (B) MTT analysis of wild-type and ATF3-/- MEFs following 48hrs treatment with afatinib with or without a 24hr pre-treatment with 20μM DGBP. (C) Trypan blue exclusion assay confirming the enhancement of the combination of DGBP and afatinib effects compared to each agent alone in the WT only. The error bars represent the standard deviation from the mean (±SD) of 2 biological replicates (n=2). Statistical significance was determined by two-way ANOVA with P<0.05 and with Bonferroni's post-hoc. Asterisks in the MTT graphs are determined to have a statistically significant difference when comparing the single wile type to the ATF3 null MEFs, while significant differences between column groups are displayed as P-values above the comparison.

P- value: *P<0.05, **P<0.01, ***P<0.001.

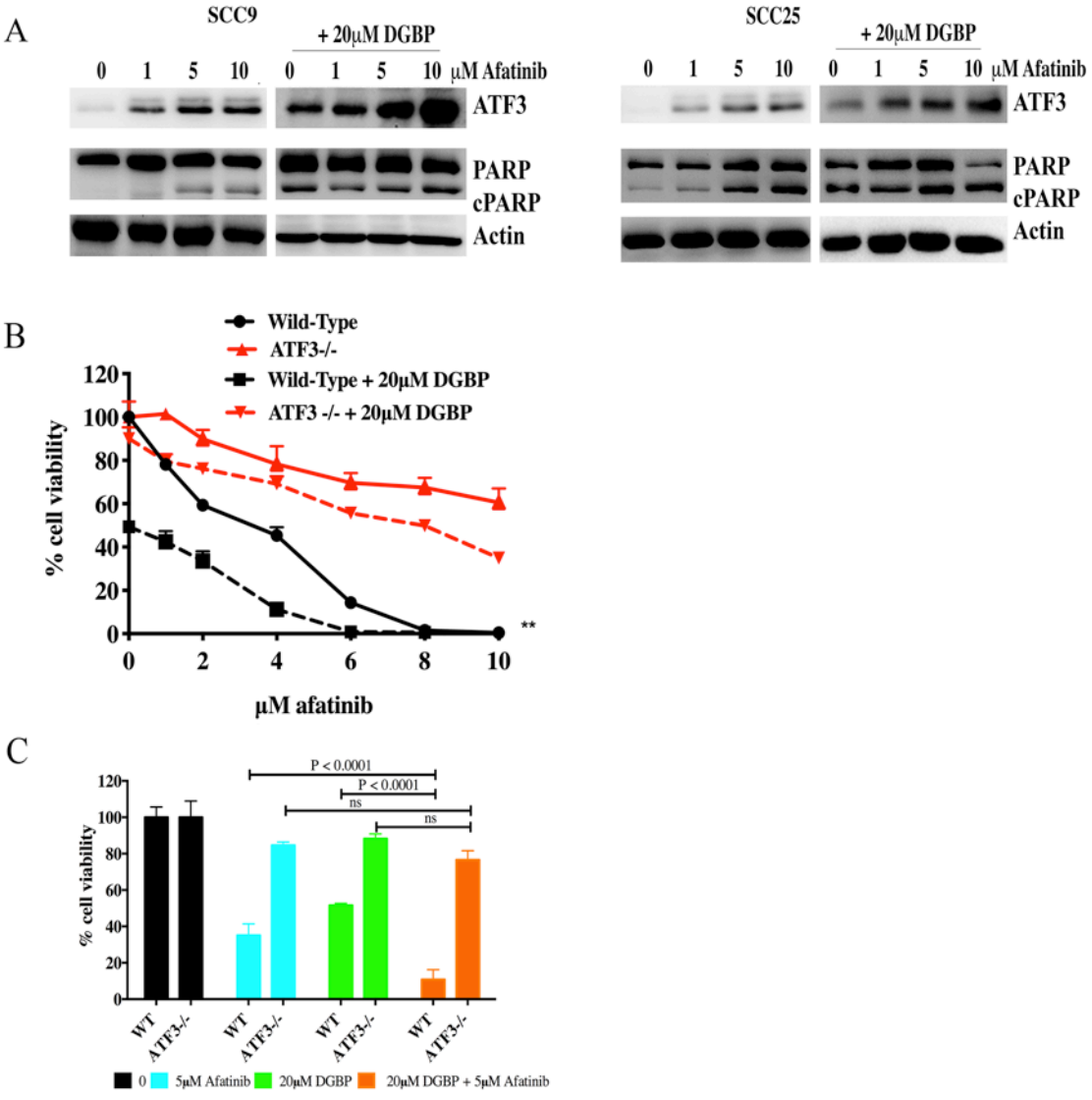
A
SCC9
+ 20μM DGBP
0 1 5 10 0 1 5 10 μM Afatinib
ATF3
PARP
cPARP
Actin
SCC25
+ 20μM DGBP
0 1 5 10 0 1 5 10 μM Afatinib
ATF3
PARP
cPARP
Actin
B
Wild-Type
ATF3-/-
Wild-Type + 20μM DGBP
ATF3 -/- + 20μM DGBP
% cell viability
120
100
80
60
40
20
0
0 2 4 6 8 10
μM afatinib
**
C
% cell viability
P < 0.0001
P < 0.0001
ns
ns
WT
ATF3-/-
0 5μM Afatinib 20μM DGBP 20μM DGBP + 5μM Afatinib

Conclusions

In this study, we evaluated the effect of targeting GGPP synthase on afatinib cytotoxicity, where we demonstrated that DGBP significantly enhances the cytotoxic activity of afatinib in SCC and NSCLC cells. DGBP as well as afatinib treatment induced ATF3 expression in SCC and NSCLC cells *in vitro* and in a cohort of *ex-vivo* tumor tissues. We also showed that the co-administration of GGPP inhibited the induction of ATF3 and the cytotoxic and apoptotic effects associated with DGBP treatment. Furthermore, the synergistic cytotoxicity induced by the combinations of DGBP and afatinib in SCC and NSCLC cells was dependent on their enhanced expression of ATF3 in combination through the induction of ISR pathway regulated by GCN2. In conclusion, this study suggests the potential clinical utility of combining GGPP synthase inhibitors with afatinib in SCC and NSCLC.

CHAPTER 5: DISCUSSION

Despite improvements in cancer therapy involving better surgical techniques, radiation therapy, and chemotherapeutic agents, many patients with advanced stages will succumb to their disease. The use of EGFR targeted therapy in treatment regimens of cancers with a high EGFR expression, such as HNSCC and NSCLC, has demonstrated promising outcomes in both *in vitro* and *in vivo* cancer models (25,27,78). The treatment for advanced stage HNSCC may benefit from strategies that involve targeting the EGFR, which plays a role in their proliferation and survival (1,60,208). EGFR-TKIs have been widely used in the treatment of HNSCC; however, they have demonstrated limited efficacy as single agents, and a combinatorial treatment approach is likely required to enhance EGFR-TKI efficacy (9,25). This current study, in combination with our previous work (104,105,108,109,148,209), suggests that treatment of advanced stage HNSCC will benefit from a novel combination strategy by targeting of the EGFR in concert with the mevalonate pathway.

The mevalonate pathway is an important cellular metabolic pathway whose end products play an essential role in maintaining cellular homeostasis and proliferation, and are essential in mediating EGFR activation and its downstream signaling pathways (87). Malignant cells appear highly dependent on the sustained availability of the mevalonate metabolites (86,108). Deregulated or elevated activity of HMG-CoA reductase has been demonstrated in a variety of different tumor types including HNSCC (86). The statin family of drugs are potent inhibitors of HMGR that are widely used to treat hypercholesterolemia. As cancer therapeutic agents, statins can directly block tumor cell growth, invasion and metastatic potential both *in vitro* and *in vivo* at high doses (5-10x the hypercholesterolemia dose) (86,95,210,211). These studies led to a Phase I study of lovastatin monotherapy in 88 patients with solid tumors comprised of mostly breast and prostate cancer

patients, where the MTD was determined to be 25 mg/kg/day, a dose that is 25x higher than the hypercholesterolemia treatment dose (212). No objective responses were observed in this patient cohort. However, gastrointestinal dysfunction and musculoskeletal system diseases that include myalgia and muscle weakness were associated with a high-dose of statin (212). Supplementation with ubiquinone reduced the severity but did not decrease the incidence of muscle toxicity (212).

Our laboratory and clinical studies provide an excellent example of the re- iterative process utilizing bench to bedside evaluations and going back to the bench to refine our bedside approach. Initially, we identified HMGR, the rate-limiting enzyme of the mevalonate pathway, as a retinoid responsive gene and that its targeting with the statin family of agents demonstrated that a subset of retinoid responsive cancers, including neuroblastoma, acute myeloid leukemia, juvenile monomyelocytic leukemia, pediatric solid malignancies (rhabdomyosarcoma and medulloblastoma), HNSCC and SCC of the cervix, are susceptible to lovastatin-induced apoptosis and cell-cycle arrest in G1 within therapeutically achievable levels (97,101,102,213). Others demonstrated similar results in medulloblastoma, neuroblastoma, mesothelioma, and glioblastomas (100,111).

These results rekindled the interest of HMGR inhibitors as anticancer agents and resulted in the clinical evaluation of lovastatin in retinoid responsive cancers. Our initial clinical trials utilizing high dose lovastatin as a single agent in a Phase I setting were performed at the Princess Margaret Hospital in AML (99) and SCC (103). In the 6 AML patients treated with lovastatin, one patient displayed a remarkable durable response where control of blast cell population for greater than 200 days was observed (99). The other 5 AML patients treated displayed significant dose-limiting toxicity (DLT) consisting of reversible muscle toxicity in all cases that were not reported to this extent in previous Phase I studies in the solid tumors tested (212). In our completed Phase

I trial in recurrent SCC, (103), 23% of our patients exhibited stable disease of greater than 3 months, and 4 had DLT exclusively from muscle toxicities (103). Our clinical results suggested that the most effective use of statins would be as part of a combined modality approach. Thus, agents targeting the mevalonate pathway required the identification of rationale combination therapeutic strategies.

Our previous studies have demonstrated such an approach where statins enhanced the cytotoxicity of EGFR-TKIs in combination through the induction of enhanced apoptotic response in various malignancies, including HNSCC. Combination of lovastatin and gefitinib represented an attractive possibility. To this end, our laboratory was the first to demonstrate that targeting mevalonate synthesis with statins inhibited the activation and downstream signaling of the EGFR in a mechanism distinct from EGFR-TKIs (104,108). Additionally, by targeting Rho family protein prenylation and their cellular localization, activation and function, lovastatin inhibited ligand-induced dimerization and activation of the EGFR and its downstream target AKT in SCC cell lines (105). Furthermore, we demonstrated synergistic cytotoxicity of lovastatin in combination with EGFR-TKIs in SCC and NSCLC cell lines (104,105,108). This combination is robust and specific as a 1200 compound screen that we performed employing FDA approved drugs showed that gefitinib and erlotinib enhanced lovastatin-induced cytotoxicity (2/7 hits identified) (109). Importantly employing the same library to identify enhancers of erlotinib cytotoxicity, two mevalonate pathway inhibitors were identified as enhancers (2/8 hits identified) (109).

Statin-induced ATF3 expression was a key regulator of its cytotoxicity and synergy with EGFR-TKIs (105,166). ATF3 is a stress-inducible gene that is a member of the CREB/CAAT-binding family of transcription factors, and it is usually expressed at basal levels in normal cells, but rapidly induced by a variety of cell stressors including the ISR and can regulate its apoptotic

response (177,183). A recent study found ATF3 and ATF4 are important regulators that induce pro-apoptotic protein Noxa by cisplatin treatment of HNSCC in a p53-independent manner (214). Importantly, we assessed the effect of statin usage in patients enrolled in the National Cancer Institute of Canada Clinical Trials Group (NCIC- CTG) study BR.21 (62), the first Phase III study to demonstrate a survival advantage in NSCLC patients with erlotinib from 4.7 to 6.7 months (62). In the erlotinib arm of this trial, patients on statins to control serum cholesterol performed better regarding overall survival than non-statin users further demonstrating the potential of this therapeutic strategy (105).

The pre-clinical data generated from our work was the basis for the recently completed Phase I study at OHRI Institute evaluating rosuvastatin and erlotinib in combination (110). These agents were chosen based on their superior clinical performances (215). This trial assessed the safety of this approach and to determine the Phase II dose to be employed in subsequent clinical analyses. Patients with a wide variety of solid tumors were assessed including breast, prostate, and pancreas that are not generally considered to be sensitive to EGFR-TKI treatments (111,213). The high dose of rosuvastatin used had undesirable muscle pathologies in 34% patients (110). Of particular interest, there were 6 evaluable patients in this trial with NSCLC and SCC. While 3 were on study for less than 2 months, 3 were on study for greater than 150 days with 2 of these patients on study for greater than 275 days (110). For these patients with advanced disease that have failed standard therapies, this represents a significant improvement over expected outcomes for single agent erlotinib treatments (62).

Notwithstanding statins benefit in cancer treatment, where they positively induce apoptosis and prevent tumor progression in a variety of cancers (122), they have also been associated with muscular complaints including benign myopathy or myalgia to myositis, and possibly life-

threatening rhabdomyolysis (114,216). According to Thompson and co-workers, there are 3 possible mechanisms of statin-induced muscle pathology: [1] reduction of the levels of ubiquinone, [2] reduction of the cholesterol content of skeletal muscle membranes, or [3] reduction in FPP, which is required for the activation of small GTP-binding regulatory proteins, where muscle fibre degeneration has shown to be linked to dysregulation of small-GTPases (113,217,218). Yet, several observational and clinical studies have suggested that statin treatment is associated with muscle damage likely by decreasing the production of ubiquinone that plays an important role in the mitochondrial respiratory chain (114,216,219). Although CoQ10 supplementation is the standard therapy option in this matter, conflicting evidence of its efficacy are shown as well, where other studies demonstrated CoQ10 supplementation does not reduce myopathic symptoms in statin-treated patients (114,220).

Interest in targeting protein geranylgeranylation was prompted from the realization in previous studies highlighting the importance of GGPP in maintaining cellular homeostasis. Biochemical add-back approaches determined which end products downstream of the mevalonate pathway metabolites are essential for statin-induced cytotoxicity. We demonstrated that GGPP co-administration reverses the apoptotic effects of lovastatin, its inhibitory effects on EGFR function, its induction of metabolic stress, and its synergistic cytotoxicity in combination with EGFR-TKIs (105). Supplementing cells with other mevalonate metabolites such as cholesterol, squalene, dolichol, ubiquinone, and IPP did not show any effect in mitigating lovastatin-induced apoptosis (221).

The goal of this study was to identify novel therapeutic strategies that can recapitulate the efficacy of statins in combination with EGFR-TKIs while circumventing the muscle toxicities associated with statin usage. In summary, this study demonstrated that targeting GGPP synthesis

or activity show synergistic cytotoxicity in combination with EGFR-TKIs that was regulated by ATF3 and the ISR pathway.

5.1 GGTI - Effects on EGFR Activity and Synergy with EGFR-TKIs

In this initial study, we focused on targeting protein geranylgeranylation as targeting GGPP incorporation represents a viable therapeutic target in combination with EGFR-TKIs. Geranylgeranylation is a crucial biochemical post-translational modification for the cellular localization and functional activation of small G proteins to enhance their hydrophobicity in order to bind to cellular membranes (123,222). Over the past 2 decades, several reports showed that these small G proteins contribute to tumor proliferation, development, progression, invasion, and metastasis (123,222,223). Geranylgeranyl transferase I is a heterodimeric prenyl transferase that is essential for the prenylation of these small G proteins (223).

Inhibitors of GGtase-I are clinically advanced agents and are available for clinical evaluations and as such were the primary focus of this study. GGTI-298 is a peptidomimetic-based GGTI that contains aminobenzoic acid (223). It has been reported that the administration of GGTI-298 as a monotherapy impairs tumor formation in cell cultures and in animal models by arresting cancer cells at G0/G1 phase of the cell cycle and inducing apoptosis through the upregulation of $p21^{wafi/cip1}$ CDK inhibitor and the downregulation of AKT phosphorylation, respectively, in oral SCC, breast, bladder, and pancreatic cancers (117,126,223–225). Additionally, conditional knockout of the GGtase-I disrupted actin cytoskeleton, reduced cell migration, reduced tumor cell proliferation and improved survival in mice with oncogenic $K\text{-}Ras^{G12D}$-induced lung cancer (223,226). Also, GGTI-298 has been reported to inhibit the processing of RhoA and RalB and impaired oral SCC, prostate, and pancreatic cell migration and invasion, which led to decreased disease progression (223,227). GGTI-2418, is another small molecule peptidomimetic inhibitor

which was designed based on the CAAL termini of RhoA and RhoC (129,223). Importantly, the GGTI-2418 completed a first-in-human Phase I clinical trial on 14 patients with advanced solid tumors in the does-escalation cohort (129). The administration of GGTI-2418 was safe and well tolerated at all the tested dose levels with some evidence of disease stability, where 4/14 patients had stable disease for up to 6.7 months (129). GGTI-2418 administration showed minimal side effects, with nausea and diarrhea as the main adverse event and importantly without demonstrating muscle pathologies. Plasma concentrations of GGTI-2418 achieved in this trial exceeded concentrations required for the *in-vitro* inhibition of GGtase-I, and durable stable disease was achieved in three colorectal cancer patients as well as one hepatocellular patient (128). Therefore, during this study, we focused on the potential of the commercially available first-generation analogue GGTase-I inhibitor GGTI-298 to enhance tarceva cytotoxicity. GGTI-298 and GGTI-2418 are identical drugs, and we used GGTI-298 because GGTI-2418 was not commercially available at that time when we start working on this project.

Biochemical add-back approaches have been widely used to pinpoint that GGPP mediates the cytotoxic and apoptotic effects of several mevalonate pathway inhibitors (131,140,191). Our previous studies demonstrated that GGPP reversed lovastatin effects on HNSCC and AML cell viability (191,221). Interestingly, supplementing AML cells with other mevalonate metabolites did not affect lovastatin's apoptotic effects (221). In the study presented here, we confirmed our previous findings, where GGPP rescued the cytotoxic effects of lovastatin alone or in combination with tarceva in HNSCC SCC9 and SCC25 (Figure 3.1 A and B). In this study we also observed the overexpression of the key enzymes of the mevalonate pathway in the cancerous cell lines but not in the normal cell line (Fig 3.1 C), which in line with the literatures (131,222).

A growing number of studies demonstrated the interaction between RhoA and various signaling molecules on cell proliferation and apoptosis (228–230). The Rho family, a widely studied group of small-GTPase proteins were shown to influence gene expression of various proteins involved in cell signalling, regulation of actin cytoskeleton and cell mobility, and in cell cycle progression and cell survival (118,201,227). The activation of this family is important for cancer cell transformation. There are 5 members of Rho GTPase proteins: RhoA, RhoB, and RhoC, Rac1, and cdc42, which are highly homologous and share about 85% of amino acid sequence (227). RhoA is involved in the actomyosin contractility; RhoB modulates cellular trafficking and survival; RhoC plays a role in cell locomotion; while Rac1 and cdc42 transduce extracellular signals to lamellipodia and filopodia, respectively (118,227). These RhoA proteins are post-translationally modified by the GGTase-I enzyme; therefore, they are important targets of the inhibitor GGTI-298.

A number of in vitro studies highlighted the importance of actin cytoskeleton to EGFR activation (105,231,232). Since the bioactivity of RhoA modulates actin organization, RhoA could potentially play a role in EGFR activation. Using immunofluorescence microscopy, F-actin showed the ability to colocalize with EGFR (105,231,232). This reveals the mechanism by which actin cytoskeleton forms a matrix that stabilizes EGFR dimerization and facilitates the interaction of EGFR and its downstream signaling proteins (233–235). Previous work in our lab delineated the mechanism of lovastatin-induced inhibition of EGFR activation through the actin cytoskeleton (105). In that model, it was found that lovastatin treatment diminished GGPP cellular pool, which affects RhoA geranylgeranylation, its localization and activation. Lovastatin significantly induced the expression of Rho proteins RhoA, and Cdc42, but not Rac1 (105). Using a colorimetric RhoA activation assay, it was shown that lovastatin inhibited EGF-induced RhoA activation in SCC9

and SCC25 HNSCC cells (105). Consequently, the inactivation of RhoA resulted in the disorganization of the actin cytoskeleton, the inhibition of ligand-induced EGFR dimerization and trafficking, and subsequently, the inhibition of EGFR activation and its downstream signaling via AKT phosphorylation (105). An inhibitor of ROCK, a downstream effector of RhoA, Y-27632 also showed similar inhibitory effects of lovastatin (105), which supports the involvement of RhoA in the EGFR dimerization and actin disorganization. Additionally, using a co-immunoprecipitation assay, the same study demonstrated that F-actin was pulled down with EGFR in control-treated cells, but not in lovastatin-treated cells suggesting that EGFR has direct interaction with the actin cytoskeleton (105). The addition of GGPP reversed all lovastatin's effects on EGFR activation (105).

In this study we assessed the effects of GGTI-298 on the prenylation of RhoA, Rac1, and Cdc42 in SCC9 and SCC25. Using Western blot analysis, the expression of the 3 proteins was induced along with a slight shift in gel mobility following GGTI-298 treatment indicative of the absence of their prenylation (Figure 3.2 A). Although our data showed the induction of RhoA protein expression, it remains non-functional due to their lack of GGPP, as supported by our recent report suggesting that the induction of RhoA by lovastatin resulted in inactive RhoA protein (105). The co-administration of GGPP reversed lovastatin effects on these Rho proteins, but not the effects of GGTI-298, confirming that these proteins are geranylgeranylated and the incorporation of GGPP in the post-translation modification of small-GTPase proteins and not the levels of intracellular GGPP was regulating this response. We also observed that GGTI-298, similarly to our work with lovastatin (105), impaired actin cytoskeleton organization and reduced cell migration through its ability to inhibit RhoA protein geranylgeranylation (Figure 3.2B and C). This phenomenon is likely the mechanism regulating GGTI-298 inhibitory effects on ligand-induced

dimerization and trafficking of the EGFR in the cells (data not shown). Targeting the geranylgeranylation of RhoA is likely the mechanism by which GGTI-298 inhibited EGFR dimerization. A study in 2011 demonstrated that GGTI-298 increased the expression of, but also a reduction in the membrane localization of RhoA and RalB, but not Ras in oral SCC cells (227). Our results in Figure 3.2 also confirmed their findings, where GGTI-298 suppressed oral SCC migration and invasion supporting the utility of GGTI in the inhibition of SCC invasion and metastasis (227). Moreover, a recent report also showed that GGTI-298 inhibited RhoA activation in the NSCLC A549 cells (222) further supporting our findings. Furthermore, that study also demonstrated that the downregulation of RhoA with small interfering RNA (siRNA) impaired the phosphorylation of EGFR supporting our suggestion that GGTI-298 may exert its effects on EGFR through a similar mechanism whereby inactive RhoA results in inhibition of EGFR activity (222).

As stated, the end products of mevalonate pathway play a crucial role in EGFR signaling. Our previous work demonstrated the synergistic effects between the HMGCR inhibitor, lovastatin, with the EGFR inhibitor, gefitinib. In this study, using MTT cell viability assay, treatment with GGTI-298, similar to lovastatin (Figure 3.3), synergistically enhanced cytotoxicity with the combination of tarceva in HNSCC (Figure 3.4A). To confirm our MTT data, the non-enzymatic trypan blue exclusion assay was performed corroborating the enhanced reduction of cell viability following these treatments in combination (Figure 3.4B). To confirm that apoptosis induction was regulating this combination effect, flow cytometric analysis of propidium iodide-stained cells showed the enhanced accumulation of apoptotic cells, which contain nuclear fragments, at the pre-G1 phase in cells treated with the combination treatments of lovastatin and tarceva (Figure 3.4C). At the molecular level, the combination of both drugs also resulted in the enhancement of cleaved apoptotic protein PARP by Western blotting (Figure 3.4D). PARP is a nuclear DNA repair protein

and a direct target of caspases upon initiation of apoptosis that is cleaved during apoptosis by activated caspases resulting in the emergence of a signature cleaved 89 kDa fragment (207). Our data also seems to corroborate the results obtained from a study conducted on NSCLC using the combination of GGTI-298 with another EGFR-TKI, gefitinib (222). Similar to our findings, GGTI-298 synergistically enhanced the antiproliferative effects of gefitinib in NSCLC cell lines A549 and HCC827 (222). These synergistic effects were also observed to induce apoptosis and to inhibit cellular migration in these NSCLC cells (222).

In this study we focused on the metabolic stress pathways that we identified previously (105,148,166) as playing a role in regulating statin-induced apoptosis (Figure 1.10): [1] the EGFR/AKT pathway; [2] the LKB1/AMPK pathway; and [3] the ISR pathway. In our recent work, we identified these three metabolic stress pathways were modulated by statin treatment. Firstly, our study in 2010 demonstrated that growth factor withdrawal manifested through the inhibition of EGFR and its downstream signaling target AKT by lovastatin (105). Secondly, our study in 2012 revealed the role of lovastatin in the energy stress response pathway (148). The LKB/AMPK pathway senses ATP depletion, which is associated with LKB1 and AMPK activation (148). LKB1 is a CAXX containing FPP modified protein, where FPP modification plays a role in its membrane localization and activity (146). Lovastatin treatment in HNSCC, similar to a known inducer of LKB/AMPK pathway Metformin, impaired mitochondrial function and decreased ADP/ATP ratios, and induced expression and activation of the LKB1 and AMPK upon cellular shortage (148). Upon LKB1 activation of AMPK, AMPK directly phosphorylates TSC2, raptor, and mTOR leading to the suppression of signaling from the mTORC1 complex (144). This inhibition results in the increased levels of non-phosphorylated 4EBP1 with its continued binding to the eukaryotic translation initiation factor 4E (eIF4E) inhibiting cap-dependent translation (144). Thirdly, our

studies in 2007 and 2013 exhibited the role of lovastatin in the Integrated Stress Response (ISR) pathway that is also activated by a wide variety of insults (166,183). Our study was the first to demonstrate that lovastatin induced the ISR through GCN2 activation in SCC cells associated with eIF2α phosphorylation, inhibition of protein translation, enhanced expression of ATF4, ATF3 and CHOP and subsequent induction of apoptosis (166).

Herein, the elucidation of the additional mechanism(s) by which GGTI-298 induces tumor cell apoptosis was uncovered; we demonstrated the role of GGTI-298 in dysregulating the expression of key proteins in the three metabolic stress pathways. In the study presented here, we confirmed the previous findings (105,222), where GGTI-298 treatment induced growth factor withdrawal through the inhibition of the phosphorylation of EGFR and AKT proteins (Figure 3.6A). Interestingly, GGTI-298 treatment enhanced the inhibitory effects of tarceva on the activation of EGFR and AKT (data not shown). Similar to this notion, Liu *et al* also showed GGTI-298 augmented the inhibitory effects of gefitinib on the activation of EGFR and AKT in NSCLC cell lines (222). Additionally, in this study we also demonstrated that GGTI-298 treatment played a role in the energy stress pathway through the up regulation of the phosphorylation of LKB1 and AMPK proteins (Figure 3.6B), which aligned with our recent findings (148). Similar to our previous work (166,183), we also showed that GGTI-298 activity involves in the ISR pathway through the induction of ATF3 expression (Figure 3.7B). Therefore, the ability of GGTI-298 to modulate the activity of multiple metabolic stress pathways is a novel finding with the potential to regulate GGTI-298 -induced tumor cell apoptosis.

To gain further insight into the common potential mechanism of action of lovastatin and GGTI-298, RNA-seq analysis was performed in SCC cells treated with either agent. ATF3 and ATF3 regulated genes were up regulated following treatments of SCC25 cells with either of these

agents (Figure 3.7A). Furthermore, ATF3 null MEFs were resistant to lovastatin and GGTI-298 treatment in comparison to their wild-type counterparts demonstrating a role for ATF3 in regulating GGTI-298 cytotoxicity (Figure 3.9). Interestingly, these results supported our previous work, where we showed that by knock down ATF3 in HeLa, the cells become resistant to lovastatin treatment in comparison to the GFP control cells (183), which highlights the importance of ATF3 in lovastatin activity. In addition, numerous attempts to transfect HNSCC cell lines failed, and thus we were forced to used alternative relevant model system as a result. ATF3 expression was also up regulated in a more clinically relevant *ex vivo* models of HNSCC and other tumor tissues (Figure 3.7D). Additionally, evaluating the key proteins of the three metabolic stress pathways in SCC9 GGTI-resistant clones identified ATF3 induction as the only pathway differentially expressed compared to the parental SCC9 (Figure 3.8). We also found that GGTI-298 treatment induced synergistic cytotoxicity with tarceva in HNSCC which was regulated by the induction of the ATF3. This strategy suggested the potential clinical utility of combining GGTIs with tarceva in HNSCC as a therapeutic strategy.

Although other pathways seem to be dysregulated in the SCC9 GGTI-resistant clones (Figure 3.8B), of clinical significance, our recent report demonstrated that lovastatin synergistically induced the cytotoxic effects of gefitinib in the LKB1+/+, LKB1-/- MEFs, as well as in the LKB1-deficient HeLa cells (148). This suggests that while the energy stress LKB1/AMPK pathway regulates lovastatin cytotoxicity, the ability of lovastatin to affect a number of cellular stress pathways can overcome the lack of LKB1, which highlights the broad therapeutic applications of statins through their pleiotropic effects on different cellular signaling pathways (148).

As stated, the small-GTPase proteins Rho, Rap1A, Rac1, Rab, and Cdc42 are geranylgeranylated. Post-translational modification of these proteins is required for their localization and biochemical functions that play a critical role in oncogenesis and cancer metastasis (236). Of a particular interest, Rab proteins, including rab5 and rab7, unlike other prenylated proteins that are modified at their terminal cysteine residue with a single moiety, are modified by the addition of two GGPP moieties at two cysteine residues by RabGGTase (118,131). They play vital roles in the internalization and trafficking of amino acid transporters and their aberrant transport has been associated with the induction of cellular stress (118). Rab 5 is a key regulator of protein trafficking to early endosomes, and it was shown to regulate EGFR internalization following its ligand activation (237–239); rab7 regulates transport from late endosomes to lysosomes (118). Endocytosed EGFR can then be recycled back to the cell surface or be targeted for degradation via transport through late endosomes to lysosomes regulated by rab11 and rab7, respectively (238,239), suggesting inhibition of their GGPP modifications. Currently, few specific RabGGTase inhibitors are available (240,241). Phosphonocarboxylates have been shown to inhibit this enzyme (240,241) with lower potency than described for GGTIs. Due to the lack of available inhibitors of RabGGTase at the time when the experiments initiated in our lab, a former student in the lab employed an RNA interference method to silence this gene. In preliminary results, similar to our results with lovastatin treatment of SCC9 and SCC25 cells, it was shown that siRNAs targeting of RabGGTase inhibited GGPP modification and endosomal localization of rab5 and rab7. However, targeting RabGGTase failed to enhance the cytotoxic effects of either lovastatin or tarceva (Data not shown).

Another approach that may show improved specificity and minimize off-target effects of statins is by direct targeting of GGPP synthase, which will deplete cellular pools of GGPP similar

to statin treatment and could also represent a viable therapeutic target that more closely mimics the anticancer effects of statins.

5.2 Targeting GGPP Synthase - Potential as Novel Enhancer of EGFR Inhibitors

In the second part of the study, we focused on targeting GGPP synthesis as a representative viable therapeutic target in combination with EGFR-TKIs. GGDPS is a prenyl synthase enzyme that catalyzes the condensation of FPP and IPP to form GGPP via an ionization-condensation-elimination mechanism (131). Several studies, including our own, have linked the apoptotic and anticancer effects of statins to the depletion of GGPP (105,131,138).

In this study, we expanded on the biochemical add-back experiment in Figure 3.1 by testing this approach in NSCLC cells; as expected we confirmed that the addition of exogenous GGPP through add-back approaches prevented lovastatin-induced cytotoxic effects in SCC and NSCLC as well (Figure 4.1). Interestingly, when we repeated the experiments of Figure 3.1 on SCC9 and SCC25 at a later date using newly thawed younger passaged cells, we noticed that these SCC9 and SCC25 were more sensitive to lovastatin treatment in Figure 4.1 than in Figure 3.1. We think that this difference in sensitivity is due to a couple of reasons: [1] The age of the cells: in Figure 3.1, the cells were already in culture prior to my receipt of them, older, and had higher passage number; whereas in Figure 4.1, the cells were freshly newly thawed, younger, and had lower passage number. [2] The heterogeneity of the cells: HNSCC is known to be heterogenous, therefore, if we culture them for too long, they might change, suggesting cells used in Figure 3.1 maybe a different subpopulation with more resistance to lovastatin. [3] The efficacy of lovastatin: at the time when the experiment of Figure 3.1 performed, lovastatin drug was already reconstituted in the freezer, and with multiple freezing/thawing events, the drug could lose its efficacy; whereas in Figure 4.1, the drug was freshly made and aliquoted into smaller volumes in part due to less frequent freezing-

thawing cycles, therefore it is more effective. Although some discrepancy was seen in SCC9 and SCC25 in Figures 3.1 and 4.1, were there was a slight difference in the (~1.3-fold difference). However, both figures demonstrated the same principle where we showed does-dependent cytotoxic effects of lovastatin in SCC9 and SCC25, and that the addition of GGPP rescued the cytotoxic effects of lovastatin in both figures.

Targeting GGPP synthase via blocking the intermediate enzymes of the mevalonate pathway will deplete cellular pools of GGPP similar to statin treatment and may represent a viable therapeutic approach in combination with EGFR-TKIs. In this study, we evaluated the effects of combining inhibitors of GGPP synthase in combination with an irreversible second-generation EGFR-TKI, afatinib. We chose afatinib for these experiments, as recently published results demonstrated the superiority of afatinib efficacy to erlotinib in NSCLC when compared head-to-head in the Lux-Lung-8 clinical trial (82,83).

A number of inhibitors of GGPP synthase have been developed (131,135,140) with DGBP being a first-generation agent, where it was the most potent inhibitor described when these studies were initiated (136). DGBP is a synthetic experimental structural diphosphate analog chemical inhibitor (134,135). DGBP has a different molecular target, selectivity, and cellular effects compared with other bisphosphonates such as zoledronate which inhibits farnesyl pyrophosphate synthesis, where DGBP specifically inhibits the activity of GGPP synthase (135). Due to its bulky structure, DGBP is more lipophilic than statins and NBPs; therefore, it requires more time to enter the cells (135). DGBP has been previously shown to induce apoptosis of cancer cells including prostate, breast, and lymphocytic leukemia (131,135,137–140,206).

Previous work on DGBP showed that DGBP was found to induce apoptosis through the

activation of cleaved PARP and cleaved Caspase-3 and increased annexin V and PI staining in a variety of cancers (131,135,138–140). Also, DGBP significantly reduces MDA-MB-231 breast cancer cell migration and motility (137). It was also shown that DGBP induces autophagy in PC3 prostate and MDA-MB-231 breast cells through the up regulation of LC3-II expression (242). Interestingly, a recent report demonstrated that inhibitors of GGDPS disrupted Rab geranylgeranylation, which impairs protein trafficking processes leading to the induction of unfolded proteins and ultimately activating the unfolded protein response pathway (UPR) leading to cellular apoptosis (136,141,243,244). Importantly, exogenous addition of GGPP prevented most of the effects observed with DGBP, suggesting specific inhibition of GGDPS by DGBP.

In a mouse model of prostate cancer, a DGBP analog disrupted Rap1a geranylgeranylation and decreased tumor burden up to 50% in the adrenal gland and prolonged survival compared to the vehicle-treated mice (245,246). Interestingly, in a recent report by Agabiti and co-workers, DGBP did not affect the human normal blood mononuclear cells (PBMCs) in contrast to ZOL (138). A recent work published by Haney *et al* in early 2019 showed that targeting GGDPS by RAM2061, another GGDPS inhibitor, impairs cellular invasion, induces apoptosis through the activation of cleaved PARP and cleaved Caspases-3,8,9 and increased annexin V and PI staining in vitro (142). The same group also demonstrated that GGDPS inhibitor induces the UPR pathway through the upregulation of ATF4, ATF6, CHOP, PERK and IRE1α expression in pancreatic ductal adenocarcinoma cells in vitro and slowed pancreatic tumor growth in vivo (142). Moreover, there was no evidence of hematological, renal, cardiac, muscular, or neurological toxicities associated with this inhibitor (142). These data indicated that GGDPS can be targeted to interfere with the progression of cancer cells; therefore, it is another candidate agent to be used to enhance EGFR-TKIs efficacy.

In this study, we initially evaluated the cytotoxicity of DGBP in SCC and NSCLC cells (Figure 4.3), where DGBP induces cytotoxicity in SCC and NSCLC cells in a concentration-dependent manner. Then, we demonstrated that the co-administration of exogenous GGPP through add-back approaches prevented the cytotoxic effects of DGBP in SCC cell lines (Figure 4.4A and B), which is aligned with previous findings (138), suggesting the role of GGPP in the cytotoxic effect of DGBP. In addition, our data confirmed the previous findings (135,137,138,140–142), where we showed that DGBP inhibited the prenylation of geranylgeranylated proteins Rap1 and RhoA small-GTPases, which led to changes in their expression (Figure 4.4C). Increased accumulation of unprenylated forms of Rho proteins by limiting geranylgeranylation of these G-proteins may disrupt Rho-dependent regulation of cytoskeletal organization (247).

Although our data showed the induction of RhoA and Rap1 expression, they remain non-functional due to their lack of GGPP, as our previous study and a recent report by Agabiti *et al* suggested that the induction of RhoA or Rac1 by lovastatin or DGBP resulted in inactive RhoA or Rac1 protein, respectively (105,138). More importantly, our findings as shown in Figure 4.5 are similar to the results obtained by Agabiti *et al* (2017), thereby supporting our hypothesis that targeting GGDPS by DGBP would demonstrate tumor cell specificity as it did not display cytotoxicity in the normal fibroblast cell line, WI-38. These results coincide with our results in Figure 3.1C and those reported literature, that the basal levels of GGDPS is higher in the cancerous cells than the normal cell line (WI-38), which indicates the involvement of this enzyme in the tumorigenesis of the cancer cell lines. Therefore, GGDPS is a useful target. Additionally, lovastatin targets HGMCR, so it depletes all the downstream metabolites of the mevalonate pathway including both the GGPP and FPP cellular pools which may affect cellular functions important for normal cell survival. Also, according to our recent clinical trial (110), which showed

that lovastatin has cytotoxic effects on the normal tissue, leading to the muscle pathology. However, DGBP specifically targets GGPP cellular pool only and did not affect the viability of the normal cells, thereby making it a better drug than lovastatin for clinical use.

Previously in Dr. Dimitroulakos' lab, it was shown that lovastatin-induced apoptosis of SCC cells is regulated by the induction of the ISR that activates ATF3 expression (166). Elevated and sustained expression of ATF3 drives apoptosis through the expression of apoptosis enhancing proteins that include CHOP/GADD153 (180,183). As we demonstrated in our recent report, combining lovastatin and salubrinal, an agent that can sustain the activity of ATF3, enhanced ATF3 induction and induced synergistic cytotoxicity in SCC25 cells (183). These results suggest that combining inducers of ATF3 through different mechanisms may enhance their apoptotic responses. Our data confirmed our previous studies (166,183), where we also demonstrated a similar mechanism of action to statins that was dependent on ATF3, where DGBP treatment induced ATF3 expression in human SCC cell lines i*n vitro* (Figure 4.6A and Figure 4.7A) and in surgically resected human tumor tissues *ex-vivo* (Figure 4.7B) that more closely mimics the clinical setting. These findings were replicated in the NSCLC cells; interestingly, DGBP treatment induced ATF3 expression in human NSCLC cell lines i*n vitro* (Figure 4.6B) and in surgically resected human tumor tissues *ex-vivo* (Figure 4.7B).

In this study, the pro-apoptotic role of ATF3 in regulating DGBP cytotoxicity was confirmed through evaluating ATF3 null MEFs that demonstrated attenuation of DGBP cytotoxicity in the absence of ATF3 (Figure 4.8). Our data confirmed the recent findings (138,141,142), where DGBP treatment induced apoptosis through the activation of cleaved PARP and cleaved Caspase-3 (Figure 4.9), which indicate the importance of the ATF family in GGDPS-inducing apoptosis. Interestingly, as we show in Figure 4.9, the co-administration of exogenous

GGPP inhibits the induction of ATF3 and apoptotic effects associated with DGBP treatment in SCC cells.

As stated in (166), there is a potential link between the mevalonate pathway and the ISR pathway to affect cellular homeostasis, where depletion of the mevalonate downstream metabolites by lovastatin treatment have the potential to trigger cellular ISR leading to apoptosis (166). Cholesterol plays a role in the membrane integrity of ER proteins and the alteration of the cholesterol composition can induce ER stress (166). Dolichol is required for the *N*-linked glycosylation of ER proteins for their proper maturation, and the inhibition of glycosylation has been demonstrated to result in ER stress in vitro (87,166,248). GGPP is vital for the localization and activation of Rab family proteins that plays critical roles in ER homeostasis, where they regulate the internalization and trafficking of amino acid transporters and their perturbation have also been shown to induce ER stress (166,248). Ubiquinone is an important antioxidant that play a role in mitochondrial respiration, and the inhibition of this metabolite resulted in oxidative cellular stress (166). In addition, isopentyladenine is crucial for some tRNA modifications for protein production (166,249). Interestingly, a number of studies have shown that targeting the mevalonate metabolites by statins or NBPs resulted in elevated ER stress and the activation of the UPR pathway (236,250–253). Thus, a previous study in our lab hypothesized that the depletion of mevalonate downstream metabolites by lovastatin treatment have the potential to trigger cellular stress resulting in apoptosis (166).

Previously, our lab showed that lovastatin treatment activates the GCN2 kinase that senses amino acid deprivation (166), and that GCN2 phosphorylates eIF2α, which inhibits the recycling of eIF2 to its active GTP- bound form leading to the inhibition of global translation and ATF4 induction allowing cell recovery (166). We have also showed that GCN2 regulates lovastatin-

induced ATF3 induction and cytotoxicity in the MEFs cell lines (166). According to the literature review, it is still not clear how GCN2 is exactly activated by lovastatin treatment. However, one possibility is that cancer cells lose their ability to uptake amino acids following lovastatin treatment, due to either the attenuation or the inactivation in the expression of cell surface receptors or the modulation of amino acid permeases thereby leading to activation of GCN2 (166,254). Some studies support this hypothesis, where they found that modulating mTOR signaling by statins, thereby blocking the leucine amino acid transporter (LAT1), enhances cisplatin-ISR induction and its cytotoxicity in Hep-2a HNSCC cells (254–257).

An alternative possible mechanism of lovastatin-induction of the GCN2 is through tRNA. As stated above, IPP, one of the mevalonate pathway end products, is crucial for some tRNA posttranscriptional modification in the isopentylation of the adenosine at position 37 (the site immediately 3' of the anticodon), creating N^6-isopentyladenosine (i^6A) (258,259). Isopentenyltransferase enzyme (IPP transferase), an intermediate in cellular isoprenoid biosynthesis, is responsible for isopentenylation of this adenosine (258,259). This modified isopentyladenine is required for efficient amino acid translation by stabilizing tRNA.mRNA interactions, decoding the UGA and the synthesis of selenoprotein (selenocysteine), and for efficient binding of aminoacyl-tRNA to ribosomes (258,260–262). Lovastatin treatment of cultured cells in vitro decreased selenoprotein expression in a selenoprotein-specific pattern (261–263). Therefore, if we deplete the mevalonate pathway, we would deplete all its end products, no tRNA modification would occur, and that would lead to amino acids starvation and ultimately to GCN2 and ISR activation. GCN2 is not only activated by the reduction of cellular levels of charged tRNAs, but the increase in the binding affinity of GCN2 to the uncharged tRNA can also produce similar effects as amino acid deprivation thereby increasing its its kinase function (264,265). Some

studies showed that treating yeast cells with the mTOR inhibitor rapamycin increased the binding affinity of the uncharged tRNA to the phosphorylated levels of GCN2 (254,266–268).

In this study, we also demonstrated that DGBP significantly induced ISR and ATF3 expression in WT MEFs that are sensitive to its cytotoxic and apoptotic effect, which was also regulated by GCN2 (Figure 4.10). Our findings are supported by recent work (142), which highlights the importance of the IRS pathway in the GGDPS inhibitory effect. It is likely that DGBP, similar to lovastatin, may target intracellular protein trafficking, and thus, may limit the levels of accessible free amino acids from recycled proteins and/or inhibit their uptake, thereby promoting the activation of GCN2. During amino acid deprivation, the uncharged tRNA accumulates and binds to the regulatory binding region within GCN2 homologous to histidyl-tRNA synthetase (HisRS) enzyme, leading to enhanced kinase catalytic activity of the GCN2 and its activation (160,162,269). In support of this notion, GCN2 was also shown to be activated by UV exposure in mouse embryonic fibroblasts and human keratinocytes (166,270). Moreover, similar to our previous finding (166), CHOP-/- MEFS attenuated the cytotoxic effects of both DGBP and afatinib (Figure 4.10), which confirm the role of the ISR in the drug-induced apoptosis (166).

In some studies such as the one published in 2010 by Koromilas group (271), they noticed that the wild type MEFs of PERK, PKR, and GCN2 did not produce identical responses following glucose deficiency. However, the observed different responses of these wild type MEFs were attributed to differences in the genetic background of the cells (271). Although we did not have the isogenic wild type pairs for the other MEFs (ATF4, GCN2, and CHOP), all these MEFs shared the same genetic background, whereby they were made in the C57BL/6J mouse strain, I speculate that we would have similar results if these wild type paired MEFs were available to me. Moreover,

this is a common practice where a lot of labs have used a single wild type MEF from the same mouse strain of the same ISR pathway, so they are appropriate control (158,160,166,182,272–275).

In this study, we evaluated the cytotoxicity of afatinib in SCC and NSCLC cells (Figure 4.11). This study is the first to demonstrate that afatinib treatment of SCC and NSCLC cells induce a potent ISR regulated by ATF3 (Figures 4.6B, 4.7A). Afatinib significantly induces the ISR and ATF3 expression in SCC and NSCLC cell lines that are sensitive to their cytotoxic and apoptotic effects, and thus may represent a novel ATF3 dependent agent. We have also shown that ATF3 mRNA expression is induced in a subset of HNSCC and lung *ex vivo* tumor tissues by afatinib treatments (Figure 4.7B). The pro-apoptotic role of ATF3 in regulating afatinib-induced cytotoxicity was confirmed through evaluating ATF3-depleted MEFs that demonstrated attenuation of afatinib cytotoxic effects (Figure 4.10). Remarkably, afatinib treatment significantly induces the ISR and ATF3 expression in WT MEFs that are sensitive to its cytotoxic and apoptotic effect, which was regulated by GCN2 (Figure 4.10). It is still not clear how GCN2 is exactly activated by afatinib treatment. In 2010, Ye *et al* demonstrated that amino acid or glucose starvation, activated the GCN2-eIF2α and upregulated ATF4 expression and its downstream target genes involved in amino acid synthesis and transportation in tumor cells; thereby this GCN2-eIF2α-ATF4 pathway is critical for tumor cells survival and proliferation in response to glucose deficiency (160). Another study in 2010 by Muaddi *et al* demonstrated that the phosphorylation of eIF2α at Serine 51 is an important modulator of cell fate, where GCN2 plays a proapoptotic role whereas PERK and PKR are cytoprotective targets in response to glucose deprivation (271). It has been shown that the interplay between the oncogene AKT/PKB and tumor suppressor P53 pathways is involved in the apoptotic effects of glucose deficiency, where under low glucose, ATP

supply decreases, so protein folding becomes less efficient in the lumen of endoplasmic reticulum (ER), leading to the accumulation of unfolded or misfolded proteins, and that leads to the activation of the GCN2 to cope with the stress induced by protein misfolding (271). In 2011, Mounir *et al* demonstrated the role of AKT in the activation of the PERK-eIF2α-ATF4 pathway. During this study, they found that the direct inhibition of the PIK3-AKT pathway, either pharmacologically using LY294002 or genetically using si-RNA, increased the phosphorylation and activation of the eIF2α in MEFs and mammalian glioblastoma cells lines (276). On the other hand, the treatment with the mTOR inhibitor KU0063794 or the MEK inhibitor PD98059 did not affect the induction of eIF2 α, suggesting that the induction of eIF2α abundance was specific to the inhibition of PI3K (276–278). The effect of AKT inhibition could also modulate GCN2 activation. A similar study in budding yeast demonstrated the indirect role of TOR in the activation of GCN2-eIF2α pathway, where the inhibition of TOR by rapamycin induces the dephosphorylation of GCN2 at Serine 577, leading to the activation of GCN2-eIF2α pathway (276,279). To support this notion, in 2016, Gandin *et al* demonstrated that during nutrient starvation, mTORC1 phosphorylates the beta subunit of eIF2 and recruits NCK1 phosphatase to eIF2, which then decreases and inactivates eIF2α phosphorylation and strengthens translational ternary complex recycling (280). Additionally, a recent findings by Liu *et al* (81), revealed that afatinib downregulated AKT phosphorylation by activating the PERK-eIF2α-ATF4 pathway, and diminished the expression of anti-apoptotic protein MCL-1 thereby mediating apoptosis in HNSCC cells (81). Another study demonstrated that erlotinib and gefitinib activated the eIF2α-ATF4 pathway in A549 NSCLC cells (281). Interestingly, our results confirmed these findings where we showed that afatinib downregulated AKT phosphorylation leading to the accumulation of mis-folded proteins and the activation of the GCN2-eIF2α-ATF4-CHOP pathway resulting in apoptosis. These results

including ours indicated the importance of the ISR pathway in the cytotoxic effects mediated by EGFR-TKIs in the HNSCC and NSCLC cells.

Interestingly, similar to our findings in chapter 3, in this study, we demonstrated that both specific shRNA targeting of GGPP synthase (Figure 4.2), as well as treatment with the inhibitor DGBP significantly and synergistically enhanced afatinib-induced SCC and NSCLC cells cytotoxicity (Figures 4.12 and 4.13). Using MTT cell viability assay, treatment with DGBP, similar to lovastatin (Figure 3.3) and GGTI-298 (Figure 3.4), synergistically enhanced cytotoxicity with the combination of erlotinib in HNSCC (Figure 4.12) and NSCLC (Figure 4.13). To confirm our MTT data, the non-enzymatic trypan blue exclusion assay was performed validating the enhanced reduction of cell viability following these treatments in combination in comparison to either agent alone (Figures 4.12C and 4.13C). In Figure 4.13, different sensitivity was observed in these NSCLC. H23 cells are $EGFR^{WT}$ and Kras mutant lung adenocarcinoma, and it is known in the literature that cells with the wild type EGFR are generally more resistant to EGFR-TKIs in contrast to the EGFR mutant cells, which are more sensitive than the WT cells (36). On the other hand, HCC827 and HCC4006 are lung adenocarcinoma that have an acquired EGFR mutation in the exon 19 in the kinase domain of the EGFR (E746-A750 deletion) and (L747-E749 deletion), respectively, and are generally more resistance to EGFR-TKIs. However, a recent study in 2019 showed that clinically, patients with EGFR mutation (L747-E749), similar to that mutation in HCC4006, showed superior outcomes when treated with afatinib than patient with EGFR mutation (E746-A750), similar to that mutation in HCC827. These findings are in line with our results in Figure 4.13, where HCC4006 were more sensitive than the HCC827 to afatinib treatment.

In this study, the pro-apoptotic role of ATF3 in regulating cytotoxicity of DGBP and afatinib combination was confirmed through evaluating ATF3 null MEFs that demonstrated

attenuation of the cytotoxic effects of both drugs in combination (Figure 4.14). Importantly, combinations of DGBP and afatinib in SCC cells showed enhanced ATF3 induction compared to either agent alone (Figure 4.14), suggesting that independent induction of ATF3 may regulate this synergistic cytotoxic effect in SCC cells. This study is also the first to demonstrate that both DGBP and afatinib treatments induce ATF3 expression and that ATF3 plays a role in regulating the apoptotic responses in SCC cells. This strategy suggested the potential clinical utility of combining GGPP synthase inhibitors with afatinib in SCC as a therapeutic strategy.

5.3 Conclusion and Future direction

Overall, our findings in this study have successfully demonstrated that targeting protein geranylgeranylation activity with GGTI-298 or GGPP synthesis with DGBP affects EGFR function through distinct mechanisms. Combining downstream mevalonate inhibitors with EGFR-TKIs resulted in synergistic enhancement of the cytotoxic effects of both first-generation and second-generation EGFR-TKIs. ATF3 plays an essential role in regulating this synergistic relationship mediated by the integrated stress response (Figure 5.1). This study is the first to demonstrate that combining downstream mevalonate metabolites with EGFR-TKIs of SCC and NSCLC induce a potent ISR regulated by ATF3. More importantly, our findings taken together provide new insight into a potential novel combination strategy for advanced SCC and NSCLC by combining inhibitors of downstream mevalonate pathway enzymes with EGFR-TKIs. In the future, expanding these pre-clinical studies will provide invaluable data that will play a role in developing this novel therapeutic strategy. Additionally, the application of targeting GGPP synthesis and activity in combination with EGFR-TKIs in *ex vivo* HNSCC and NSCLC human biopsies and *in vivo* HNSCC and NSCLC models will allow the validation of the efficacy and toxicity of this combination strategy, and the ability to test the effect of the combination on the

muscle pathology. These pre-clinical evaluations will allow translation of this combination-based approach into clinical studies to evaluate the potential of this novel combination therapy.

Figure 5. 1 Overall proposed model of the study.

This figure outlines the overall model of the study. Inhibiting GGPP cellular pools by statins or GGPP synthase inhibitors affect the GGPP modification of the Rab proteins, which impair protein trafficking leading to the induction of unfolded protein response and ultimately the activation of the ISR and GCN2. The activation of GCN2 will induce the phosphorylation of eIF2α and ATF4, leading to the inhibition of the global protein translation and ultimately to ATF3 activation and cellular apoptosis. Additionally, inhibiting the GGPP modification of RhoA proteins will affect EGFR activation, and the downstream signaling through AKT, which leads to the inhibition of the global protein translation and cellular apoptosis through the ATF3 activation. On the other hand, the inhibition of EGFR activity by EGFR-TKIs would lead to the inhibition of the AKT pathway, leading to the activation of the GCN2-eIF2α-ATF4 pathway, then the inhibition of the global protein translation, ATF3 activation and apoptosis. Combining the two inhibitors EGFR-TKIs with the mevalonate pathway inhibitors would lead to synergistic cytotoxicity that was regulated by enhancing the induction of ATF3 expression and the apoptosis than either agent alone.

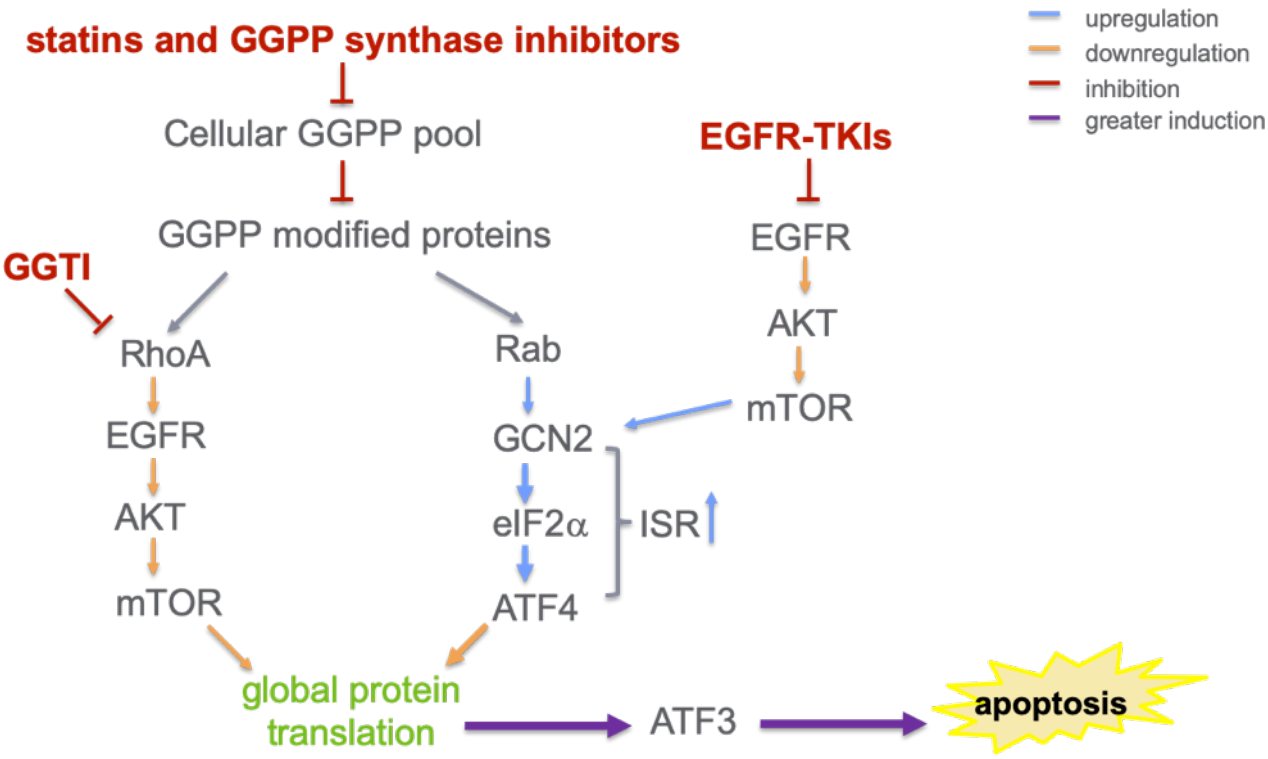
statins and GGPP synthase inhibitors
Cellular GGPP pool
GGPP modified proteins
GGTI
RhoA
EGFR
AKT
mTOR
Rab
GCN2
eIF2α
ATF4
ISR
EGFR-TKIs
EGFR
AKT
mTOR
global protein translation
ATF3
apoptosis
upregulation
downregulation
inhibition
greater induction

APPENDIX I

Supplemental Figure S1. Densitometry analysis of Figure 3-1C demonstrating HMG-CoR and GGPS1 levels normalized to actin levels. Error bars and ±SD are from the mean of three replicates.

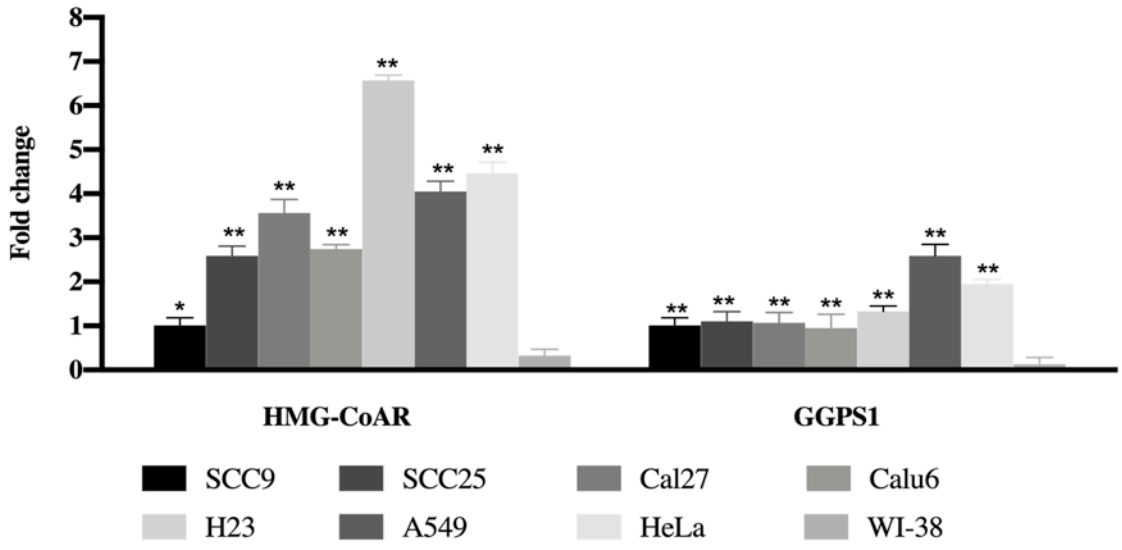

Supplemental Figure S2. Densitometry analysis of Figure 3-6 demonstrating phosphorylated EGFR, AKT, LKB1 and AMPK levels normalized to their corresponding total EGFR, AKT, LKB1 and AMPK levels. Error bars and ±SD are from the mean of three replicates.

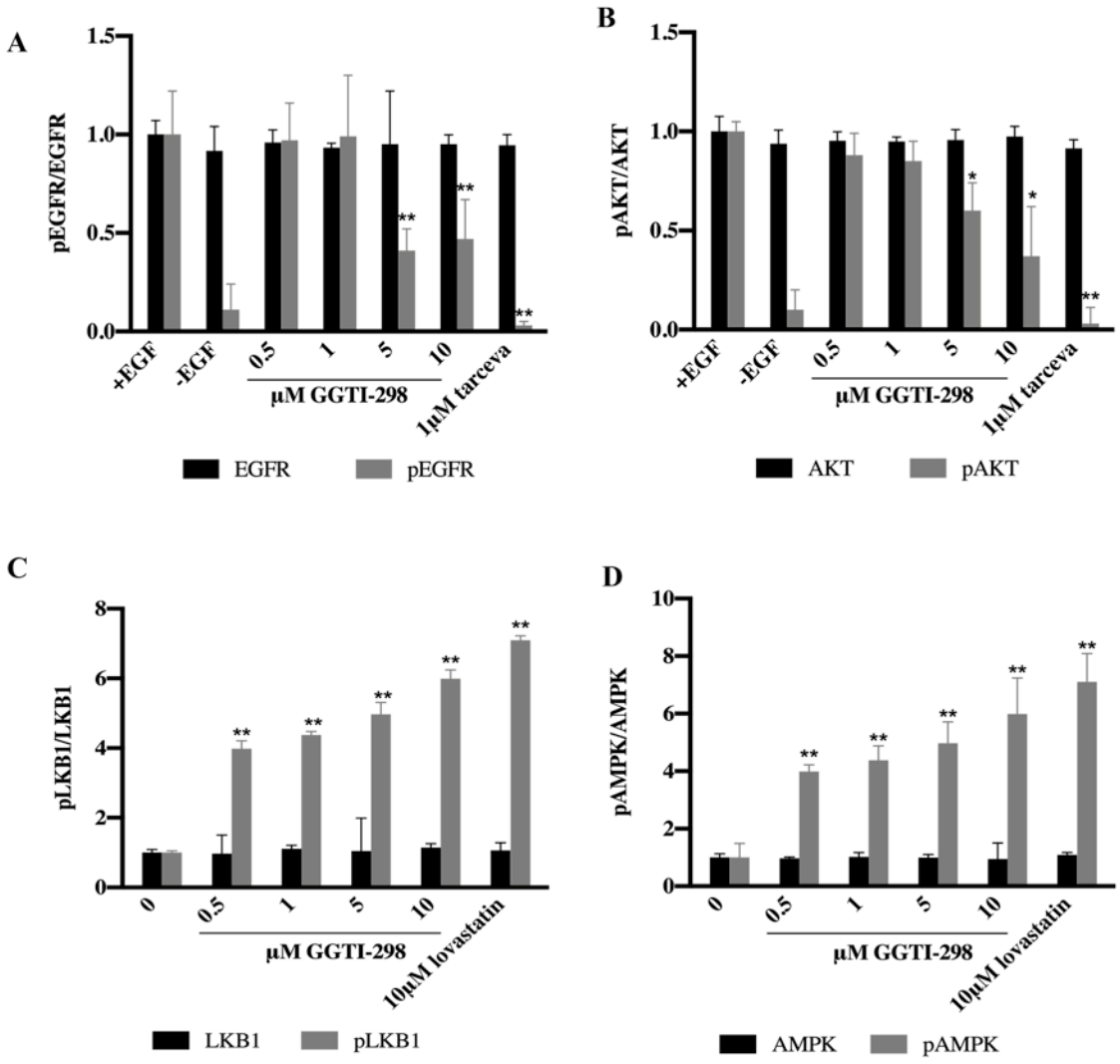

Supplemental Figure S3. Densitometry analysis of Figure 3-7B demonstrating ATF3 levels normalized to actin levels. Error bars and ±SD are from the mean of three replicates.

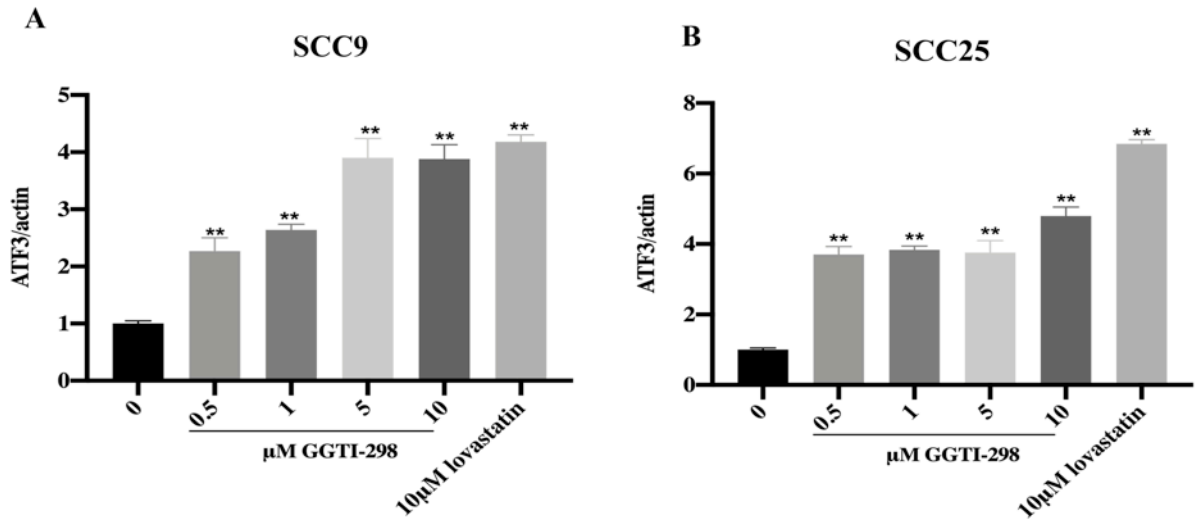

Supplemental Figure S4. Densitometry analysis of Figure 3-8 demonstrating phosphorylated EGFR, AKT, LKB1 and AMPK levels normalized to their corresponding total EGFR, AKT, LKB1 and AMPK levels, as well as ATF3 and RhoA levels to actin level. Error bars and ±SD are from the mean of three independent experiments.

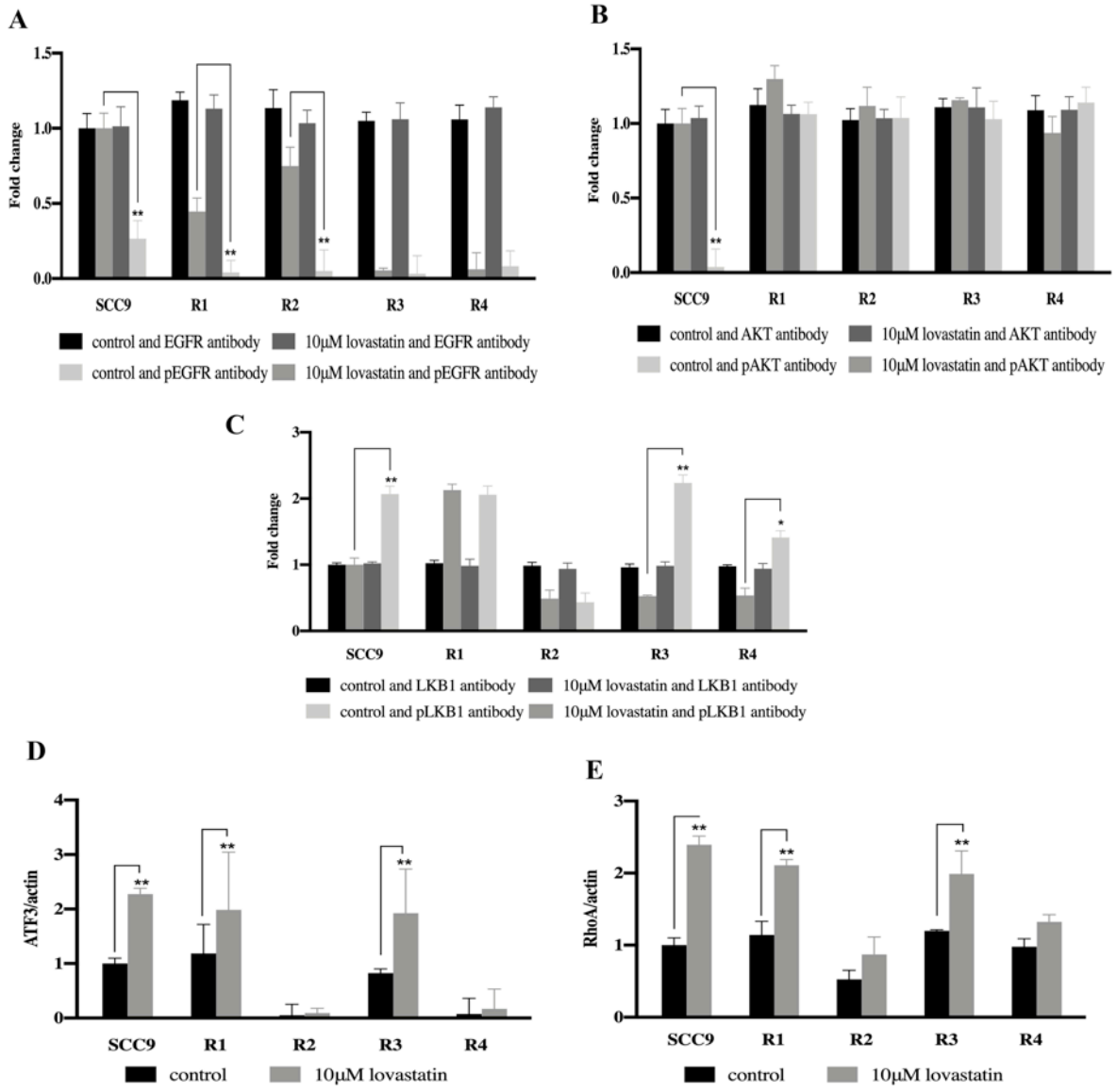

Supplemental Figure S5. Densitometry analysis of Figure 4-4C demonstrating Rap1, RhoA, and pan-Ras levels normalized to actin levels. Error bars and ±SD are from the mean of three replicates.

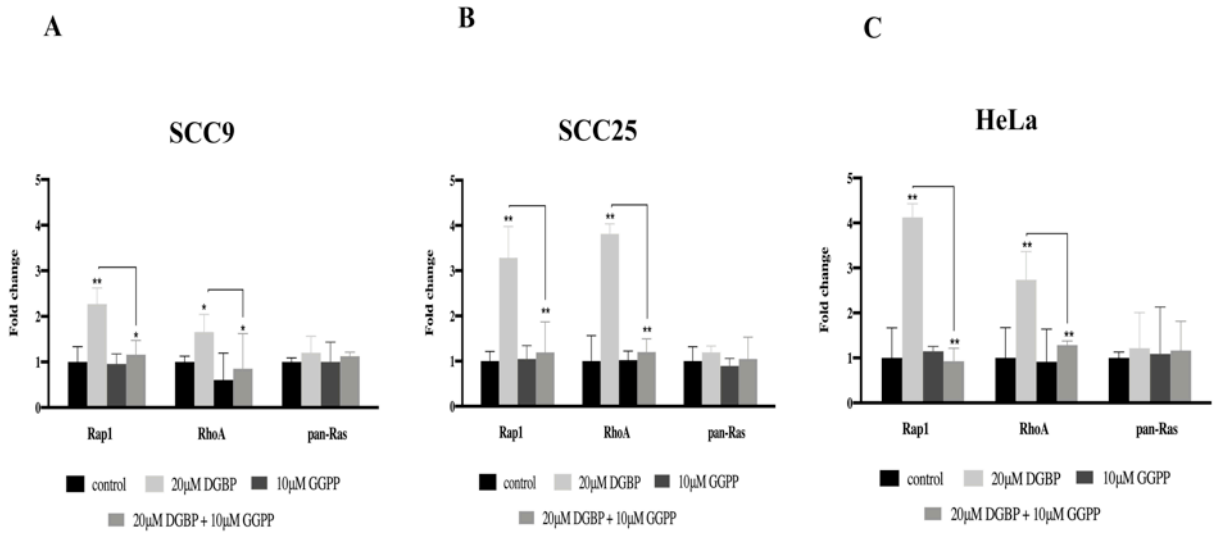

Supplemental Figure S6. Densitometry analysis of Figure 4-6A demonstrating ATF3 and cPARP levels normalized to actin and total PARP levels, respectively. Error bars and ±SD are from the mean of three replicates.

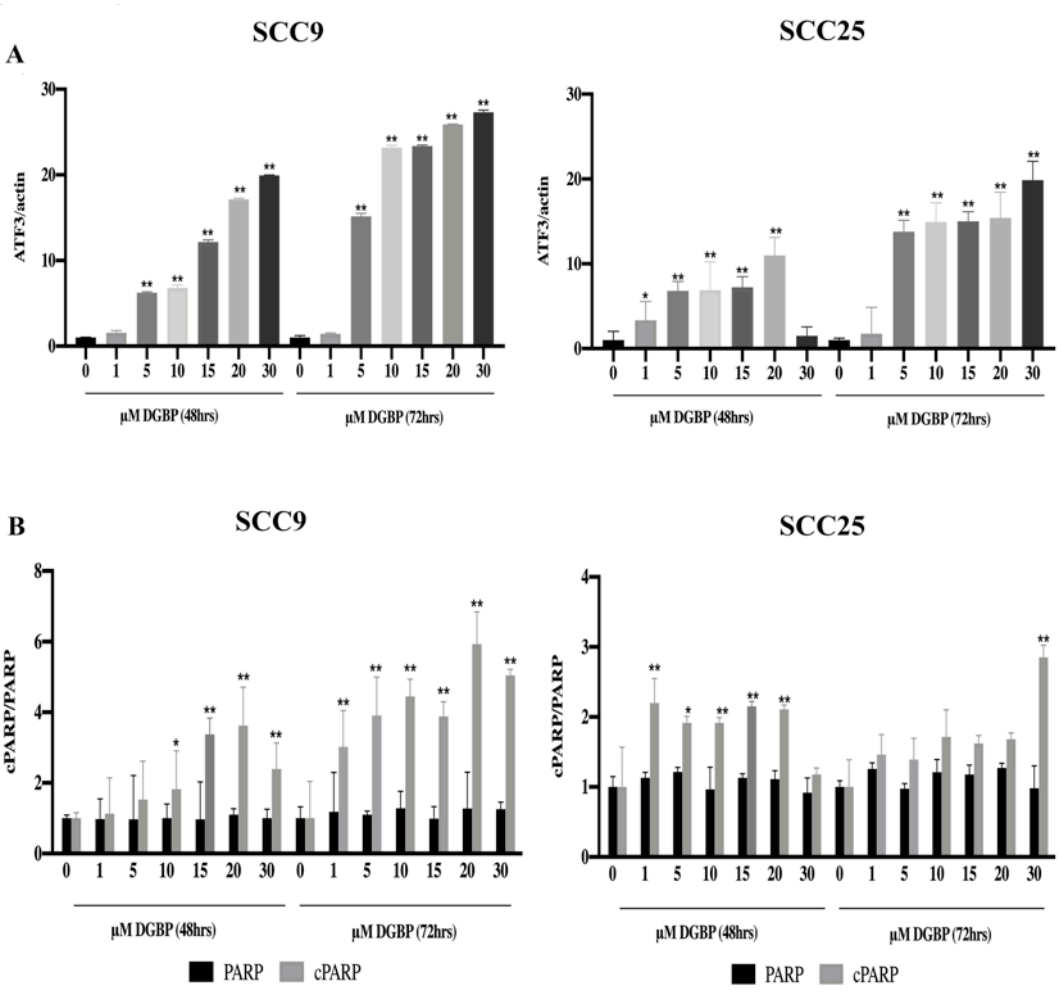

Supplemental Figure S7. Densitometry analysis of Figure 4-6B demonstrating ATF3 and cPARP levels normalized to actin and total PARP levels, respectively. Error bars and ±SD are from the mean of three replicates.

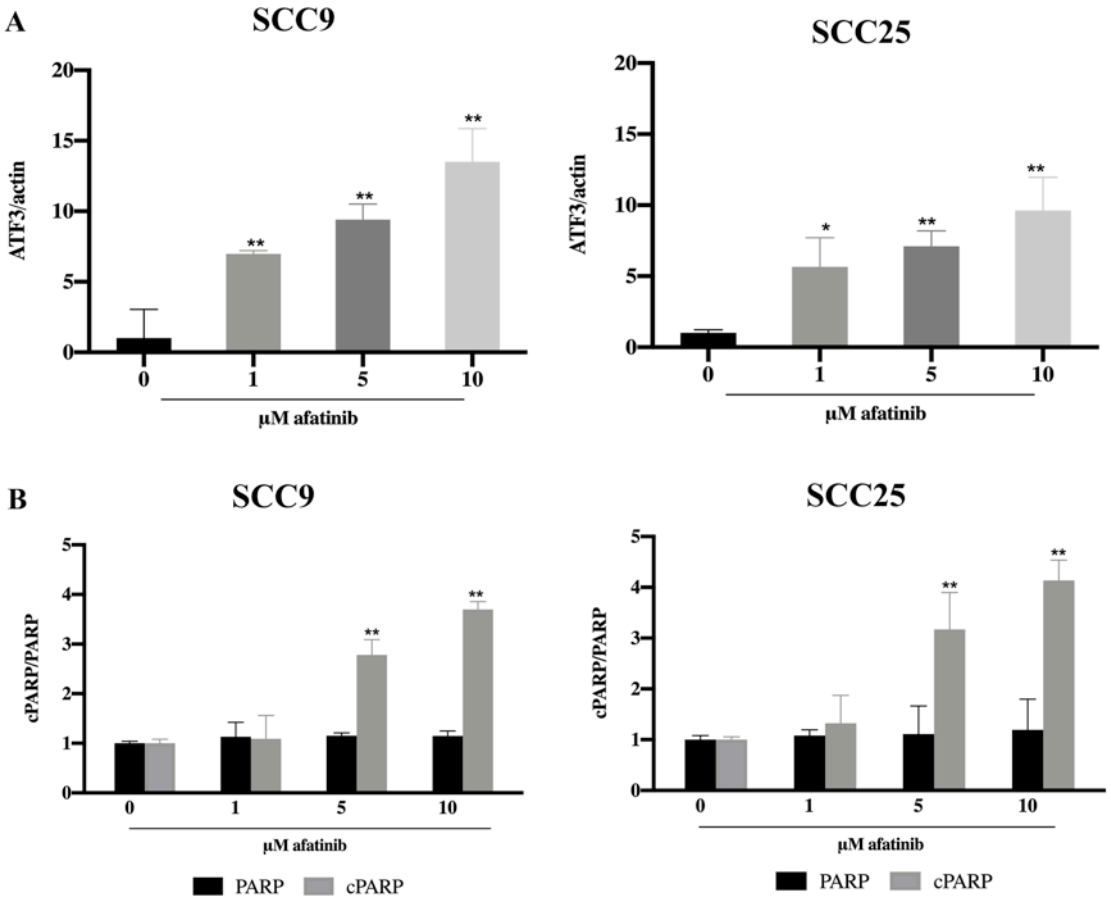

.

Supplemental Figure S8. Densitometry analysis of Figure 4-7A demonstrating ATF3 and cPARP levels normalized to actin and total PARP levels, respectively. Error bars and ±SD are from the mean of three replicates.

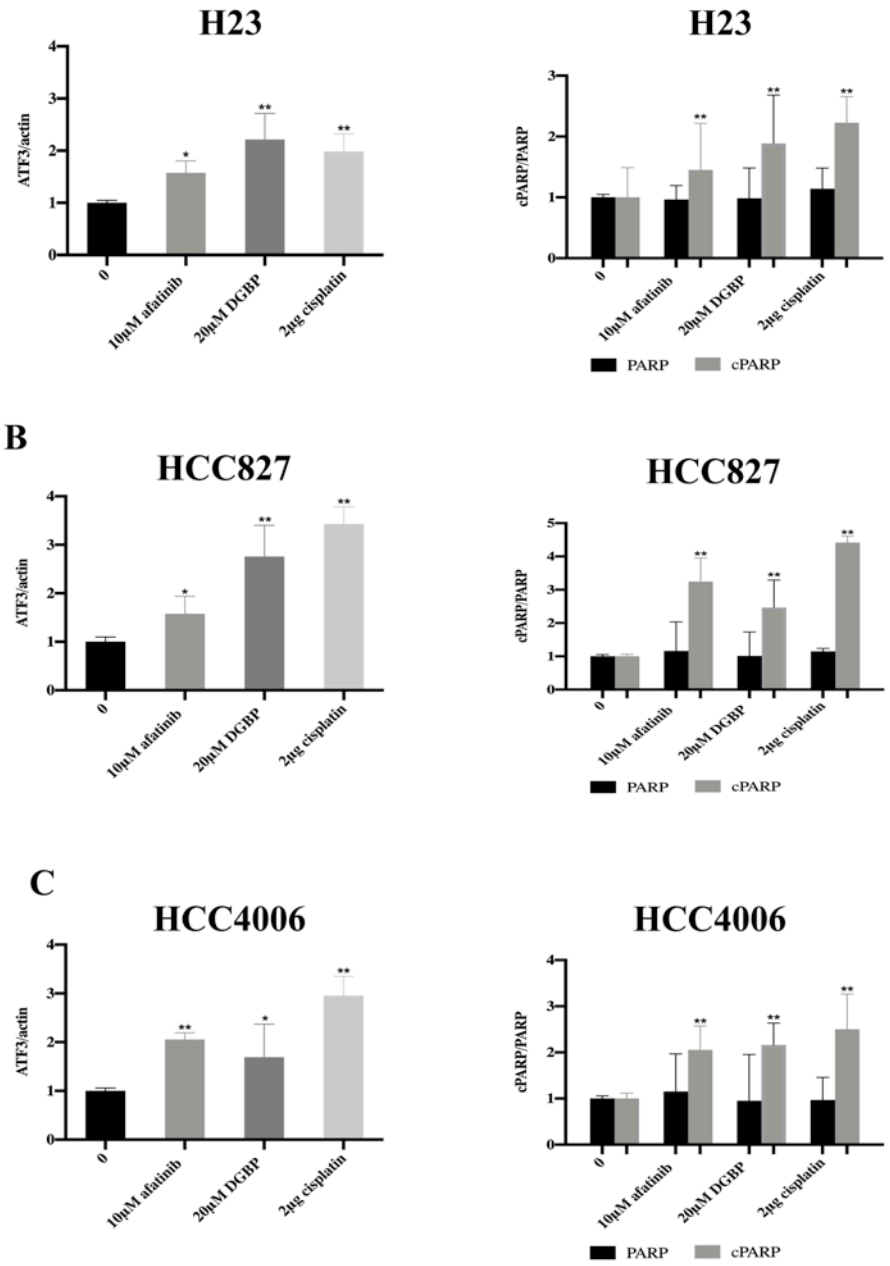

Supplemental Figure S9. Densitometry analysis of Figure 4-8A demonstrating ATF3 and cPARP levels normalized to actin and total PARP levels, respectively. Error bars and ±SD are from the mean of three replicates.

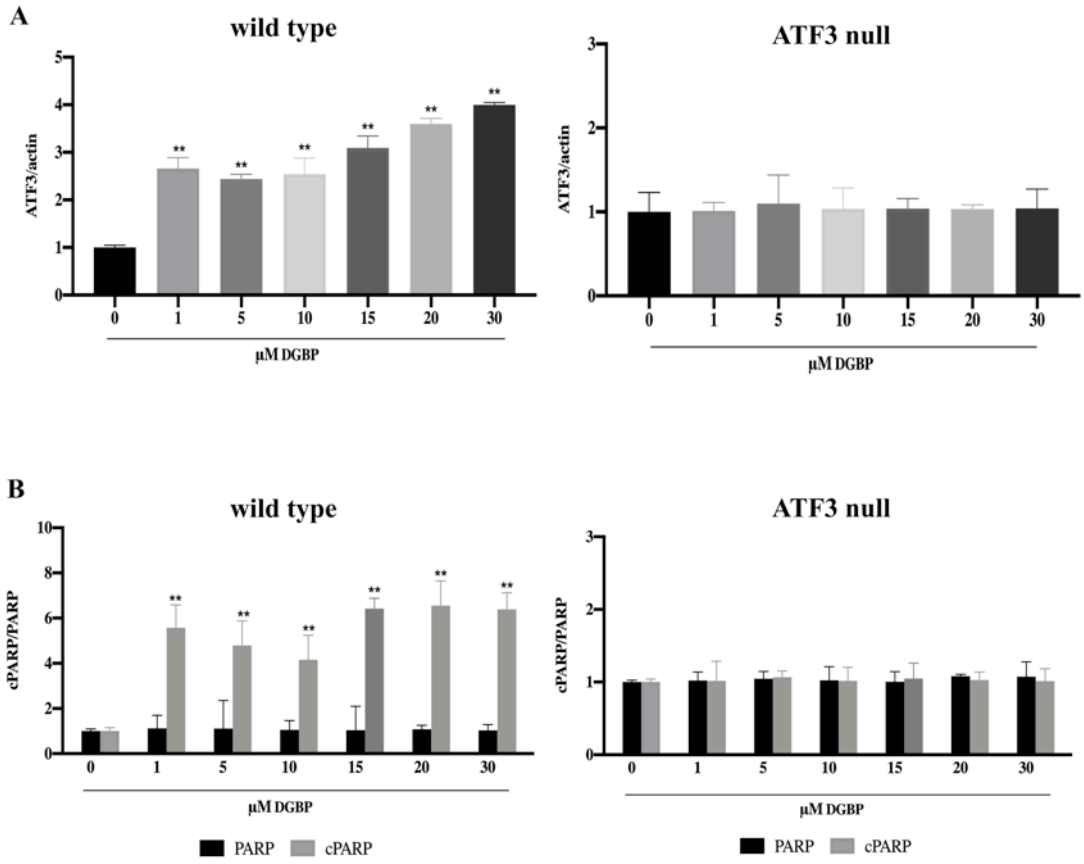

Supplemental Figure S10. Densitometry analysis of Figure 4-8B demonstrating ATF3 and cPARP and cCaspase3 levels normalized to actin and total PARP and Caspase3 levels, respectively. Error bars and ±SD are from the mean of three replicates.

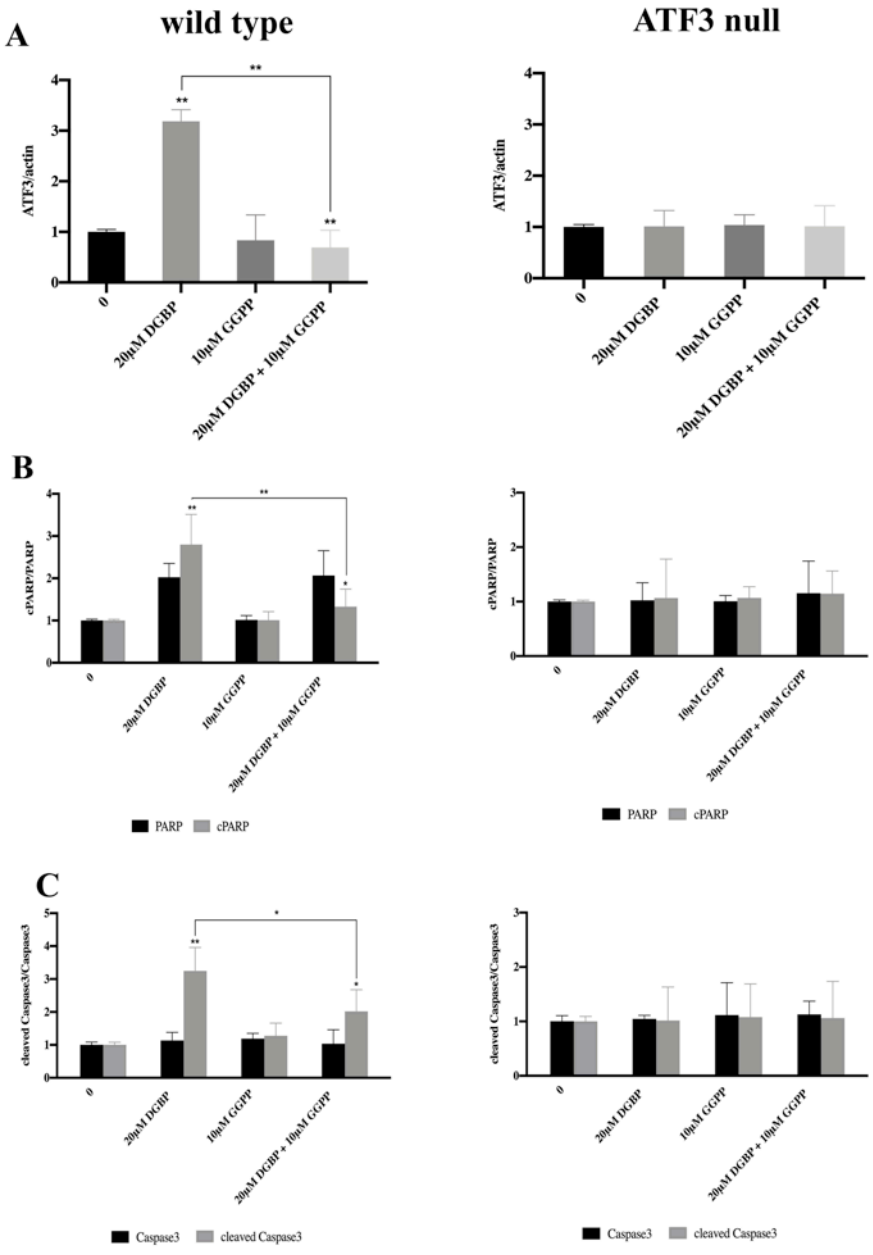

Supplemental Figure S11. Densitometry analysis of Figure 4-9 demonstrating ATF3 and cPARP and cCaspase3 levels normalized to actin and total PARP and Caspase3 levels, respectively. Error bars and ±SD are from the mean of three replicates.

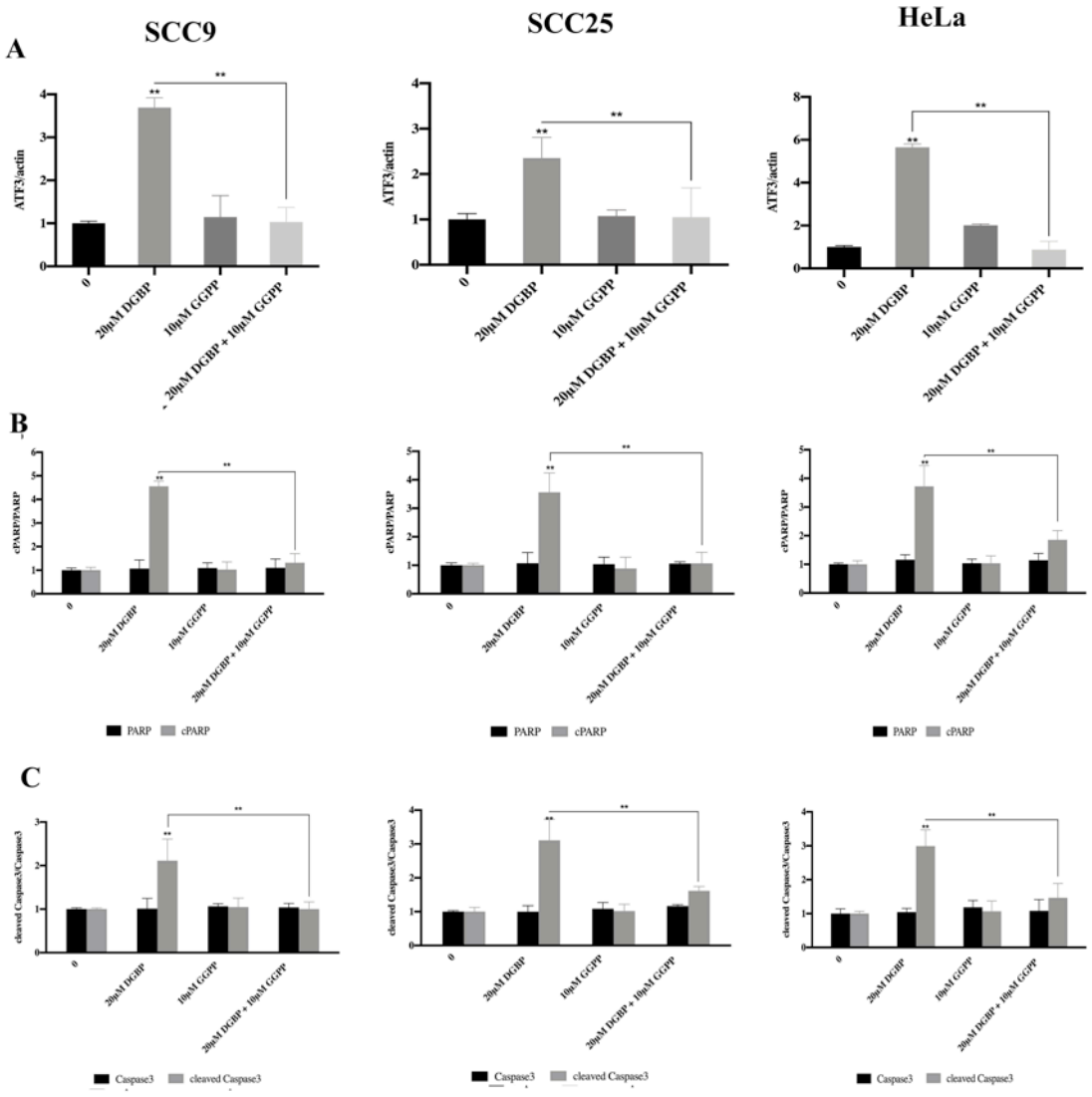

Supplemental Figure S12. Densitometry analysis of Figure 4-10A demonstrating ATF3 levels normalized to actin following DGBP treatment. Error bars and ±SD are from the mean of three replicates.

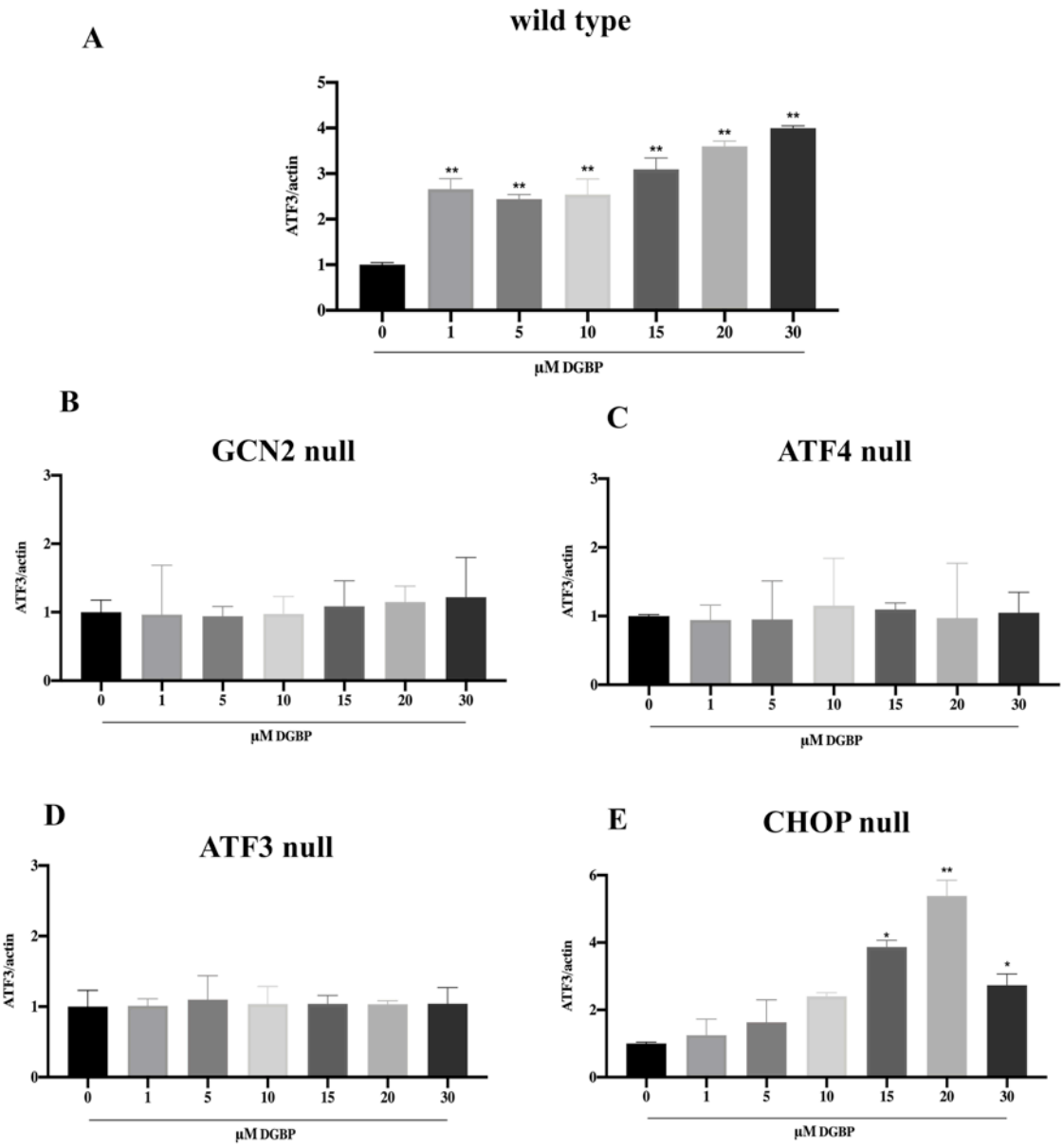

Supplemental Figure S13. Densitometry analysis of Figure 4-10A demonstrating cPARP levels normalized to total PARP levels following DGBP treatment. Error bars and ±SD are from the mean of three replicates.

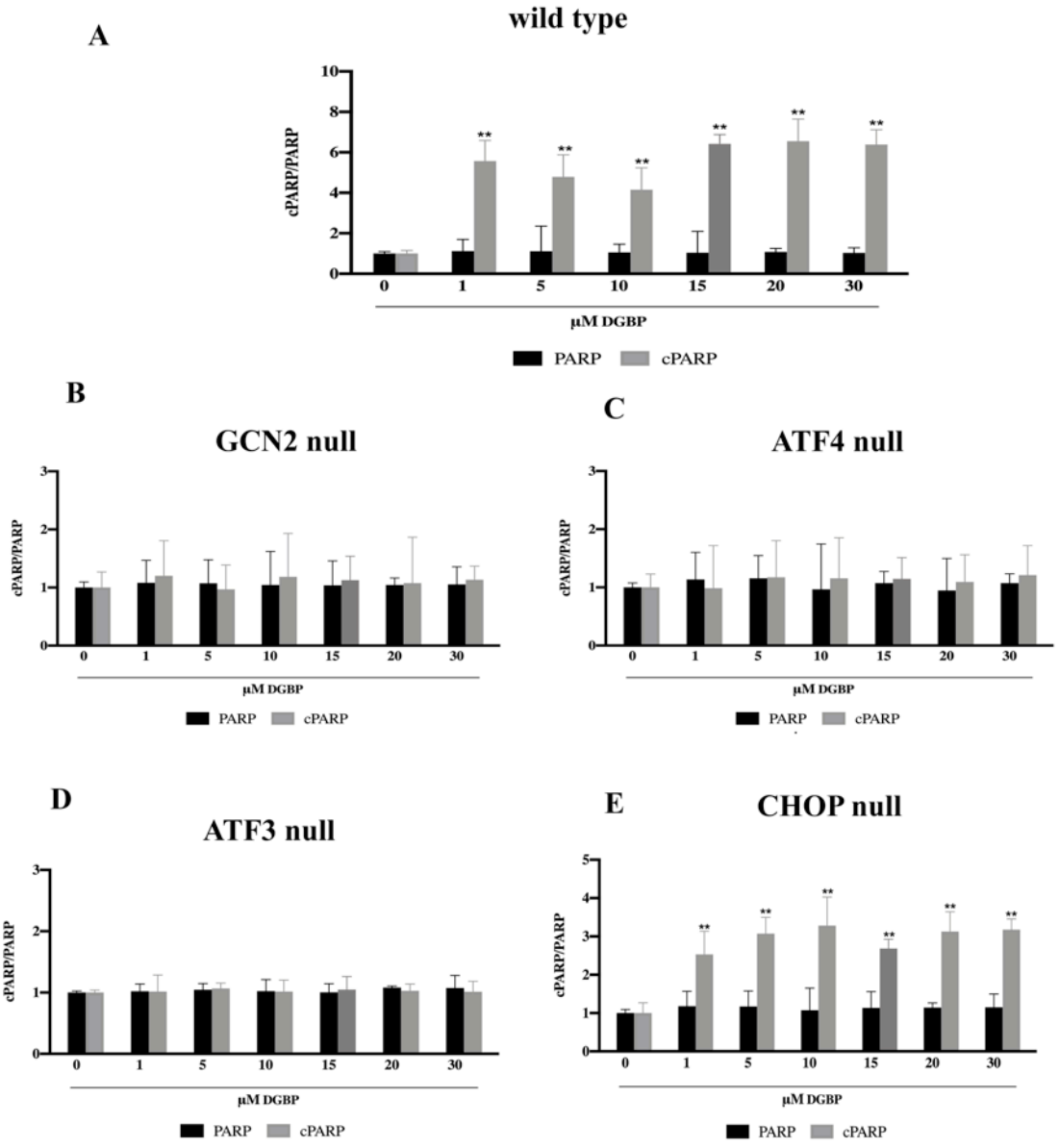

Supplemental Figure S14. Densitometry analysis of Figure 4-10A demonstrating ATF3 levels normalized to actin levels following afatinib treatment. Error bars and ±SD are from the mean of three replicates.

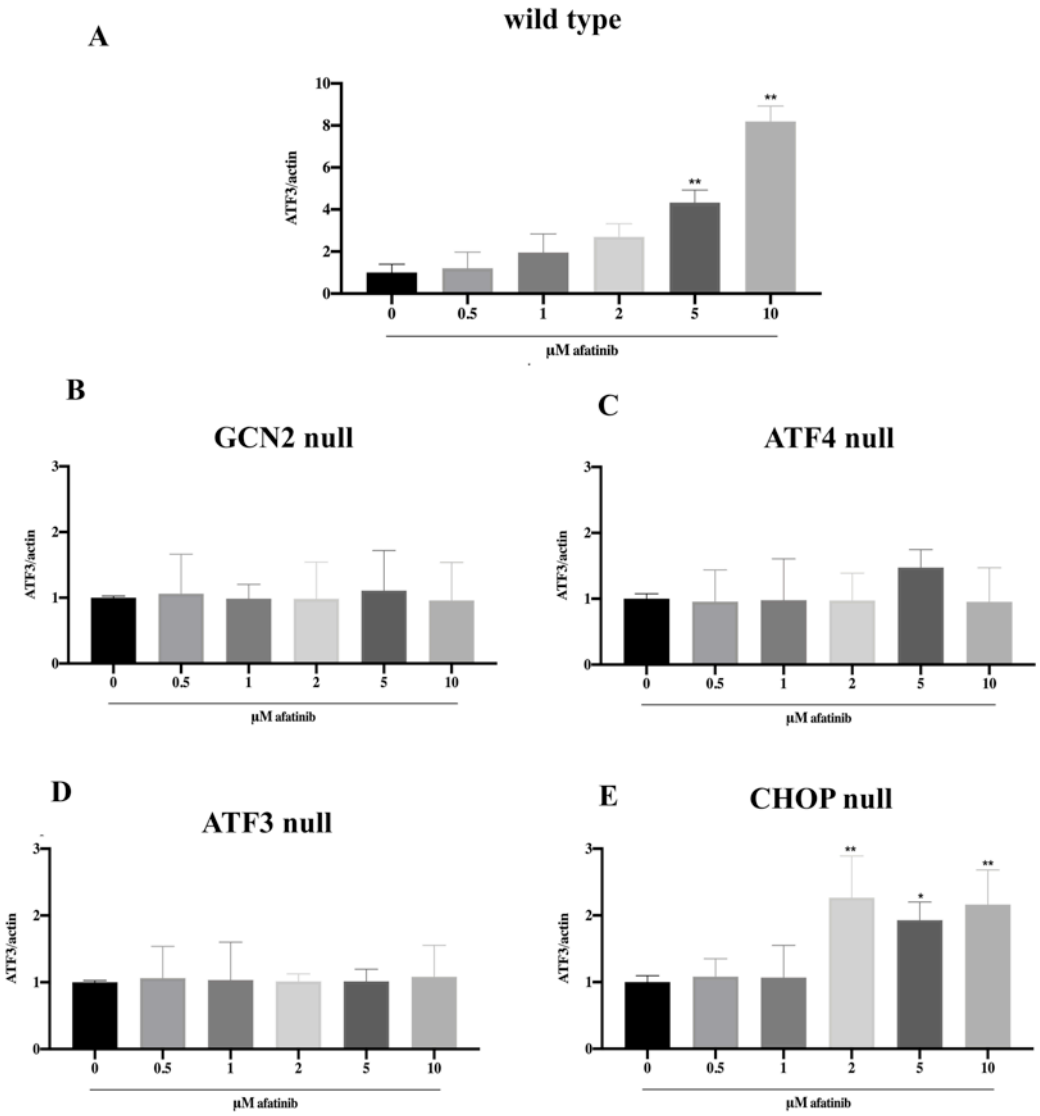

Supplemental Figure S15. Densitometry analysis of Figure 4-10A demonstrating cPARP levels normalized to total PARP levels following afatinib treatment. Error bars and ±SD are from the mean of three replicates.

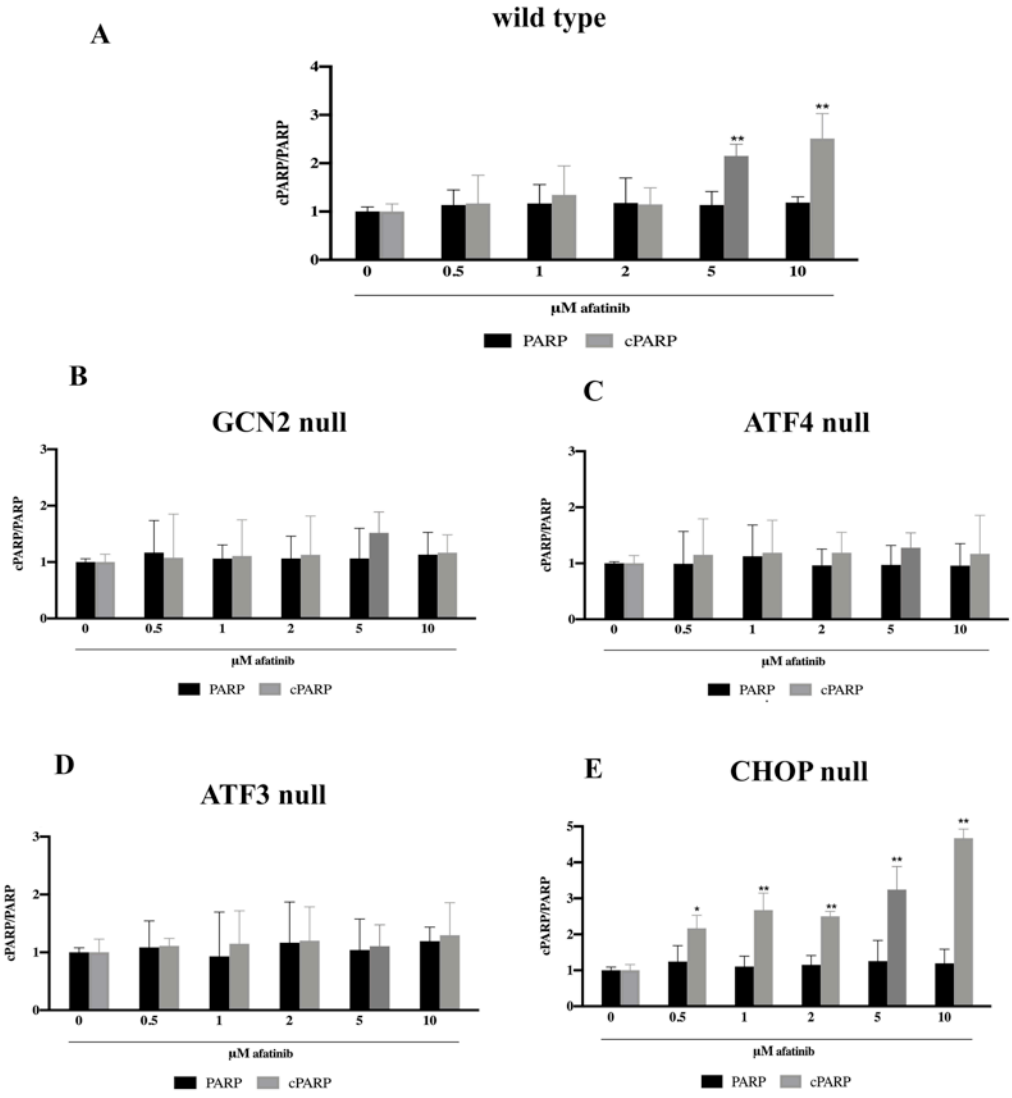

Supplemental Figure S16. Densitometry analysis of Figure 4-14A demonstrating ATF3 levels normalized to actin. Error bars and ±SD are from the mean of three replicates.

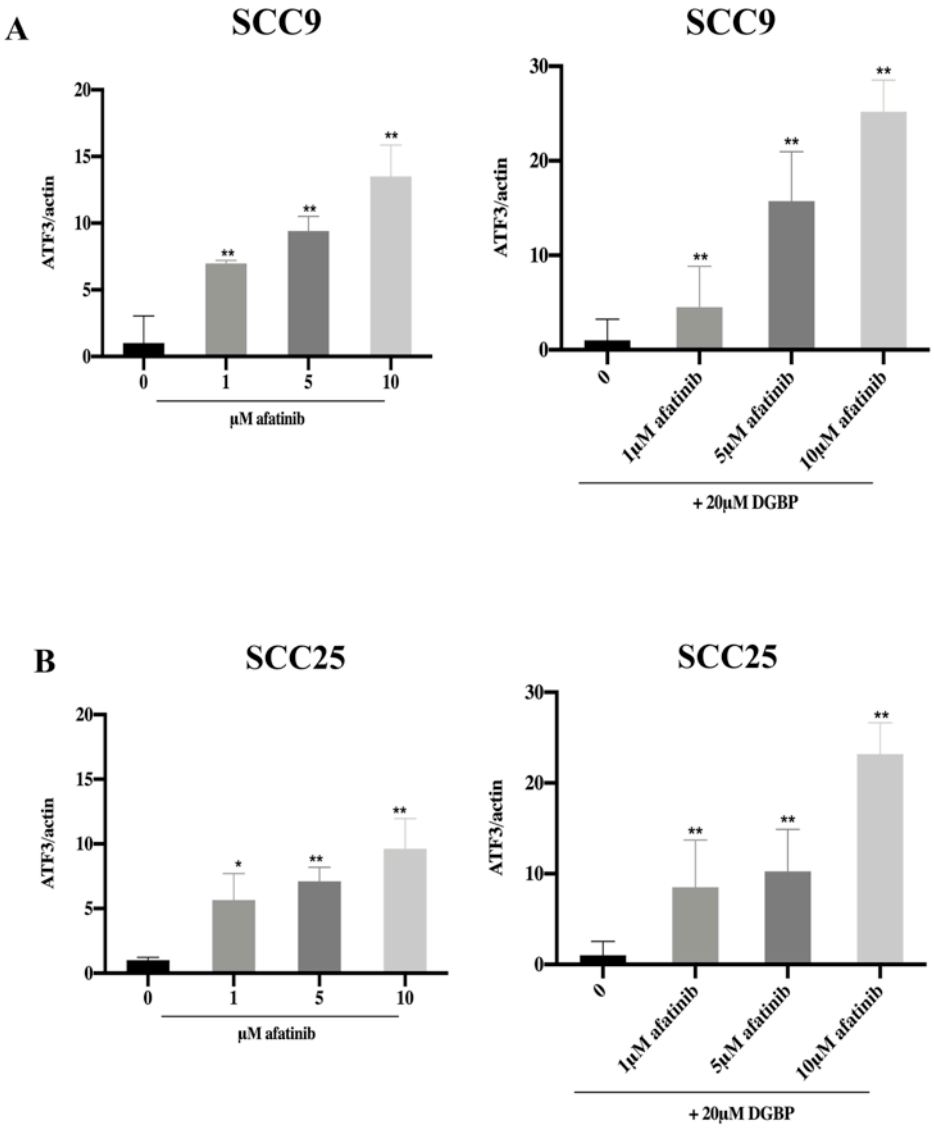

Supplemental Figure S17. Densitometry analysis of Figure 4-14A demonstrating cPARP levels normalized to total PARP levels. Error bars, ±SD from the mean of three replicates.

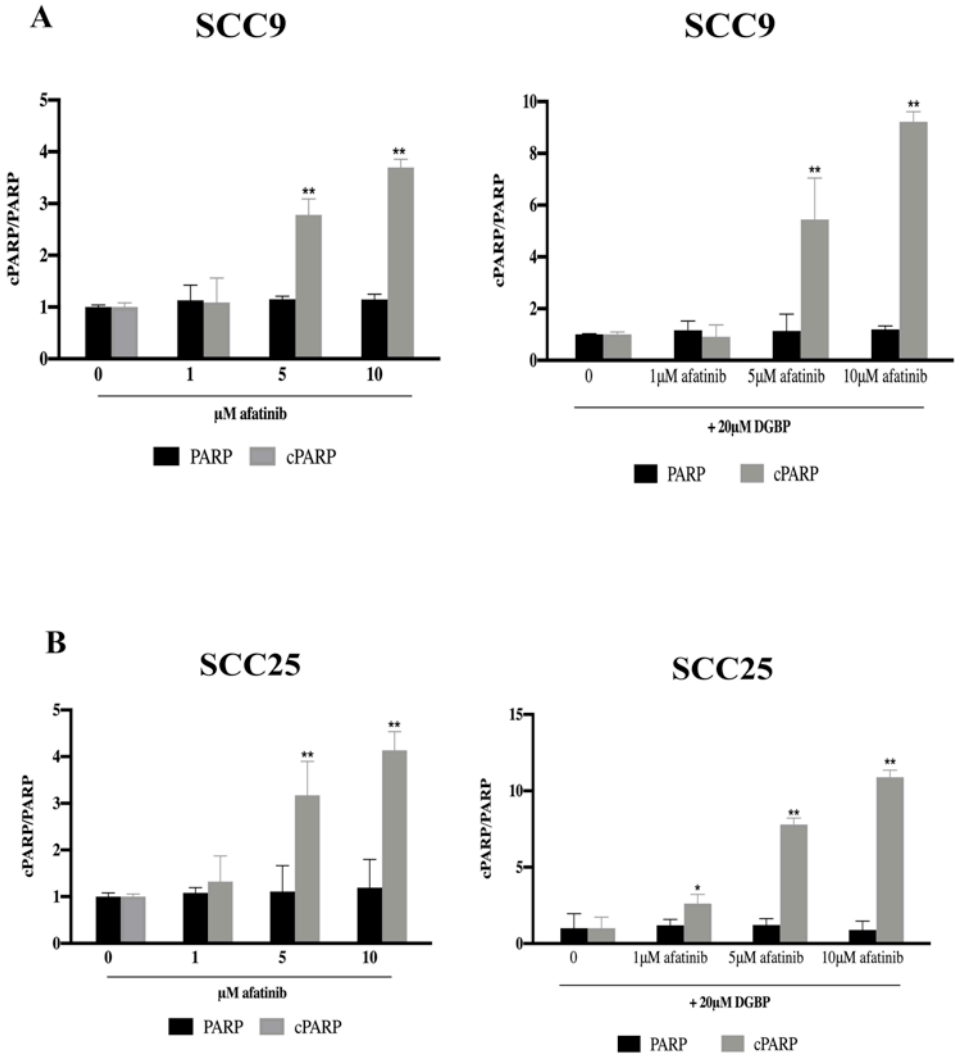

APPENDIX II

Supplemental Figure S18. Venn diagram demonstrating the number of the genes that were differentially expressed following the treatment of SCC25 with 10μM lovastatin or 10μM GGTI-298.

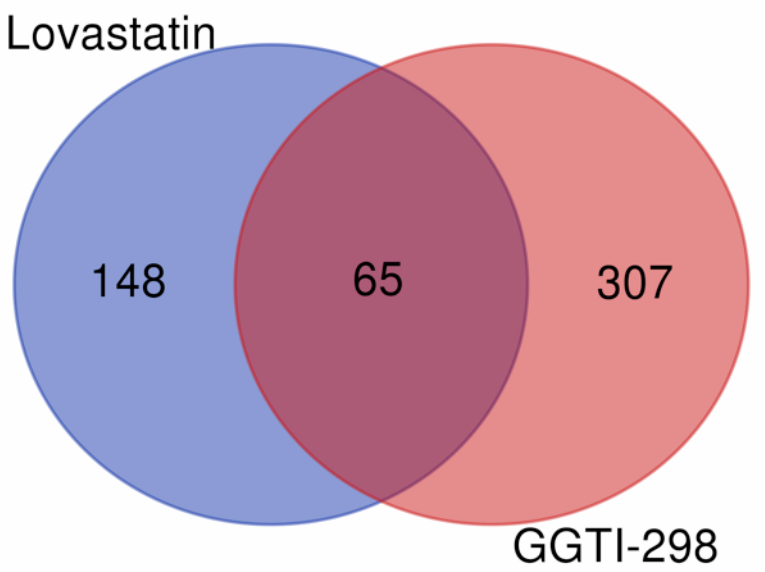

Supplemental Figure S19. GO analysis of the differentially expressed genes following (A) 10μM lovastatin and (B) 10μM GGTI-298 in SCC25 highlighting the top 8 terms showing fold enrichment based on the FDR values and (Log2N±2).

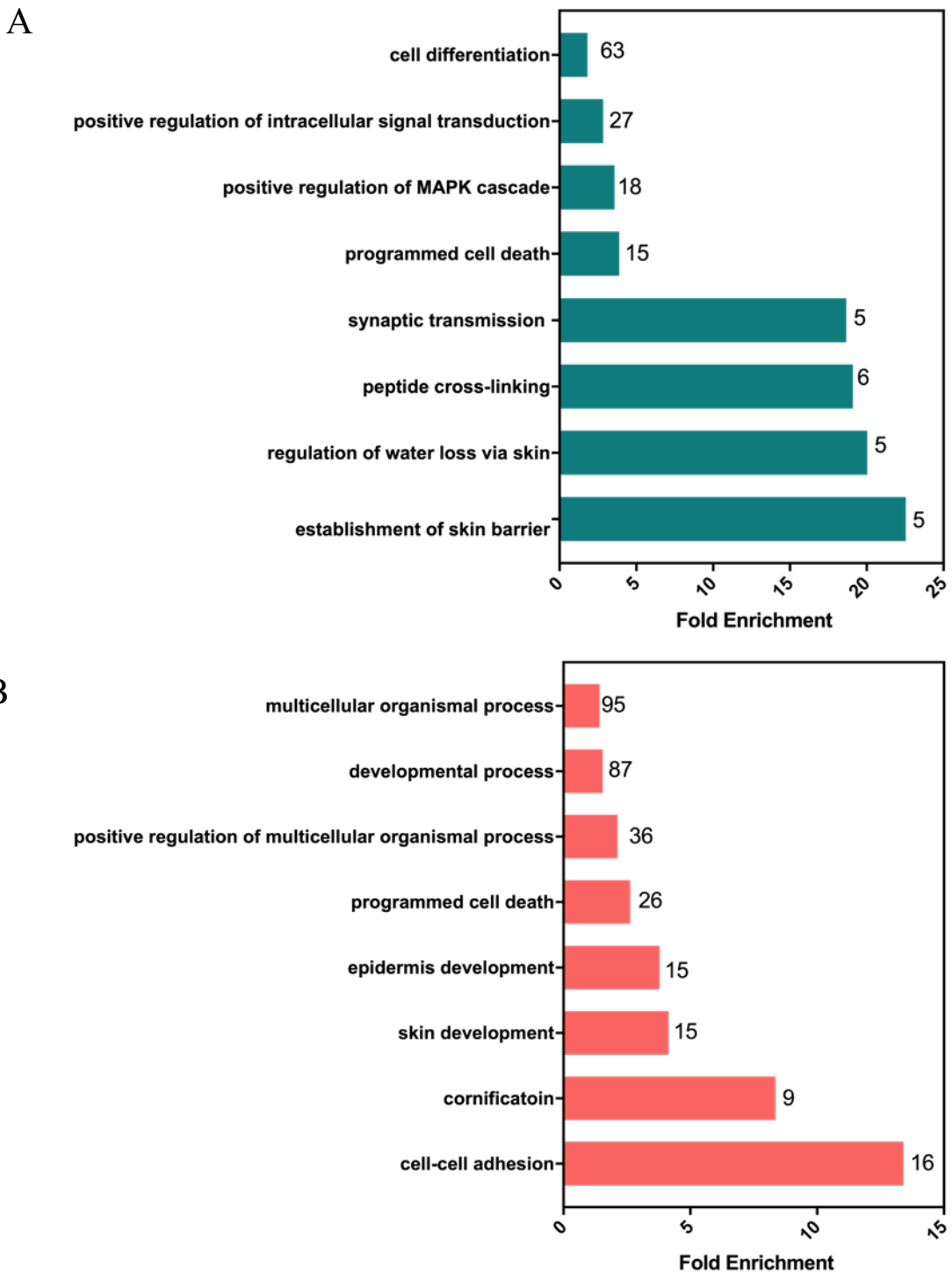

Supplemental Figure S20. (A) Venn diagram demonstrating the subset of the genes that were differentially induced following the 24hrs treatment of SCC25 with 10μM lovastatin and 10μM GGTI-298. (B) GO analysis of the differentially upregulated genes following 10μM lovastatin and 10μM GGTI-298 in SCC25 highlighting the top 16 terms showing fold enrichment based on the FDR values and ($Log_2N\pm2$).

A

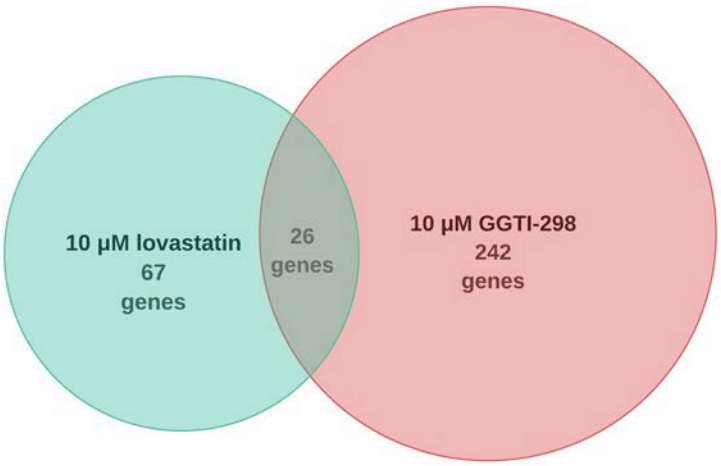

B

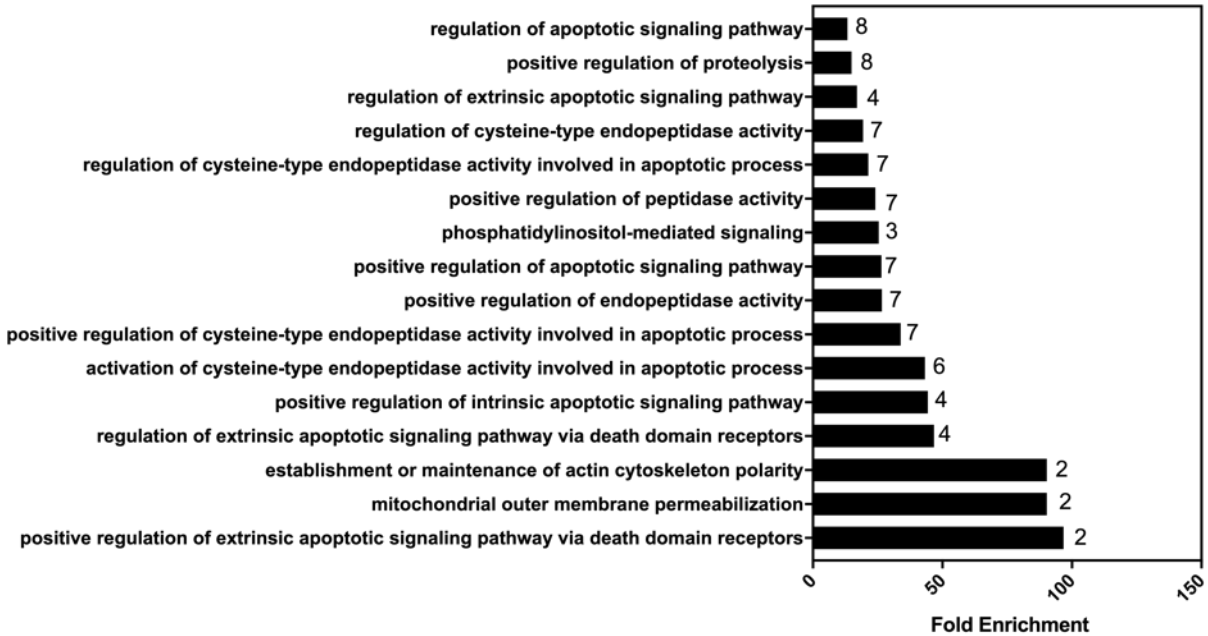

APPENDIX III

Supplemental Table S1. A table highlights the gene names of the 26 upregulated genes following the 24hrs treatment of SCC25 with 10μM lovastatin and 10μM GGTI-298.

GO biological process complete	Gene	Gene name
Apoptosis Regulagtor	AMIGO2	Amphoterin-induced protein 2
	ACTN2	Alpha-actinin-2
	ATF3	Cyclic AMP-dependent activating transcription factor ATF-3
	BBC3/PUMA	Bcl-2-binding component 3
	BMF	Bcl-2-modifying factor
	LGALS7	Galectin-7
	rhoA	Transforming protein Ras homolog family member A
	rhoB	Transforming protein Ras homolog family member B
Death Ligand Pathways	Fas	Fatty acid synthase-Tumor necrosis factor receptor superfamily member 6
	TRAIL-R	TNF-related apoptosis-inducing ligand-receptor
	TRADD	Tumor necrosis factor receptor type 1-associated DEATH domain protein
	FLIP	FLICE-like inhibitory protein
Growth Factor Signaling	EGF	Epidermal growth factor
	FGF	Fibroblast growth factor ligand
	NGF	Beta-nerve growth factor
	FGFR	Fibroblast growth factor receptor
	PDGFR	Platelet-derived growth factor receptor beta
	Ras	rat sarcoma viral oncogene
	JNK	c-Jun N-terminal kinases
	JUND	Transcription factor jun-D
	c-JUN	cellular human protein that encoded by the JUN gene
	DDIT4	DNA damage-inducible transcript 4 protein
Calcium Homeostasis	S100A8	Protein S100-A8
	S100A9	Protein S100-A9
	SLC8A1	Sodium/calcium exchanger 1
	MAL	T-cell surface glycoprotein CD8 alpha chain CD8A

REFERENCES

1. Wen Y, Grandis JR. Emerging drugs for head and neck cancer. Expert Opin Emerg Drugs. 2015;20:1–17.
2. Egle A, Greil R, Melchardt T. Update on squamous cell carcinoma of the head and neck ASCO annual meeting 2017. 2017;220–3.
3. Fitzmaurice C, Allen C, Barber RM, Barregard L, Bhutta ZA, Brenner H, et al. Global, regional, and national cancer incidence, mortality, years of life lost, years lived with disability, and disability-adjusted life-years for 32 cancer groups, 1990 to 2015: A Systematic Analysis for the Global Burden of Disease Study Global Burden . JAMA Oncol. 2017;3:524–48.
4. Marur S, Forastiere AA. Head and Neck Squamous Cell Carcinoma: Update on Epidemiology, Diagnosis, and Treatment. Mayo Clin. Proc. 2016. page 386–96.
5. José Silva-Oliveira R, Melendez M, Martinho O, Zanon MF, de Souza Viana L, Lopes Carvalho A, et al. AKT can modulate the in vitro response of HNSCC cells to irreversible EGFR inhibitors. Oncotarget. 2017;8:53288–301.
6. Bose P, Brockton NT, Dort JC. Head and neck cancer: From anatomy to biology. Int J Cancer. 2013;133:2013–23.
7. Martinez-Useros J, Garcia-Foncillas J. The challenge of blocking a wider family members of EGFR against Head and neck squamous cell carcinomas. Oral Oncol. 2015;51:423–30.
8. Shah JP. Staging for Head and Neck Cancer: Purpose, Process and Progress. Indian J Surg Oncol. Indian Journal of Surgical Oncology; 2018;9:116–20.
9. Rieke DT, Klinghammer K, Keilholz U. Targeted Therapy of Head and Neck Cancer. Oncol. Res. Treat. 2016. page 780–6.
10. Johnson-Obaseki S, McDonald JT, Corsten M, Rourke R. Head and neck cancer in Canada: Trends 1992 to 2007. Otolaryngol - Head Neck Surg (United States). 2012. page 74–8.
11. Guo T, Califano JA. Molecular Biology and Immunology of Head and Neck Cancer. Surg. Oncol. Clin. N. Am. 2015. page 397–407.
12. Faraji F, Zaidi M, Fakhry C, Gaykalova DA. Molecular mechanisms of human papillomavirus-related carcinogenesis in head and neck cancer. Microbes Infect. 2017. page 464–75.
13. Straight SW, Hinkle PM, Jewers RJ, McCance DJ. The E5 oncoprotein of human papillomavirus type 16 transforms fibroblasts and effects the downregulation of the epidermal growth factor receptor in keratinocytes. J Virol. 1993;67:4521–32.
14. Scheffner M, Werness BA, Huibregtse JM, Levine AJ, Howley PM. The E6 oncoprotein encoded by human papillomavirus types 16 and 18 promotes the degradation of p53. Cell. 1990;63:1129–36.
15. Dyson N, Howley P, Munger K, Harlow E. The human papilloma virus-16 E7 oncoprotein is able to bind to the retinoblastoma gene product. Science. 1989;243:934–7.
16. Echrri MJ, Lopiz-Martin A, Hit R. Targeted Therapy in Locally Advanced and Recurrent/Metastatic Head and Neck Squamous Cell Carcinoma (LA-R/M HNSCC). Cancers (Basel). 2016;8.
17. Woolgar JA, Triantafyllou A. Pitfalls and procedures in the histopathological diagnosis of oral and oropharyngeal squamous cell carcinoma and a review of the role of pathology in prognosis. Oral Oncol. 2009. page 361–85.
18. Aung KL, Siu LL. Genomically personalized therapy in head and neck cancer. Cancers Head Neck. 2016;1:2.
19. Yamamoto VN, Thylur DS, Bauschard M, Schmale I, Sinha UK. Overcoming radioresistance in head and neck squamous cell carcinoma. Oral Oncol. 2016. page 44–51.
20. Seiwert TY, Salama JK, Vokes EE. The chemoradiation paradigm in head and neck cancer. Nat Clin Pract Oncol. 2007;4:156–71.
21. Pan Q, Gorin M a, Teknos TN. Pharmacotherapy of head and neck squamous cell carcinoma. Expert Opin Pharmacother. 2009;10:2291–302.
22. Machiels JPH, Licitra LF, Haddad RI, Tahara M, Cohen EEW. Rationale and design of LUX-Head

& Neck 1: A randomised, Phase III trial of afatinib versus methotrexate in patients with recurrent and/or metastatic head and neck squamous cell carcinoma who progressed after platinum-based therapy. BMC Cancer. 2014;14.
23. Winquist E, Agbassi C, Meyers BM, Yoo J, Chan KKW. Systemic therapy in the curative treatment of head and neck squamous cell cancer: a systematic review. J Otolaryngol - Head Neck Surg. 2017;46:29.
24. Moon C, Chae YK, Lee J. Targeting epidermal growth factor receptor in head and neck cancer: lessons learned from cetuximab. Exp Biol Med. 2010;235:907–20.
25. Moreira J, Tobias A, O'Brien MP, Agulnik M. Targeted Therapy in Head and Neck Cancer: An Update on Current Clinical Developments in Epidermal Growth Factor Receptor-Targeted Therapy and Immunotherapies. Drugs. 2017. page 843–57.
26. Nicholson RI, Gee JM, Harper ME. EGFR and cancer prognosis. Eur J Cancer. 2001;37 Suppl 4:S9–15.
27. Mendelsohn J, Baselga JM. The EGF receptor family as targets for cancer therapy. Oncogene. 2000;19:6550–65.
28. Roskoski R. The ErbB/HER family of protein-tyrosine kinases and cancer. Pharmacol. Res. 2014. page 34–74.
29. Yarden Y. The EGFR family and its ligands in human cancer. signalling mechanisms and therapeutic opportunities. Eur J Cancer. 2001;37 Suppl 4:S3–8.
30. Herbst RS. Review of epidermal growth factor receptor biology. Int. J. Radiat. Oncol. Biol. Phys. 2004. page 21–6.
31. Roskoski R. ErbB/HER protein-tyrosine kinases: Structures and small molecule inhibitors. Pharmacol Res. 2014;87:42–59.
32. Singh AB, Harris RC. Autocrine, paracrine and juxtacrine signaling by EGFR ligands. Cell. Signal. 2005. page 1183–93.
33. Sibilia M, Kroismayr R, Lichtenberger BM, Natarajan A, Hecking M, Holcmann M. The epidermal growth factor receptor: From development to tumorigenesis. Differentiation. 2007. page 770–87.
34. Carpenter G, Cohen S. Epidermal Growth Factor. Annu Rev Biochem. 1979;48:193–216.
35. Cohen S. The epidermal growth factor (EGF). Cancer. 1983;51:1787–91.
36. Yewale C, Baradia D, Vhora I, Patil S, Misra A. Epidermal growth factor receptor targeting in cancer: A review of trends and strategies. Biomaterials. 2013. page 8690–707.
37. Ferguson KM, Berger MB, Mendrola JM, Cho HS, Leahy DJ, Lemmon MA. EGF activates its receptor by removing interactions that autoinhibit ectodomain dimerization. Mol Cell. 2003;11:507–17.
38. Lemmon MA. Ligand-induced ErbB receptor dimerization. Exp. Cell Res. 2009. page 638–48.
39. Singh B, Carpenter G, Coffey RJ. EGF receptor ligands: recent advances. F1000Research. 2016;5:2270.
40. Dawson JP, Bu Z, Lemmon MA. Ligand-Induced Structural Transitions in ErbB Receptor Extracellular Domains. Structure. 2007;15:942–54.
41. Tomas A, Futter CE. Stress reveals new destination for EGF receptor. Cell Cycle. 2015;14:3343–4.
42. Chen X, Su M, Chen T, Hong H, Han A, Li W. Oxidative stress affects retinal pigment epithelial cell survival through epidermal growth factor receptor/AKT signaling pathway. Int J Ophthalmol. 2017;10:507–14.
43. Daub H, Weiss FU, Wallasch C, Ullrich A. Role of transactivation of the EGF receptor in signalling by G-protein-coupled receptors. Nature. 1996;379:557–60.
44. Lemmon MA, Schlessinger J. Cell signaling by receptor tyrosine kinases. Cell. 2010. page 1117–34.
45. Chappell WH, Steelman LS, Long JM, Kempf RC, Abrams SL, Franklin RA, et al. Ras/Raf/MEK/ERK and PI3K/PTEN/Akt/mTOR inhibitors: rationale and importance to inhibiting these pathways in human health. Oncotarget. 2011;2:135–64.
46. Molina JR, Adjei AA. The Ras/Raf/MAPK pathway. J. Thorac. Oncol. 2006. page 7–9.

47. Plotnikov A, Zehorai E, Procaccia S, Seger R. The MAPK cascades: Signaling components, nuclear roles and mechanisms of nuclear translocation. Biochim Biophys Acta - Mol Cell Res. 2011;1813:1619–33.
48. Vivanco I, Sawyers CL. The phosphatidylinositol 3-Kinase AKT pathway in human cancer. Nat Rev Cancer. 2002;2:489–501.
49. Stransky N, Egloff AM, Tward AD, Kostic AD, Cibulskis K, Sivachenko A, et al. The mutational landscape of head and neck squamous cell carcinoma. Science. 2011;333:1157–60.
50. Hanahan D, Weinberg RA. Hallmarks of cancer: the next generation. Cell. 2011;144:646–74.
51. Haddad R, Wirth L, Posner M. Emerging drugs for head and neck cancer. Expert Opin Emerg Drugs. 2015;20:313–29.
52. Ang KK, Berkey B a, Tu X, Zhang H-Z, Katz R, Hammond EH, et al. Impact of epidermal growth factor receptor expression on survival and pattern of relapse in patients with advanced head and neck carcinoma. Cancer Res. 2002;62:7350–6.
53. Qian G, Jiang N, Wang D, Newman S, Kim S, Chen Z, et al. Heregulin and HER3 are prognostic biomarkers in oropharyngeal squamous cell carcinoma. Cancer. 2015;121:3600–11.
54. Mak MP, William WN. Targeting the epidermal growth factor receptor for head and neck cancer chemoprevention. Oral Oncol. 2014;50:918–23.
55. Crombet T, Torres O, Neninger E, Catala M, Rodriguez N, Ramos M, et al. Phase I clinical evaluation of a neutralizing monoclonal antibody against epidermal growth factor receptor. Cancer Biother Radiopharm. 2001;16:93–102.
56. Specenier P, Vermorken JB. Cetuximab: Its unique place in head and neck cancer treatment. Biol Targets Ther. 2013;7:77–90.
57. Goldstein NI, Prewett M, Zuklys K, Rockwell P, Mendelsohn J. Biological efficacy of a chimeric antibody to the epidermal growth factor receptor in a human tumor xenograft model. Clin Cancer Res. 1995;1:1311–8.
58. Stamos J, Sliwkowski MX, Eigenbrot C. Structure of the epidermal growth factor receptor kinase domain alone and in complex with a 4-anilinoquinazoline inhibitor. J Biol Chem. 2002;277:46265–72.
59. Arora A, Scholar EM. Role of tyrosine kinase inhibitors in cancer therapy. J Pharmacol Exp Ther. 2005;315:971–9.
60. Yang Z, Hackshaw A, Feng Q, Fu X, Zhang Y, Mao C, Tang J. Comparison of gefitinib, erlotinib and afatinib in non-small cell lung cancer: A meta-analysis. Int J Cancer Comp. 2017.
61. Bareschino MA, Schettino C, Troiani T, Martinelli E, Morgillo F, Ciardiello F. Erlotinib in cancer treatment. Ann Oncol. 2007.
62. Shepherd FA, Pereira JR, Ciuleanu T, Tan EH, Hirsh V, Thongprasert S, et al. Erlotinib in Previously Treated Non–Small-Cell Lung Cancer. J Med. 2005;353:9–19.
63. Soulieres D, Senzer NN, Vokes EE, Hidalgo M, Agarvala SS, Siu LL. Multicenter phase II study of erlotinib, an oral epidermal growth factor receptor tyrosine kinase inhibitor, in patients with recurrent or metastatic squamous cell cancer of the head and neck. J Clin Oncol. 2004;22:77–85.
64. Siu LL, Soulieres D, Chen EX, Pond GR, Chin SF, Francis P, et al. Phase I/II trial of erlotinib and cisplatin in patients with recurrent or metastatic squamous cell carcinoma of the head and neck: A Princess Margaret Hospital Phase II Consortium and National Cancer Institute of Canada Clinical Trials Group study. J Clin Oncol. 2007;25:2178–83.
65. Cohen EEW, Rosen F, Stadler WM, Recant W, Stenson K, Huo D, et al. Phase II trial of ZD1839 in recurrent or metastatic squamous cell carcinoma of the head and neck. J Clin Oncol. 2003;21:1980–7.
66. Cohen EEW, Kane MA, List MA, Brockstein BE, Mehrotra B, Huo D, et al. Phase II trial of gefitinib 250 mg daily in patients with recurrent and/or metastatic squamous cell carcinoma of the head and neck. Clin Cancer Res. 2005;11:8418–24.
67. Kozakiewicz P, Grzybowska-Szatkowska L. Application of molecular targeted therapies in the treatment of head and neck squamous cell carcinoma. Oncol Lett. 2018;15:7497–505.

68. Perisanidis C. Prevalence of EGFR Tyrosine Kinase Domain Mutations in Head and Neck Squamous Cell Carcinoma : Cohort Study and Systematic Review. In Vivo (Brooklyn). 2017;34:23–34.
69. Vatte C, Cyrus C, Chathoth S, Al Amri AM, Al Ali Z, Alshreadah ST, et al. Tyrosine kinase domain mutations of EGFR gene in head and neck squamous cell carcinoma. Onco Targets Ther. 2017;10:1527–33.
70. Paez JG, Jänne P, Lee JC, Tracy S, Greulich H, Gabriel S, et al. EGFR mutations in lung cancer: correlation with clinical response to gefitinib therapy. Science. 2004;304:1497–500.
71. Lynch TJ, Bell DW, Sordella R, Gurubhagavatula S, Okimoto RA, Brannigan BW, et al. Activating mutations in the epidermal growth factor receptor underlying responsiveness of non-small-cell lung cancer to gefitinib. N Engl J Med. 2004;350:2129–39.
72. Yun C-H, Mengwasser KE, Toms A V., Woo MS, Greulich H, Wong K-K, et al. The T790M mutation in EGFR kinase causes drug resistance by increasing the affinity for ATP. Proc Natl Acad Sci. 2008;105:2070–5.
73. Zhou W, Ercan D, Chen L, Yun CH, Li D, Capelletti M, et al. Novel mutant-selective EGFR kinase inhibitors against EGFR T790M. Nature. 2009;462:1070–4.
74. Kobayashi S, Boggon TJ, Dayaram T, Jänne PA, Kocher O, Meyerson M, et al. *EGFR* Mutation and Resistance of Non–Small-Cell Lung Cancer to Gefitinib. N Engl J Med. 2005;352:786–92.
75. Abdallah SM, Hirsh V. Epidermal Growth Factor Receptor Tyrosine Kinase Inhibitors in Treatment of Metastatic Non-Small Cell Lung Cancer, with a Focus on Afatinib. 2017;7.
76. Wind S, Schnell D, Ebner T, Freiwald M, Stopfer P. Clinical Pharmacokinetics and Pharmacodynamics of Afatinib. Clin. Pharmacokinet. 2017. page 235–50.
77. Specenier P, Vermorken J. Expert Opinion on Pharmacotherapy Afatinib in squamous cell carcinoma of the head and neck. 2016;6566.
78. Hirsh V. New developments in the treatment of advanced squamous cell lung cancer : focus on afatinib. 2017;2513–26.
79. De Pauw I, Lardon F, Van den Bossche J, Baysal H, Fransen E, Deschoolmeester V, et al. Simultaneous targeting of EGFR, HER2 and HER4 by afatinib overcomes intrinsic and acquired cetuximab resistance in head and neck squamous cell carcinoma cell lines. Mol Oncol. 2018.
80. Seiwert TY, Fayette J, Cupissol D, del Campo JM, Clement PM, Hitt R, et al. A randomized, phase II study of afatinib versus cetuximab in metastatic or recurrent squamous cell carcinoma of the head and neck. Ann Oncol. 2014;25:1813–20.
81. Liu X, Lv Z, Zou J, Liu X, Ma J, Wang J, et al. Afatinib down-regulates MCL-1 expression through the PERK-eIF2α-ATF4 axis and leads to apoptosis in head and neck squamous cell carcinoma. 2016;6:1708–19.
82. Soria J-C, Felip E, Cobo M, Lu S, Syrigos K, Lee KH, et al. Afatinib versus erlotinib as second-line treatment of patients with advanced squamous cell carcinoma of the lung (LUX-Lung 8): an open-label randomised controlled phase 3 trial. Lancet Oncol. 2015;
83. Felip E, Hirsh V, Popat S, Cobo M, Fülöp A, Dayen C, et al. Symptom and Quality of Life Improvement in LUX-Lung 8 , an Open-Label Phase III Study of Second-Line Afatinib Versus Erlotinib in Patients With Advanced Squamous Cell Carcinoma of the Lung After First-Line Platinum-Based Chemotherapy. Clin Lung Cancer. 2017.
84. Zhou F, Chen X, Zhou C. Epidermal growth factor receptor tyrosine kinase inhibitors in patients with EGFR wild-type lung cancer: When there is a target, there is a targeted drug. J. Clin. Oncol. 2015. page 523–4.
85. Buhaescu I, Izzedine H. Mevalonate pathway: A review of clinical and therapeutical implications. Clin. Biochem. 2007. page 575–84.
86. Iannelli F, Lombardi R, Milone MR, Pucci B, De Rienzo S, Budillon A, et al. Targeting Mevalonate Pathway in Cancer Treatment: Repurposing of Statins. Recent Pat Anticancer Drug Discov. 2018.
87. Goldstein JL, Brown MS. Regulation of the mevalonate pathway. Nature. 1990;343:425–30.
88. Xu N, Shen N, Wang XX, Jiang S, Xue B, Li CJ. Protein prenylation and human diseases: a balance

of protein farnesylation and geranylgeranylation. Sci China Life Sci. 2015;58:328–35.
89. Fritz V, Benfodda Z, Henriquet C, Hure S, Cristol JP, Michel F, et al. Metabolic intervention on lipid synthesis converging pathways abrogates prostate cancer growth. Oncogene. 2013;32:5101–10.
90. Parrales A, Thoenen E, Iwakuma T. The interplay between mutant p53 and the mevalonate pathway. Cell Death Differ. Springer US; 2017.
91. Endo A. A historical perspective on the discovery of statins. Proc Jpn Acad, Ser B. 2010;
92. Ahmadi Y, Ghorbanihaghjo A, Argani H. The balance between induction and inhibition of mevalonate pathway regulates cancer suppression by statins: A review of molecular mechanisms. Chem Biol Interact. 2017;273:273–85.
93. Istvan ES, Deisenhofer J. Structural mechanism for statin inhibition of HMG-CoA reductase. Science. 2001;292:1160–4.
94. Shitara Y, Sugiyama Y. Pharmacokinetic and pharmacodynamic alterations of 3-hydroxy-3-methylglutaryl coenzyme A (HMG-CoA) reductase inhibitors: Drug-drug interactions and interindividual differences in transporter and metabolic enzyme functions. Pharmacol. Ther. 2006. page 71–105.
95. Altwairgi AK. Statins are potential anticancerous agents (Review). Oncol Rep. 2015;33:1019–39.
96. Pavan LM, Rego DF, Elias ST, De Luca Canto G, Guerra EN. In vitro Anti-Tumor Effects of Statins on Head and Neck Squamous Cell Carcinoma: A Systematic Review. PLoS One. 2015;10:e0130476.
97. Dimitroulakos J, Ye LY, Benzaquen M, Moore MJ, Kamel-Reid S, Freedman MH, et al. Differential sensitivity of various pediatric cancers and squamous cell carcinomas to lovastatin-induced apoptosis: Therapeutic implications. Clin Cancer Res. 2001;7:158–67.
98. Khurana V, Bejjanki HR, Caldito G, Owens MW. Statins reduce the risk of lung cancer in humans: A large case-control study of US Veterans. Chest. 2007;131:1282–8.
99. Minden MD, Dimitroulakos J, Nohynek D, Penn LZ. Lovastatin induced control of blast cell growth in an elderly patient with acute myeloblastic leukemia. Leuk Lymphoma. 2001;40:659–62.
100. Macaulay RJBB, Wang W, Dimitroulakos J, Becker LE, Yeger H. Lovastatin-induced apoptosis of human medulloblastoma cell lines in vitro. J Neurooncol. 1999;42:1–11.
101. Dimitroulakos J, Yeger H. HMG-CoA reductase mediates the biological effects of retinoic acid on human neuroblastoma cells: lovastatin specifically targets P-glycoprotein-expressing cells. Nat Med. 1996;2:326–33.
102. Dimitroulakos J, Thai S, Wasfy GH, Hedley DW, Minden MD, Penn LZ. Lovastatin induces a pronounced differentiation response in acute myeloid leukemias. Leuk Lymphoma. 2000;40:167–78.
103. Knox JJ, Siu LL, Chen E, Dimitroulakos J, Kamel-Reid S, Moore MJ, et al. A Phase I trial of prolonged administration of lovastatin in patients with recurrent or metastatic squamous cell carcinoma of the head and neck or of the cervix. Eur J Cancer. 2005;41:523–30.
104. Mantha AJ, McFee KE, Niknejad N, Goss G, Lorimer IA, Dimitroulakos J. Epidermal growth factor receptor-targeted therapy potentiates lovastatin-induced apoptosis in head and neck squamous cell carcinoma cells. J Cancer Res Clin Oncol. 2003;129:631–41.
105. Zhao TT, Le Francois BG, Goss G, Ding K, Bradbury P a, Dimitroulakos J. Lovastatin inhibits EGFR dimerization and AKT activation in squamous cell carcinoma cells: potential regulation by targeting rho proteins. Oncogene. 2010;29:4682–92.
106. Ringerike T, Blystad FD, Levy FO, Madshus IH, Stang E. Cholesterol is important in control of EGF receptor kinase activity but EGF receptors are not concentrated in caveolae. J Cell Sci. 2002;115:1331–40.
107. Garcia-Ruiz C, Morales A F-CJ. Statins and protein prenylation in cancer cell biology and therapy. Anticancer Agents Med Che. 2012;12(4):303-:303–15.
108. Mantha AJ, Hanson JEL, Goss G, Lagarde AE, Lorimer IA, Dimitroulakos J. Targeting the mevalonate pathway inhibits the function of the epidermal growth factor receptor. Clin Cancer Res.

2005;11:2398–407.
109. Dayekh K, Johnson-Obaseki S, Corsten M, Villeneuve PJ, Sekhon H, Weberpals JI, et al. Monensin Inhibits Epidermal Growth Factor Receptor Trafficking and Activation: Synergistic Cytotoxicity in Combination with EGFR Inhibitors. MolCancer Ther. 2014;2559–72.
110. Goss GD, Jonker DJ, Laurie SA, Weberpals JI, Oza AM, Spaans JN, et al. A phase I study of high-dose rosuvastatin with standard dose erlotinib in patients with advanced solid malignancies. J Transl Med. BioMed Central; 2016;14:83.
111. Wong WWL, Dimitroulakos J, Minden MD, Penn LZ. HMG-CoA reductase inhibitors and the malignant cell: the statin family of drugs as triggers of tumor-specific apoptosis. Leuk Off J Leuk Soc Am Leuk Res Fund, UK. 2002;16:508–19.
112. Furberg CD, Pitt B. Withdrawal of cerivastatin from the world market. Curr Control Trials Cardiovasc Med. 2001;2:205–7.
113. Apostolopoulou M, Corsini A, Roden M. The role of mitochondria in statin-induced myopathy. Eur J Clin Invest. 2015;45:745–54.
114. Ramachandran R, Wierzbicki A. Statins, Muscle Disease and Mitochondria. J Clin Med. 2017;6:75.
115. Wang M, Casey PJ. Protein prenylation: Unique fats make their mark on biology. Nat Rev Mol Cell Biol. 2016;17:110–22.
116. Amaya M, Baranova A, Van Hoek ML. Protein prenylation: A new mode of host-pathogen interaction. Biochem Biophys Res Commun. 2011;416:1–6.
117. Berndt N, Hamilton AD, Sebti SM. Targeting protein prenylation for cancer therapy. Nat Rev Cancer. 2011;11:775–91.
118. Takai Y, Sasaki T, Matozaki T. Small GTP-binding proteins. Physiol Rev. 2001;81:153–208.
119. Cox AD, Der CJ. Ras history: The saga continues. Small GTPases. 2010;1:2–27.
120. Bos JL. ras Oncogenes in human cancer: A review. Cancer Res. 1989. page 4682–9.
121. Sebti S, Hamilton AD. Inhibitors of prenyl transferases. Curr Opin Oncol. 1997;9:557–61.
122. Mullen PJ, Yu R, Longo J, Archer MC, Penn LZ. The interplay between cell signalling and the mevalonate pathway in cancer. Nat Rev Cancer. 2016;16:718–31.
123. Shen M, Pan P, Li Y, Li D, Yu H, Hou T. Farnesyltransferase and geranylgeranyltransferase I: Structures, mechanism, inhibitors and molecular modeling. Drug Discov Today. 2015;20:267–76.
124. Mesa RA. Tipifarnib: Farnesyl transferase inhibition at a crossroads. Expert Rev Anticancer Ther. 2006;6:313–9.
125. Agrawal AG, Somani RR. Farnesyltransferase inhibitor as anticancer agent. Mini-Reviews Med Chem. 2009;9:638–52.
126. Miquel K, Pradines A, Sun J, Qian Y, Hamilton AD, Sebti SM, et al. GGTI-298 induces G0-G1 block and apoptosis whereas FTI-277 causes G2- M enrichment in A549 cells. Cancer Res. 1997;57:1846–50.
127. Sun J, Ohkanda J, Coppola D, Yin H, Kothare M, Busciglio B, et al. Geranylgeranyltransferase I Inhibitor GGTI-2154 Induces Breast Carcinoma Apoptosis and Tumor Regression in H-Ras Transgenic Mice. Cancer Res. 2003;63:8922–9.
128. O'Dwyer PJ, G., M., Nguyen, B., Waddell, M.!J. & Chiorean EG. Phase I accelerated dose escalating safety and pharmacokinetic (PK) study of GGTI2418, a novel geranylgeranyltransferase I inhibitor in patients with refractory solid tumors. Ann Oncol. 2010;21.
129. Karasic TB, Chiorean EG, Sebti SM, Dwyer PJO. A Phase I Study of GGTI-2418 (Geranylgeranyl Transferase I Inhibitor) in Patients with Advanced Solid Tumors. Target Oncol. 2019;2418.
130. Russell RGG. Bisphosphonates: The first 40 years. Bone. 2011;49:2–19.
131. Agabiti SS, Liang Y, Wiemer AJ. Molecular mechanisms linking geranylgeranyl diphosphate synthase to cell survival and proliferation. Mol Membr Biol. 2017;7688:0–11.
132. Agarwal B, Bhendwal S, Halmos B, Moss SF, Ramey WG, Holt PR. Lovastatin augments apoptosis induced by chemotherapeutic agents in colon cancer cells. Clin Cancer Res. 1999;5:2223–9.
133. Neville-Webbe HL, Rostami-Hodjegan A, Evans CA, Coleman RE, Holen I. Sequence- and schedule-dependent enhancement of zoledronic acid induced apoptosis by doxorubicin in breast and

prostate cancer cells. Int J Cancer. 2005;113:364–71.
134. Shull LW, Wiemer AJ, Hohl RJ, Wiemer DF. Synthesis and biological activity of isoprenoid bisphosphonates. Bioorganic Med Chem. 2006;14:4130–6.
135. Wiemer AJ, Tong H, Swanson KM, Hohl RJ. Digeranyl bisphosphonate inhibits geranylgeranyl pyrophosphate synthase. Biochem Biophys Res Commun. 2007;353:921–5.
136. Matthiesen RA, Varney ML, Xu PC, Rier AS, Wiemer DF, Holstein SA. α-Methylation enhances the potency of isoprenoid triazole bisphosphonates as geranylgeranyl diphosphate synthase inhibitors. Bioorganic Med Chem. 2018;26:376–85.
137. Dudakovic A, Tong H, Hohl RJ. Geranylgeranyl diphosphate depletion inhibits breast cancer cell migration. Invest New Drugs. 2011;29:911.
138. Agabiti SS, Li J, Wiemer AJ. Geranylgeranyl diphosphate synthase inhibition induces apoptosis that is dependent upon GGPP depletion , ERK phosphorylation and caspase activation. Cell Death Dis. 2017;8:e2678-12.
139. Dudakovic A, Wiemer AJ, Lamb KM, Vonnahme L a, Dietz SE, Hohl RJ. Inhibition of geranylgeranyl diphosphate synthase induces apoptosis through multiple mechanisms and displays synergy with inhibition of other isoprenoid biosynthetic enzymes. J Pharmacol Exp Ther. 2008;324:1028–36.
140. Wiemer a J, Wiemer DF, Hohl RJ. Geranylgeranyl diphosphate synthase: an emerging therapeutic target. Clin Pharmacol Ther. 2011;90:804–12.
141. Haney SL, Chhonker YS, Varney ML, Talmon G, Murry DJ, Holstein SA. Preclinical investigation of a potent geranylgeranyl diphosphate synthase inhibitor. Invest New Drugs. Investigational New Drugs; 2018;36:810–8.
142. Haney SL, Varney ML, Chhonker YS, Shin S, Mehla K, Crawford AJ, et al. Inhibition of geranylgeranyl diphosphate synthase is a novel therapeutic strategy for pancreatic ductal adenocarcinoma. Oncogene. 2019;38:5308–20.
143. Carnero A. The PKB/AKT pathway in cancer. Curr Pharm Des. 2010;16:34–44.
144. Shackelford DB, Shaw RJ. The LKB1-AMPK pathway: Metabolism and growth control in tumour suppression. Nat. Rev. Cancer. 2009. page 563–75.
145. Boudeau J, Sapkota G, Alessi DR. LKB1, a protein kinase regulating cell proliferation and polarity. FEBS Lett. 2003. page 159–65.
146. Hardie DG, Alessi DR. LKB1 and AMPK and the cancer-metabolism link - ten years after. BMC Biol. 2013.
147. Pakos-zebrucka K, Koryga I, Mnich K, Ljujic M, Samali A, Gorman AM. The integrated stress response. EMBO Rep. 2016;1–22.
148. Ma L, Niknejad N, Gorn-Hondermann I, Dayekh K, Dimitroulakos J. Lovastatin Induces Multiple Stress Pathways Including LKB1/AMPK Activation That Regulate Its Cytotoxic Effects in Squamous Cell Carcinoma Cells. PLoS One. 2012;7.
149. Jorissen RN, Walker F, Pouliot N, Garrett TPJ, Ward CW, Burgess AW. Epidermal growth factor receptor: Mechanisms of activation and signalling. Exp Cell Res. 2003;284:31–53.
150. Wek RC, Jiang H-Y, Anthony TG. Coping with stress: eIF2 kinases and translational control. Biochem Soc Trans. 2006;34:7.
151. Alexander A, Walker CL. The role of LKB1 and AMPK in cellular responses to stress and damage. FEBS Lett. 2011. page 952–7.
152. Hemminki A, Markie D, Tomlinson I, Avizienyte E, Roth S, Loukola A, et al. A serine/threonine kinase gene defective in Peutz-Jeghers syndrome. Nature. 1998;391:184–7.
153. Sanchez-Cespedes M, Parrella P, Esteller M, Nomoto S, Trink B, Engles JM, et al. Inactivation of LKB1/STK11 is a common event in adenocarcinomas of the lung. Cancer Res. 2002;62:3659–62.
154. Ji H, Ramsey MR, Hayes DN, Fan C, McNamara K, Kozlowski P, et al. LKB1 modulates lung cancer differentiation and metastasis. Nature. 2007;448:807–10.
155. Wingo SN, Gallardo TD, Akbay EA, Liang MC, Contreras CM, Boren T, et al. Somatic LKB1 mutations promote cervical cancer progression. PLoS One. 2009;4.

156. Qiu W, Schönleben F, Thaker HM, Goggins M, Su GH. A novel mutation of STK11/LKB1 gene leads to the loss of cell growth inhibition in head and neck squamous cell carcinoma. Oncogene. 2006;25:2937–42.
157. Li X, Lu Y, Lu H, Luo J, Hong Y, Fan Z. AMPK-mediated energy homeostasis and associated metabolic effects on cancer cell response and resistance to cetuximab. Oncotarget. 2015;6:11507–18.
158. Harding HP, Zhang Y, Zeng H, Novoa I, Lu PD, Calfon M, et al. An integrated stress response regulates amino acid metabolism and resistance to oxidative stress. Mol Cell. 2003;11:619–33.
159. Ron D. Translational control in the endoplasmic reticulum stress response. J. Clin. Invest. 2002. page 1383–8.
160. Ye J, Kumanova M, Hart LS, Sloane K, Zhang H, De Panis DN, et al. The GCN2-ATF4 pathway is critical for tumour cell survival and proliferation in response to nutrient deprivation. EMBO J. 2010;29:2082–96.
161. Denoyelle C, Abou-Rjaily G, Bezrookove V, Verhaegen M, Johnson TM, Fullen DR, et al. Anti-oncogenic role of the endoplasmic reticulum differentially activated by mutations in the MAPK pathway. Nat Cell Biol. 2006;8:1053–63.
162. Donnelly N, Gorman AM, Gupta S, Samali A. The eIF2alpha kinases: their structures and functions. Cell Mol Life Sci. 2013;70:3493–511.
163. García MA, Meurs EF, Esteban M. The dsRNA protein kinase PKR: Virus and cell control. Biochimie. 2007. page 799–811.
164. Garcia MA, Gil J, Ventoso I, Guerra S, Domingo E, Rivas C, et al. Impact of Protein Kinase PKR in Cell Biology: from Antiviral to Antiproliferative Action. Microbiol Mol Biol Rev. 2006;70:1032–60.
165. Han AP, Yu C, Lu L, Fujiwara Y, Browne C, Chin G, et al. Heme-regulated eIF2α kinase (HRI) is required for translational regulation and survival of erythroid precursors in iron deficiency. EMBO J. 2001;20:6909–18.
166. Niknejad, Nima; Morley, Melissa; and Dimitroulakos J. Activation of the Integrated Stress Response Regulates Lovastatin-induced Apoptosis. J Biol Chem. 2007;282:29748–56.
167. Novoa I, Zeng H, Harding HP, Ron D. Feedback inhibition of the unfolded protein response by GADD34-mediated dephosphorylation of eIF2alpha. J Cell Biol. 2001;153:1011–22.
168. Ameri K, Harris AL. Activating transcription factor 4. Int J Biochem Cell Biol. 2008;40:14–21.
169. Rutkowski DT, Arnold SM, Miller CN, Wu J, Li J, Gunnison KM, et al. Adaptation to ER stress is mediated by differential stabilities of pro-survival and pro-apoptotic mRNAs and proteins. PLoS Biol. 2006;4:2024–41.
170. Ghosh AP, Klocke BJ, Ballestas ME, Roth KA. CHOP potentially co-operates with FOXO3a in neuronal cells to regulate PUMA and BIM expression in response to ER stress. PLoS One. 2012;7.
171. Li Y, Guo Y, Tang J, Jiang J, Chen Z. New insights into the roles of CHOP-induced apoptosis in ER stress Structure and Properties of C / EBP Homologous Protein Roles of CHOP in ER Stress-Mediated Apoptosis. Acta Biochim Biophys Sin. 2014;46:629–40.
172. Hoque MO, Begum S, Sommer M, Lee T, Trink B, Ratovitski E, et al. PUMA in head and neck cancer. Cancer Lett. 2003;199:75–81.
173. Sun Q, Sakaida T, Yue W, Gollin SM, Yu J. Chemosensitization of head and neck cancer cells by PUMA. Mol Cancer Ther. 2007;6:3180–8.
174. Sun Q, Ming L, Thomas SM, Wang Y, Chen ZG, Ferris RL, et al. PUMA mediates EGFR tyrosine kinase inhibitor-induced apoptosis in head and neck cancer cells. Oncogene. 2009;28:2348–57.
175. Jadhav K, Zhang Y. Activating transcription factor 3 in immune response and metabolic regulation. Liver Res. 2017;1:96–102.
176. Hai, Tsonwin; Wolford, Christopher; and Chang Y-S. ATF3, a hub of the cellular adaptive-response network, in the pathogenesis of diseases: is modulation of inflammation a unifying component? Gene Expr. 2010;15:1–11.
177. Hai T, Wolfgang CD, Marsee DK, Allen AE, Sivaprasad U. ATF3 and stress responses. Gene Expr.

1999;7:321–35.
178. Yin X, DeWille JW, Hai T. A potential dichotomous role of ATF3, an adaptive-response gene, in cancer development. Oncogene. 2008;27:2118–27.
179. St Germain C, O'Brien A, Dimitroulakos J. Activating Transcription Factor 3 regulates in part the enhanced tumour cell cytotoxicity of the histone deacetylase inhibitor M344 and cisplatin in combination. Cancer Cell Int. 2010;10:32.
180. Bar J, Hasim MS, Baghai T, Niknejad N, Perkins TJ, Stewart DJ, et al. Induction of Activating Transcription Factor 3 Is Associated with Cisplatin Responsiveness in Non–Small Cell Lung Carcinoma Cells. Neoplasia. 2016;18:525–35.
181. St. Germain C, Niknejad N, Ma L, Garbuio K, Hai T, Dimitroulakos J. Cisplatin Induces Cytotoxicity through the Mitogen-Activated Protein Kinase Pathways ana Activating Transcription Factor 3. Neoplasia. 2010;12:527–38.
182. Jiang H-Y, Wek S a, McGrath BC, Lu D, Hai T, Harding HP, et al. Activating transcription factor 3 is integral to the eukaryotic initiation factor 2 kinase stress response. Mol Cell Biol. 2004;24:1365–77.
183. Niknejad N, Gorn-Hondermann I, Ma L, Zahr S, Johnson-Obeseki S, Corsten M, et al. Lovastatin-induced apoptosis is mediated by activating transcription factor 3 and enhanced in combination with salubrinal. Int J Cancer. 2014;134:268–79.
184. Pignon JP, Maître A le, Maillard E, Bourhis J. Meta-analysis of chemotherapy in head and neck cancer (MACH-NC): An update on 93 randomised trials and 17,346 patients. Radiother Oncol. 2009;92:4–14.
185. Jiang L, Ji N, Zhou Y, Li J, Liu X, Wang Z, et al. CAL 27 is an oral adenosquamous carcinoma cell line. Oral Oncol. 2009;45:e204–7.
186. Nichols A, Yoo J, Palma D, Fung K, Franklin J, Koropatnick J, et al. Frequent Mutations in Frequent Mutations in TP53 and CDKN2A Found by Next-Generation Sequencing of Head and Neck Cancer Cell Lines. Arch Otolaryngol Head Neck Surg. 2012;138:732–9.
187. Hartman MG, Lu D, Kim M-L, Kociba GJ, Shukri T, Buteau J, et al. Role for Activating Transcription Factor 3 in Stress-Induced -Cell Apoptosis. Mol Cell Biol. 2004;24:5721–32.
188. Zinszner H, Kuroda M, Wang XZ, Batchvarova N, Lightfoot RT, Remotti H, et al. CHOP is implicated in programmed cell death in response to impaired function of the endoplasmic reticulum. Genes Dev. 1998;12:982–95.
189. Harding HP, Novoa I, Zhang Y, Zeng H, Wek R, Schapira M, et al. Stress-Induced Gene Expression in Mammalian Cells. Mol Cell. 2000;6:1099–108.
190. Hettmann T, Barton K, Leiden JM. Microphthalmia due to p53-mediated apoptosis of anterior lens epithelial cells in mice lacking the CREB-2 transcription factor. Dev Biol. 2000;222:110–23.
191. Dimitroulakos J, Marhin WH, Tokunaga J, Irish J, Gullane P, Penn LZ, et al. Microarray and biochemical analysis of lovastatin-induced apoptosis of squamous cell carcinomas. Neoplasia. 2002;4:337–46.
192. Mantha A, Hanson J, Goss G, Lagarde A, Lorimer I, Dimitroulakos J. Targeting the mevalonate pathway inhibits the function of the epidermal growth factor receptor: synergistic cytotoxicity induced by lovastatin and gefitinib. Clin Cancer Res. 2005;11:2398–407.
193. Chou TC. Drug combination studies and their synergy quantification using the chou-talalay method. Cancer Res. 2010;70:440–6.
194. Strober W. Trypan Blue Exclusion Test of Cell Viability. Curr Protoc Immunol. 2015;Appendix 3:Appendix 3B.
195. Trapnell C, Roberts A, Goff L, Pertea G, Kim D, Kelley DR, et al. Differential gene and transcript expression analysis of RNA-seq experiments with TopHat and Cufflinks. Nat Protoc. 2012;7:562–78.
196. Mi H, Huang X, Muruganujan A, Tang H, Mills C, Kang D, et al. PANTHER version 11: Expanded annotation data from Gene Ontology and Reactome pathways, and data analysis tool enhancements. Nucleic Acids Res. 2017;45:D183–9.

197. Carmichael J, Degraff WG, Gazdar AF, Minna JD, Mitchell JB. Evaluation of a Tetrazolium-based of Chemosensitivity Testing1 Semiautomated Colorimetrie Assay : Assessment. Cancer Res. 1987;47:936–42.
198. Tong JJ, Yan Z, Jian REN, Tao H, Hui OTAO, Jian C. RhoA regulates invasion of glioma cells via the c-Jun NH2-terminal kinase pathway under hypoxia. Oncol Lett. 2012;4:495–500.
199. Virtanen SS, Sandholm J, Yegutkin G, Kalervo Vaananen H, Harkonen PL, Va HK. Inhibition of GGTase-I and FTase disrupts cytoskeletal organization of human PC-3 prostate cancer cells. Cell Biol Int. 2010;34:815–26.
200. Kaibuchi K, Kuroda S, Amano M. Regulation of the cytoskeleton and cell adhesion by the Rho family GTPases in mammalian cells. Annu Rev Biochem. 1999;68:459–86.
201. Schmitz AAPP, Govek EE, Böttner B, Van Aelst L, Bo B, Aelst L Van. Rho GTPases: Signaling, migration, and invasion. Exp Cell Res. 2000;261:1–12.
202. Piacentini L, Wainwright CL PJ, Piacentini L, Wainwright CL, Parratt JR. The antiarrhythmic effect of ischaemic preconditioning in isolated rat heart involves a pertussis toxin sensitive mechanism. Cardiovasc Res. 1993;27:674–80.
203. Costa V, Angelini C, Feis I De, Ciccodicola A. Uncovering the Complexity of Transcriptomes with RNA-Seq. J Biomed Biotechnol. 2010;2010.
204. Tanaka Y, Nakamura A, Morioka MS, Inoue S, Tamamori-adachi M, Yamada K, et al. Systems Analysis of ATF3 in Stress Response and Cancer Reveals Opposing Effects on Pro-Apoptotic Genes in p53 Pathway. PLoS One. 2011;6.
205. Park J, Matralis AN, Berghuis AM, Tsantrizos YS. Human isoprenoid synthase enzymes as therapeutic targets. Front Chem. 2014;2:50.
206. Holstein SA, Hohl RJ. Is there a future for prenyltransferase inhibitors in cancer therapy? Curr Opin Pharmacol. 2012;12:704–9.
207. Ivana Scovassi A, Diederich M. Modulation of poly(ADP-ribosylation) in apoptotic cells. Biochem Pharmacol. 2004;68:1041–7.
208. Young NR, Soneru C, Liu J, Grushko TA, Hardeman A, Olopade OI, et al. Afatinib efficacy against squamous cell carcinoma of the head and neck cell lines in vitro and in vivo. Target Oncol. 2015;
209. Zhao TT, Trinh D, Addison CL, Dimitroulakos J. Lovastatin inhibits VEGFR and AKT activation: Synergistic cytotoxicity in combination with VEGFR inhibitors. PLoS One. 2010;5:1–11.
210. Hindler K, Cleeland CS, Rivera E, Collard CD. The role of statins in cancer therapy. Oncologist. 2006;11:306–15.
211. Sopková J, Vidomanová E, Strnádel J, Škovierová H HE. The role of statins as therapeutic agents in cancer. Gen Physiol Biophys. 2017;36:501–11.
212. Thibault A, Samid D, Tompkins AC, Figg WD, Cooper MR, Hohl RJ, et al. Phase I study of lovastatin, an inhibitor of the mevalonate pathway, in patients with cancer. Clin Cancer Res. 1996;2:483–91.
213. Dimitroulakos J, Nohynek D, Backway KL, Hedley DW, Yeger H, Freedman MH, et al. Increased sensitivity of acute myeloid leukemias to lovastatin-induced apoptosis: A potential therapeutic approach. Blood. 1999;93:1308–18.
214. Sharma K, Vu T-T, Cook W, Naseri M, Zhan K, Nakajima W, et al. p53-independent Noxa induction by cisplatin is regulated by ATF3/ATF4 in head and neck squamous cell carcinoma cells. Mol Oncol. 2018.
215. Dimitroulakos J, Lorimer IA, Goss G. Strategies to enhance epidermal growth factor inhibition: Targeting the mevalonate pathway. Clin Cancer Res. 2006.
216. Banach M, Serban C, Ursoniu S, Rysz J, Muntner P, Toth PP, et al. Statin therapy and plasma coenzyme Q10 concentrations-A systematic review and meta-analysis of placebo-controlled trials. Pharmacol Res. 2015;99:329–36.
217. Thompson PD, Clarkson P, Karas RH. Statin-Associated Myopathy. J. Am. Med. Assoc. 2003. page 1681–90.
218. Taylor BA, Lorson L, White CM, Thompson PD. A randomized trial of coenzyme Q10 in patients

with confirmed Statin Myopathy. Atherosclerosis. 2015;238:329–35.
219. Pinal-fernandez I, Casal-dominguez M, Mammen AL. Statins : pros and cons. Med Clin. 2017;S0025-7753:30914–4.
220. Littlefield N, Beckstrand RL, Luthy KE. Statins' effect on plasma levels of Coenzyme Q10 and improvement in myopathy with supplementation. J. Am. Assoc. Nurse Pract. 2014. page 85–90.
221. Xia Z, Tan MM, Wong WW, Dimitroulakos J, Minden MD, Penn LZ. Blocking protein geranylgeranylation is essential for lovastatin-induced apoptosis of human acute myeloid leukemia cells. Leukemia. 2001;15:1398–407.
222. Liu BS, Dai XY, Xia HW, Xu HJ, Tang QL, Gong QY, et al. Geranylgeranyl transferase 1 inhibitor GGTI-298 enhances the anticancer effect of gefitinib. Mol Med Rep. 2018;18:4023–9.
223. Ullah N, Mansha M, J. Casey P. Protein Geranylgeranyltransferase Type 1 as a Target in Cancer. Curr Cancer Drug Targets. 2016;16:563–71.
224. Vogt A, Sun J, Qian Y, Hamilton AD SS. The geranylgeranyltransferase-I inhibitor GGTI-298 arrests human tumor cells in G0/G1 and induces p21(WAF1/CIP1/SDI1) in a p53-independent manner. J Biol Chem. 1997;272:27224–9.
225. Kazi A, Carie A, Blaskovich M a, Bucher C, Thai V, Moulder S, et al. Blockade of protein geranylgeranylation inhibits Cdk2-dependent p27Kip1 phosphorylation on Thr187 and accumulates p27Kip1 in the nucleus: implications for breast cancer therapy. Mol Cell Biol. 2009;29:2254–63.
226. Sjogren AKM, Andersson KME, Liu M, Cutts BA, Karlsson C, Wahlstrom AM, et al. GGTase-I deficiency reduces tumor formation and improves survival in mice with K-RAS-induced lung cancer. J Clin Invest. 2007;117:1294–304.
227. Hamada M, Miki T, Iwai S, Shimizu H, Yura Y. Involvement of RhoA and RalB in geranylgeranyltransferase i inhibitor-mediated inhibition of proliferation and migration of human oral squamous cell carcinoma cells. Cancer Chemother Pharmacol. 2011;68:559–69.
228. Del Re DP, Miyamoto S, Brown JH. Focal adhesion kinase as a RhoA-activable signaling scaffold mediating akt activation and cardiomyocyte protection. J Biol Chem. 2008.
229. Basile JR, Gavard J, Gutkind JS. Plexin-B1 utilizes RhoA and Rho kinase to promote the integrin-dependent activation of Akt and ERK and endothelial cell motility. J Biol Chem. 2007.
230. Hébert M, Potin S, Sebbagh M, Bertoglio J, Bréard J, Hamelin J. Rho-ROCK-Dependent Ezrin-Radixin-Moesin Phosphorylation Regulates Fas-Mediated Apoptosis in Jurkat Cells. J Immunol. 2008.
231. Rijken PJ, Hage WJ, Van Bergen En Henegouwen PMP, Verkleij Boonstra AJJ. Epidermal growth factor induces rapid reorganization of the actin microfilament system in human A431 cells. J Cell Sci. 1991;100:491–9.
232. Wiegant FAC, Blok FJ, Defize LHK, Linnemans WA, Verkley AJ, Boonstra J. Epidermal growth factor receptors associated to cytoskeletal elements of epidermoid carcinoma (A431) cells. J Cell Biol. 1986;103:87–94.
233. Lohi O, Lehto VP. EAST, a novel EGF receptor substrate, associates with focal adhesions and actin fibers. FEBS Lett. 1998.
234. Akiyama T, Kadowaki T, Nishida E, Kadooka T, Ogawara H, Fukami Y, et al. Substrate specificities of tyrosine-specific protein kinases toward cytoskeletal proteins in vitro. J Biol Chem. 1986.
235. Stoorvogel W, Kerstens S, Fritzsche I, Den Hartigh JC, Oud R, Van Der Heyden MAG, et al. Sorting of Ligand-activated Epidermal Growth Factor Receptor to Lysosomes Requires Its Actin-binding Domain. J Biol Chem. 2004.
236. Waller DD, Park J, Tsantrizos YS. Inhibition of farnesyl pyrophosphate (FPP) and/or geranylgeranyl pyrophosphate (GGPP) biosynthesis and its implication in the treatment of cancers. Crit Rev Biochem Mol Biol. 2019;54:41–60.
237. Taub N, Teis D, Ebner HL, Hess MW, Huber LA. Late endosomal traffic of the epidermal growth factor receptor ensures spatial and temporal fidelity of mitogen-activated protein kinase signaling. Mol Biol Cell. 2007;
238. Ceresa BP. Regulation of EGFR endocytic trafficking by rab proteins. Histol. Histopathol. 2006.

239. Ceresa BP. Determining the role of rab7 in constitutive and ligand- mediated epidermal growth factor receptor endocytic traffi cking using single cell assays. Methods Mol Biol. 2015.
240. Baron RA, Tavaré R, Figueiredo AC, Błazewska KM, Kashemirov BA, McKenna CE, et al. Phosphonocarboxylates inhibit the second geranylgeranyl addition by Rab geranylgeranyl transferase. J Biol Chem. 2009.
241. Coxon FP, Ebetino FH, Mules EH, Seabra MC, McKenna CE, Rogers MJ. Phosphonocarboxylate inhibitors of Rab geranylgeranyl transferase disrupt the prenylation and membrane localization of Rab proteins in osteoclasts in vitro and in vivo. Bone. 2005.
242. Wasko BM, Dudakovic A, Hohl RJ. Bisphosphonates induce autophagy by depleting geranylgeranyl diphosphate. J Pharmacol Exp Ther. 2011;337:540–6.
243. Dykstra KM, Allen C, Born EJ, Tong H, Holstein SA. Mechanisms for autophagy modulation by isoprenoid biosynthetic pathway inhibitors in multiple myeloma cells. Oncotarget. 2015;6:41535–49.
244. Holstein SA, Hohl RJ. Isoprenoid biosynthetic pathway inhibition disrupts monoclonal protein secretion and induces the unfolded protein response pathway in multiple myeloma cells. Leuk Res. 2011;35:551–9.
245. Reilly JE, Neighbors JD, Hohl RJ. Targeting protein geranylgeranylation slows tumor development in a murine model of prostate cancer metastasis. Cancer Biol Ther. 2016;4047:00–00.
246. Reilly JE, Neighbors JD, Tong H, Henry MD, Hohl RJ. Targeting geranylgeranylation reduces adrenal gland tumor burden in a murine model of prostate cancer metastasis. Clin Exp Metastasis. Springer Netherlands; 2015;32:555–66.
247. von Zee CL, Richards MP, Bu P, Perlman JI, Stubbs EB. Increased RhoA and RhoB protein accumulation in cultured human trabecular meshwork cells by lovastatin. Investig Ophthalmol Vis Sci. 2009;50:2816–23.
248. Schröder M, Kaufman RJ. ER stress and the unfolded protein response. Mutat. Res. - Fundam. Mol. Mech. Mutagen. 2005.
249. Sinensky M, Logel J. Defective macromolecule biosynthesis and cell-cycle progression in a mammalian cell starved for mevalonate. Proc Natl Acad Sci U S A. 1985;82:3257–61.
250. Mollazadeh H, Atkin SL, Butler AE, Ruscica M, Sirtori CR, Sahebkar A. The effect of statin therapy on endoplasmic reticulum stress. Pharmacol Res. Elsevier; 2018;137:150–8.
251. Ghavami S, Yeganeh B, Stelmack GL, Kashani HH, Sharma P, Cunnington R, et al. Apoptosis, autophagy and ER stress in mevalonate cascade inhibition-induced cell death of human atrial fibroblasts. Cell Death Dis. 2012.
252. Lan YC, Chang CL, Sung MT, Yin PH, Hsu CC, Wang KC, et al. Zoledronic acid-induced cytotoxicity through endoplasmic reticulum stress triggered REDD1-mTOR pathway in breast cancer cells. Anticancer Res. 2013.
253. Chen JC, Wu ML, Huang KC, Lin WW. HMG-CoA reductase inhibitors activate the unfolded protein response and induce cytoprotective GRP78 expression. Cardiovasc Res. 2008.
254. Schmidt A, Beck T, Koller A, Kunz J, Hall MN. The TOR nutrient signalling pathway phosphorylates NPR1 and inhibits turnover of the tryptophan permease. EMBO J. 1998;17:6924–31.
255. Woodard J, Sassano A, Hay N, Platanias LC. Statin-dependent suppression of the Akt/mammalian target of rapamycin signaling cascade and programmed cell death 4 up-regulation in renal cell carcinoma. Clin Cancer Res. 2008;14:4640–9.
256. Yamauchi K, Sakurai H, Kimura T, Wiriyasermkul P, Nagamori S, Kanai Y, et al. System L amino acid transporter inhibitor enhances anti-tumor activity of cisplatin in a head and neck squamous cell carcinoma cell line. Cancer Lett. 2009;276:95–101.
257. Goberdhan DCI, Ögmundsdóttir MH, Kazi S, Reynolds B, Visvalingam S, Wilson C. Amino acid sensing and mTOR regulation ; inside or out ? Biochem Soc Trans. 2010;37:248–52.
258. Warner GJ, Berry MJ, Moustafa ME, Carlson BA, Hatfield DL, Faust JR. Inhibition of selenoprotein synthesis by selenocysteine tRNA([Ser]Sec) lacking isopentenyladenosine. J Biol Chem.

2000;275:28110–9.
259. Faust JR, Dice JF. Evidence for isopentenyladenine modification on a cell cycle-regulated protein. J Biol Chem. 1991;266:9961–70.
260. Konevega AL, Soboleva NG, Makhno VI, Semenkov YP, Wintermeyer W, Rodnina M V., et al. Purine bases at position 37 of tRNA stabilize codon-anticodon interaction in the ribosomal A site by stacking and Mg2+-dependent interactions. Rna. 2004;10:90–101.
261. Schweizer U, Bohleber S, Fradejas-Villar N. The modified base isopentenyladenosine and its derivatives in tRNA. RNA Biol. 2017;14:1197–208.
262. Moosmann B, Behl C. Selenoproteins, cholesterol-lowering drugs, and the consequences: Revisiting of the mevalonate pathway. Trends Cardiovasc Med. 2004;14:273–81.
263. Miller BT, Ueta CB, Lau V, Jacomino KG, Wasserman LM, Kim BW. Statins and downstream inhibitors of the isoprenylation pathway increase type 2 iodothyronine deiodinase activity. Endocrinology. 2012;153:4039–48.
264. Dirheimer G, Baranowski W, Keith G. Variations in tRNA modifications, particularly of their queuine content in higher eukaryotes. Its relation to malignancy grading. Biochimie. 1995;77:99–103.
265. Dong J, Qiu H, Garcia-Barrio M, Anderson J, Hinnebusch AG. Uncharged tRNA activates GCN2 by displacing the protein kinase moiety from a bipartite tRNA-binding domain. Mol Cell. 2000;6:269–79.
266. Garcia-Barrio M, Dong J, Cherkasova VA, Zhang X, Zhang F, Ufano S, et al. Serine 577 is phosphorylated and negatively affects the tRNA binding and eIF2α kinase activities of GCN2. J Biol Chem. 2002;277:30675–83.
267. Lageix S, Zhang J, Rothenburg S, Hinnebusch AG. Interaction between the tRNA-Binding and C-Terminal Domains of Yeast Gcn2 Regulates Kinase Activity In Vivo. PLoS Genet. 2015;11:1–28.
268. Zaborske JM, Wu X, Wek RC, Pan T. Selective control of amino acid metabolism by the GCN2 eIF2 kinase pathway in Saccharomyces cerevisiae. BMC Biochem. 2010;11:1–9.
269. Sood R, Porter AC, Olsen DA, Cavener DR, Wek RC. A mammalian homologue of GCN2 protein kinase important for translational control by phosphorylation of eukaryotic initiation factor-2α. Genetics. 2000.
270. Deng J, Harding HP, Raught B, Gingras AC, Berlanga JJ, Scheuner D, et al. Activation of gcn2 in uv-irradiated cells inhibits translation. Curr Biol. 2002;12:1279–86.
271. Muaddi H, Majumder M, Peidis P, Papadakis AI, Holcik M, Scheuner D, et al. Phosphorylation of eIF2α at serine 51 is an important determinant of cell survival and adaptation to glucose deficiency. Mol Biol Cell. 2010;21:3220–31.
272. Liu Y, László C, Liu Y, Liu W, Chen X, Evans SC, et al. Regulation of G1 arrest and apoptosis in hypoxia by PERK and GCN2-mediated eIF2α phosphorylation. Neoplasia. 2010;12:61–8.
273. B'Chir W, Maurin AC, Carraro V, Averous J, Jousse C, Muranishi Y, et al. The eIF2α/ATF4 pathway is essential for stress-induced autophagy gene expression. Nucleic Acids Res. 2013;41:7683–99.
274. Tsuru A, Imai Y, Saito M, Kohno K. Novel mechanism of enhancing IRE1α-XBP1 signalling via the PERK-ATF4 pathway. Sci Rep. Nature Publishing Group; 2016;6:1–8.
275. Hamanaka RB, Bennett BS, Cullinan SB, Diehl JA. PERK and GCN2 Contribute to eIF2alpha Phosphorylation and Cell Cycle Arrest after Activation of the Unfolded Protein Response Pathway. Mol Biol Cell. 2005;16:5493–501.
276. Mounir Z, Krishnamoorthy JL, Wang S, Papadopoulou B, Campbell S, Muller WJ, et al. Akt determines cell fate through inhibition of the PERK-eIF2α phosphorylation pathway. Sci Signal. 2011;4.
277. Dudley DT, Pang L, Decker SJ, Bridges AJ, Saltiel AR. A synthetic inhibitor of the mitogen-activated protein kinase cascade. Proc Natl Acad Sci U S A. 1995;92:7686–7689.
278. García-Martínez JM, Moran J, Clarke RG, Gray A, Cosulich SC, Chresta CM, et al. Ku-0063794 is a specific inhibitor of the mammalian target of rapamycin (mTOR). Biochem J. 2009;421:29–42.

279. Cherkasova VA, Hinnebusch AG. Translational control by TOR and TAP42 through dephosphorylation of eIF2α kinase GCN2. Genes Dev. 2003;17:859–872.
280. Gandin V, Masvidal L, Cargnello M, Gyenis L, McLaughlan S, Cai Y, et al. MTORC1 and CK2 coordinate ternary and eIF4F complex assembly. Nat Commun. Nature Publishing Group; 2016;7.
281. Koyama S, Omura T, Yonezawa A, Imai S, Nakagawa S, Nakagawa T, et al. Gefitinib and erlotinib lead to phosphorylation of eukaryotic initiation factor 2 alpha independent of epidermal growth factor receptor in A549 cells. PLoS One. 2015.
282. Ferguson KM. Structure-Based View of Epidermal Growth Factor Receptor Regulation. Annu Rev Biophys. 2008;37:353–73.
283. Zhao TT. Mechanism and Therapeutic Potential of Statin-Mediated Inhibition of Tyrosine Kinase Receptors. University of Ottawa; 2011.
284. Korsse SE, Peppelenbosch MP, Van Veelen W. Targeting LKB1 signaling in cancer. Biochim. Biophys. Acta - Rev. Cancer. 2013. page 194–210.